Ultrasonic nodal point: a new configuration for ultrasonic moulding. Advances towards the complete industrialisation of the technology

Marcel Janer Angelet

Doctoral thesis – Industrial Ph.D.

Supervised by Dr. Maria Dolors Riera Colom

Company coordination by Francisco Javier Plantà Torralba

Barcelona, July 2022

UNIVERSITAT POLITÈCNICA DE CATALUNYA
BARCELONATECH
Escola d'Enginyeria de Barcelona Est

Department of Materials Science and Engineering

eurecat

Advanced Manufacturing Unit

Acknowledgements

First of all, I would like to express my gratitude to my advisor, Dr. Mª Dolors Riera for her support and inspiration, whilst guiding me through this thesis. Without her dedication, it would have been impossible for me to accomplish this work.

I would also like to thank my advisor Xavier Plantà, Head of Eurecat's Industrial Area, for giving me the opportunity to work in this project and for supporting me in the research done during these years.

I would like to express my sincere gratitude to my colleagues at Eurecat Dr. Carles Rubio, Dr. German Perez, David Montes and all the "Advanced Manufacturing Systems" unit, who have helped me in my day-to-day tasks related to this research. I would also like to acknowledge Ultrasion ® employees, especially Toni Lopez, for helping me during the experimental tests.

I would also like to express my gratitude to the industrial PhD initiative from the *Generalitat de Catalunya* that has co-funded this research.

I would like to finish with a big thank you to my family, my parents and specially my partner Jorgina, for their patience and unconditional support.

Dedicated to my son Bernat, my endless source of happiness

Abstract

The new European industrial strategy for the Green Deal seeks to promote low-emission technologies in order to achieve climate neutrality by 2050. In this context, ultrasonic moulding (USM) is a promising technology, which could be used as a substitute for conventional injection moulding techniques. This relatively new technology has a lower energy consumption due to the removal of the injection screw and its heaters. Hence, it could be a sustainable alternative in an industrial environment. In addition, the supply of the material processed in USM is delivered shot-by-shot, which makes this technology extremely feasible for processing small batches of samples without wastage. However, until now, USM technology has not been adopted in industrial environments due to the lack of robustness and poor repeatability of its results. Further, inadequate knowledge about the influence of the process parameters in the polymer melt also acts as an obstacle for the industrial operator.

In this dissertation, applied research and numerical simulation were carried out to improve USM technology and to deepen the knowledge of the process to promote its industrialization.In this context, this thesis presents three main areas of work.

First, the evolution of ultrasonic moulding machines and configurations was examined. This examination analysed the major findings and drawbacks identified through the experiments published in existing literature.
Based on the above-mentioned review of literature, the development and validation of a new configuration for USM was completed. This led to a great improvement in the performance of USM in terms of repeatability and reduction of impurities in the samples. The new configuration was used to process polyexymethylene and cyclic olefin polymer, and the results were compared to conventional injection moulding. The analysis of the results revealed that the newly developed method is successful in correct, repetitive processing of polymers. Thus, USM was proved to be a reliable industrial technology.

Finally, research was carried out to study the viscoelastic behaviour of polypropylene cylinders subjected to ultrasonic heating. Results obtained from the numerical simulation of the process were compared to experimental measurements obtained using an infrared camera. The analysis of the results showed an inhomogeneous temperature distribution along the cylinder, and distinct stages of heating could be identified over a period of time. In addition, the comparison between the numerical and the experimental results showed that the interaction between the sample and the mould directly influences the temperature distribution along the cylinder. Last, the effects of the main parameters of ultrasonic heating were documented and compared, both numerically and experimentally.

Thus, in the final analysis, the research undertaken for this dissertation improves the applicability of USM technology in industrial environments by increasing its repeatability and robustness, and contributing to a better understanding of its main parameters.

Contents

List of Figures

List of Tables

Nomenclature

Abbreviations

μIM	Micro-injection moulding	1
POM	Polyoxymethylene	28
COP	Cyclic olefin copolymer	40
DMA	Dynamic mechanical analysis	91
DOE	Design of experiments	44
FEA	Finite element analysis	117
FTIR	Fourier-transform infrared	48
HDPE	High-density polyethylene	49
NPUSM	Nodal point ultrasonic moulding	55
PA12	Polyamide 12	41
PBS	Polybutylene succinate	41
PCL	Polycaprolactone	41
PEEK	Polyether ether ketone	45
PLA	Polylactide	45
PMMA	polymethyl methacrylate	36
PP	Polypropylene	40
PPSU	Polyphenylsulfone	41
PS	Polystyrene	45
PZT	Lead zirconate titanate	10
TTS	Time-temperature superposition principle	106

UAIM	Ultrasonic assisted injection moulding	2
UHMWPE	Ultra-high molecular weight polyethylene	41
USM	Ultrasonic moulding	1
WLF	Williams-Landel-Ferry equation	108

Symbols

β	Coefficient of volume expansions	39
δ	Time phase	35
ϵ	Strain	35
η	Viscosity	103
$\frac{\partial}{\partial t}$	Partial derivate of time	12
κ	Thermal conductivity	34
ρ	Material density	34
σ	Stress	35
σ_s	Surface tension of the polymer melt	38
τ	Relaxation time	105
$\tau(\vec{t})$	Equivalent friction stress	37
$\vec{g}$	Gravity	39
$\vec{u}$	Flow velocity	39
$v(\vec{t})$	Relative sliding velocity	37
a	Ultrasonic amplitude	38
a_T	Horizontal shift factor	106
b_T	Vertical shift factor	106
c_0	Speed of sound	12
c_p	Specific heat capacity at constant pressure	34
E	Young's Modulus	103

Motivation

During my earliest days as a researcher in the field of ultrasonic moulding (USM), there existed an assumption that the lack of knowledge about the variables of the process was the main reason for all the challenges faced by USM technology. Those days, we used an initial version of Sonorus® 1G machine from Ultrasion® in all our experiments; there were numerous problems: lack of repeatability, sample contamination, burnt samples, fragile samples, dispersion in the processing parameters, among many others. The more optimistic researchers thought that most of these problems could be easily solved using the data gathered from in-mould sensors during the experiments. The pessimistic ones felt that the intrinsic features of ultrasonic heating (very fast heating in a very short time) would make the process chaotic and unmanageable. All in all, it was a very interesting challenge for us to try to address.

We started working with the optimistic approach, using temperature and pressure sensors during the process, and trying to correlate the information with the machine outputs and samples properties. Multiple sensors were used at multiple locations. *Design of experiments* methodologies and visualisation techniques were applied. However, even after the generation of several gigabytes of data, no proper correlation was found. After all, the so-called easy problem-solving was not so easy.
Fortunately, the pessimistic approach also was not true. Ultimately, we found out that a major redesigning of the USM method was needed. This new configuration, complemented by a better understanding of the major variables and their behaviour during the process, proved that the technology was stable and fit for industrial use.

1 Introduction

1.1 General overview

Ultrasonic moulding (USM) is a relatively new technology specifically designed for the production of mini and micro plastic parts. This technology was first developed in 2002 by Michaeli et al. [1], using high-power ultrasound to melt a small quantity of polymer and shape it inside a mould. Since then, multiple experimentation has been carried out by several authors with the aim of exploring new processing possibilities and overcoming some of the limitations of micro-injection moulding (μIM).

μIM is a well-established technology for low-cost mass production, which has been able to successfully process parts with sub-micron or even nano sizes. However, for some applications wherein the moulded parts display cross-scale features, μIM could be challenging in terms of replication fidelity, material utilisation and energy consumption.
On the other hand, the use of high-power ultrasound in conjunction with injection moulding has proved to facilitate the melt filling and to enhance the replication of micro features [2]. In addition, the use of high-power ultrasound to process polymers can lead to very repetitive results with low energy-consumption ratios, as has been demonstrated in consolidated processes such as ultrasonic welding or ultrasonic hot-embossing. Thus, power ultrasonics are applied in injection moulding processes with the aim of enhancing their performance in challenging applications and, at the same time, reducing their energy consumption.

High-power ultrasound applications involve the use of low ultrasonic frequencies (typically from 16kHz to 100kHz) and high amplitudes of vibration.

This technology has been applied since the 1950s to process polymers and is extensively used in common industrial applications such as ultrasonic welding [3] or ultrasonic cutting [4], among several others [5]. One of the distinctive elements of this technology is the *sonotrode* (also known as ultrasonic horn), which is the element that delivers the ultrasonic vibration to the processed material (see section 2.2 for a more detailed explanation).

At present, two main approaches are used to apply ultrasonic energy to mould polymers: ultrasonic assisted injection moulding (UAIM), and USM (see Figure 1.1). The UAIM process applies ultrasonic energy in conventional injection machines, introducing the ultrasonic horn directly into the polymer melt, with the objective of improving the fluidity of the material. The use of UAIM has proved to increase the surface replication ratio of the samples, which can lead to interesting applications for lens and optical parts [6]. However, this process does not replace the traditional way of heating and melting the material, and a conventional screw is still needed in order to plasticise the polymer. On the contrary, USM technology fully replaces the injection screw and uses high-power ultrasonic energy as an alternative to resistance heaters, in order to melt the polymer.

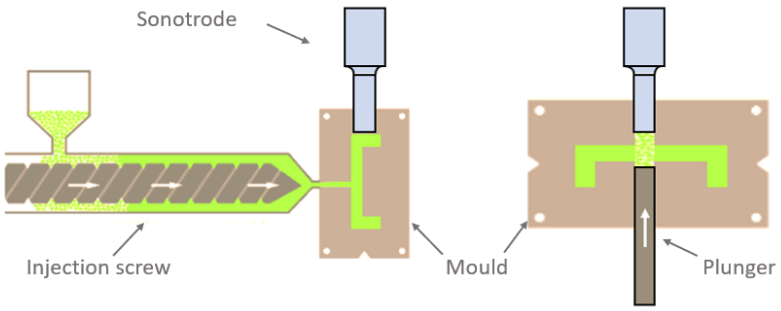

Figure 1.1: Two main approaches for applying ultrasonic energy to mould polymers: UAIM (left) and USM (right)

This dissertation focusses only on USM technology and compares it with conventional injection moulding. One of the major differences between both technologies arises from the removal of the plasticising screw. In conventional injection moulding, there is a clear sequentiality between the plasticising step and the injection step. This is even more evident in μIM, wherein some dedicated machines have separated plasticising and injection units (see section 2.3). Instead, in the USM process, the plasticising of the polymer (known as *Heating step*) and its injection into the mould (known as *Filling*

step) take place almost simultaneously. This leads to various advantages, such as a notable reduction of the time of residence of the material at high temperatures, or the possibility to change the processed material without incurring any wastage. However, the coupling between the heating and the filling steps makes it very difficult to separate the influence of each variable of the process at each step, and impedes the knowledge of basic properties such as the temperature of processing of the polymer. Therefore, the influence of the chief variables of the process has been one of the main topics of research in literature, ever since the emergence of the technology.

The main steps in a typical USM application are as follows: feeding the material, heating the polymer pellets until they melt, filling the mould with the melt, packing the material and cooling it until it can be de-moulded (see Figure 1.2). These steps are similar to the ones used in conventional injection moulding. However, the coupling of the steps and the high speed of the heating step pose a challenge to the complete understanding of the process.

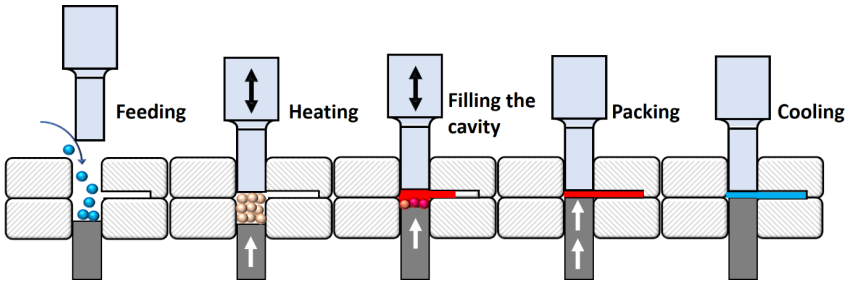

Figure 1.2: Main steps in USM

The use of high-power ultrasound applications in the industry has been favoured due to energy savings, wastage reduction and better sample quality. With regard to USM technology, a shorter time of residence of the polymer at high temperatures and the capacity to mould the material at lower injection pressures are some of the quantified advantages, in comparison with conventional injection techniques.

Nevertheless, despite USM being a promising technology, its adoption in the industrial market has been very limited due to two main factors. On the one hand, USM is a very complex process, and there is a lack of knowledge of the influence of its main parameters which, in addition, tend to have coupled influences. On the other hand, the stability of USM process, as found in the experiments reported, is significantly lower in comparison to conventional injection moulding.

In terms of opportunities, the μIM market is expected to grow from \$904.3 million in 2020 to \$1.6 billion by 2025 [7]. Within this market, the medical healthcare segment hold the largest market share, and is expected to be the fastest-growing end-user segment during the period forecasted. Also, the use of electronic precision components in the automotive industry is further driving the μIM market. Thus, if the problems in the industrial implementation of USM are resolved, USM could be used in niche industrial sectors, such as the fast-growing biomedical, electronics and telecommunications sectors. These sectors are in need of a system to manufacture micro-components comprising of high-performance polymers. In addition, the new trends in manufacturing processes, which ar marked by personalised orders, offer a remarkable opportunity for USM technology. This is because the USM process is able to manufacture short production batches, without needing any purging of the machine or resulting in material wastage.

1.2 Problem statement

As explained earlier, USM is a promising technology with a potential niche market, but with a very low adoption in the industrial market.

The main reasons for the lack of industrialisation of this technology are, on the one hand, the poor knowledge of the influence of its chief parameters and, on the other hand, the lack of robustness of the technology. It will be possible to advance towards a complete industrialisation of this technology, only by resolving both these issues.

This research study has investigated various aspects, with the aim of solving the afore-mentioned problem. First of all, a new configuration for USM has been presented. This configuration focuses upon maximizing the stability of the method for its industrial use. Thus, the repeatability of the processing conditions of the materials, as well as of the mechanical and chemical properties of the samples, is a milestone of this configuration.

Further, experimentation, modelling and simulation of ultrasonic heating in polymers have also been carried out as part of this study. The resultant understanding gained about the heating stage in the USM process is of vital importance in reducing the uncertainty of the method. Due to the complexity of the technology, it is difficult to isolate the effect of each parameter experimentally. Hence, it has been concluded that, modelling efforts are needed to determine the influence of the major variables during the heating of the polymer.

1.3 Objectives and contribution

As previously expressed, the research presented in this thesis focussed on improving USM technology, both in terms of knowledge and performance, in order to make it suitable for industrial use. In order to successfully achieve this purpose, the following specific objectives were identified:

- The generation of a detailed analysis of the evolution of USM, including varied machine configurations, methodology, and materials used, as identified in the literature.
- The design and validation of a robust configuration for USM processing of polymeric materials.
- The design and execution of an experimental plan to obtain a good processing window for any set of polymers.
- The comparison of the performance of USM technology with the industrial standard (conventional injection moulding technology).
- The modelling, simulation and experimental validation of the temperature evolution in polymers due to ultrasonic heating.
- The analysis of the effect of each parameter and of their mutual interactions, as part of the ultrasonic heating evolution.

Apart from these specific objectives, this study mainly sought to contribute towards the improvement of the performance of USM technology.

1.4 Outline of the chapters

Based on the above-mentioned objectives, this dissertation has been divided into the following chapters:

Chapter 2 provides an extensive review of the actual state of the technology. In this chapter, USM technology is presented in detail. An extended review of the experimental work as well as the modelling approaches recorded in literature is included. A part of the study carried out in this chapter has been already published as a peer-reviewed article [8].

Chapter 3 presents the new USM configuration developed to overcome the main drawbacks of existing USM technology. The performance of this configuration is analysed, comparing the processed samples with the ones obtained by using standard USM as well as conventional injection moulding.

Some of the results presented in this chapter have been published in a peer-reviewed article [9].

Chapter 4 presents a numerical model for ultrasonic heating of polymers and its validation using experimental data. The ultrasonic heating evolution of the polymer is presented and the effect of its main parameters is analysed.

Finally, in **Chapter 5** general conclusions are summarised and the main contributions of this study are highlighted. In addition, suggestions for future research work are also offered.

2

Ultrasonic moulding technology

2.1 Introduction

Ultrasonic moulding (USM), or ultrasonic micro moulding [10, 11, 12, 13, 14, 15], is a relatively new technology that uses high-power ultrasound energy to melt and mould thermoplastic polymer pellets for producing mini and micro components. This manufacturing technique was developed by Michaeli et al. in 2002 [1] and, nowadays, it constitutes an interesting alternative to conventional μIM [16]. This technology, along with its main parameters and steps, will be explained in detail in section 2.4. However, most of the elements that compose this technology come from two main areas of expertise: high-power ultrasound and polymer injection moulding.

Thus, in order to present a broader scope of USM technology, the use of high-power ultrasound equipment for industrial processes will be reviewed in section 2.2 and conventional μIM will be presented in section 2.3. The evolution of the USM configurations used in the literature, as well as the details of the machines used in this work are presented in section 2.5. Finally, a state of the art of USM modelling is presented in section 2.6, and a literature the review of the experimental analysis in the field is exposed in section 2.7. This chapter serves as a summary of all the work done in USM technology prior to the findings of this dissertation.

2.2 High-power ultrasound

Ultrasonic waves are vibratory oscillations at frequencies above the hearing range of a person (typically 16 kHz). These waves may be considered as

acoustic waves, which are compression waves that propagate in gases and several liquids, or as elastic waves, which are propagated in solids and depend on the elastic properties of the medium [17].
As there is a very broad field of application for ultrasonic energy (from medical devices to industrial inspection of solids and liquids), for the sake of simplicity, ultrasonic applications can be divided in two main categories: low-power ultrasound and high-power ultrasound. In the sphere of industrial ultrasonics, applications involving low-power ultrasound are used for measurement and control, whereas high-power ultrasonics are used for processing (see Figure 2.1). Currently, power ultrasonics are attracting increased attention in industrial applications, as they might constitute flexible green alternative for energy efficient processes [18].

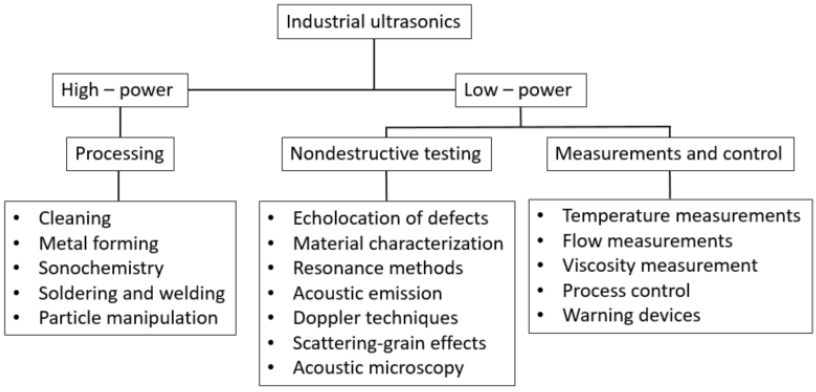

Figure 2.1: Main scope of industrial ultrasonics (adapted from [17])

High-power ultrasound waves, which are defined as "...those that produce effects on the media, or its contents through which the waves propagate..." [19], have been applied since the 1950s to process polymers in multiple fields, with the following three main objectives:

1. To improve the material processability in conventional manufacturing technologies, such as extrusion [20, 21] and injection moulding [22, 23];

2. To define and prepare new polymeric materials or composites or new properties in polymers [24] ;

3. To weld components [3, 25, 26], to manufacture them by means of different processes of plastic deformation [5, 27] and, recently, also to mould polymers [10, 11, 12, 13, 14, 15].

The use of high-power ultrasound waves in polymer melts is reviewed by Ávila-Orta [24]. The study concludes that even though the use of ultrasounds has been shown to be successful for a wide range of applications, there is still a lack of understanding about the fundamental mechanisms underlying the

effects of the ultrasound in polymer melts. In other fields, such as ultrasonic welding, there is much experimental knowledge documented [3] and yet, the modelling and understanding of the main factors of the process are still under study [28].

2.2.1 Acoustic unit

Industrial high-power ultrasound waves are created by the *acoustic unit*, which encompasses the main elements needed to generate and deliver the mechanical vibrations at ultrasonic frequency: an ultrasonic generator, an ultrasonic transducer, a booster and a sonotrode (see Figure 2.2). High-power ultrasonics means larger piezoelectrics; so, it involves lower ultrasonic frequencies (typically between 16kHz to 100 kHz) [18]. In order to be able to deliver high power with minimum losses, all the elements must be tuned to work near the resonance frequency of the ultrasonic transducer.

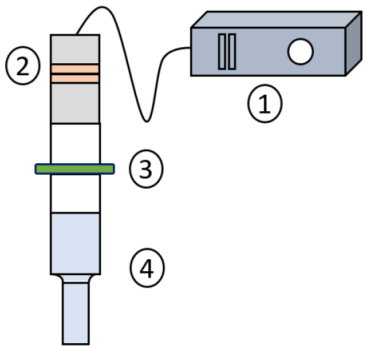

Figure 2.2: Sketch of the main elements of an acoustic unit: 1) ultrasonic generator, 2) ultrasonic transducer, 3) booster, 4) sonotrode

Ultrasonic generator

The ultrasonic generator is responsible for supplying the proper electrical signal to the transducer and for controlling the entire process. In order to transmit power to the transducer in the most efficient way, the output waveform of an ultrasonic generator is sinusoidal, and the frequency delivered is fixed at a very narrow range [29]. Typical powers delivered by generators range from a few hundred watts to 4 kW. Most commercial generators are equipped with phase-locked loop-frequency systems, which automatically match the generator frequency and phase with the ultrasonic transducer using a VCO (voltage-controlled oscillator) [30]. Some of the newest generators can also provide real-time power consumption, amplitude and frequency through analogue outputs.

Ultrasonic transducer

Two types of transducers (also known as converters) are most widely applied across industrial applications, that is, magnetostrictive and piezoelectric transducers [18]. Particularly, when using high-power ultrasound equipment in polymer applications, transducers are usually piezoelectric and built following a Langevin design. This type of converter, also called *sandwich transducer*, was invented by physicist Paul Langevin in 1920s for the development of SONAR. However, his scope of use has expanded since then, due to its high-power ratio and high energy conversion efficiency [31]. Langevin transducers are usually made of two or four lead zirconate titanate (PZT) ceramics sandwiched between two resonator metal blocks [32]. Usually, steel is used as a back-mass, and aluminium is used as a front-mass. The sandwich is clamped using a bolt, to force the system to resonate according to the entire structure. A sketch of a typical Langevin transducer is shown in Figure 2.3. Since the piezoelectric elements are located in the middle of the transducer, near the vibrating node, the long displacements are supported by the metal blocks, and it is possible to get high power without braking the ceramics [33].

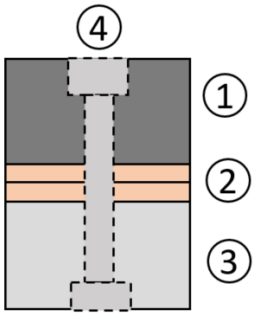

Figure 2.3: Sketch of the main elements of a Langevin transducer: 1) back mass, 2) ceramic piezoelectrics, 3) front mass, 4) bolt

Booster

A booster is a mechanical element designed to amplify or reduce the vibration of the transducer, and can also be used as a mounting point for the acoustic assembly. The gain of the booster is related with the mass of the booster at each side of the nodal point, and is usually displayed as a ratio between input amplitude and output amplitude. Typical gain values for commercial boosters range from 1 to 2.5 (see Figure 2.4). In some devices, such as handheld equipment, boosters may be not necessary.

Figure 2.4: Commercial ultrasonic boosters with gain ratios displayed (input amplitude:output amplitude). Adapted from [34]

Sonotrode

A sonotrode (also called *ultrasonic horn*) is an element that delivers the mechanical energy into the material. This element has to be carefully designed to match the resonance frequency of the ultrasonic transducer attached. Typical sonotrode geometries for ultrasonic welding are axisymmetrical with different profiles, depending on the amplitude desired and stress supported by the material. As it can be seen in Figure 2.5, stepped sonotrodes can achieve higher gains (difference between input and output amplitudes) but have higher stress.

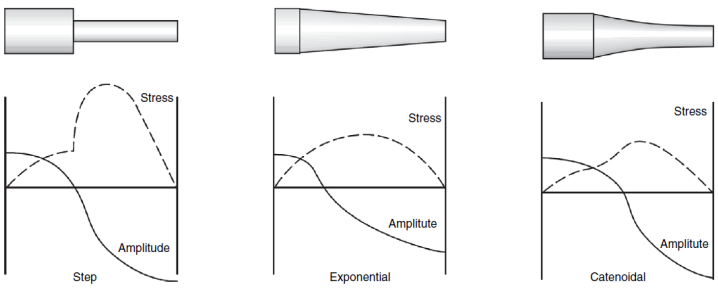

Figure 2.5: Sketch of three typical sonotrode horn profiles: stepped (left), exponential (middle) and catenoidal (right). Extracted from [35]

Apart from these common geometries, it is possible to find really complex sonotrodes fabricated for specific uses (see Figure 2.6).

On the other hand, not all materials are suitable for manufacturing sonotrodes, as they may have to bear ultra-high cycle fatigue. This means that a material with good acoustical properties and low internal damping is needed. Besides, complex geometries require material easy to machine. Thus, the established criteria for material selection constitute a balance among cost, affordability, machinability, good fatigue behaviour and good acoustic properties. Accordingly, some of the typical materials used for sonotrode fabrication are listed in Table 2.1.

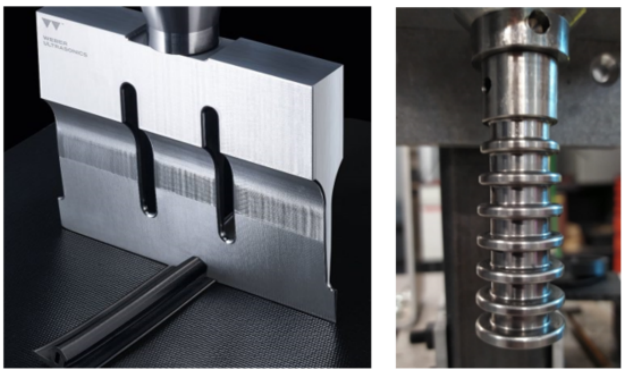

Figure 2.6: Examples of complex sonotrodes: On the left, a cutting sonotrode from [36]; on the right a multistep sonotrode for sonication designed and fabricated by the author in Eurecat

Material	Alloy	Benefits	Drawbacks
Titanium	Ti6Al4V Ti7Al4Mo	Good fatigue strength Good surface hardness	Expensive Difficult to machine
Aluminium	Al7075	Easy to machine Low cost	Poor surface hardness
Steel		Good wear resistance	Low fatigue strength
Niobium		Erosion resistance during cavitation	Very expensive
Syalon		Erosion resistance during cavitation Temperature resistance	Very expensive Very difficult to machine

Table 2.1: Typical materials for sonotrode fabrication

In the USM process, a titanium, stepped, profile sonotrode has been used up to now in all the published works [10, 11, 12, 13, 14, 15, 37].

Stepped sonotrode design: To estimate the design of a stepped sonotrode, one starts with the wave equation for plane waves in the axial direction z (direction of movement of the transducer):

$$\frac{\partial^2 u}{\partial t^2} = c_0^2 \frac{\partial^2 u}{\partial z^2} \tag{2.1}$$

where u is the wave displacement, and c_0 is the speed of sound.

Considering that the acoustic wave propagates as a plane wave through all the sonotrode without boundary reflections (Poisson coefficient is neglected), the Webster equation is obtained:

$$\frac{1}{c_0^2}\frac{\partial^2 u}{\partial t^2} - \frac{1}{S}\frac{\partial S}{\partial z}\frac{\partial u}{\partial z} - \frac{\partial^2 u}{\partial z^2} = 0 \tag{2.2}$$

where $S(z)$ is the section of the sonotrode in z. If we use variable separation, $u(z) = U(z)T(t)$, the spatial part of the equation can be written as:

$$\frac{\partial^2 u}{\partial z^2} + \frac{1}{S}\frac{\partial S}{\partial z}\frac{\partial u}{\partial z} + \frac{w^2}{c_0^2}u = 0 \tag{2.3}$$

where w is the angular frequency. Considering a double-cylinder stepped sonotrode with the step at the midplain along the length, as described in Figure 2.7, the wave displacement along the sonotrode can be obtained from Equation 2.3 as [19]:

$$\text{For } x \leq \lambda/4 \qquad u_x = u_1 cos\left(\frac{wx}{c}\right) cos(wt) \tag{2.4}$$

$$\text{For } \lambda/4 \leq x \leq \lambda/2 \qquad u_x = u_2 cos\left(\frac{w(l-x)}{c}\right) cos(wt) \tag{2.5}$$

where u_1 and u_2 are the input and output amplitudes of the sonotrode, which, in this ideal case, are related by the following identity:

$$\frac{u_2}{u_1} = \frac{S_2}{S_1} = \frac{r_2^2}{r_1^2} \tag{2.6}$$

where S_1 and S_2 are the input and output sections of the sonotrode, while r_1 and r_2 are the radii of the input and output cylinders that form the stepped sonotrode.

The former equation gives the *gain of the sonotrode* and, although it is only valid for this ideal case, it can be used to estimate the approximate gain of any stepped sonotrode.

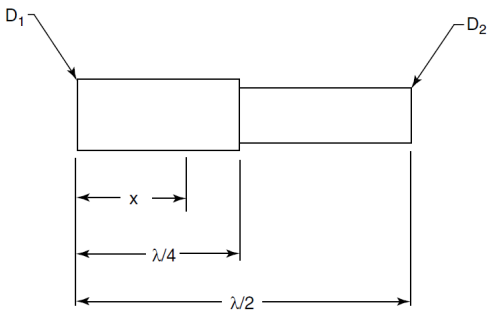

Figure 2.7: Double cylinder stepped sonotrode. Reproduced from [19]

In practice, real, stepped sonotrodes have a radius between both cylinders and, although they are half-wave sonotrodes, they no longer measure $\lambda_0/2$ (where $\lambda_0 = c_0/f$). Thus, to design a sonotrode to resonate at a certain frequency, the total length must be carefully calculated. As a first guess, there are several analytical equations that can be used to estimate the geometry based on empirical data [38], or on network methods [39]. However, currently most sonotrodes are designed using finite element methods, through a simple modal analysis study [40, 37]. Finite element methods can also be used to ensure that the gain of the sonotrode and the stress supported by the material are correct.

Once the sonotrode is designed and machined, a tuning step must be performed, in order to adjust the entire acoustic system to the desired frequency. This step is executed, partly to account for possible differences between the real material properties and the given ones, and partly to account for the influence of the different parts of the acoustic unit that have not been simulated (i.e booster, transducer). For this step, an impedance measuring equipment must be used to match the resonance frequency of the acoustic unit with the one delivered by the ultrasonic generator. Although professional impedance analysers can be prohibitive in terms of their cost, currently there exist some cheap impedance analysers, specifically designed for ultrasonic equipment (see Figure 2.8). The analysis of the impedance curve provides important information about the overall performance of the acoustic unit, such as the resonance frequencies and the quality factor. For further information about the design of customised high-power sonotrodes, one can consult references [32] and [41].

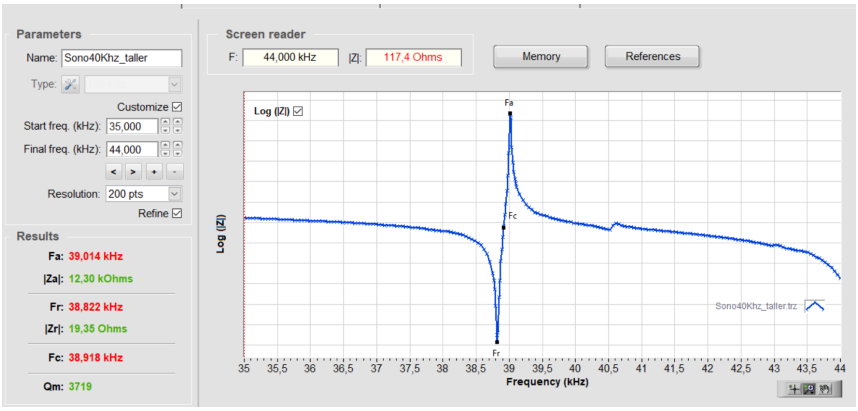

Figure 2.8: Impedance analyser results for a 40 kHz acoustic equipment, measured using a TRZ® analyser from ATCP [42]

2.3 Micro-injection moulding

Injection moulding is a manufacturing process aimed to produce identical parts by injecting molten material into a mould. Nowadays, injection moulding is the most widely used polymer processing operation [43]. Some of the main advantages of this process include its high production rates and its capacity for fabricating complex geometries.

The evolution of the injection moulding machine started with the packing machine invented by the Hyatt brothers in 1972, which used a plunger to inject the plastic into a mould. Since then, several developments have been made to achieve the actual conventional injection machine, which is sketched in Figure 2.9. The injection moulding process starts when material is fed using gravity, through a hopper, into the screw system. Next, the rotating screw plasticises the polymer inside the heated barrel, until it is completely melted within the injection chamber. When the sufficient polymer has been melt, the screw pushes the material into the mould cavity. Once the polymer is solidified, the mould opens and the part is ejected. A more detailed description of some of the main stages of this process will be presented later in this section.

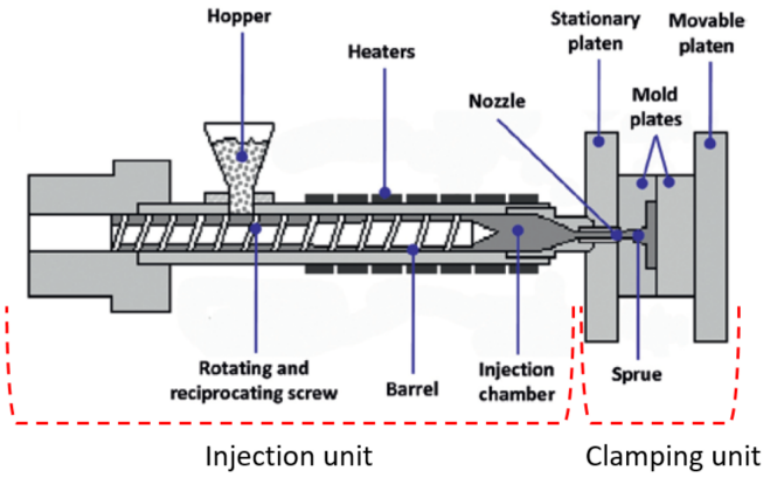

Figure 2.9: Sketch of a conventional injection moulding machine. Adapted from [44]

μIM involves the fabrication of micro-moulded parts with high dimensional accuracy. When an injected sample has the mass of the part of few milligrams, exhibits dimensions with tolerances in the micro-metric range, or has some features in the order of micrometers, the process can be defined as a micro-injection moulding process [45]. μIM is a key technology used in the micro-manufacturing process, due to its low cost and the capacity

for mass production. Replicability, repeatability and high precision are the main features of this process [46]. Moreover, the wide range of thermal, optical and mechanical properties of thermoplastic materials makes μIM a suitable process for a large variety of applications. Lenses, waveguides, micro-mechanical components, sensors, micro-electromechanical systems (MEMS) and micro-fluidic devices are some examples of products made using μIM. According to the *"Institute of design and production in precision engineering (IKKF)"* micro-injection comprises of [47]:

- Components with very low weight (milligrams), small dimensions (millimetres) and micro-metric details
- Parts with standard dimensions, with features having micro-structural details
- Parts of any size, with tolerances in the order of a micro-metre.

2.3.1 Main steps in μIM

The main steps in a typical μIM process, from the point of view of the polymer processing, include: plasticising, filling, packing and cooling.

Plasticising

Plasticising is the process of melting the material to be able to inject it. This process is done by the *plasticising unit* or *injection unit* of the moulding machine (see Figure 2.9). Injection machines used for the micro-injection process may use two types of plasticising systems:

- A one-stage extruder with a scaled plasticiser, having a small-diameter conventional screw
- A two-stages extruder and injection plunger, wherein the extruder inserts the dosage into a chamber, and then, the piston pushes the material into the injection process.

In the case of the two-stages extruder, there is an additional metering step between the plasticising and the filling stages, to ensure the accurate injection volume of material (see Figure 2.10). Fantoni et al. [48] have carried out a step-by-step functional analysis of the μIM process, concluding that the two-stages extruder with smaller screws and injection plungers allow for faster and more accurate injection of small shot volumes.

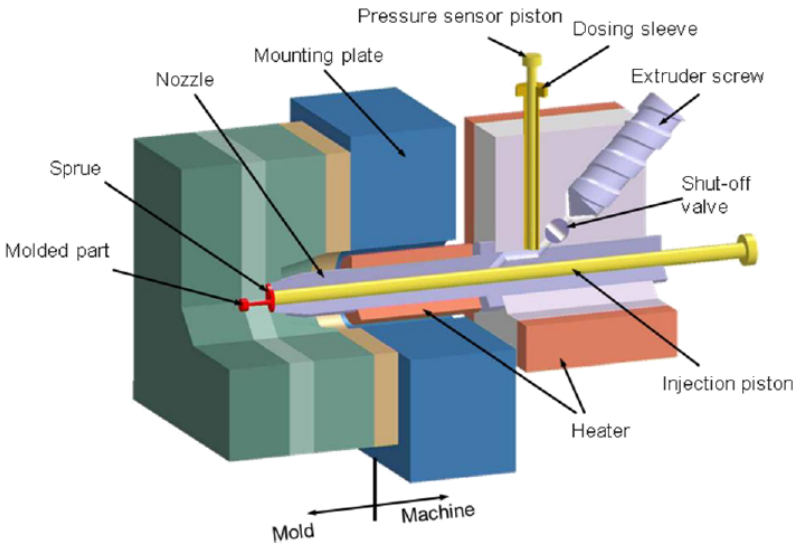

Figure 2.10: Sketch of a μIM machine. Adapted from [44]

Filling

One of the biggest problems with the μIM process is the *high-aspect ratio* of the parts (ratio between thickness and lateral dimensions). In these kinds of geometries, the polymer melt solidifies rapidly and creates solid layers that ultimately become filling defects. To be able to inject these geometries, micro parts must be usually processed at higher mould temperatures than the ones recommended by the datasheet [47]. Although the influence of injection moulding parameters may be different for each material, usually, high injection speed and high temperatures are needed, in order to achieve a completely-filled cavity (see Figure 2.11). High injection rates cause frictional heating that can degrade the material [49], and requires the use of machines able to deliver high pressures to the polymer.

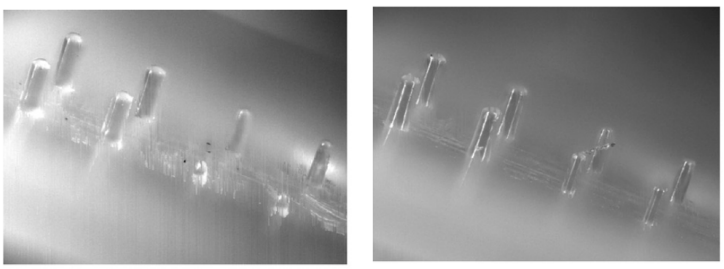

Figure 2.11: Comparison of the filling of micro-needle cavities at different processing parameters. Left: low speed ($100mm/s$) and low mould temperature (60 °C). Right: high speed ($200mm/s$) and high mould temperature (120 °C). Adapted from [46]

On the other hand, a physical phenomenon typical of the micro world, is the *hesitation effect* (see Figure 2.12). This effect occurs when the injection moulded part has *high-aspect ratio* microstructures in thick substrates. In that case, the melt freezes within the microstructures before the substrate is completely filled.

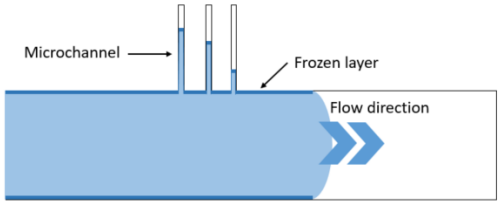

Figure 2.12: Hesitation effect in μIM. Adapted from [50]

Packing

Once the sample is almost completely filled, a packing or holding stage is needed, in order to maintain the sample properties until the material freezes. At this stage, pressure is applied, and a little volume of material is added, in order to compensate the loss of volume of the part due its shrinkage [51]. However, due to the rapid solidification of the material, switchover between filling and packing must be extremely precise.
In micro-injection machines, this transition mode from the injection pressure to the holding pressure is generally based on the injection plunger position (and not on the injection pressure as in the conventional injection), and can have a significant influence on the final weight of the parts [52].

Cooling

Liang et al. [53] defined a model for the calculation of the cooling time in conventional injection moulding, wherein this magnitude is directly related to the square of the thickness of the part being manufactured. Thus, cooling time in μIM is usually a fast step due to the low thickness of the moulded parts. However, as moulds usually need to be heated above the desired temperature for facilitating the complete filling of parts, an extra cooling is needed before the demoulding of the samples. Thus, the cooling time is greater than the time estimated for conventional injection moulding. An option used to reduce this time is the *variotherm process*, wherein mould cavity is heated using induction and cooled with water. This process improves the replication of the high aspect ratio, and allows a better controlled cooling of the material, thereby lowering the residual stress [51].

2.3.2 Challenges in micro-injection technology

Although μIM is considered to be one of the technologies *"with the greatest future potential development for the manufacture of plastic components"* [47], there are still some challenges related to this technology that need to be addressed:

- **Limited geometries:** There exist difficulties in replicating geometries with very *high-aspect ratios* [54].
- **High temperatures:** The long residence time of the material in the screw and the high temperatures needed in the mould (near the melting point of the polymer) can degrade it [55].
- **High shear:** High pressures and velocities must be applied to cause the material to flow through small-sized gates; this can result in higher shear rates and high friction heating, which can lead to polymer degradation [49] and to anisotropy in the properties of the moulded parts [56].
- **Material wasting:** Due to the large difference in weight between the piece and the sprue, approximately 90% of the raw material is lost. In some applications, even the weight of a pellet is bigger than the weight of the figure [1].

With the aim of solving all or part of these challenges, high-power ultrasound energy was introduced to enhance the performance of the injection moulding process. As previously described in Chapter 1, the application of ultrasound to μIM followed two variants, i.e., ultrasonic moulding (USM) and ultrasonic assisted injection moulding (UAIM). The main differences between both these approaches is that, while UAIM still uses a conventional screw to plasticise and melt the polymer, USM replaces it with an acoustic unit that heats the polymer using mechanical ultrasonic energy. In this chapter, only USM technology has been presented and reviewed. However, an exhaustive review of UAIM technology can be found in the work done by Zhao et al. [2].

2.4 USM process

As previously stated, the USM technique was created with the aim of overcoming some of the drawbacks and limitations of micro-injection moulding technology. In this case, the main advantages of USM technology over the conventional process are:

- **Shorter time of residence at high temperatures:** Due to the rapidity of the process, the polymer is subjected to high temperatures within a very short period of time [57], which allows its injection without degradation of the polymer.

- **Lower temperature needed to inject the material:** The material can flow at a lower temperature as the application of ultrasonic waves to a polymer reduces its viscosity due to physical and chemical factors [58, 59].
- **Lower pressure of injection:** The better fluidity of the material makes USM technology capable of injecting materials at pressures much lower than in conventional micro-injection. Masato et al. injected a polypropylene specimen using USM at a pressure three times lower than in conventional injection moulding [60]. This should allow the USM technology to process materials with geometries beyond the scope of conventional injection methods.
- **Energy savings:** As each pellet in the polymer is heated locally, the energy needed to increase the temperature of the material is expected to be much lesser than that used in conventional machines. Although some studies confirm this hypothesis [12], more work is still needed in this field to obtain a quantitative measure [1].
- **Material savings:** The only material melted is the one injected. That means that there is no remaining material in the plasticising chamber, and it is even possible to change the material without wasting material. In comparison with conventional injection moulding, the USM can save 40% to 70% of the material [2].

The principle on which the USM is based is the transmission of the oscillatory energy from a sonotrode to a thermoplastic polymer with which it is in contact. The mechanical energy is then transformed into thermal energy, which heats and melts the polymeric pellets. In the second stage, the melt is introduced into a mould wherein it solidifies. These steps, along with the main elements involved in the process will be described in this section.

2.4.1 Nomenclature

The technology, in which this study contributes to, uses ultrasonic energy instead of a screw, to plasticise and inject material in a mould. This technology is called *"ultrasonic moulding"*, but is also known as *"ultrasonic plasticisation"*, *"ultrasonic plasticising for injection moulding"* [57, 61, 62, 63], or *"ultrasonic microinjection moulding"* [64, 65]. Besides, there are other technologies that share some elements with the one studied here, and, in some articles, also its name. Ultrasonic assisted injection moulding (UAIM) is one of them. As previously explained, this technology does not replace the screw used in conventional injection machines, but uses ultrasounds to enhance the performance of these machines. On the other hand, there is a technology known as ultrasonic compression moulding (UCM), wherein the material is

compacted and plasticised by a sonotrode directly within the mould cavity [66]. This technology is more related to a hot embossing method than to an injection process (an extensive review of UCM is done by Heredia et al [66]). Both of these later technologies also are found under the name of *"ultrasonic moulding"* in the literature (see Table 2.2).

	Ultrasonic Moulding	Ultrasonic Assisted Injection Moulding	Ultrasonic Compression Moulding
Acronym	USM	UAIM	UCM
Cited as	Ultrasonic Moulding (USM) [10, 11, 12, 13, 14, 15]; Ultrasonic Plasticising for Injection Moulding (UPIM) [57, 61, 62, 63, 2], Ultrasonic Micro Injection Moulding (UMIM) [64, 65, 67]	Ultrasonic Assisted Injection Moulding (UAIM) [21, 22]; Ultrasonic Injection Moulding (UIM) [6, 68]; Ultrasonic Assisted Micro-Injection Moulding (UAMIM) [2]	Ultrasonic Compresion Moulding (UCM) [66]; Ultrasonic Moulding (UM) [69, 70]; Micro Ultrasonic Powder Moulding (MUPM) [71]

Table 2.2: Nomenclature for ultrasonic moulding and similar technologies

2.4.2 Main elements of the process

USM technology combines: an acoustic unit similar to the ones used in other high-power ultrasound applications, a moulding unit adapted from the injection moulding technology, and a feeding unit usually designed and fabricated exclusively for this technology (see Figure 2.13).

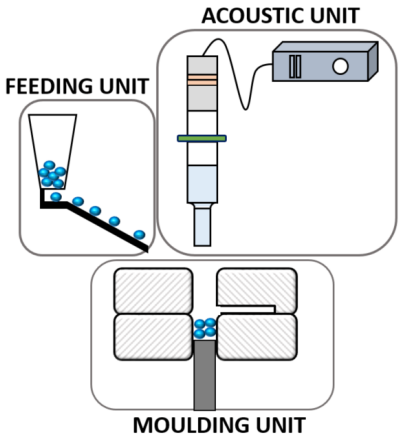

Figure 2.13: Main units of the USM equipment: an acoustic unit, a feeding unit and a moulding unit

As the acoustic unit has been described in detail in section 2.2, the other two elements are explained in this section.

Feeding unit

The feeding unit is designed to automate the dosage of material in USM technology. As the metering of injection material in USM is done at the feeding stage, the same amount of material needs to be dosed each time. In Sonorus®1G machines this is done using the device patented in 2015 by Puliga et al.[72], which was specifically designed to count and dose polymer pellets into the mould. The feeder is composed of a dosing apparatus that includes a hopper, which pours pellets into a vibrating chute (see Figure 2.14). The vibration aligns and moves the pellets until they drop into the mould. A laser is used to count the pellets at the end of the vibrating chute. The dosing can also be done manually, by counting the pellets, or by using a balance, which is more accurate due to the weight dispersion of some polymer pellets.

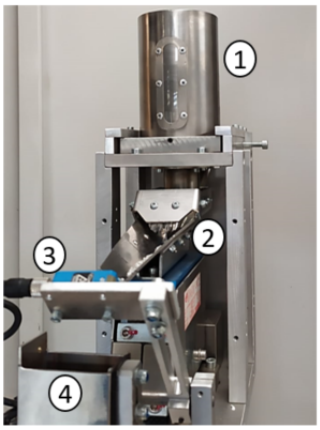

Figure 2.14: Image of a feeder for USM process used in Sonorus ®, with a hopper (1), a vibrating chute (2), a laser to count the pellets (3) and a case connected to the mould (4)

An improved device was later designed by the research group, wherein the author works, for its use in Sonorus® 2G and has been patented recently [73].

Moulding unit

Moulds used in USM are adapted from conventional micro-injection technology. In USM, the moulds are placed horizontally and divided into two parts: a moving part (superior) and a fixed part (inferior). Electrical heaters are usually included, along with an ejection unit to demould parts. In addition, ultrasonic moulds also include a plasticising chamber where the material is deposited, and holes to introduce the sonotrode and the plunger (a piston used to push the material into the mould). The main components of a typical USM mould are presented in Figure 2.15.

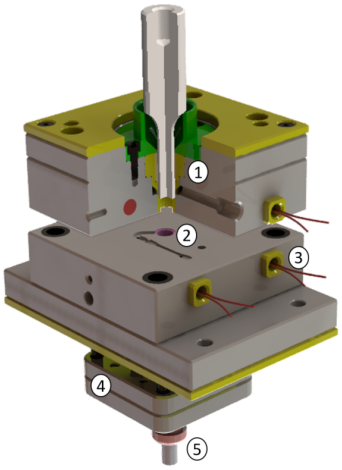

Figure 2.15: Render image of an USM mould; main elements are: hole and sleeves for the sonotrode (1), plasticisation chamber and mould cavity (2), heaters (3), ejection unit (4), plunger and sleeves (5)

2.4.3 Main steps of the process

The main steps of the USM process are similar to the ones used in micro-injection technology (see Figure 1.2). However, as previously discussed in Chapter 1, some of these steps are coupled and can take place almost simultaneously. In this section, the different steps of the process will be analysed considering that the sonotrode remains fixed during the heating and filling steps, and the plunger is the element that pushes the material. This is known historically as *Configuration 2* option. However, the steps and the explanation given here would be the same even for the case wherein the plunger is fixed and the sonotrode pushes the material (*Configuration 1*). Both configurations are explained in detail in section 2.5.

Material feeding

The first step required for the USM process is to count and place the material in the plasticisation chamber. The dosage of the material can be set manually or by using an automated feeder system like the one described in Figure 2.14. The variability of the volume of dosing associated with the dispersion of the volume of the pellets is thought to be one of the main problems affecting the stability of the process [15]. Although this particular machine is optimised to work with pellets, some studies have also been carried out using powder [12, 13, 74] and irregular-shaped polymers [64].

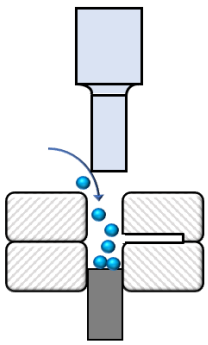

Figure 2.16: USM feeding step

Polymer heating

Once the polymer is placed in the plasticising chamber, the upward advance of the plunger (in the *Configuration 2* of the forming system) compresses the pellets against themselves, against the walls of the chamber and against the sonotrode that is already vibrating.

In the first stage, the particles get rearranged and the friction developed in the areas of contact among the particles and with the tools is the basic mechanism responsible for the heating of the material. When the applied stress reaches a certain value, the particles begin to deform and their contact areas increase progressively. Once the particles are compacted and a complete contact is established between the sonotrode and the polymer, the high frequency vibration intensely increases the temperature of the material closest to the sonotrode until it melts. Conversely, the material that is in contact with the plunger, continues to be in a solid state since its heating rate is much lower than the one developed in the region directly in contact with the sonotrode.

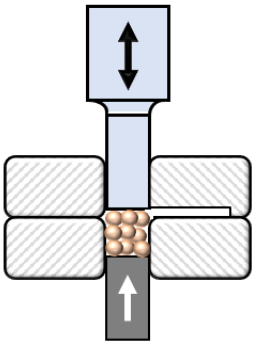

Figure 2.17: USM heating step

Most of the studies published in extant literature have applied ultrasonic energy in a continuous manner during the heating step. However, Sánchez-Sánchez et al. [64] considered the mode of activation of the wave as a new parameter. They evaluated the possibility of using an intermittent methodology in the application of the ultrasound energy during the heating stage. In continuous ultrasound mode, the ultrasonic wave is continuously applied throughout the process, while in intermittent mode, ultrasound is activated only during a specific phase of the plunger path. The objective of this strategy is to have a larger surface area prior to the application of ultrasonic irradiation, thus improving interfacial friction heating

Cavity filling

The filling stage takes place simultaneously along with the heating. Once the first polymer layer has melted, the upward movement of the plunger against the material makes it flow towards the cavity in the mould, while the rest of the polymer is still heating under the action of ultrasonic vibration. The latest USM machines allow the mould filling to be carried out by keeping the force exerted by the plunger constant (similar to an ultrasonic welding press), or by maintaining constant a speed of advancement (as in conventional injection moulding machines).

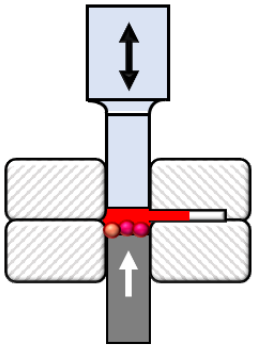

Figure 2.18: USM filling step

A comparison with the results obtained by injecting with either a constant force or constant velocity, in the study carried out by Montes [75], does not show significant differences between the methodologies. However, velocity driven injection is more stable and allows the use of a force value as a *"switchover point"*, as described below.

Packing

As in conventional injection moulding, the USM process also includes packing as the final step in cavity filling. In this step, a holding force is applied to the polymer to compensate the shrinkage and to ensure the correct geometrical properties of the sample. The transition between the filling and the packing steps is known as the *"switchover point"* and is one of the most critical aspects in conventional injection moulding. Various factors can be used as a switchover point in conventional injection moulding, although the ones most used are the screw position and the hydraulic pressure [76].

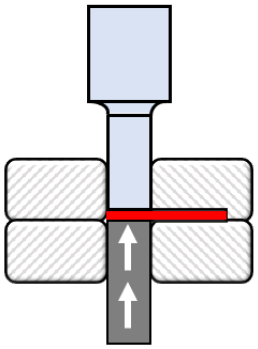

Figure 2.19: USM packing step

As explained in section 2.3, in case of μIM, the position of the piston is usually used as a switchover point. However, in the USM process, the position of the plunger cannot be used as a switchover point, because there can be

a significant variation in material from shot-to-shot, depending upon the dispersion of volume between pellets. Thus, the factor used as a switchover point across all the works analysed is the ultrasonic time [14, 15, 64]. However, the newest versions of Sonorus® 1G machine allow the value of the force induced by the plunger to be used as a switchover point. In this case, when the plunger reaches the force chosen, the filling step is switched to the packing step.

In the USM process, when the polymer has filled almost all of the mould cavity, the plunger needs to increase the force to continue pushing the material into this cavity. Then, when a certain value of force is reached, the cavity can be considered to be filled, and the process can be switched to the packing step. Figure 2.16 compares the evolution of the force developed by the plunger and its vertical position with the process time, obtained from the injection of two equal polypropylene samples moulded with the same parameters. Sample 1 reaches the trigger force at 7.8 seconds and -4 mm of plunger, while sample 2 reaches the trigger force at 8.8 seconds and -2 mm of plunger. This difference is caused because there were four more pellets of material in sample 1. Even so, with the force switchover, both samples are completely filled without degradation. Recently, some research has been performed using the force as a switchover point with promising results [77].

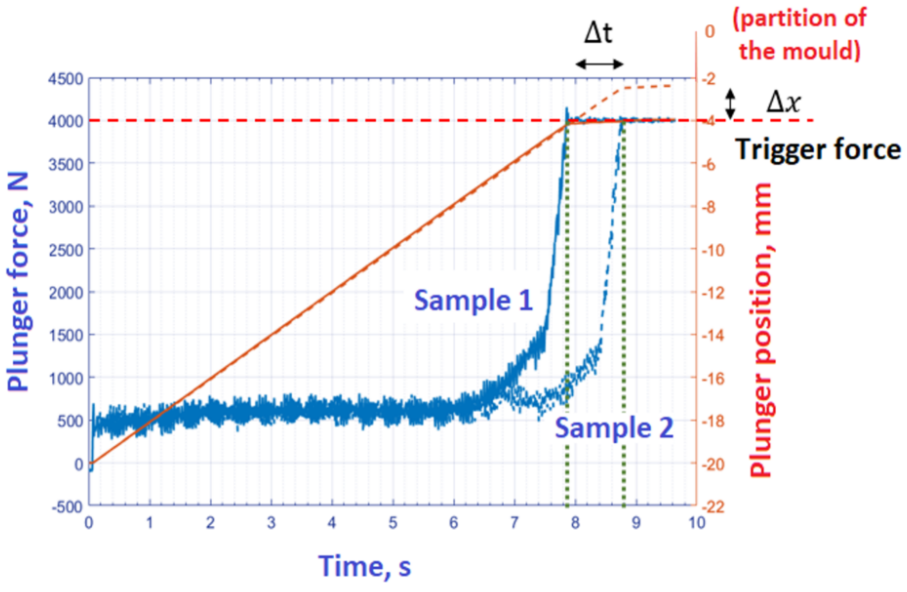

Figure 2.16: Real example of the machine graphs obtained for two polypropylene samples moulded using the same parameters

Cooling

As explained in section 2.3, during the cooling stage, the polymer injected is cooled down inside the mould, from the melting state to the de-moulding temperature. Although the cooling stage is the most time-consuming one among all the injection processes, while manufacturing micro-samples, there is no need for such long time periods due to the small volume of material to be cooled. In any case, the time needed to demould depends on several parameters: the thickness of the sample, the thermal properties of the polymer, the material of the mould and on the thermal contact conductance (the quality of the contact between the sample and the mould).

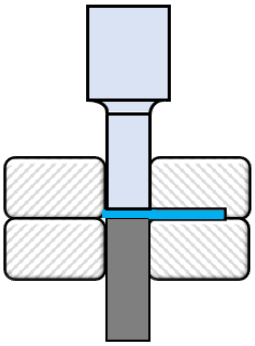

Figure 2.17: USM cooling step

As an order of magnitude example, the expected cooling time for samples with a thickness of less than 1 mm, is around a few seconds. However, as explained before, mould temperatures in μIM technology are usually higher than the ones provided by the manufacturer datasheet, which increases the cooling time.

In principle, since ultrasonic energy decreases the viscosity of the material and the mould temperature needed to process it, one would expect cooling time for USM to be lesser than that required for conventional micro-moulding. However, to date, no study has been carried out to prove this.

2.5 USM configurations

Although USM is a novel technology, it has been studied using different moulding machines and configurations. In this section a review of the main ultrasonic configurations found in the literature is presented, and the specifications of the configurations used in this work are detailed.

2.5.1 Ultrasonic machine evolution

In 2002, Michaeli et al.[1] analysed different plasticising concepts using high-power ultrasound equipment to overcome the difficulties of processing samples weighing less than 1 mg in conventional injection moulding (where 90% of the raw material was wasted in the sprue). The results obtained with polyoxymethylene (POM) were promising (regarding the homogeneity and the melted polymer morphology), and they considered the production of micro-samples through ultrasonic moulding. After an initial validation of the ultrasonic pellet melting with a laboratory apparatus [1], a prototype was presented [61] in which the sonotrode was used not only to melt but also to inject the material into a cavity. This technology was called *Ultrasonic direct injection*. In Figure 2.17, a sketch of this technology that uses plastic sheets as raw material is shown.

Nevertheless, the poor moulding quality due to the low injection pressure and the missing holding pressure forced the direct injection concept to be completely modified [57], as sketched in Figure 2.18. In this new design, polymer pellets were used as raw material, and the melted material was pushed to the mould cavity through common runners and sprues.

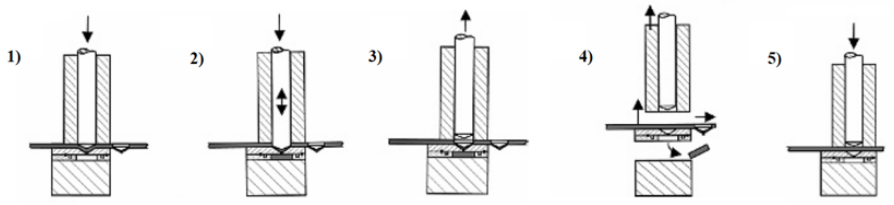

Figure 2.17: Ultrasonic direct injection process steps. The sonotrode pushes downwards and starts to plasticise the sheet (step 1). During the plasticising the sonotrode injects the melt into the cavity located below the plasticising chamber (step 2). After the plasticising the sonotrode is moved upward (step 3) and the part can be demoulded (step 4). Meanwhile the plastic film is moved in position to provide new material for the next cycle (step 5). Adapted from [61]

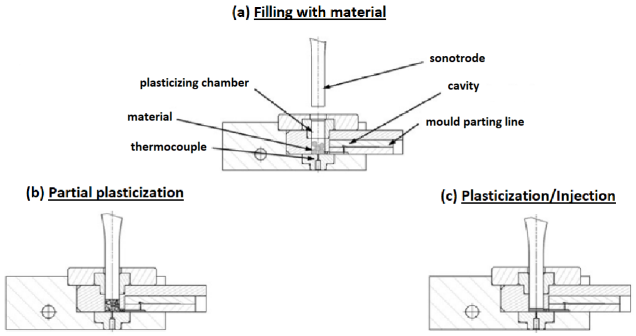

Figure 2.18: Direct injection modified configuration and steps of the process [1]

In 2009, Bas et al. patented an ultrasonic machine prototype [78] that used a similar configuration, adding the necessary elements to automate the process of fabrication. Figure 2.19 represents the initial scheme of this equipment, and its first experimental device, constructed by the same group.

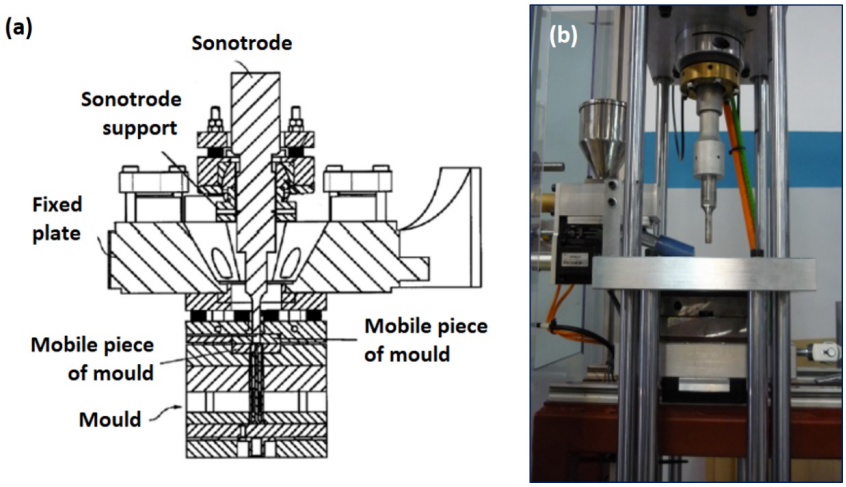

Figure 2.19: On the left, adapted sketch of the ultrasonic machine prototype corresponding to the patent [78]. On the right, a photograph of its experimental version [79]

Several research groups involved in this field have been using this type of prototype to perform their works [10, 11, 80, 81]. In fact, this equipment can be prepared from a welding machine to which the moulding system have been added. An example of a similar in-house developed USM setup, is that of Jiang et al. [63, 82, 83], shown in Figure 2.20.

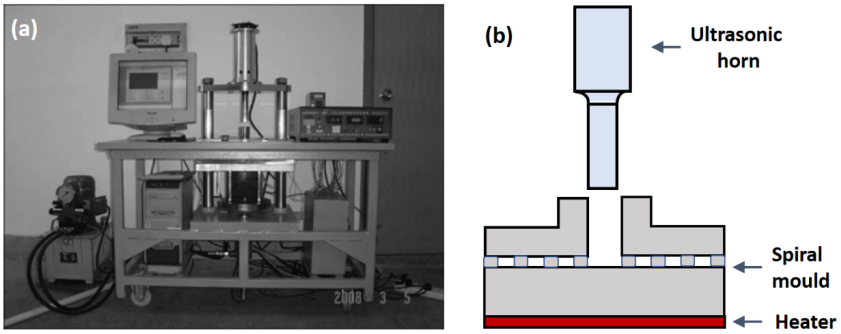

Figure 2.20: (a) Experimental ultrasonic plasticisation device developed by Jiang et al.[83]. (b) Configuration of Jiang's setup with a spiral mould, adapted from [82]

In 2014, Puliga et al. [84] patented an improved version of the USM machine with the objective of putting into the market the first and, to the knowledge of the author of this dissertation, up to know the unique USM commercial machine (*Sonorus*®, fabricated by *Ultrasion, S.L.*). Figure 2.21 corresponds to a photograph and a scheme showing its main elements and initial configuration.

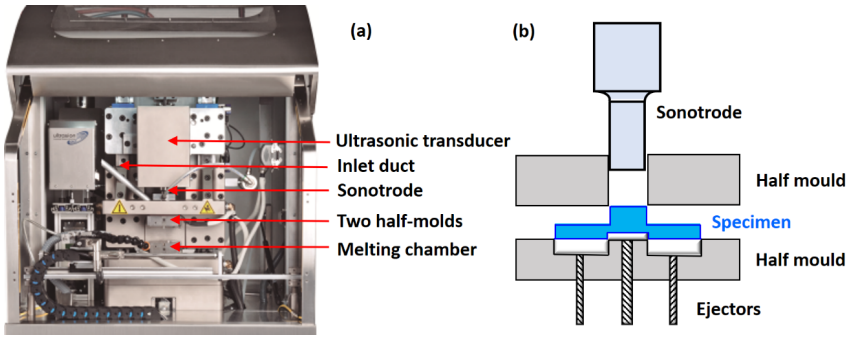

Figure 2.21: (a) Commercial version of the Sonorus® 1G machine [85]. Red arrows indicate the location of the elements (b) Diagram of the main parts of this equipment, adapted from Planellas et al. [12]

Several works reported in this chapter have been performed with this machine [12, 13, 74, 86, 87, 88].

All the devices represented in Figures 2.18 to 2.21, correspond to a configuration for ultrasonic injection moulding, *Configuration 1*, schematized in Figure 2.22, in which the ultrasonic horn is performed by moving the sonotrode down while the material is melted. The plunger, when it exists, acts as a fixed base of the mould during the stages of heating and melting of the material, and as an ejector of the finished piece.

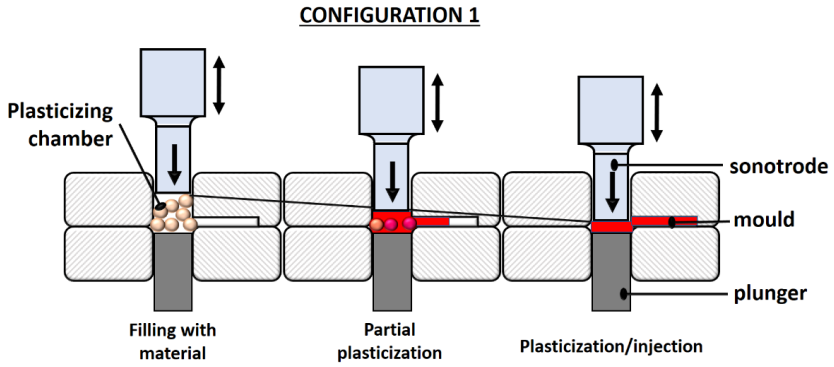

Figure 2.22: USM *Configuration 1*. This element configuration was adopted in the first USM machines

This type of equipment has been improved incorporating the *Configuration 2*, schematised in Figure 2.22, and characterised by a change in the kinematics of the sonotrode and the plunger. Now, the sonotrode has a static position; the plunger is in this case the element which injects the material into the mould cavity.

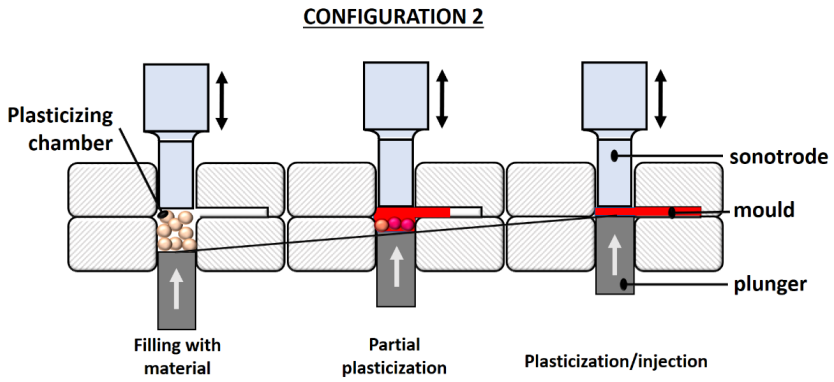

Figure 2.23: USM *Configuration 2*. This element configuration has been adopted in the newest USM machines

This later configuration was developed with the objective of solving, above all, two problems of the manufacturing process. On the one hand, the formation of an intense flash in the gap between the sonotrode and the mould. On the other hand, in *Configuration 1*, the molten polymer drags solid material into the mould, especially when processing of powder or very small pellets. As a result, parts with internal and/or external inclusions can be obtained. Some of the works carried out by means of machines with *Configuration 2*, are those of the references [14, 60, 65, 89, 90, 91].

2.5.2 Ultrasonic machine versions used in this work

In this dissertation two different versions have been used. A commercial Sonorus®1G has been used for all the heating experiments reported in Chapter 4, while a new prototype of machine (Sonorus® 2G) has been used for all the experiments reported in Chapter 3. In the former case, Sonorus®1G machine was better fitted for the experiments, as the relationship between the real plunger force and force obtained by the motors is known. Also this machine has a more tested software. In the later case, the new methodology developed needs for a machine with more clamping force and more available plunger travel. In that case, the new prototype is better fitted for these experiments.
Main differences of both machines from the mechanical point of view are listed below (see Figure 2.24):

- **Machine plates moving mechanism:** Commercial machine Sonorus®1G is constructed using a goose-neck system to move the machine plates (and the mould between them). This system allows a bigger space to manipulate the samples and better accessibility to the mould. However, the system is not well fitted to withstand high forces, as it bends. On the contrary, Sonorus®2G prototype uses a four-column system, which is able to withstand high forces without loosing the perpendicularity. This new prototype is more adequate for technical materials requiring high forces even though the access to the mould and figure is more complicate.

- **Clamping unit:** Sonorus® 1G closes the mould using the goose-neck and the force is supported by a spindle and its motor. This system allows to have a smaller machine but, again, does not withstand high forces (3 kN maximum). To solve this issue, the new Sonorus® 2G configuration uses a toggle-type clamping unit (15 kN maximum).

- **Plunger travel:** As the Sonorus 2G prototype is taller, plunger travel has been increased from 100 to 180 millimetres. This allows to have a bigger plasticisation chamber and increases the maximum shot weight up to 2.5 grams (see Table 2.3).

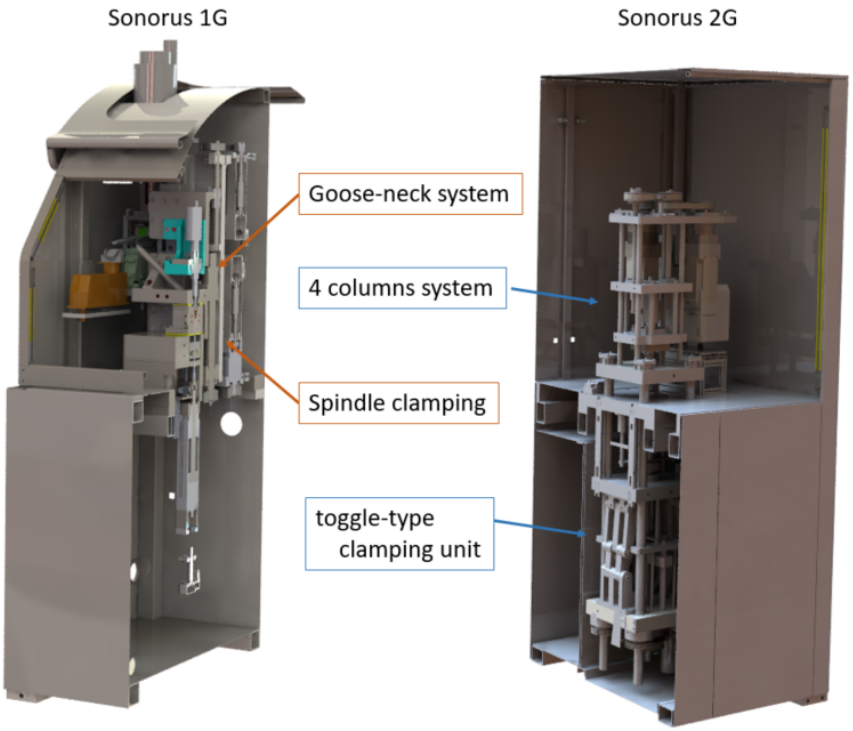

Figure 2.24: Mechanical comparison between Sonorus® 1G and Sonorus® 2G

	Sonorus® 1G	Sonorus® 2G
Ultrasonic frequencies	20 kHz and 30 kHz	20 kHz and 30 kHz
Maximum mould height	100 mm	180 mm
Maximum dosing	1.5 grams	2.5 grams
Maximum injection force	1.5 kN	12 kN
Maximum clamping force	3 kN	15 kN

Table 2.3: Sonorus® machine versions main specifications

2.6 State of the art of USM modelling

Due to the novelty of the process and its complexity, only few papers are focused on the theoretical analysis of the USM process [11, 62, 63]. Even so, there is a large amount of literature related to the simulation and modelling of the ultrasonic welding process that can be used as a starting point to identify the mechanisms and factors involved in the USM heating step [3, 92, 93, 25, 94], and micro-injection moulding modelling approaches can be used to study the USM filling step [51, 95, 44]. The packing and cooling steps are analogous to their conventional counterparts and will not be analysed in this section.

2.6.1 Heating step

The USM process differs from conventional injection moulding mainly in the way that the polymer is heated until it melts. In USM, the energy needed to heat a polymer must be provided by the different thermomechanical contributions of all the elements that constitute the USM: the viscoelastic behaviour of the polymer for processing [57]; the friction between polymer pellets with the tools; the kinematics of the plunger and the sonotrode, which can generate high strains in the material; and, according to some authors [83, 96], the ultrasonic cavitation. Instead, there is a thermal dissipation between the polymer and the surrounding tools; however, due to the rapidity of ultrasonic heating [61], thermal dissipation can be neglected in the heating step.

When trying to solve the coupled model, the different time scales of the process makes solving the thermomechanical coupled problem very difficult and computationally costly [97], and some authors approach it as a thermal problem using the following conservation of energy equation [63, 94]:

$$\rho c_p \dot{T} - \nabla \cdot (\kappa \nabla T) = \dot{W} \tag{2.7}$$

Where ρ is the material density, C_p is the specific heat, T is the temperature, κ is the material thermal conductivity, and $\dot{W}$ is the generated energy, which includes all the heating mechanisms considered before.

Viscoelastic heating

It is well known that applying a cyclic deformation to a viscoelastic material can increase its temperature and even bring it to the melting point. This behaviour is a consequence of the internal structure of this type of material: the friction between the molecular chains that constitute the polymer is the cause of the dissipation of a part of the mechanical deformation. A fraction of this dissipated energy is transformed into heat, causing an increase in

the local temperature of the polymer [98], which is both strain- and strain-rate dependent [99, 100] (an example of this behaviour will be presented in section 4.3).

Benatar et al. modelled the viscoelastic heating of polymers when a sinusoidal deformation is applied [3]. In these type of materials, the ratio of stress to strain in vibratory conditions is called the complex modulus E^*, which can be divided into: a storage modulus E' that represents the ability of the material to store energy; and a loss modulus E'', which represents the ability of the material to dissipate energy.

$$E^*(w) = E'(w) + iE''(w) \tag{2.8}$$

where w is the angular frequency of excitation. The storage and loss terms can be better understood if the mechanical work in each cycle is considered. Here, we consider that the sonotrode is imposing a sinusoidal strain on the polymer:

$$\epsilon = \epsilon_0 sin(wt) \tag{2.9}$$

where ϵ_0 is the strain amplitude. The stress generated is also sinusoidal, with the same angular frequency but with a phase change of δ:

$$\sigma = \sigma_0 \sin(wt + \delta) \tag{2.10}$$

Here σ_0 is the stress amplitude. The previous equation can be written as:

$$\sigma = \sigma_0' sin(wt)\cos(\delta) + \sigma_0' \cos(wt)\sin(\delta) \tag{2.11}$$

On the other hand, the storage and loss moduli can be defined as [101]:

$$\begin{aligned} E' &= \frac{\sigma_0}{\epsilon_0}\cos\delta \\ E'' &= \frac{\sigma_0}{\epsilon_0}\sin\delta \end{aligned} \tag{2.12}$$

The value of $sin\delta$ is obtained from the hysteresis loop of the stress-strain relationship. Substituting equation 2.12 in 2.11, the equation that relates the strain and stress is written as follows:

$$\sigma = E' \cdot \epsilon_0 sin(wt) + E'' \cdot \epsilon_0 cos(wt) \tag{2.13}$$

The strain energy for volume and cycle units is:

$$W = \oint \sigma d\epsilon = \oint \sigma \dot{\epsilon} dt \tag{2.14}$$

Integrating the parts of both the in-phase and out-of-phase components, the following expression is obtained:

$$W = \int_0^{2\pi/w} E'\epsilon_0 sin(wt)\epsilon_0 wcos(wt)dt + \int_0^{2\pi/w} E''\epsilon_0 cos(wt)\epsilon_0 wcos(wt)dt$$
$$= \left[\frac{E'\epsilon_0^2}{2}\sin wt^2\right]_0^{2\pi/w} + \left[\frac{E''\epsilon_0^2}{2}\left(wt + \sin(wt)\cos(wt)\right)\right]_0^{2\pi/w} \tag{2.15}$$

The first element in the right of the equality is "0" because it corresponds to the purely elastic energy that, in a full cycle, is totally recovered. Therefore, the dissipated energy for a unit of volume per cycle is:

$$W_{cycle} = \pi E''\epsilon_0^2 \tag{2.16}$$

Thus, the dissipated energy for a unit of volume per time is:

$$W = \frac{W_{cycle}}{2\pi/w} = \frac{1}{2}w\epsilon_0^2 E'' \tag{2.17}$$

Only a fraction of this dissipated energy is converted into heat. The other fraction is absorbed by internal changes in the material, as has been previously indicated.

Viscoelastic heating was studied by Jiang et al. as a mechanism in ultrasonic plasticising [63]. The results obtained both by numerical simulation and by experimentation pointed to the relationship between the initial temperature of the experiment and the glass transition of the polymer as a determining factor of viscoelastic heat generation. Viscoelastic heating proved to be relatively low at the beginning, evolving to a steep increase after reaching the glass transition temperature (the material studied was an amorphous polymethyl methacrylate (PMMA) polymer). The authors conclude that for the development of the ultrasonic plasticising, it would be better to heat the plasticising chamber up to the glass transition temperature.

In addition to the sinusoidal displacement imposed by the sonotrode, during the heating step of USM process the plunger is also applying a compression force to the polymer. Although this force is needed to inject the molten polymer into the mould cavity, high pressures can be achieved in the polymer pellets during the heating step before the polymer melts. These pressures will induce high strains in the material, which can also contribute to its heating [100, 102]. High strains induced by plunger pressures could also mean that the polymer can no longer be represented by linear

viscoelasticity equations and that non-linear models must be used. This issue is not considered in this dissertation although it should be addressed in future works.

Friction heating

Several studies have considered the friction heating mechanism between two polymer samples in the ultrasonic welding process [6, 28] and, recently, also in the USM process [62]. The dry friction type is considered to be the main contribution of inter-facial friction heating in which the heat rate at the interface between two granules can be described as:

$$Q(t) = \tau(\vec{t}) \prod v(\vec{t}) \tag{2.18}$$

where $\tau(\vec{t})$ is the equivalent friction stress, and $v(\vec{t})$ is the relative sliding velocity. Wu et al. [62] studied the friction heating in PMMA during ultrasonic excitation showing that the friction heating phenomenon occurs and lasts only until the interfaces disappear (at the initial stage of the USM process). From the analysis of their results, it can be observed that the temperature increases with ultrasonic amplitude and that the pressure seems to have less influence (see Figure 2.25).Recently, Jiang et al. [103] studied the influence of friction in pellets during the initial stages of ultrasonic heating. Their results show that friction increases with higher ultrasonic amplitudes and vibration times, but only for some inter-facial friction angles between pellets, showing a highly inhomogeneous behaviour.

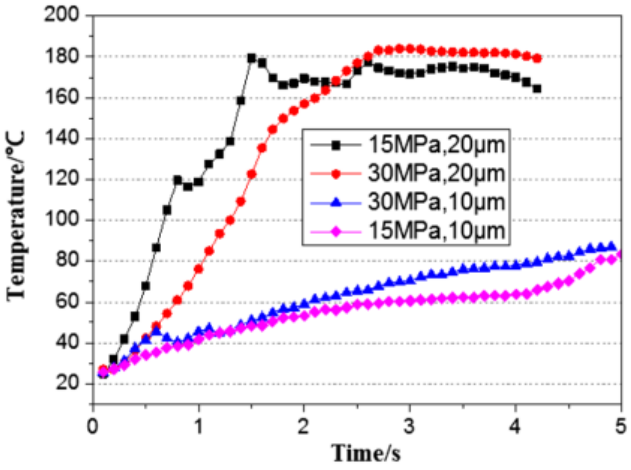

Figure 2.25: Temperature evolution in the interface between two half cylinders of PMMA under different pressure and ultrasonic amplitude conditions [62]

Ultrasonic cavitation

Ultrasonic cavitation refers to the formation and collapse of cavities, or bubbles, in a liquid medium being subjected suddenly to low pressures. When a liquid is exposed to a high-intensity ultrasonic wave, during the rarefaction part of the cycle the pressure in the wave is below the ambient pressure. This forces gas pockets to expand until they collapse violently due to the high stresses developed in the walls [19].

The cavitation formula for a single gas bubble under the influence of an oscillating sound wave is given by the following [104]:

$$R\ddot{R} + 3/2\dot{R}^2 = \frac{1}{\rho}\left(p_0 + \frac{2\sigma_s}{R_0}\right)\left(\frac{R_0}{R}\right)^{3k} - \frac{2\rho}{R} - 4v\frac{\dot{R}}{R} - p_0 - p_v + a \cdot sin(wt) \quad (2.19)$$

where R is the real bubble radius,R_0 is the initial bubble radius, $\dot{R}$ and $\ddot{R}$ are the velocity and acceleration of the bubble, respectively, p_0 is the initial pressure, p_v is the gas pressure inside the bubble, σ_s is the surface tension of the polymer melt, v is the viscosity of the polymer melt, k is the polytropic index, A is the ultrasonic amplitude, and w is the angular ultrasonic frequency.

Cavitation has an important effect on many high-power ultrasonic applications to liquids, such as degassing or cleaning [105]. However, the knowledge about the effect of the cavitation on polymers is still incomplete. Some authors assign a main role to the ultrasonic cavitation mechanism in the polymer heating step of the USM process [15, 83, 89, 106]. In contrast, Avila et al. [24] concluded that ultrasonic cavitation should have much less of an influence in non-Newtonian fluids, such as polymers, because polymer chains confer a higher resistance to the extensional flow and significantly reduce the intensity of the microjet developed during bubble collapse in comparison with Newtonian fluids.

The heating mechanisms explained above are independent from each other and can take place simultaneously during the process. However, the magnitude and duration of each mechanism in USM process is still not known properly.

In this dissertation a numerical modelling of the viscoelastic heating mechanism will be presented in Chapter 4. For this study, a generalised Maxwell model will be used to characterise the viscoelastic behaviour of the material. This material is introduced using Prony series to a thermomechanical model, which is solved using a commercial finite element software.

2.6.2 Filling step

In the filling step of the USM process, the polymer melt is pushed into the mould cavity in a similar way as in conventional injection moulding. In this later case, the fluid mechanics and heat transfer of the injection mould filling stage can be described by the Navier-Stokes equations that consists of [107]:

$$\text{Conservation of mass:} \quad \frac{\partial \rho}{\partial t} + \nabla \cdot (\rho \vec{u}) = 0 \tag{2.20}$$

$$\text{Conservation of momentum:} \quad \rho \frac{\partial \rho}{\partial t} = -\nabla p + \nabla \cdot \vec{\sigma} + \rho \vec{g} \tag{2.21}$$

$$\text{Conservation of energy:} \quad \rho c_p \frac{DT}{Dt} = \beta T \frac{Dp}{Dt} + p \nabla \cdot \vec{u} + \nabla(\kappa \nabla T) + \vec{\sigma} : \nabla \vec{u} \tag{2.22}$$

where ρ is the material density, $\vec{u}$ is the flow velocity, p is the pressure, $\vec{\sigma}$ is the stress, $\vec{g}$ is the gravity, c_p is the specific heat capacity, β is the coefficient of volume expansions, T is the absolute temperature and κ is the thermal conductivity.

These equations are used in commercial software applications able to simulate the process [108, 109]. Therefore, the filling stage of injection moulding is a well-known process. However, when dealing with micro features, there are some differences to consider, as:

- Higher shear rates (up to two order of magnitudes greater than in conventional injection) are obtained due to the presence of micro-sized runners [51]. This is due to the need to use higher pressures and injection velocities to maintain the polymer flow.
- Some approximations used in commercial software for conventional injection (as 2.5D modelling approaches, or the use of Hele-Shaw flow approximation) are no longer valid for μIM. In this case, full 3D modelling is required with a multi-scale mesh[95]

Guido et al. [44] has recently written an extensive review of the state of the art of μIM modelling and its main issues.

On the other hand, the filling step in USM also differs from that in conventional injection moulding in the following two main ways:

- The use of ultrasound lowers the viscosity of the material, which will become more fluid than in conventional injection moulding due to a reduced chain entanglement [58, 59].
- In the USM process, there is a strong coupling between the heating and the filling steps. Both steps are not completely consecutive, since part of polymer is introduced into the mould while there are still pellets in a solid state. This means that injection velocity is coupled with the heating speed (and limited to the melting rate of the process [60]).

Fortunately, these two singular characteristics of USM counteract themselves, thus allowing a polymer melt to fill at very low velocities (i.e., 50 mm^3/s [90]) in comparison with typical micro-injection flow rates (2500-10000 mm^3/s [60]). In contrast, the change in fluidity of the material could mean that mathematical models, such as the power-law model [110] or the Cross model [111], cannot be used to describe the material viscosity when applied to ultrasound; therefore, the simulation results from commercial software could be inaccurate. In fact, the modelling of micro-injection moulding also presents differences in the microscale viscosity of the polymer [95] Finally, although Heredia et al. [14] used simulation software to study the feasibility of part filling in the USM process, there is currently no analysis comparing the simulation results with the experimental filling behaviour of the polymer in the USM process.

2.7 USM experimental review

2.7.1 Materials and applications

USM technology has already been tested with multiple materials and applications. Customer tests made by *Ultrasion, S.L.* have shown that this technology offers great benefits for moulding high-aspect ratio (height to width ratio) textures, samples with low pressure requirements, or when a hopper needs to be avoided due to the lack of thermal resistance of the material. In Figure 2.26, two examples of samples obtained with USM technology are presented.

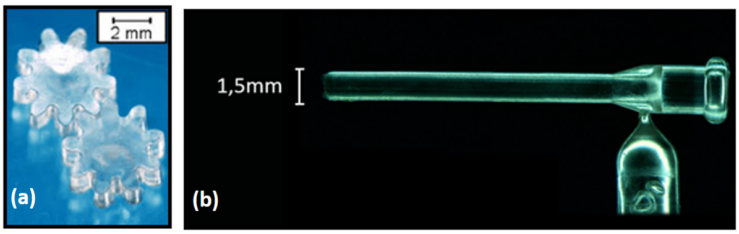

Figure 2.26: Examples of figures obtained by USM: a) A polypropylene (PP) microgear[57], and b) a cannula made from cyclic olefin polymer (COP), courtesy of *Ultrasion, S.L.*

Although there is still a great deal of work pending, the technology has shown to be able to process a large variety of polymers. Among them, polypropylene (PP) was one of the first polymers to be tested [57] and has been successfully processed by Negre et al. [13]. Polyoxymethylene (POM) was also studied by Michaeli et al. [57, 61], and the research done in this dissertation shows that it can be processed with very good results (see Chapter 3). The application of USM to process polylactic acid (PLA) was widely studied by several authors [10, 12, 14, 81, 86]. PMMA was

also processed without degradation [81]. Other materials tested with USM technology are polyphenylsulfone (PPSU) [15], polybutylene succinate (PBS) [12], ultra-high molecular weight polyethylene (UHMWPE) [64], polyamide 12 (PA12) [80, 81], polycaprolactone (PCL) [87] and synthesized polymers, such as poly(nona-methylene azelate) [88]. In addition, there is a recent publication that reviews the advances of USM technology in processing biomaterials[66]. In this research study, polyoxymethylene (POM) and cyclic olefin polymer (COP) were processed using a new configuration for USM technology.

Due to the novelty of the USM application, most of the research documented is focused on obtaining a processing window or an optimal processing point for a determined material [10, 11, 13, 15, 81]. Even so, there are also other applications of USM technology, such as the works published by Diaz et al. focused in studying the dispersion of nanoclays [86], and that of Olmo et al. [87] about the dispersion of nanotubes, both in a polymeric matrix. USM has also been successfully applied to disperse graphite in UHMWPE [65]. All these results show that this technology is capable of obtaining moulded nanocomposite specimens without degradation and without needing any further processing. Recently, Heredia et al. [66], have showed the great potential of USM technology for biomedical applications including drug delivery or fabrication of tailored implants.

2.7.2 Study of the main factors

As has been shown in section 2.6, there are several process parameters that might affect the USM process. Some of these parameters are specific to this technology, and its influence on the experimental results is still not completely understood. Additionally, different machine configurations have been used in the literature, implying the use of different moulding methodologies and different control parameters. In this section, the main factors of USM technology used in the literature are reviewed.

Amplitude of the sonotrode: The ultrasonic amplitude is the amplitude delivered to the polymer by the sonotrode. This amplitude is directly related to the maximum strain (ϵ_0) induced in the polymer by the vibrating sonotrode and therefore, according to Equation 2.17, is related to the average power dissipated due to the viscoelastic heating [94]. Consequently, most of the articles reviewed identify the amplitude as the main factor to be considered to find the optimal processing window [10, 12, 15, 64, 81]. In fact, the effect of the amplitude is so high that some studies prefer to fix its value to be able to study the influence of the remaining factors [11, 13, 65]. The experiments carried out show that processing a material with too lower amplitudes can

introduce non-melted material in the cavity [112] or produce incomplete parts [10]. In contrast, too higher amplitudes can degrade the material, especially when low forces are applied [10]. In general, higher amplitude values give better filling results and geometry accuracy [11]. From the extant literature, it can be observed that the amplitude interacts greatly with the other factors governing this manufacturing process; such as the compression pressure [10], the velocity [15], or the shape of the polymer pellets [64].
In this research study, the numerical simulation developed in Chapter 4 identifies ultrasonic amplitude as the main parameter in the viscoelastic heating of the material, which is in accordance with the literature results presented here.

Frequency: In high-power ultrasonic devices, all the elements must be tuned to work at the same frequency. In the present case, the ultrasonic generator and transducer are only capable of delivering one resonant frequency, and they work at 30 kHz. Thus, there is very little information about the effect of the frequency in the USM process. It is known that larger piezoelectrics are required for lower frequencies, which can deliver more amplitude and more power. However, Jian et al. [63] calculated the heat generation rate at different frequencies using the same amplitude. The results show that, although the viscoelastic heating rate increases slightly with the frequency, it has a limited influence on the temperature of the polymer.

Compression pressure: Pressure is needed to push the polymeric melt into the mould cavity. However, too much pressure can introduce non-melted material in the figure [57] and can produce incomplete and inhomogeneous parts [10, 81]. On the other hand, higher forces seem to provide better filling ratios and better dimensional accuracy of the samples, although no relationship has been found between the pressure and the mechanical properties of the sample [11].

Injection velocity: As explained in section 2.5, velocity was added in newer versions of the commercial machine Sonorus® as an alternative control factor of compression force. Since then, the effect of the sonotrode velocity has been studied for the *Configuration 1* methodology [13], and the effect of the plunger velocity has been analysed for the *Configuration 2* [15, 64, 65]. Dorf et al [15] concluded that for lower velocities, there were more bubbles in the final part (which the author relates to a greater cavitation) and higher velocities produce higher mechanical strength but can produce unfilled samples. In contrast, no influence of the injection speed was found by Masato et al. [60] when processing polypropylene with USM. In this case, the coupling between the melting and filling steps and the use of a very low force for the movements of the plunger, could mask the influence of the velocity.

Thanks to the possibility of including a variable injection velocity in the most recent version of the commercial machine, different authors have studied the influence of velocity profiles. The experiments carried out by Negre et al. [13] show that profiles with increasing sonotrode velocities give better filling results when processing polypropylene. If *Configuration 2* is used, the U-shaped velocity profile gives better tensile strength results when processing ultra-high molecular weight polyethylene (UHMWPE) [64, 65]. Although there is still no clear experimental relationship between USM parameters and the polymer temperature evolution during the process, a recent study with sensorised moulds shows that higher plunger velocities have less dispersion in the temperature values obtained from an infrared sensor placed at the mould cavity [75].

Raw material shape: There are few studies documented that have analysed the influence of the shape of the raw material in USM. The most relevant method was performed by Sanchez-Sanchez et al. [64], showing that the material shape is the most important factor to process UHMWPE with high tensile strength. On the other hand, as displayed in Figure 2.27, the research performed by Montes et al. [75] showed that polymers dosed with smaller pellets can be injected with a lower temperature. These results are in accordance with the fact that less amplitude is needed to process powder than to process pellets of PLA [12].

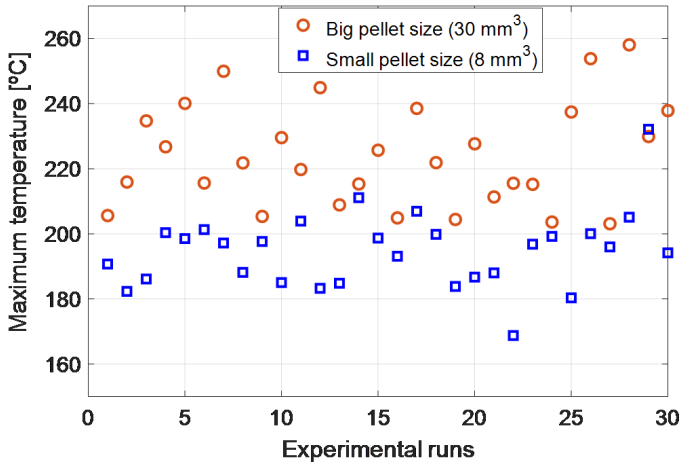

Figure 2.27: Temperature results obtained using extruded PP with different pellet sizes and with the same process parameters [75]. The temperature of the polymer when it arrives at the sensor (placed at the end of the mould figure) is lower when the pellets of the material are smaller

Ultrasonic time: The ultrasonic time is the time in which the sonotrode is vibrating. This variable is directly related to the energy applied to the material, and several authors have considered it as one of the main factors for USM [10, 12, 81]. In addition, Grabalosa et al. [11] showed that the ultrasonic time has a very strong effect on the part filling but only up to a certain time when the sample is already filled. If ultrasonic energy is still applied when the sample is filled, it is easy to degrade the polymer [89]. Thus, the ultrasonic time is a key parameter because with too short times, the sample is unfilled, and with too long times, the polymer can degrade. Typical ultrasonic time values go from 2 seconds [11] , to 10 seconds [81]. As the material is dosed in pellets and can have substantial differences in weight, the ultrasonic time should not be the same for different shots. This is related to the switchover point explained at section 2.4. The initial results obtained by Janer et al. showed that using a trigger force as a switchover point stabilizes the filling of the figures [77].

In addition to the main process parameters, there are multiple factors that can affect the USM process and have to be taken into account. The mould temperature is normally set according to conventional injection data sheet parameters. However, the study done by Sanchez- Sanchez et al. [65] concluded that the mould temperature is the main effect factor to obtain a good tensile strength with UHMWPE with graphite additivities. In another context, the study performed by Heredia et al. [14] showed that using venting holes increases the filling of the samples. Negre et al. [13] proved that drying the pellets before processing seems to be necessary to reduce the porosity of the final samples. Finally, although not studied as a factor, it seems that the position of the heaters in the mould can affect the filling of the samples [14].

The influence of the main factors involved in USM technology has been studied with different approaches. However, the best way to fully characterise a process, knowing the main variables that have an effect and having its impact quantified, is through a design of experiments (DOE). DOE methodology is extensively used for novel process characterisation and is commonly used in the published USM literature.

A full factorial matrix design is generally employed for the control factors when the goal of the research is to obtain the processing window for a particular material [10, 57, 81]. If the influence of each parameter is also an objective, most authors use a two-step design of experiments with an initial screening step and a full factorial, or a fractional factorial, step [11, 15, 64], or they use a three-step design of experiments [90]. In these cases, the cavity filling or the mechanical properties of the sample are usually chosen as a response.

On the other hand, some articles are more interested in obtaining good samples without degradation, and the influence of each parameter is not so relevant. In this case, normally, the approach known as one factor at a time is used [12, 13, 86, 87]. One problem that these studies have in common is that they are unable to quantify the influence of each parameter and their interactions. Strong interactions, such as those observed between the ultrasonic amplitude and the compression force, make finding trends impossible and the optimisation of the parameters difficult [10, 12].

In a recent publication, Sánchez-Sánchez et al. [65] used a Taguchi optimisation to optimise the USM parameters in order to maximize the tensile strength of the moulded samples.

2.7.3 Study of responses

In conventional injection moulding, a sample can be considered well processed when it has the desired geometry, the adequate mechanical properties, and no signs of defects or impurities. To evaluate the use of the USM process, different responses related to the quality of the sample have to be studied. In the literature, the following responses have been considered:

- **Filling capability:** A completely filled sample is an indispensable requirement for a good moulding process. If this requirement is not fulfilled, most of the rest of the requirements are worthless. Thus, the filling capability is a common response used to find the processing window of a material [10, 12, 81, 90]. However, few authors study in depth the repeatability of the process. Although USM process is capable to fill completely figures with commodity polymers as PP [13] or PS [90], there is a low repeatability of the process for certain high performance materials like PPSU [15]. In general, to obtain completely filled samples, a minimum ultrasonic time and pressure are needed [11, 81]. Most studies find that higher amplitudes improve the filling of the samples [10, 11, 15, 64, 91]. Velocity also has a key influence on the part filling, although its effect can be contradictory depending on the material and cavity shape. Ferrer et al. [90] found that better filling results were obtained when injecting thin-wall shaped PS with lower velocities. On the contrary, Dorf et al. [89] obtained better filling of PEEK samples with higher velocities. As this later material is a technical polymer with high melting temperature, probably higher velocities are needed in order to prevent the material from cooling before filling the cavity. High mould temperatures also influence part filling positively [64]. The best parameter values for part filling are listed in Table 2.4.

Material	Geometry	Amplitude	US time	Force/Velocity	Reference
PA	Tensile bar $33 \times 2.5 \times 1.2mm^3$	35 μm	$>$ 2 sec	2-4 bars	[11, 80]
PLA	Tensile bar $15 \times 1 \times 1mm^3$	48 μm	3 sec	0.5 or 3 bars	[10, 81],
PMMA	Tensile bar $15 \times 1 \times 1mm^3$	48 μm	10 sec	6 bars	[81]
PP	Tensile bar $33 \times 2.5 \times 1.2mm^3$	56 μm	3 sec	5 mm/s or increasing velocity ramp	[13]
UHMWPE	Tensile bar $30 \times 2 \times 1mm^3$	50-56 μm	Not specified	U velocity profile	[64, 91]
PPSU	Tensile bar $30 \times 2 \times 2mm^3$	58 μm	$\leq$ 2.8 sec	$\geq$ 5 mm/s	[15]
PEEK	Tensile bar $30 \times 2 \times 2mm^3$	58 μm	7-8 sec	5-7 mm/s	[89]
PS	Rectangular specimen $155 \times 8 \times 0.55mm^3$	14-70 μm	Not specified	1 mm/s	[90]

Table 2.4: Best parameter values for part filling obtained from literature. In this table, only main parameters are listed, for detailed configurations and optimal processing points, please refer to the sources

- **Mechanical properties:** To ensure the applicability of a polymeric sample, mechanical requirements must be fulfilled. The common method to study the mechanical properties of a material is the stress-strain curve obtained from a tensile stress test. Thus, several authors used the tensile strength of the samples [15, 89] and the Young's modulus [65] as responses for their studies. Other authors only studied the mechanical properties in the optimal moulding points. In this case, good repeatability of the stress-strain curves are found for PLA [10] and PMMA [81].

  From the literature, it can be observed that the influence of the process parameters on the mechanical properties of the samples may vary depending on the material. Sacristan et al. [10] found that, when processing PLA, low moulding pressures led to higher variability, lower modulus and lower elongation values. According to the authors, low pressures do not allow the reduction of the polymer viscosity, and the ultrasonic vibration degrades the material. In contrast, when processing

PA12, Grabalosa et al. [80] found that tensile strength is reduced when larger pressure values are applied. However, in a later study with the same material geometry and machine configuration, the same authors concluded that changes in applied pressure did not present any significant influence, while longer ultrasonic times presented higher weld strength values [11]. When processing UHWMPE, better results were found when higher mould temperatures were used [64]. According to the authors, at higher mould temperature, the crystalline phase increases, thus resulting in a greater stiffness. This effect is also found when UHMWPE/graphite composites are manufactured using USM [65]. Dorf et al. [15] found that the process was not stable for PPSU in terms of the mechanical properties of the samples. Even so, a mathematical model was developed to predict the tensile strength of the samples from the process parameters. The results from this study show that a high velocity produces higher mechanical strength in the samples (although a velocity that is too high creates unfilled samples).

Comparing other processes, Dorf et al. [89] found that the PEEK specimens obtained from USM had similar tensile strengths to the ones obtained by conventional injection moulding but presented a 56% higher crosshead extension. On the other hand, in comparison with the compression moulding process, greater values of the elastic modulus and tensile strength but lower values of tensile strain were found [64]. Conversely, Masato et al. [60] found that the mechanical properties obtained when processing PP were significantly better than those obtained with conventional micro-injection, although lower repeatability was observed.

- **Molecular weight:** It is known from the literature that ultrasonic energy reduces the molecular chain entanglement and increases the fluidity of a polymer [58, 59]. However, the application of ultrasonic energy can also cause chain breakages and degrade the material [24]. The measurement of the average molecular weight of the polymer is a method to estimate if there have been chain breakages during the process. Sacristan et al. [10] studied the effect of processing conditions on the average molecular weight of PLA samples. Although a general behaviour could not be observed, the authors found that the moulding pressure plays a significant role in the molecular weight, while there was no clear tendency with the ultrasonic amplitude. Moreover, the average molecular weight was maintained when the samples were processed at optimal conditions. Additionally, PLA and PBS could be moulded in powder form with an average molecular weight decrease lower than 6% [12]. Sanchez-Sanchez et al. [64] studied the molecular weight at different regions of the samples, concluding that the molecular weight

decreased along the flow direction (see Figure 2.28). According to these authors, the material at the end of the sample was nearer the sonotrode during the heating stage and was more exposed to the ultrasonic energy.

Due to economic factors and accessibility, Dorf et al. used FTIR spectroscopy as an alternative method to determine the degradation of PEEK [89] and PPSU [15]. Changes in the absorption bands of the infrared spectra between the raw material and the processed material can indicate degradation.

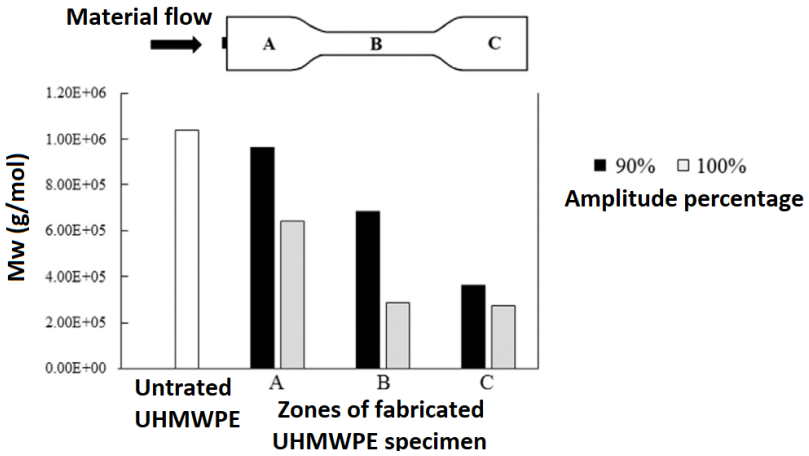

Figure 2.28: Average molecular weight at three zones of the samples processed at 90% (50.6μm) and 100% (56.2μm) amplitudes. The results are reproduced from [64]

- **Crystallization:** The first USM tests reported that it was possible to process materials with regular crystallization and homogeneous structures [61]. An amorphous outer layer was observed for ultrasonic moulded PP and POM specimens [57]. In fact, the detailed chemical analysis performed by Sacristan et al. [10] with PLA suggests that ultrasonic processing increases the amorphous phase content of the samples. Although it is beyond the scope of this review, several studies have analysed the influence of additives on the crystallinity of nanocomposites processed with USM [12, 86, 88]. Jian et al. [106] showed that for HDPE, under ultrasonic excitation, the molecular chain becomes shorter, the chain structure becomes simpler, and the symmetry stereo-regularity of the molecule is better. According to these authors, these results lead to faster crystallization velocity, lower crystallization temperature and more uniform grains of the polymer. Dorf et al. [89] used the endothermic and exothermic peaks obtained in a DSC analysis to calculate the crystallization of PEEK samples. The results showed that the crystallization levels were similar to those of the raw material. In comparison with conventional injection, Masato et al. [60] found higher crystallization in USM processed PP. Finally, when processing

UHWMPE, Sanchez-Sanchez et al. [64] concluded that at a higher mould temperature, the crystalline phase increases to the detriment of the amorphous phase, which results in a greater stiffness.

- **Dimensional accuracy**. Grabalosa et al [11] studied the average width and thickness of a PA tensile specimen, concluding that thickness accuracy improves with maximum pressures and maximum ultrasonic time. On the contrary, width dimensions did not show any trend under different processing conditions. The authors of the article attributed this due to that the width dimension is two times larger than the thickness (it has greater contact with the mould), so it solidifies earlier and reduces the influence of the packing pressure. Negre et al. [13] when processing polypropylene found that both thickness and width were better when increasing velocity ramps were used. These means that the material is subjected to greater pressures during the last step of the injection, which is consistent with the results obtained by Grabalosa et al [11] with thickness behaviour.

  Heredia et al. [14] also measured the thickness of processed PLA in a thin wall plate shape. Two different process conditions varying ultrasonic time and a pre-compaction of the pellets have been studied, performing 10 trials for each configuration. However, the dispersion of the results makes it difficult to obtain any influence of the process parameters. The authors point out that maybe the location of the thermal resistances are affecting the results (the location is different for both configurations). Similar results were obtained by Ferrer et al. [90] when measuring the thickness of Polystyrene thin plates at different points and analysed the results using principal components analysis. Both Heredia et al. [14] and Ferrer et al. [90] found that the thickness of the samples were, on average, greater than the thickness of the mould, which it would expected to be lower due to the shrinkage effect. The hypothesis provided by the authors of the article is that the cooling time used in the experiments was too low, so the polymer is still warm when the mould is opened and the geometry is not correctly replicated. In this case, the thickness obtained is greater at lower injection velocities (the material is heated during longer times and can achieve higher temperatures), which is consistent with the hypothesis. However, due to the influence of the cooling time, these results are not comparable with the ones obtained by Grabalosa et al. [11] and Negre et al. [13].

2.8 Conclusions

USM has been proven to be a promising new technology for the processing of multiple polymers types with micro and mini features. In this chapter, the main properties of this technology have been discussed, and a review of the work performed to date in this field has been carried out. The main conclusions drawn from this chapter may be summarised as follows:

- USM has been successfully applied to process a large quantity of thermoplastic polymers. This technology is capable of moulding high-aspect ratio parts and is suitable for multiple applications from electronic overmoulding to the dispersion of nanocomposites.
- According to the extant literature, ultrasonic amplitude is one of the most important factors in the USM process. Although it has strong interactions with the pressure or velocity of the injection and the polymer shape, the results show that the high values of the amplitudes give better results as long as the material is not degraded.
- High injection velocity or high injection pressure seems to provide better mechanical results but can produce unfilled samples. Additionally, the use of increasing velocity profiles is found to have better filling results for the *Configuration 1* methodology, whereas the use of U-shaped velocity profiles is found to have better filling results for the *Configuration 2* methodology.
- Despite all the efforts made, the influence of the processing factors on the measurable responses (filling, mechanical properties, degradation) has not been completely understood. The instability of the process along with the varying machine configurations used in the research articles studied here do not help to solve the problem.
- Given the great number of parameters of this process, the authors think that the use of the full factorial or one-factor-at-a-time design of experiments makes it difficult to quantify the influence of the parameters and their interactions. Studies using systematic methodology seem better suited to evaluate the influence of each parameter.
- As most of the research studies focus on new applications, there is little information about the repeatability of the USM process in existing literature. However, this has been identified by the author as one of the main drawbacks of the technology and is one of the main reasons behind the development of the *nodal point* configuration presented in the next chapter.

3

New configuration for ultrasonic moulding process

3.1 Introduction

As described previously, ultrasonic moulding (USM) technology is an interesting alternative to conventional injection moulding and has been applied to process multiple materials for different applications. However, up to now, its use has mainly been limited to research centres and universities due to the lack of repeatability of the technology. It can be said that the performance of standard USM methodology does not meet the requirements from industry standards, preventing its adoption in most of the markets. Thus, the improvement of the repeatability of USM method is the main objective behind the development of the new configuration presented in this dissertation. This new configuration has been called as *nodal point* due to the use of the resonance vibration properties of the sonotrode involved.

Nodal point layout is developed with the aim to solve all the main drawbacks encountered in standard USM process. Particularly, this configuration is designed to improve the repeatability and robustness of the method to allow the adoption of the USM technology in the industry.

In this chapter, the main drawbacks of the USM technology used with the standard method are identified and the new configuration is presented and validated with two different materials. *Nodal Point* configuration has been protected by Eurecat [114] and some of the results presented here have been previously published by the authors in [9].

3.2 Identified drawbacks of USM standard methodology

Most of the experimental tests performed with USM in the literature use the *standard configuration* as described in section 2.4. The standard USM configuration uses a sonotrode placed in the mould partition level and a plunger to push the material against the sonotrode as it is shown in Figure 3.1. This configuration has a plasticising chamber where the polymer is melt just above the partition level, and a runner that connects the mold cavity with the plasticising chamber. However, this chamber is not completely sealed because there is a gap between the mould and the sonotrode, which is necessary to allow the vibration of the sonotrode.

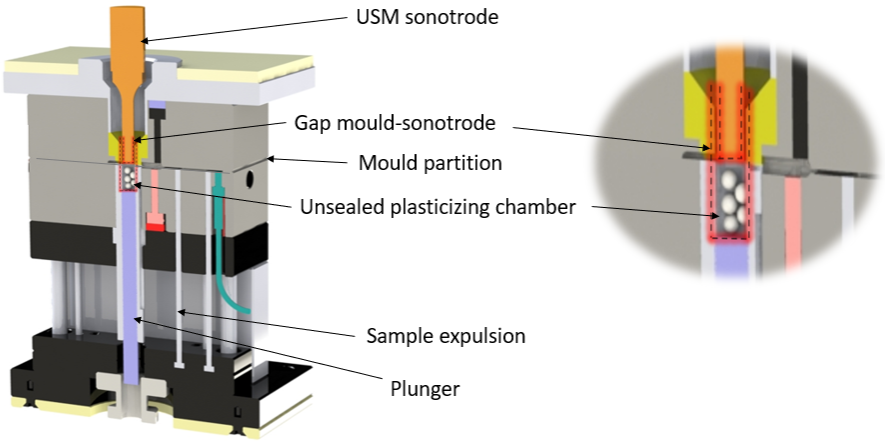

Figure 3.1: Standard USM configuration

The presence of this gap has two big implications in USM technology. On one hand, it implies the need of a centring ring around the acoustic unit to avoid the contact between a moving sonotrode tip and the mould, which would contaminate the sample. To be able to have a correctly centred sonotrode, most of ultrasonic machines used in the experiments reported in the literature, use copper centring rings and place PEEK sleeves between the sonotrode and the copper element to prevent the sonotrode from touching the mould (see Figure 3.2).

On the other hand, even with the centring system, this gap between the mould and sonotrode is believed to be a key element in the instability of the process. The main problems associated with USM technology due to the presence of this gap are listed below:

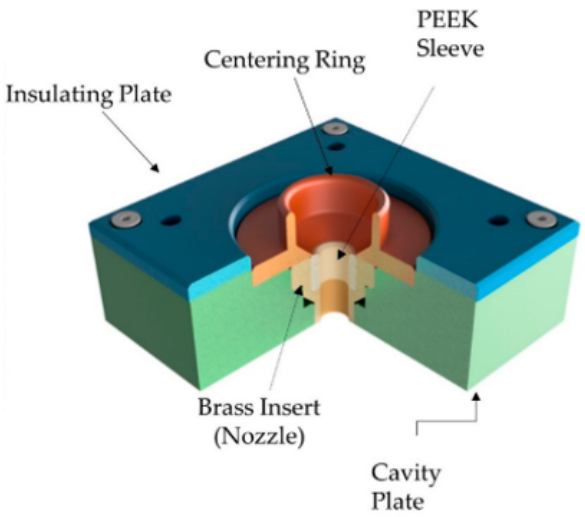

Figure 3.2: Upper mould partition with a centring ring and a PEEK sleeve, reproduced from [66]

- **Flash in the material**. The standard configuration allows the leakage of material through the sonotrode-mould gap. This is more critical when the cavity gate has a similar dimension than the sonotrode-mould gap, or when processing polymers with low viscosity, but can appear in almost all the situations. In fact, as showed in Figure 3.3, there are multiple images in the literature where it can be observed flash in the samples processed.

- **Contamination**. If the gap is reduced or the force applied during the filling step is high, the sonotrode will bend and it can eventually touch the centring ring of the mould, leaving copper particles (or, eventually, titanium particles) in the sample . This can be seen in the sample of Figure 3.4.

- **Lack of repeatability**. The sonotrode - mould gap prevents to have a completely sealed plasticisation chamber. This causes instability during the filing process and this seems to be directly related to the poor repetitiveness of the process. This lack of repeatability can be detected in the dispersion of in-mould temperatures and it is related with large deviations in mechanical properties, as shown in strain stress curves of Figure 3.5. The hypothesis of the influence of the plasticising chamber in this behaviour of the method will be discussed in depth in section 3.4.

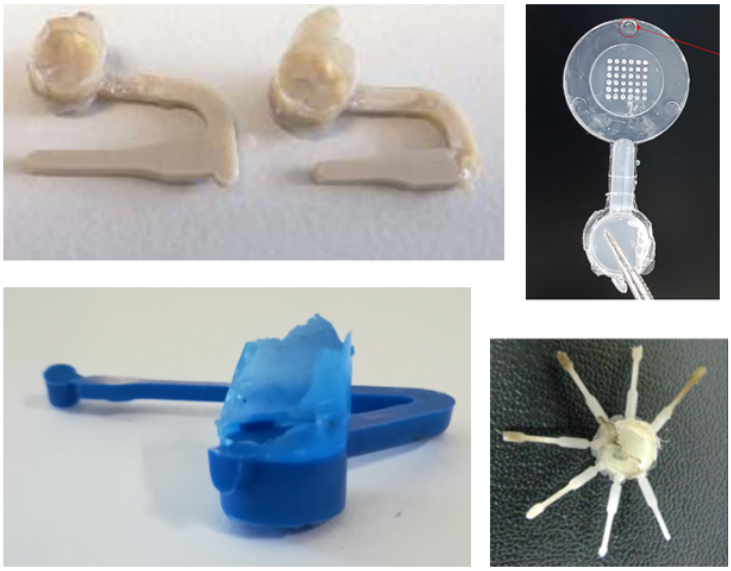

Figure 3.3: Flash in the sprue due the leakage of material in the sonotrode-mould gap obtained for several materials and geometries: PEEK samples from [89] (upper left), polypropylene lens from [115] (upper right), Eltex MED 100 polypropylene sample processed by the author (lower left), and polycaprolactone samples from [87] (lower left)

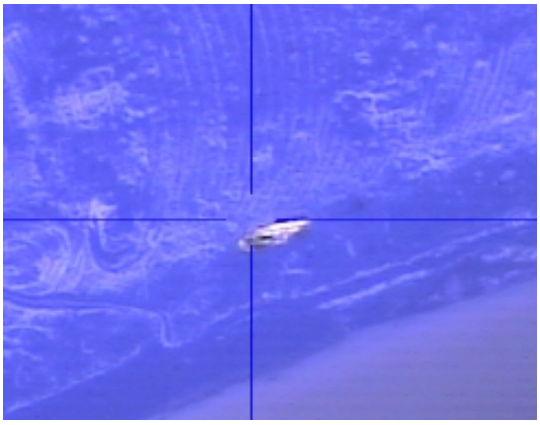

Figure 3.4: Copper contamination in samples when processing Eltex MED 100 polypropylene

3.3 Nodal point configuration

The new nodal point method aims at improving the performance of USM technology. In particular, the lack of repeatability in filling, in the in-mould measurements and in the mechanical properties of the samples are the main issues to be addressed from standard USM method. Nodal point method attempts to solve these issues using a new mould configuration and a dedicated methodology.

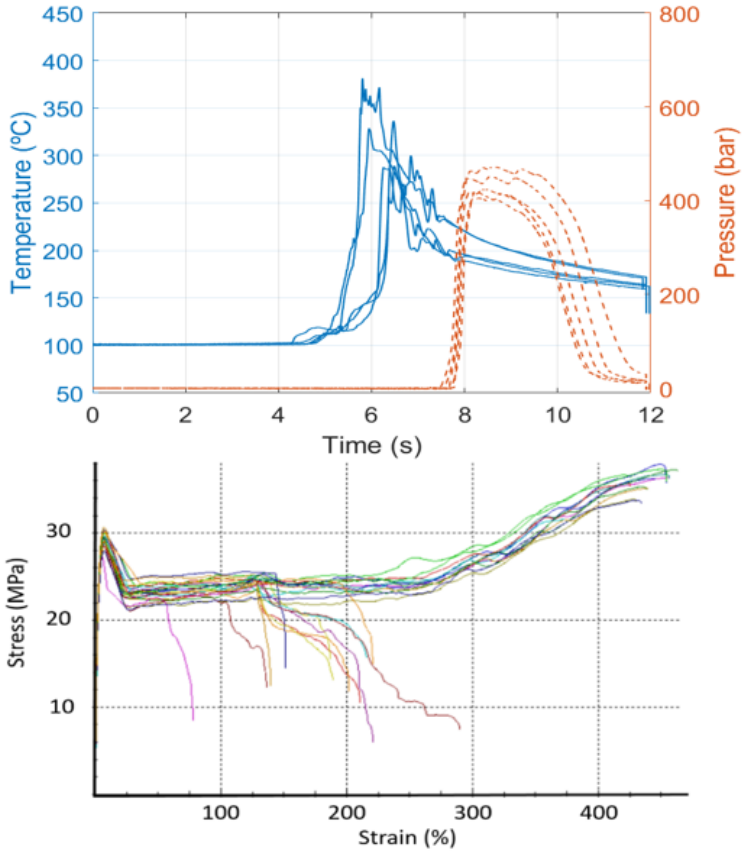

Figure 3.5: Instability in in-mould data of processed samples of POM Delrin® (top) and in mechanical properties of processed samples of Hostacom® PPU X9067 polypropylene (bottom)

3.3.1 Mould

Nodal point ultrasonic moulding (NPUSM) configuration changes the placement of the ultrasonic elements in the mould in order to have a sealed plasticising chamber. A sealed chamber is expected to improve the performance of the method and prevent the problems associated with the gap between the mould and the sonotrode. Thus, NPUSM configuration places such sonotrode in a low position until its nodal point is in contact with the mould (see Figure 3.6).

3.3.2 Sonotrodes

Up to now, conventional half-wave stepped sonotrodes are used in all USM configurations. As previously explained in section 2.2.1, these types of sonotrodes have a length approximately equal to $\lambda/2$, where λ is the acoustic wavelength for the sonotrode's material.
However, due to the specific geometric requirements of NPUSM configuration, in this case a customized half-wave stepped sonotrode has been

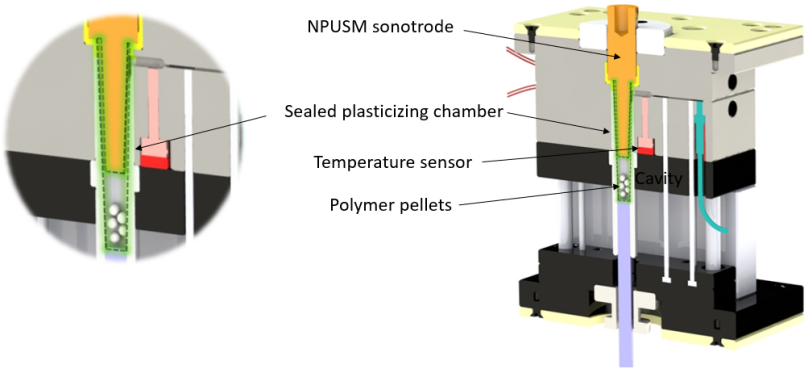

Figure 3.6: Nodal point ultrasonic moulding configuration

designed. This new sonotrode has a flat region around the nodal point to ease the contact with the mould during the process, sealing the plasticising chamber. Another significant difference of this sonotrode is the conical shape of its lower part, needed in order to de-mould the material. This new design was determined through a modal analysis performed by means of the Finite Element Method with the commercial *COMSOL® Multiphysics* software. This particular sonotrode has been made of Ti6Al4V with a gain (ratio between output and input amplitude) of 4. When working in resonance condition, the amplitude of vibration delivered varies sinusoidally through the length of the sonotrodes, as it is detailed in Figure 3.7). The use of the nodal point (also called nodal plane) properties of the ultrasonic elements has been used previously in industrial equipment to fix housing assemblies [116]. In this case, this property is used to support the sonotrode in the mould and close the plasticising chamber. Recently, a similar approach for the extrusion process has been developed by Perez et al. [117].

3.3.3 Plasticising chamber

As shown in Figure 3.6, this new configuration allows to have a sealed plasticising chamber. However, this solution comes with a price, i.e., a significant increase of the material of the sprue. Closing the plasticising chamber at the sonotrode nodal point leaves a hollow cylindrical sprue with a height around 4 centimetres and similar weight than conventional macro-injection ones. However, its weight is much higher than standard USM and conventional microinjection sprues (see Figure 3.8). This issue can be a major drawback when moulding high expensive polymers and should be addressed in future works.

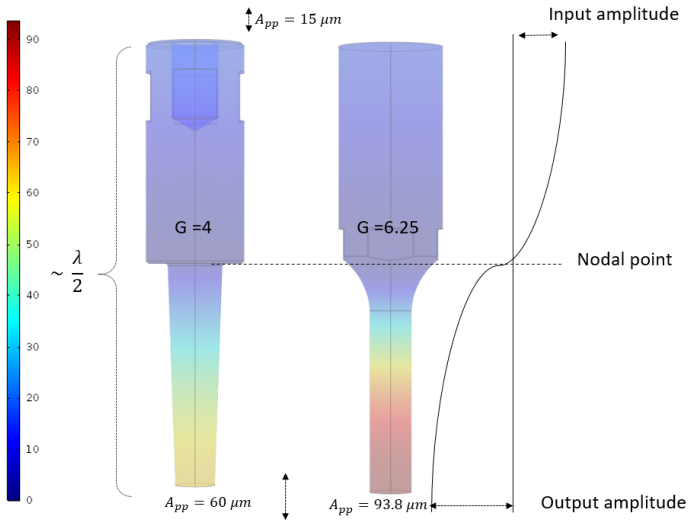

Figure 3.7: Distribution of the amplitude obtained from FEM analysis for a nodal point sonotrode (left) and a standard one (right). A_{pp} is the peak-to-peak amplitude and G is the gain of the sonotrode

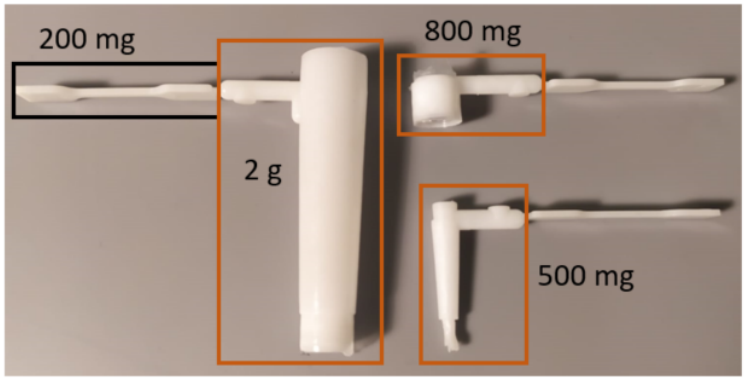

Figure 3.8: Sprue comparison between nodal point method (left), standard USM (upper right) and Babyplast ® 6/10 microinjection moulding sprue (lower right)

3.4 Nodal point plasticising chamber design

As previously discussed, the main benefit of NPUSM configuration is to have a completely sealed plasticising chamber that allows a better repeatability of the process.
One of the problems that arise when there is an open plasticising chamber is that the polymer flow may not be continuous. A qualitative study of the influence of the plasticising chamber in the polymer flow can be done using Moldex3D® software. This software is suited to simulate the conventional injection moulding process and cannot account for effects related with USM process. Temperatures and pressures obtained in the simulations won't be valid, nor will be the filling time. However, the simulation can be used to

estimate the qualitative influence of the plasticising chamber geometry in the polymer flow. In this section, Moldex3D® is used to simulate the filling of USM and NPUSM mould cavities as if they were injected using conventional injection moulding parameters.

3.4.1 Simulation setup

The mesh of the cavity is generated with the *Boundary Layer Method*, which ensures a minimum of 3 layers in each part of the sample. For these simulations, all the geometry is considered as a part (no runner is defined), and the lower surface of the sonotrode is selected as the gate for the material (see Figure 3.9).

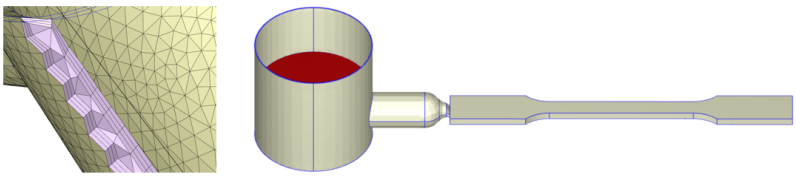

Figure 3.9: Moldex3D ® simulation setup. Detail of mesh generated using BLM method (left) and the position of the gate in red (right)

The simulation analysis is done for the filling stage only using the standard solver. A customized injection moulding machine has been created to adjust the process conditions to the ones described in Table 3.1.

Material	POM Delrin 500P NC010
Melt temperature	220 ° C
Mould temperature	100 ° C
Flow rate	0.25 cm^3/s
Injection pressure	150 MPa

Table 3.1: Process conditions used in Moldex3D ® simulation. Flow rate value is obtained considering a 8 mm diameter plunger moving at 5 mm/s

3.4.2 Analysis of the standard USM plasticising chamber

The standard USM plasticising chamber has a gap between the centring ring of the mould and the sonotrode. The size of this gap will be different in each the mould, and could increase during the time due to the wear of the sonotrode. For the sake of simplicity, in this analysis a wall of 0.05 mm and a maximum height of 4 mm for the flash are considered (see Figure 3.10).

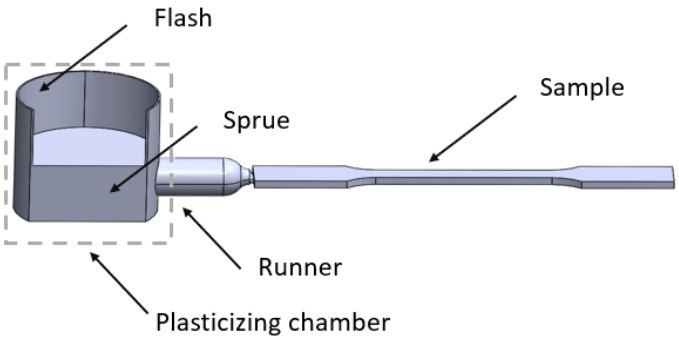

Figure 3.10: Sketch of a standard USM sample and its plasticising chamber

As previously said, this simulation can only be analysed as a qualitative indication of the polymer flow, considering that the effect of the ultrasounds is neglected and that the melt temperature is imposed from the material datasheet. In any case, the results represented in Figure show that polymer fills simultaneously the sample and the gap between the mould and the sonotrode (flash). This can lead to filling instabilities due to hesitation (see 2.3) and cool spots. In fact the simulation results show an incomplete filling with these processing conditions (see Figure 3.11).

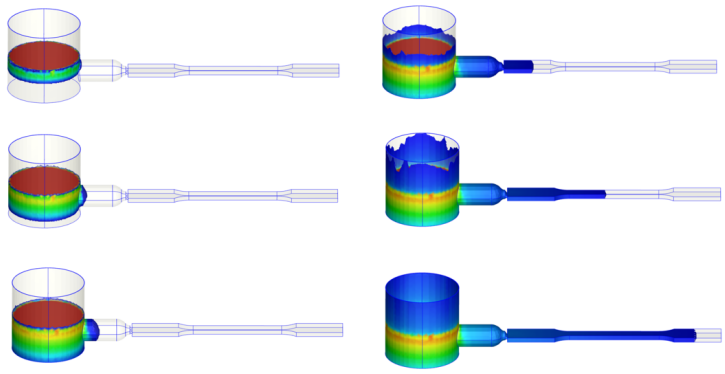

Figure 3.11: Simulation of cavity filling in standard ultrasonic moulding. From upper left: 30%, 60%, 80, %90%, 95% and 100% of volume filled

In conventional injection moulding, this behaviour would always lead to incomplete fillings. However, in ultrasonic moulding, even when the polymer flow stops due to the cooling of the melt front, the sonication energy is sustained and the sample temperature continues to increase. This effect was observed by Gülçur et al. [115] in completely filled microneedle cavities (see Figure 3.12). Although this unwanted effect can be partly avoided using

a force switchover to detect the end the filling, it is possible to still have heating peaks during the filling if the polymer flow is stopped. That would explain the high temperatures of the melt needed with standard USM to fill the samples (see section 3.6).

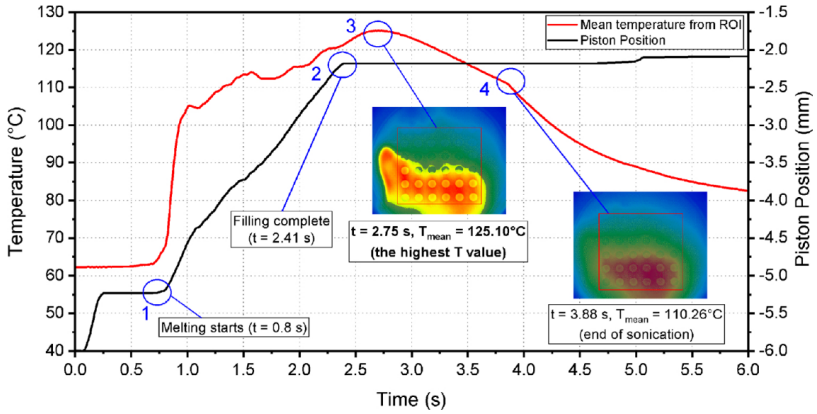

Figure 3.12: Mean temperatures recorded during ultrasonic moulding of a microneedle cavity. Reproduced from [115]

3.4.3 Design of the NPUSM plasticising chamber

To guarantee the continuity of the polymer flow, the nodal point plasticising chamber was carefully designed and a Moldex3D ® simulation was performed with the processing parameters listed in Table 3.1. As it can be seen in Figure 3.13, in this case, although the chamber is much more bigger than in standard ultrasonic moulding, the sample was completely filled.

Even with the limitations of this qualitative analysis, the results of the simulation give some insights about the need of a properly chamber design for the USM process, and the benefits of a closed chamber. In practice, the experimental filling follows a similar pattern than the one obtained in the simulations, as it can be seen in Figure 3.14. However, much more work is needed in order to adapt the Moldex3D® simulation to the USM process to be able to do a quantitative analysis.

In this dissertation only the heating step of USM process is modelled and analysed both numerically and experimentally. However, due to the strong coupling between both steps (heating and filling), the results obtained in Chapter 4 need to be used in order to estimate the temperature evolution during the filling of the mould. This work should be addressed in the future and could provide USM technology with a very useful and needed tool.

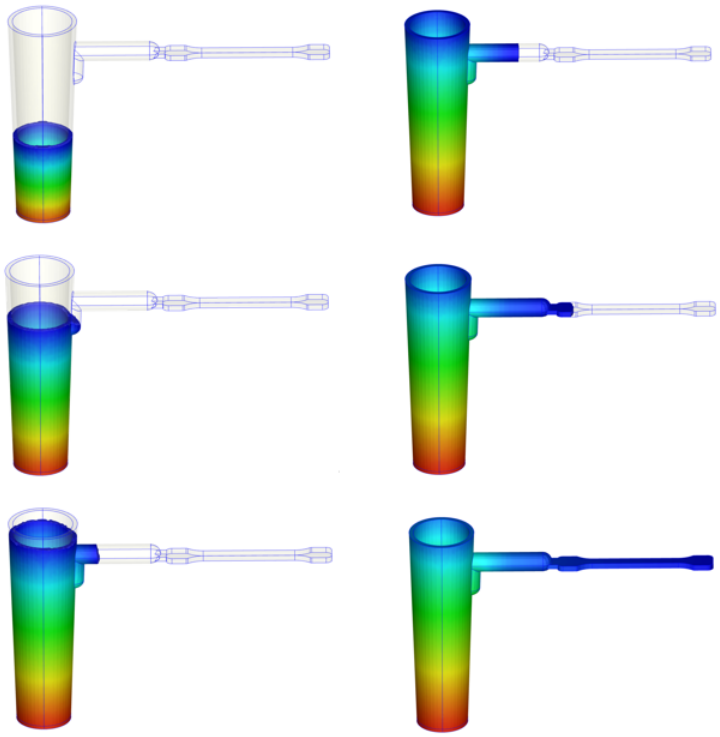

Figure 3.13: Simulation of cavity filling in nodal point ultrasonic moulding. From upper left: 30%, 60%, 80, %90%, 95% and 100% of volume filled

Figure 3.14: Filling study of a COP polymer with nodal point. Short shots at different filling times (from upper left to lower right)

3.5 Experimental setup

3.5.1 Moulding equipment

All USM experiments described in this chapter were carried out with the new Sonorus ® 2G machine prototype described in section 2.5.2. As previously indicated, the main difference between this prototype and the commercial one is the clamping system. This prototype also allows moulds up to 180 mm height while Sonorus ® 1G moulds must be lower than 100 mm. Since the nodal point method has a longer travel distance of the plunger than the standard USM method, taller moulds are needed and the new prototype is more suitable for the comparison analysis.

All the experiments made use of a Branson ® DCX 30 kHz generator with its corresponding Langevin transducer. This equipment can deliver a maximum of 15 μ of peak-to-peak amplitude. To facilitate the de-moulding of the material, the nodal point sonotrode has a conical angle which reduces its gain in comparison with conventional sonotrode used in the USM process (see Figure 3.7). This change in geometry implies that a lower amplitude is obtained with the nodal point configuration for the same percentage of power used. Thus, in order to facilitate the comparison between both configurations, the peak-to-peak output amplitude has also been included in the results.

A Babyplast ® 6/10 machine is used for the conventional injection tests in the comparison. This equipment is optimised for small samples because it can inject up to 4 cm^3 with a maximum clamping force of 62,5 kN.

3.5.2 Tools and specimens

Two moulds have been machined with the same figure cavity for USM technology and conventional injection moulding technology. In both cases the figure is a dumb-bell shaped sample with dimensions according to the EN ISO 527-2/5B standard (see Figure 3.15).

The same mould was used for both USM and NPUSM configurations, changing only the internal sleeves and the sonotrode used. An additional mould was machined for the experiments made with Babyplast ®. Both moulds contain cavities for in-mould sensors and a set of sleeves were used for each sprue and channel geometry (see Figure 3.6). Two in-mould sensors are used: a Futaba ® EPSSZL infrared sensor that is able to measure the temperature of the polymer melt up to 430 °C, and a KISTLER 6157 piezoelectric pressure sensor (0-2000 bar range). Their geometry details and locations are indicated in Figure 3.15.

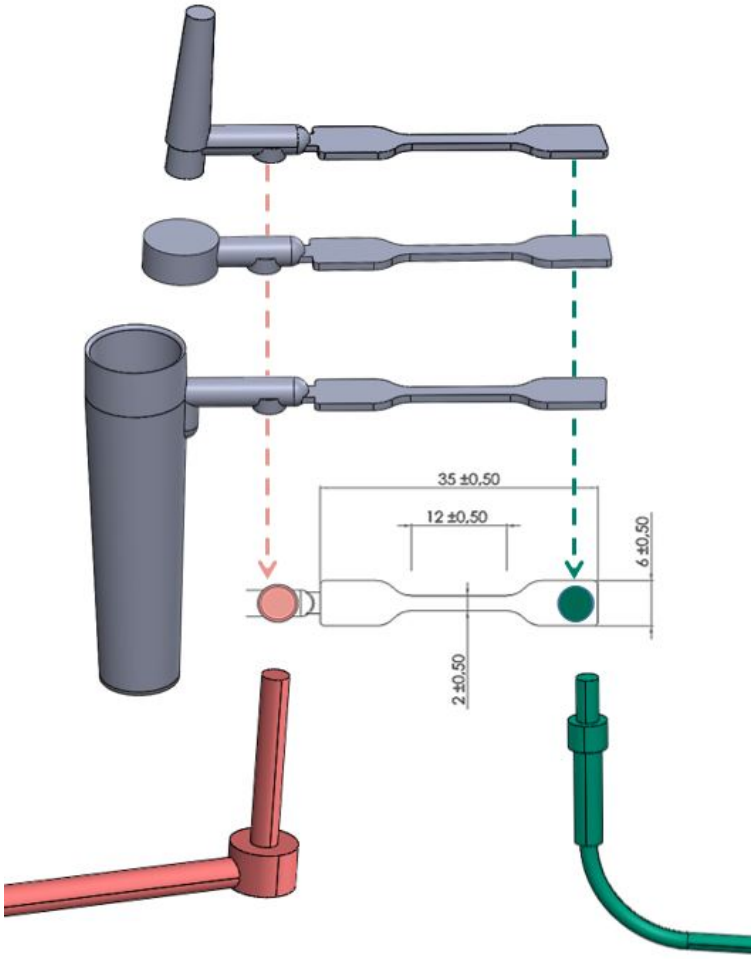

Figure 3.15: Specimens, with their sprue, obtained from: conventional injection moulding (top) , USM standard (middle), and NPUSM (bottom). Temperature sensor location is represented in red and pressure sensor in green. Sample dimensionsare in millimetres

The data obtained from the sensors is collected along with the data provided by the Sonorus® 2G machine (power, plunger displacement, frequency and plunger force) and processed and analysed using MATLAB® R2018a software.

3.5.3 Materials

In this work, two materials have been used to validate the *nodal point* configuration for ultrasonic moldeing method: A polyoxymethylene (POM) Delrin® 500P NC010 and a cyclic olefin polymer (COP) ZEONEX® E483. POM material is commonly used for high-performance engineering components such as small gear wheels, where it needs to fulfil mechanical requirements.

Moreover, POM was one of the first materials processed with USM technology [57, 61] although no study of the repeatability and performance of the method has been published. COP material is a transparent material to be used in optical and healthcare applications as an alternative to glass. Optical materials such as polycarbonate has been studied previously using ultrasonic assisted moulding by Sato et al. [6, 118]. In addition, Lu et al. [119] managed to process a similar material but much more fluid (COC Topaz ® 5013-10L) with a customized USM method. However, although the authors indicate some experimental configurations able to obtain non degraded samples, there are no details about the repeatability of the method.

All the materials used in this work have been previously dried according to the recommended processing conditions given by its manufacturer (see Table 3.2).

3.5.4 Methodology

In all the experiments of this study, the end of the filling step is determined using the force switchover point. Traditionally, ultrasonic time is the factor used as a switchover point in USM articles [14, 15, 64], . However, the newest version of Sonorus ® 1G allows to use the value of the force induced by the plunger as a switchover point. In this case, when the plunger reaches the selected force, the filling step is switched to the packing step. The use of force switchover minimizes dosing inaccuracies, as the ultrasonic time used in each shot will depend on the material dosed. For a detailed information of this method, see section 2.4.

In all the experiments, ultrasonic amplitude and plunger velocity were used as main control factors, while mould temperature, material dosage, packing conditions and cooling time were fixed for all configurations.

Material	Melt temperature	Mould temperature	Drying time	Drying temperature	Holding pressure
POM Delrin® 500P NC010	210-220 °C	80-100 °C	4h	80 °C	800-1000 bar
COP Zeonex® E483	265-295 °C	95-135 °C	4h	105 °C	no specified

Table 3.2: Injection properties of POM Delrin® 500 P NC010 [120] and COP ZEONEX® E483 [121]

Force switchover is determined as the force needed to fill the sample almost completely (similar than in conventional injection). However, in USM technology, if the force applied by the plunger is high and the material does not flow, the sonotrode receives this pressure and can produce 'overloads' (the sonotrode is unable to resonate). This phenomenon limits the maximum switchover force available and depends on the material, the dosage and the geometry of the sample. In the experiments, a 9 kN switchover force has been used for standard ultrasonic method and 11 kN for nodal point method.

In all the cases, the obtained results are compared with the samples processed by conventional injection moulding.

3.5.5 Samples characterisation

To study the USM process of POM material, a broad processing window was considered, and only 5 samples of each configuration test were analysed. Once the processing window was known, 25 samples were processed and analysed using an optimal set of parameters.
Instead, fewer configurations were studied for the processing window of COP with NPUSM, but 25 samples were analysed for each one. For each of the configurations tested, the first 5 samples were discarded from the analysis. For both materials 5 samples of each configuration were mechanically tested. Three additional POM samples were processed with the best configuration obtained in each method and molecular weight (Mw) under ISO 16014-2 regulation was evaluated. Instead, stress patterns were obtained and compared for COP samples.

The mechanical properties were determined by means of uniaxial tensile tests with the following objectives:

- Analyse the quality of the parts fabricated by USM with the new configuration of the sonotrode at nodal point,
- Compare the results of specimens obtained using the two USM techniques, and
- Evaluate the capacity of this new NPUSM configuration to manufacture medium and long series of pieces in a stable way and with repetitive quality (see section 3.6.1).

Mechanical properties of specimens were evaluated through tensile tests under UNE EN 527 regulation. A Zwick/Roell ® Z050 machine is used with a 500 N charge cell. All tests were performed at a velocity of 50 mm/min. A stress-strain curve was obtained for each sample and values of yield stress and strain at break are were calculated.

The estimated molecular weight was obtained by analysing two regions of each sample (a proximal zone, A, and a distal one, B), from the injection gate, as indicated in Figure 3.16 with a Shimadzu® LC-8A Gel Permeation Chromatography (GPC) equipment. The polymer was dissolved in hexafluorisopropanol (HFIP) at a flow rate of 1 mL/min flow and a sample concentration of 2 mg/mL. The number and weight average molecular weights were calculated using polymethacrylate standards. For the stress patterns, a binocular microscope Seafront® WF10X/20 was used along with a software to capture images.

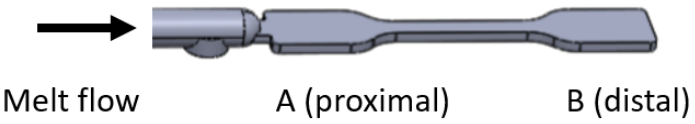

Figure 3.16: Sketch of the specimens indicating the areas, A and B, in which the molecular weight has been determined

3.6 Results: Polyexymethylene processing

First of all the shape and magnitude of the sprue obtained for each of the injection processes here considered must be highlighted. The schemes in Figure 3.15 already show this aspect, which is confirmed by the photograph of real samples in Figure 3.8. In both representations, the large sprue obtained in the USM with a nodal point configuration is clearly evident, compared to the ones obtained by the other two techniques. This is due to the fact that the closure of the plasticising chamber with the sonotrode in the nodal point position leaves a hollow cylindrical sprue of similar weight to that obtained in macro-injection, but higher in weight than that of the standard USM and of the conventional micro injection processes. This issue can be a major drawback in the moulding of high valued polymers and should be addressed in future works.

3.6.1 Processing window

Recorded data

For each experimental run, output data from the Sonorus ® machine was collected along with the data obtained from in-mould sensors. The analysis of this data allows a better understanding of the USM process. As it can be seen in Figure 3.19, maximum temperatures occur when the material reaches the sensor and it can be considered as an indirect a measurement

of the melt temperature during the moulding injection. Once the material is in contact with the sensor, the outer layer of the polymer gets frozen and the recorded temperature falls. However, the inner core is still liquid and there is a continuous flow of material until all the cavity is filled. In this moment, there is a peak in the pressure and the material switches from the filling step to the packing step. As previously discussed in section 2.4, in these experiments, the force of the plunger was used as a switchover trigger between filling and packing steps.

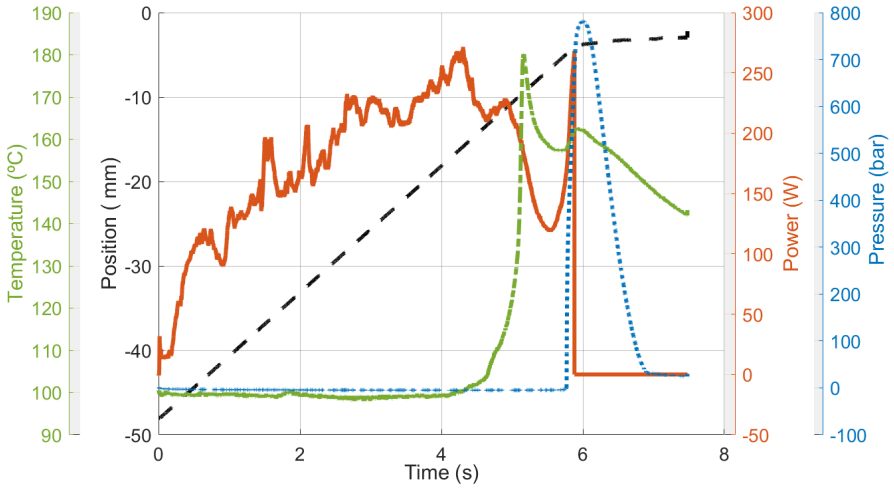

Figure 3.17: Output data obtained for a POM sample processed with NPUSM at 60% amplitude and 5 mm/s speed : Plunger position (–), Ultrasonic power (-), In-mould temperature (--.-) and in-mould pressure (-. . .)

Standard USM results

The processing window obtained with USM standard moulding method detailed in Table 3.3 shows several combinations of ultrasonic amplitude and plunger velocity with good filling repeatability. However, amplitudes higher than 46 μm were needed to fill the samples, which resulted in temperatures recorded being much higher than the ones recommended by the manufacturer, while maximum pressures reached were lower than the recommended ones. In addition, all configurations have very large scatter, which is an indicator that the mechanical properties of the specimens obtained may not be repetitive.

	Plunger velocity (mm/s) [cm^3/s]		
Ultrasonic amplitude (%) [μm]	3 [0.15]	4 [0.2]	5 [0.25]
50 [57]	$T = 327 \pm 36$ °C $P = 434.8 \pm 26.3$ bar	$T = 315.3 \pm 29.8$ °C $P = 36.2 \pm 44.3$ bar	Not filled
55 [52]	Visually degraded	$T = 314.8 \pm 20.8$ °C $P = 330.2 \pm 66$ bar	$T = 339.6 \pm 23.1$ °C $P = 162.2 \pm 68.5$ bar
60 [56]	Visually degraded	$T = 326.8 \pm 21.3$ °C $P = 429.4 \pm 52.4$ bar	$T = 350.6 \pm 43.9$ °C $P = 256.8 \pm 201.7$ bar

Table 3.3: Processing window for POM using the standard USM configuration. In-mould maximum temperatures (mean ± standard deviation) and maximum pressures (mean ± standard deviation) measured for several combinations of ultrasonic amplitude and plunger velocity

NPUSM results

NPUSM configuration allowed processing POM at lower ultrasonic amplitudes and, thus, a much bigger processing window was obtained. Recorded temperatures show that the material can be moulded at lower temperatures than with standard USM configuration. Higher pressures in cavity are measured and configurations with low scatter are obtained. Experimental configurations that fulfil the injection recommendations of the material manufacturer (melt temperatures lower than 220 °C and pressure in cavity higher than 800 bar) and have a standard deviation in temperature lower than 10 °C are highlighted in Table 3.4. The curves obtained for these configurations are displayed in Appendix A.

Ultrasonic amplitude (%) [μm]	Plunger velocity (mm/s) [cm^3/s]				
	2 [0.1]	3 [0.15]	4 [0.2]	5 [0.25]	6 [0.3]
35 [21]	$T = 154.2 \pm 47.7°$ C $P = 269.4 \pm 466$ bar	not filled	not filled	not filled	not filled
40 [24]	$T = 192.7 \pm 39.4°$C $P = 802.9 \pm 77.7$bar	$T = 112.5 \pm 17°$ C $P = 0.3 \pm 0.3$ bar	not filled	not filled	not filled
45 [27]	$T = 181.5 \pm 16.4°$C $P = 794.1 \pm 105$ bar	$T = 222.3 \pm 58.2°$C $P = 639.7 \pm 382$ bar	not filled	not filled	not filled
50 [30]	$T = 189.2 \pm 2.9°$C $P = 798.1 \pm 23.7$ bar	$T = 180.7 \pm 1.9°$C $P = 853.5 \pm 43$ bar	$T = 205.2 \pm 24.8°$C $P = 361.3 \pm 332$ bar	$T = 192.4 \pm 21.2°$C $P = 353.7 \pm 500$ bar	$T = 131.5 \pm 41.3°$C $P = 20.2 \pm 28.5$ bar
55 [33]	$T = 197.0 \pm 7.4°$C $P = 892.9 \pm 67.5$ bar	$T = 188.1 \pm 3.3°$C $P = 912.6 \pm 28.2$ bar	$T = 180.2 \pm 2.2°$C $P = 866.5 \pm 14.6$ bar	$T = 186.8 \pm 7.3°$C $P = 722.3 \pm 150$ bar	$T = 245.4 \pm 65.8°$C $P = 408.0 \pm 202$ bar
60 [36]	$T = 237.1 \pm 44.7°$C $P = 886.4 \pm 57.6$ bar	$T = 214.5 \pm 12.1°$C $P = 976.9 \pm 40.8$ bar	$T = 189.2 \pm 7.4°$C $P = 924.3 \pm 6$ bar	$T = 187.3 \pm 6°$C $P = 823.1 \pm 12.4$ bar	$T = 200.0 \pm 12.4°$C $P = 628.6 \pm 115$ bar
65 [39]	$T = 270.8 \pm 44.3°$C $P = 943.4 \pm 19.7$ bar	$T = 242.0 \pm 25.7°$C $P = 951.3 \pm 56.8$ bar	$T = 242.9 \pm 17.8°$C $P = 931.9 \pm 53$ bar	$T = 190.3 \pm 5°$C $P = 843.8 \pm 82$ bar	$T = 192.2 \pm 6.1°$C $P = 795.4 \pm 136$ bar
70 [42]	$T = 245.5 \pm 27.4°$C $P = 990.3 \pm 15.7$ bar	$T = 257.5 \pm 42.2°$C $P = 978.0 \pm 29.7$ bar	$T = 262.7 \pm 37.1°$C $P = 961 \pm 56.3$ bar	$T = 254.2 \pm 28.4°$C $P = 938.7 \pm 61.1$ bar	$T = 247.2 \pm 48.8°$C $P = 898.7 \pm 26.6$ bar
75 [45]	$T = 268.7 \pm 11.5°$C $P = 1024.6 \pm 10$ bar	$T = 238.4 \pm 42.7°$C $P = 991.8 \pm 14.7$ bar	$T = 293.3 \pm 39.7°$C $P = 983.4 \pm 26.3$ bar	$T = 292 \pm 40.5°$C $P = 964 \pm 61.4$ bar	$T = 263 \pm 28.1°$C $P = 937.3 \pm 58.9$ bar

Table 3.4: Processing window for POM using NPUSM configuration. In-mould maximum temperatures (mean $\pm$ standard deviation) and maximum pressures (mean $\pm$ standard deviation). Configurations that meet the manufacturer requirements are highlighted

Conventional injection moulding results

Conventional injection experiments were carried out with a Babyplast® 6/10 injection machine using the same in-mould temperature and pressure sensors. A dedicated mould was machined with the same cavity geometry (see Figure 3.18).

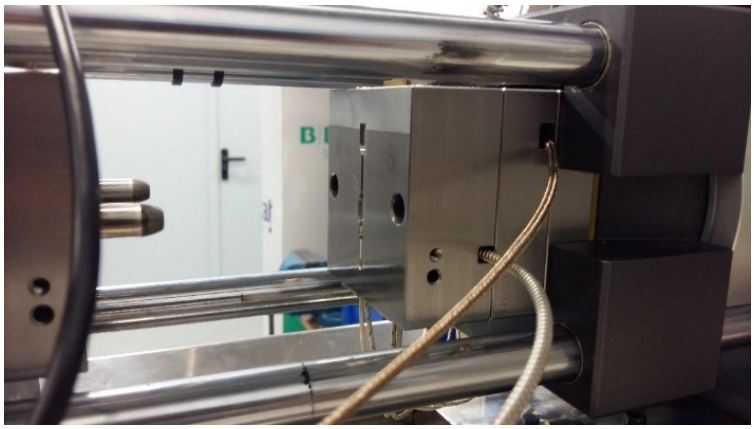

Figure 3.18: Babyplast ® mould

Plasticising temperature in hopper	200 °C
Mould temperature	66 °C
Injection velocity	9 mm/s [0.7 cm^3/s]
Injection time	1.2 s

Table 3.5: Babyplast ® 6/10 injection parameters

Main parameters used to inject POM samples are presented in Table 3.5.

Once the machine was in steady-state, 50 samples were obtained. Recorded temperatures and pressures were analysed and maximums and standard deviations were computed. In-mould maximum temperature recorded was $T = 199.7 \pm 1.7$ °C, and maximum pressure $P = 975.7 \pm 3.1$ bar These results meet the manufacturer recommendations and have a very low scatter, proving that conventional microinjection moulding is a very stable process.

Analysis of the results

Filling stability has been one of the main drawbacks of USM process, particularly when dealing with high performance polymers [61]. In view of the results obtained with standard USM, presented in Table 3.3, none of the tested configurations of parameters fulfil the recommendations of the manufacturer, as the temperature is much more higher than the recommended one and the pressure obtained in the cavity is lower. Besides, all configurations present very large scatter. These factors indicate that the polymer is not well processed, even if they show an acceptable visual aspect.

On the contrary, for certain combinations of input parameters, NPUSM method is able to process POM with the recommended temperature and pressure from the manufacturer and with low scatter in the results. In addition, when processing the material with standard USM process, only 6 configurations of process parameters produced completely filled samples with no burned parts. Instead, the processing window obtained with nodal point method shows that in 50 out of 60 configurations tested the sample was completely filled without burns and the process was repetitive.

The comparison of the results from the three methods shows that NPUSM configuration is much more stable than the standard USM one. However, still, conventional injection moulding has lower scatter. In Figure 3.19, cavity temperatures and pressures obtained in the best configurations for each method are presented. It can be visually observed that the samples processed with standard USM method have a high scatter in temperature and pressure values.

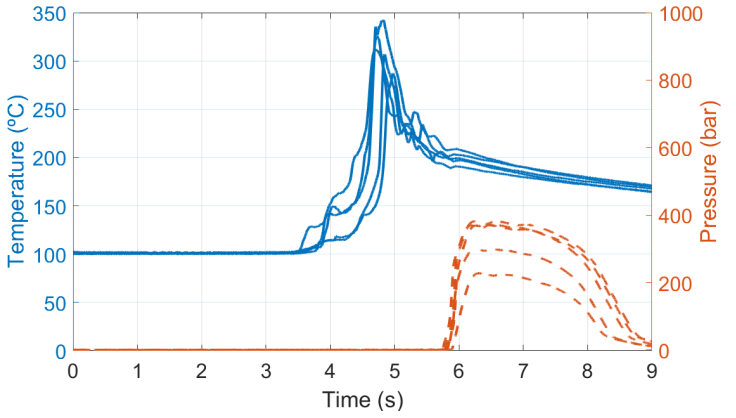

(a) USM

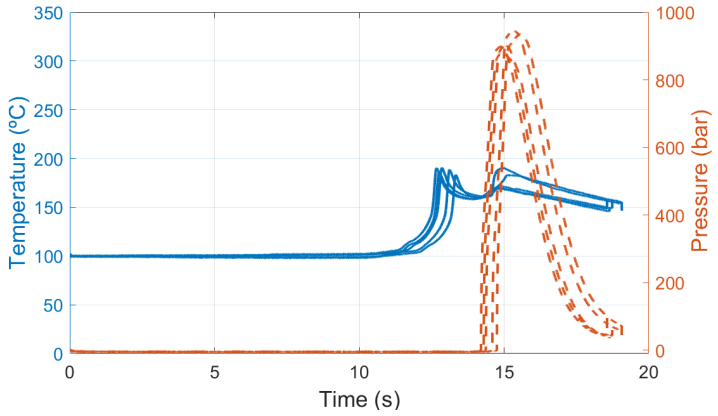

(b) NPSUM

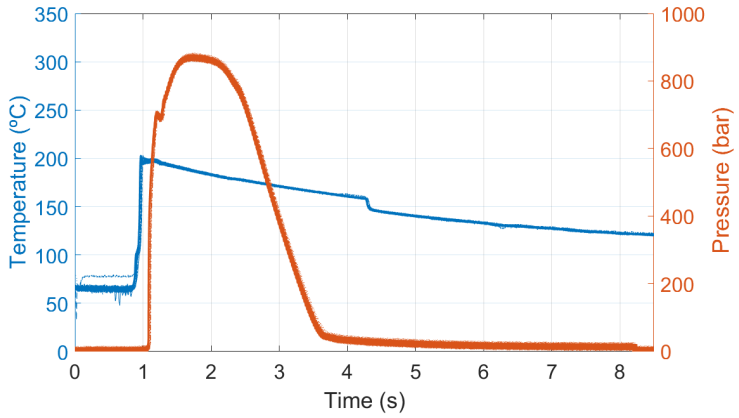

(c) Conventional Injection

Figure 3.19: In mould temperatures and pressures obtained for a) standard USM (55% amplitude, 4 mm/s velocity), b) nodal point USM (55% amplitude, 3 mm/s velocity) and c) Babyplast ® with optimised process parameters

The recommended temperature range for POM Delrin® NC10 processing is 210-220 °C, according to the manufacturer datasheet. When processing this material with standard USM methodology, the material must be heated at least 100 °C more to fill completely the sample. On the contrary, with nodal point method it is possible to process the material at the temperature recommended in the material datasheet.

Such difference on material behaviour is probably related with the hesitation effect produced by the gap between the mould and the sonotrode that obstructs the filling of the material (as it can be seen in the simulations done in section 3.4), then the material stops and increases its temperature until is able to fill again.

Another hypothesis is that the lower distance between the plasticising chamber and the cavity gate in standard USM is dragging unmelted material and making it difficult to fill the cavity unless the material is much more fluid (higher temperatures). The short distance between the plasticisation chamber to the moulded part was already identified by Grabalosa et al.[11] as a possible source for defects at the sample caused by a lack of homogenization. However, in nodal point method, there is a larger distance between the plasticisation chamber and the cavity gate, and the material is flowing through a vibrating sonotrode which is expected to help the homogenization of the material. This difference of behaviour can be observed when processing transparent material like a cyclic olefin polymer (COP) and will be discussed in section 3.7.

3.6.2 Mechanical properties

According to the material supplier, an ideally processed sample of POM Delrin ® 500P NC010 should have a yield stress of 71 MPa and a nominal strain at break of 30 % [120]. Tables 3.6 and 3.7 show the obtained results for the different combinations of parameters of both processes.

Ultrasonic amplitude (%) [μm]	Plunger velocity (mm/s) [cm^3/s]		
	3 [0.15]	4 [0.2]	5 [0.25]
50 [47]	$\sigma_\gamma = 45.2 \pm 24.5$ MPa $\epsilon_\gamma = 8.4 \pm 7.4\%$	$\sigma_\gamma = 52.2 \pm 17.2$ MPa $\epsilon_\gamma = 5.39 \pm 3.17$ %	Not filled
55 [52]		$\sigma_\gamma = 67.5 \pm 1$ MPa $\epsilon_\gamma = 13.5 \pm 4.5\%$	$\sigma_\gamma = 64.4 \pm 5.8$ MPa $\epsilon_\gamma = 8.5 \pm 3.7$ %
60 [56]		$\sigma_\gamma = 45.3 \pm 28.6$ MPa $\epsilon_\gamma = 4.3 \pm 2.9\%$	$\sigma_\gamma = 37.1 \pm 19.4$ MPa $\epsilon_\gamma = 4.5 \pm 2.6\%$

Table 3.6: Tensile properties (yield stress, σ_γ, and strain at break, ϵ_γ) of the POM Delrin ® 500P NC010 specimens manufactured by standard ultrasonic moulding

As it can be seen in Table 3.6, none of the combinations of parameters of standard USM process allows obtaining the desired mechanical properties. The low value of the ductility of the tested samples should be particularly emphasized.

Ultrasonic amplitude (%) [μm]	Plunger velocity (mm/s) [cm^3/s]				
	2 [0.1]	3 [0.15]	4 [0.2]	5 [0.25]	6 [0.3]
45 [27]	$\sigma_\gamma 74.6 \pm 0.1$ MPa $\epsilon_\gamma = 20.5 \pm 1.4\%$	$\sigma_\gamma 29.8 \pm 40.7$ MPa $\epsilon_\gamma = 10.9 \pm 9.2\%$			
50 [30]	$\sigma_\gamma 74.3 \pm 0.3$ MPa $\epsilon_\gamma = 24.4 \pm 1.6\%$	$\sigma_\gamma 73.8 \pm 0.2$ MPa $\epsilon_\gamma = 27.4 \pm 3.1\%$			
55 [33]	$\sigma_\gamma 74.6 \pm 0.43$ MPa $\epsilon_\gamma = 24.4 \pm 2.3\%$	$\sigma_\gamma 73.6 \pm 0.2$ MPa $\epsilon_\gamma = 28.7 \pm 2.4\%$	$\sigma_\gamma 72.9 \pm 0.5$ MPa $\epsilon_\gamma = 23 \pm 5.2\%$	$\sigma_\gamma 72.4 \pm 0.3$ MPa $\epsilon_\gamma = 18.7 \pm 5.6\%$	$\sigma_\gamma 54.1 \pm 30$ MPa $\epsilon_\gamma = 14.1 \pm 9.6\%$
60 [36]	$\sigma_\gamma 14.8 \pm 33.2$ MPa $\epsilon_\gamma = 6.7 \pm 6.9\%$	$\sigma_\gamma 29.3 \pm 40.1$ MPa $\epsilon_\gamma = 13 \pm 12.2\%$	$\sigma_\gamma 71.5 \pm 2.2$ MPa $\epsilon_\gamma = 25.6 \pm 1.6\%$	$\sigma_\gamma 72.1 \pm 0.2$ MPa $\epsilon_\gamma = 26.9 \pm 1.8\%$	$\sigma_\gamma 56.6 \pm 31.6$ MPa $\epsilon_\gamma = 21.7 \pm 7.9\%$
65 [39]				$\sigma_\gamma 72.1 \pm 0.3$ MPa $\epsilon_\gamma = 22,6 \pm 2\%$	$\sigma_\gamma 71.4 \pm 0.4$ MPa $\epsilon_\gamma = 24.9 \pm 2.5\%$

Table 3.7: Tensile properties (yield stress, σ_γ, and strain at break, ϵ_γ) of the POM Delrin ® 500P NC010 specimens manufactured by NPUSM. The combinations of process parameters that fulfil the material datasheet recommendations are highlighted

For the samples manufactured using NPUSM, tensile properties of the same order of magnitude of those expected are obtained for various combinations of the process parameters, as it can be seen from observing the values in Table 3.7. In these particular cases, higher yield stresses and slightly lower strain fractures than the recommended values were reached. On the other hand, the samples processed with conventional injection moulding present a yield stress of 68.2 ± 0.1 MPa and a strain at break of 26.8 ± 0.6 %.

Both values are slightly lower than the values provided by the manufacturer. In Table 3.8, the mechanical properties of the specimens prepared with the best configuration of each method are presented and compared with the values recommended in the material datasheet. These results show that the samples obtained with NPUSM configuration have the highest yield stress. In addition, although samples processed with Babyplast ® machine show the best repeatability in mechanical properties, several configurations tested with NPUSM configuration also present very low dispersion in the results

	Manufacturer Datasheet	Standard USM	Nodal Point USM	Babyplast 6/10
(Amplitude,Velocity)		$(55\%, 4mm/s)$	$(60\%, 5mm/s)$	Best parameters
Yield stress (MPa)	70	$67,5 \pm 1$	$72,1 \pm 0,23$	$68,2 \pm 0,1$
Strain at break $(\%)$	30	$13,5 \pm 4,5$	$26,9 \pm 3$	$26,8 \pm 0,6$

Table 3.8: POM tensile test results comparison for the best configurations of each moulding technology

3.6.3 Molecular weight

Average molecular weights and polydispersity index were measured in two different specimens processed using the best configuration of parameters for each method.As previously indicated in section 3.5.4, for each specimen, two measures were taken in the proximal and distal zone from the gate. The results show that the variation of the molecular weight of the samples obtained through USM processes are similar to the one observed in the specimens manufactured by conventional injection moulding. Although standard USM presents a lower weight average molecular weight (M_w) than the other processing techniques, the difference does not seem relevant enough to indicate an ultrasonic degradation due to chain scission (see Figure 3.20). On the other hand, the polydispersity index measured in the samples processed with NPSUM is slightly lower than the values obtained for the rest of samples, suggesting a uniform molecular size in the samples. These results, summarized in Table 3.9 indicate that the molecular structure has been preserved in the samples processed with NPUSM although further research is still needed to completely characterise this method.

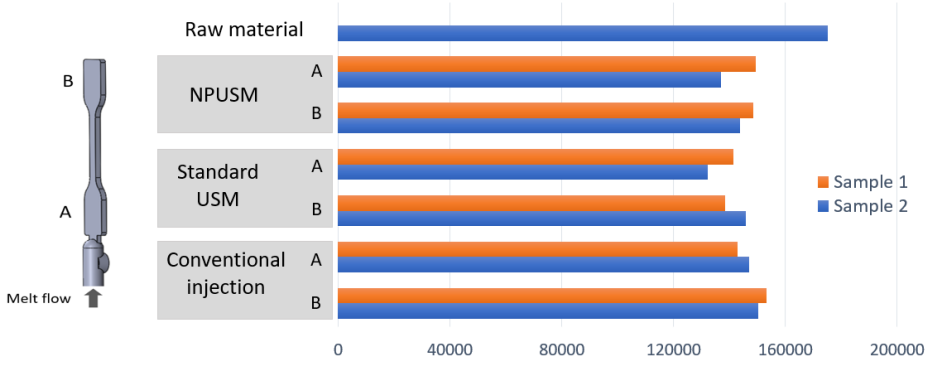

Figure 3.20: Measured molecular weight (M_w) of POM samples at proximal (A) and distal (B) zones , processed with diferent methods

		M_n (g/mol)		M_w (g/mol)		M_w/M_n	
	Zone	Sample 1	Sample 2	Sample 1	Sample 2	Sample 1	Sample 2
Raw material		40301		175242		4.35	
NPSUM	A	50957	48000	137033	149553	2.69	3.12
	B	58965	35691	143930	148673	2.44	4.17
Standard USM	A	23051	20487	132444	141532	5.75	6.91
	B	39855	35428	146074	138627	3.67	3.91
Conventional injection	A	38760	35129	147199	143105	3.80	4.07
	B	47672	29299	150351	153232	3.15	5.23

Table 3.9: Results obtained from GPC analysis: Number average molecular weight (M_n), weight average molecular weight (M_w) and polydispersity index (M_w/M_n) obtained for each analysis

3.6.4 Repeatability of NPUSM configuration

The results presented in the previous sections show that with nodal NPUSM configuration it was possible to obtain a set of parameters that produce samples with good filling and good mechanical and thermal properties. However, as repeatability is one of the major concerns of USM technology, a larger set of specimens was processed using the best NPUSM combinations of parameters, as detailed in Table 6. In this case, 25 samples were analysed and mechanically tested.

From the analysis of these results, it can be observed that the scatter in temperature and pressure values is slightly higher than that obtained in the processing window tests. In addition, a lower average yield stress and a higher strain at break were obtained. In any case, the results presented here

Material	POM Delrin ®NC010 500P	
Number of samples tested	25	
Main processing parameters	Ultrasonic amplitude	60 % [36 μm]
	Plunger velocity	5 mm/s
	Mould temperature	90 °C
	Force switchover	11000 N
Cavity sensor measurements	Maximum temperature	195 $\pm$ 15 °C
	Maximum pressure	851.24 $\pm$ 28 bar
Mechanical tensile test results	Yield stress	69.5 $\pm$ 0.6 MPa
	Strain at break	27.8 $\pm$ 6.6 %

Table 3.10: Results of POM Delrin ® NC010 500P specimens manufactured using an stable configuration of NPUSM

are repetitive and all the specimens processed have the expected mechanical tensile properties, as shown in Figure 3.21.

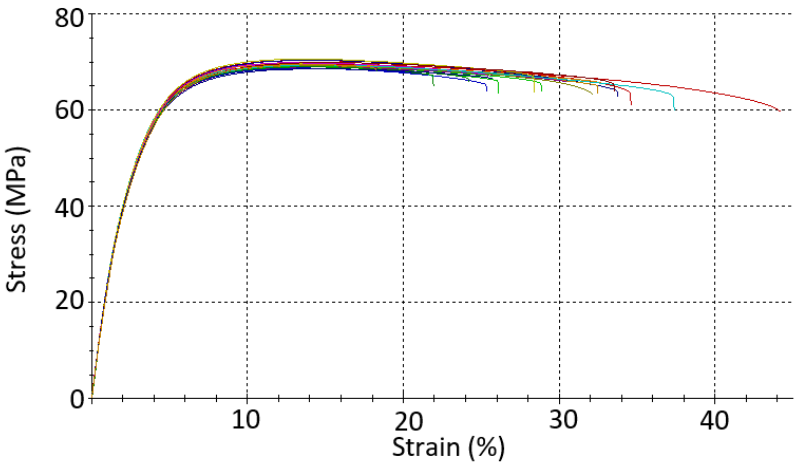

Figure 3.21: Stress–strain behaviour in uniaxial tensile tests of 25 POM specimens manufactured using the NPUSM process

3.7 Results: Cyclic olefin polymer processing

Cyclic olefin polymer (COP) is a glass-like and UV transparent polymer. It has similar barrier properties to those of glass but is less expensive. Thus, this material is very well suited to optical and healthcare applications as an alternative to glass.

3.7.1 Processing window

Recorded data

A process window for COP Zeonex ® E48R material was obtained for the nodal point method, and was compared with the samples processed using conventional injection moulding method. For each experimental run, output data from the Sonorus ® 2G machine was collected along with the data obtained from temperature and pressure in-mould sensors. The results obtained for a processed sample are displayed in Figure 3.22. As previously discussed in section 3.6, the maximum temperature can be considered as an indirect measurement of the melt temperature during the injection and is obtained when the material reaches the sensor. This material starts to cool but the inner layer is still in a melted state and causes the flow of material until the cavity is filled. At this moment, the pressure increases abruptly and indicates the end of the filling step.

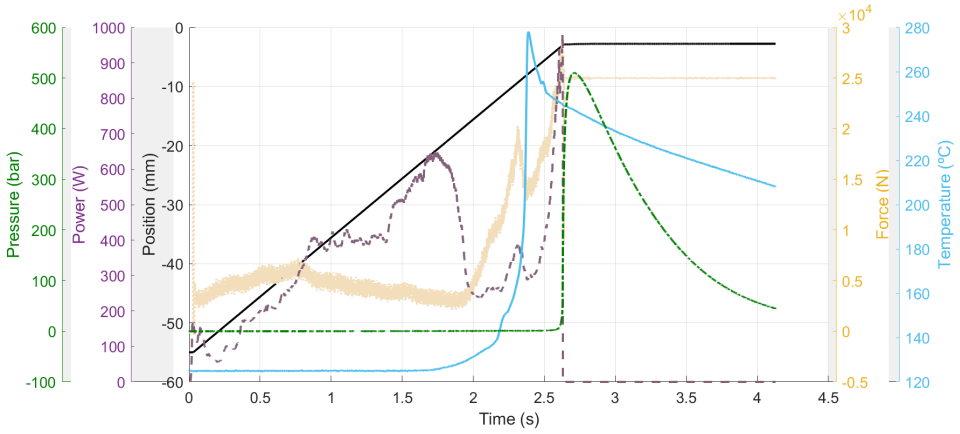

Figure 3.22: Output data obtained for a COP processed sample with NPSUM at 90 % amplitude and 10 mm/s speed: Plunger position (-), Plunger Force (-), Ultrasonic power (–), In-mould temperature (-.-) and in-mould pressure (. . .)

Standard USM results

None of the experimental configurations tested to process COP using standard USM methodology provided acceptable results. Only the configurations having a lower velocity were able to fill the cavity in a repetitive manner. However, the in-mould temperatures of the melt measured were almost 100 °C higher than the ones recommended by the manufacturer (see Table 3.11). On the other hand, the experimental configurations possessing higher velocity produced unfilled samples.
In addition, several of the experimental runs gave an *injection error* message. This error appears when the ultrasonic transducer is not able to vibrate, while maintaining the amplitude and frequency delivered by the ultrasonic generator. Although this could damage the ultrasonic transducer, nowadays, commercial ultrasonic generators are equipped with safety features that stop the signal, in order to prevent failures in the equipment.
The above-mentioned error may happen when there is frozen polymer melt attached to the sonotrode. In that case, the generator tries to maintain the amplitude and increases the frequency up to the limits of the equipment (30.75 kHz). This behaviour can be observed in Figure 3.23.

In order to find a set of parameters wherein the polymer melt is able to completely fill the sample, the plunger velocity has to be reduced to 5 mm/s. In this case, all the samples are filled, but processed at very high temperatures (see section 3.24), exhibit a fragile behaviour and break during the de-moulding.

In-mould temperatures and pressures obtained for some of these parameter configurations are displayed in Appendix A.

	Plunger velocity (mm/s) [cm^3/s]		
Ultrasonic amplitude (%) [μm]	5 [0.25]	10 [0.5]	15 [0.75]
80 [48]	$T = 393,4 \pm 35,3°$ C $P = 832,5 \pm 139,1$ bar	$T = 344,33 \pm 46,92°$ C $P = 325,83 \pm 342,37$ bar	Not filled
100 [60]	$T = 422,2 \pm 8,9°$C $P = 583,2 \pm 73,5$ bar	$T = 340,2 \pm 58,8°$C $P = 289,7 \pm 418,3$ bar	Not filled

Table 3.11: Processing window for COP using standard ultrasonic moulding configuration. In-mould maximum temperatures (mean ± standard deviation) and maximum pressures (mean ± standard deviation)

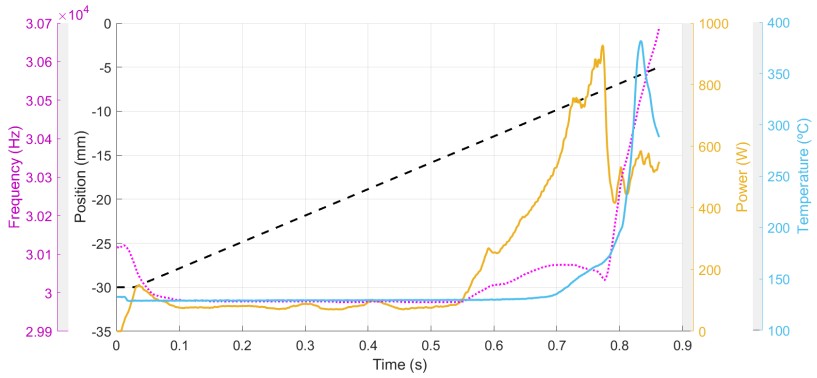

Figure 3.23: Machine data obtained for an unfilled COP sample processed with USM at 100 % amplitude and 15 mm/s plunger velocity. This cycle is prematurely stopped with an *Injection error* message as the transducer frequency is rising near its limit. Plunger position (–), Ultrasonic power (-), Frequency (..) and melt temperature (-)

NPUSM results

Several experimental configurations of parameters were obtained using NPUSM which fulfil the injection recommendations of the material manufacturer (melt temperatures lower than 295 °C [121]). In this case, a minimum pressure within the cavity is not requested. Instead, typical optical samples require as low pressure as possible, to reduce stress and birefringence. Experimental configurations that fulfil the injection recommendations and have a standard deviation in temperature lower than 10 °C are highlighted in Table 3.12. Still, there is one experimental configuration (80% amplitude and 14 mm/s velocity) that complies with the temperature requisites but has a very large standard deviation in the pressure values, which indicates an unstable point and it is not highlighted as a good configuration.
Temperatures and pressures obtained for the tested configurations are displayed in the Appendix A.

Conventional injection moulding results

Conventional injection moulding experiments have been carried out with a Babyplast®6/10 injection machine, using the same in-mould temperature and pressure sensors. Further, the same mould previously described in section 3.6.1 was used (see Figure 3.18). The main parameters used to inject POM samples are presented in Table 3.13.

Once the machine was in steady-state, 50 samples were obtained. Recorded temperatures and pressures were analysed and maximums and standard deviations were computed. In-mould maximum temperature recorded was $T = 284 \pm 0.6$ °C, and maximum pressure was $P = 668.1 \pm 4.9$ bar. As previously observed in section 3.6.1 for POM processing, the results obtained

	Plunger velocity (mm/s) [cm^3/s]		
Ultrasonic amplitude (%) [μm]	10 [0.5]	12 [0.6]	14 [0.7]
80 [48]	$T = 284,4 \pm 9,3$ °C $P = 514,7 \pm 21,1$ bar	$T = 281,6 \pm 6,2$ °C $P = 538,8 \pm 18$ bar	$T = 276,3 \pm 4,3$ °C $P = 467,9 \pm 142,4$ bar
90 [54]	$T = 302 \pm 8,4$ °C $P = 450,1 \pm 21,6$ bar	$T = 294,3 \pm 5,4$ °C $P = 498,5 \pm 14,9$ bar	$T = 293,2 \pm 6,1$ °C $P = 505,2 \pm 20,5$ bar
100 [60]	$T = 320 \pm 31,5$ °C $P = 395 \pm 30,7$ bar	$T = 310,8 \pm 10,2$ °C $P = 428,5 \pm 26,4$ bar	$T = 305,5 \pm 9,1$ °C $P = 467,5 \pm 22,9$ bar

Table 3.12: Processing window for COP using NPUSM configuration. In-mould maximum temperatures (mean ± standard deviation) and maximum pressures (mean ± standard deviation). Configurations that meet the manufacturer requirements are highlighted

Plasticising temperature in hopper	275 °C
Mould temperature	104 °C
Injection velocity	12 mm/s [0.94 cm^3/s]
Injection time	0.8 s

Table 3.13: Babyplast® 6/10 COP injection parameters

from conventional injection moulding also meet the manufacturer recommendations for COP material and have a very low scatter.

Analysis of the results

Filling COP samples in a repetitive way using standard USM method was possible with almost any of the parameters' configurations tested. In the only configuration that allowed completely filled cavities, the samples were processed at very high temperatures and exhibited fragile behaviour.
On the contrary, for multiple combinations of input parameters, the NPUSM method was able to completely fill COP samples. In several cases, the samples processed fulfil the recommended temperature from the manufacturer with low scatter in the results.

The comparison of the results between the different methods shows that, contrary to the standard USM method, the NPUSM configuration is able to correctly process COP material. Although conventional injection moulding has lower scatter in the results, in-mould recorded values for NPUSM configuration show a good stability of the method. Cavity temperatures and pressures obtained in the best configurations for each method are presented in Figure 3.24.

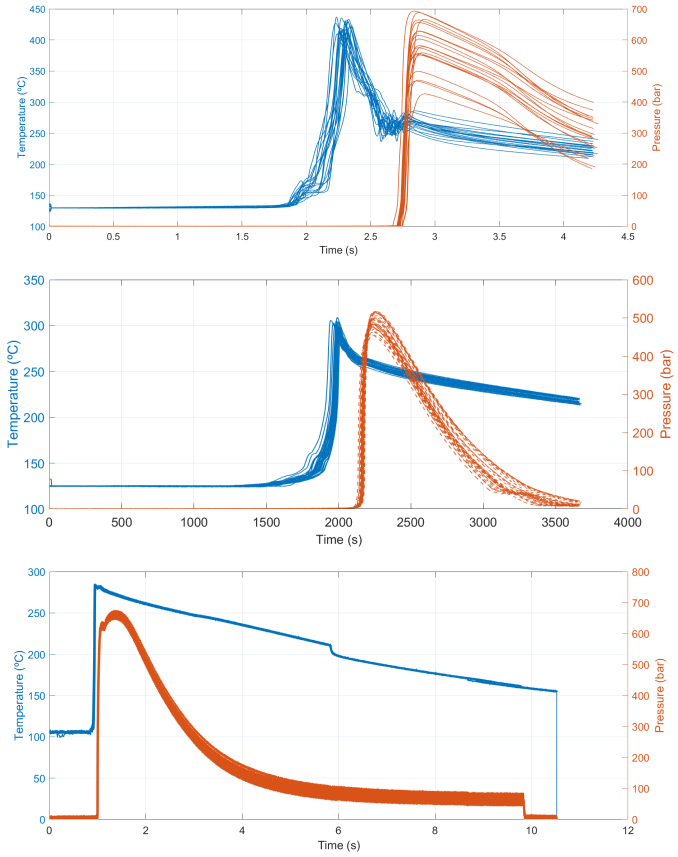

Figure 3.24: In mould temperatures and pressures obtained for (top) standard USM, (middle) NPUSM (90% amplitude, 12 mm/s velocity) and, (bottom) Babyplast ® with optimised process parameters for COP samples

The recommended temperature range for COP Zeonex ® E48R processing is 265-295 °C, according to the manufacturer datasheet [121]. Standard USM methodology is not able to correctly fill the dogbone sample with this material in a repetitive way. On the contrary, using the nodal point method it is possible to process the material at the temperature recommended in the material datasheet. Such difference in material behaviour could be related to the plasticising chamber geometry and the presence of inhomogeneities in the melt, as previously discussed in case of POM processing in section 3.6.

3.7.2 Mechanical properties

The mechanical properties of standard USM processed samples were measured only for one parameter configuration, as in the rest of the configurations, samples were fragile and broke during the de-moulding step. The values obtained from the tensile strain tests for the samples processed at 100% amplitude and 5 mm/s velocity present a yield stress of 49.8 ± 12.6 MPa and a strain at break of 5.2 ± 1.6 %. These results do not fulfil the material

	Plunger velocity (mm/s) [cm^3/s]		
Ultrasonic amplitude (%) [μm]	10 [0.5]	12 [0.6]	14 [0.7]
80 [48]	$\sigma_\gamma = 77.6 \pm 2.3$ MPa $\epsilon_\gamma = 8.2 \pm 0.2\%$	$\sigma_\gamma = 77.8 \pm 1.3$ MPa $\epsilon_\gamma = 7.9 \pm 0.3$ %	$\sigma_\gamma = 78.7 \pm 0.4$ MPa $\epsilon_\gamma = 7.7 \pm 0.1$ %
90 [54]	$\sigma_\gamma = 76.4 \pm 1.4$ MPa $\epsilon_\gamma = 8 \pm 0.8\%$	$\sigma_\gamma = 78.2 \pm 0.7$ MPa $\epsilon_\gamma = 7.9 \pm 0.1$ %	$\sigma_\gamma = 77.4 \pm 0.9$ MPa $\epsilon_\gamma = 7.6 \pm 0.4$ %
100 [60]	$\sigma_\gamma = 74.4 \pm 3.9$ MPa $\epsilon_\gamma = 7.8 \pm 1.1\%$	$\sigma_\gamma = 77.2 \pm 1.4$ MPa $\epsilon_\gamma = 7.8 \pm 0.1$ %	$\sigma_\gamma = 77.8 \pm 0.6$ MPa $\epsilon_\gamma = 7.7 \pm 0.2$ %

Table 3.14: Tensile properties (yield stress, σ_γ, and strain at break, ϵ_γ) of COP Zeonex ® E48R manufactured by NPUSM

datasheet requirements, and present a large scattering in the results. The tensile results graph is displayed in Appendix A.

Instead, the mechanical properties of five samples manufactured using ultrasonic moulding with nodal point configuration were determined for each experimental configuration. For this type of material, mechanical properties are provided for the elastic zone. According to the material supplier, a good processed sample of Zeonex® E48R should have a yield stress of 73 MPa and a nominal strain at yield of 5% [122].

The samples obtained using NPSUM fulfil the mechanical requirements in all the configurations (see Table 3.14).

The samples processed with conventional injection moulding present a yield stress of 74.3 ± 0.1 MPa and a strain at yield of 5 ± 0.1 %. Both values fulfil the specifications provided by the manufacturer. In Table 3.15, the mechanical properties of the specimens prepared with the best configuration of each method are presented and compared with the values recommended in the material datasheet. These results show that the samples obtained using NPUSM configuration have the highest yield stress and strain at break.

	Manufacturer Datasheet	Standard USM	Nodal Point USM	Babyplast 6/10
(Amplitude,Velocity)		$(100\%, 5mm/s)$	$(90\%, 12mm/s)$	Best parameters
Yield stress (MPa)	73	49.8 ± 12.6	78.2 ± 0.7	74.3 ± 0.1
Strain at break (%)	5	5.2 ± 1.6	7.9 ± 0.1	5 ± 0.1

Table 3.15: COP tensile test results comparison for the best configurations of each moulding technology

Although the samples processed using the Babyplast ® machine show the best repeatability in mechanical properties, the samples obtained using NPUSM configuration also present low dispersion in the results and better mechanical properties. Specially, the samples processed using NPUSM present a longer elongation at yield. The reason for this behaviour and its association with the influence of ultrasounds in the polymer has to be further studied.

3.7.3 Stress patterns

In this section, a qualitative analysis of stress patterns has been performed. The study of the changes in the optical properties of a material under mechanical deformation is called photoelasticity. This technique is often used to determine the stress distribution in materials and geometries. Although, in these experiments, the cavity figure was a tensile specimen instead of an optical lens, it is still possible to see if the material could be fitted for optical use by using photoelastic experiments.

Several images were taken for processed samples using the different methods presented above. Upon comparing Figures 3.25, 3.26 and 3.27, it can be seen that both NPUSM and conventional injection present a fairly homogeneous pattern, whereas standard USM shows a lot of inhomogeneities in the sample. These inhomogeneities seem to be related to the presence of unmelted material in the sample, which reinforces the hypothesis described in section 3.6.1. On the other hand, samples processed using NPSUM and conventional injection do not seem to show any presence of unmelted material.

Besides, although the colour scale could be different from shot to shot, it is worth noticing that nodal point samples have lesser stress than samples processed using conventional injection. This is particularly clear in the proximal region (the region near the gate), wherein the conventional injection sample presents some zones of high stress. A possible reason for this difference in behaviour could be the lower shear stress in NPSUM samples due to a lower injection velocity or a higher fluidity of the material, as a result of the application of ultrasounds. In any case, further work is needed in order to quantify this behaviour.

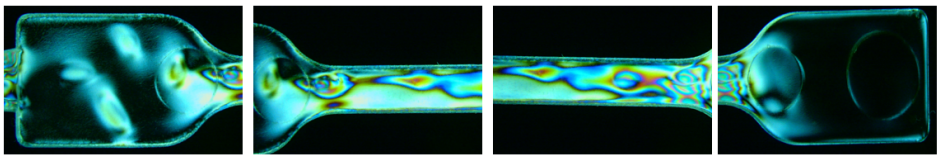

Figure 3.25: Polarized images of a COP Zeonex® 48R sample processed using standard USM

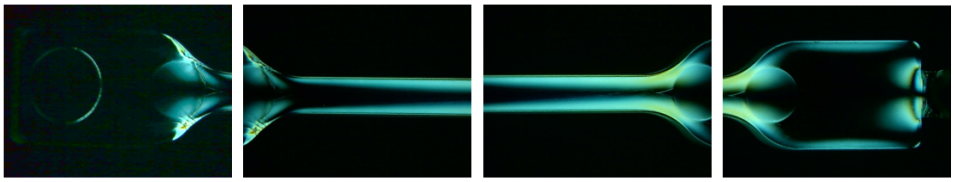

Figure 3.26: Polarized images of a COP Zeonex® 48R sample processed using nodal point USM

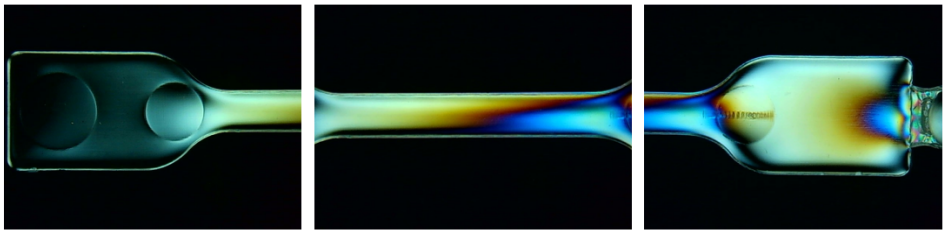

Figure 3.27: Polarized images of a COP Zeonex ®48R sample processed using conventional injection

3.8 Conclusions

The results presented in this chapter show that an improvement in the quality of the manufactured parts, as well as in the repeatability of this quality, can be achieved by incorporating the concept of *nodal point* into the standard ultrasonic micro-moulding technology. The experimental process and characterisation tests carried out demonstrate this for a polyoxymethylene (Delrin® 500P NC010) and a cyclic olefin polymer (Zeonex ® E48R).

The best processing conditions in the process window for these polymers perfectly match the recommendations given by the raw material provider, in terms of the melt temperature and the pressure developed in the mould cavity. These process parameters have allowed the manufacture under stable conditions of a large number of tensile specimens, whose physical

and mechanical properties (geometry, presence / absence of defects, stress-strain ratio in uniaxial tensile tests, molecular weight and stress patterns) meet the requirements for this type of components.

The results obtained for NPUSM processing are comparable with those obtained in equal specimens manufactured using the well-established conventional injection moulding technology. The values of the tensile properties are similar or even slightly higher for the nodal point configuration. However, the deviations in these values are still higher than those measured in the specimens prepared by conventional injection moulding. In any case, the ability to process these materials has improved greatly with the use of NPUSM configuration in comparison with standard USM.

To sum up, the results of this research show that the use of NPUSM is a robust technique, which improves the processability of polyoxymethylene and cyclic olefin. Further, it stands as a convincing industrial technique for manufacturing polymeric parts.

4
Ultrasonic heating evolution

4.1 Introduction

As described in Chapters 2 and 3, the devices used for the manufacture of specimens by ultrasonic moulding (USM) have been adapted in order to stabilise the process and ensure repetitive quality of the final component. All of them use high power generators and piezoelectric transducers to produce ultrasonic mechanical oscillations and transmit them to a sonotrode. Also, in all the cases, a plunger pushes the polymeric pellets to this vibrating sonotrode to plasticise it. The polymer is then heated, melted and pushed into the mould cavity.

However, in practice, these steps are not completely sequential and the heating and filling processes are strongly coupled (melted polymer is being pushed to the mould cavity while other parts of the polymer are still being heated). Such non-sequential processing makes the analysis of the influence of the parameters rather complicated and, as a result, it increases the experimental time needed to find an optimum configuration for a desired material and geometry.

As previously discussed in section 2.6, to date, very little research has been done with regard to modelling the ultrasonic plasticising mechanism. Jiang et al. [106] studied the mechanisms responsible for ultrasonic plasticising and pointed out that ultrasonic cavitation was the most significant effect. The viscoelastic heating mechanism in ultrasonic plasticising was also investigated by Jiang et al. [63], wherein experimental results were compared with a numerical simulation. Wu et al. [62] and Jiang et al. [103]

also studied the influence of interfacial friction of polymer granulates under ultrasonic excitation. Their results show that interfacial friction heating is a fast, transient process, which creates an inhomogeneous temperature field around the interface.

Despite the research done, there is still no model capable of completely estimating the polymer temperature evolution base on the ultrasonic parameters applied. As highlighted by Masato et al. [60], so far, the use of in-mould sensors is the only way to determine the distribution and the evolution of the temperature of the material during its USM processing. In a recent study published by Gülçür et al. [115], this process is characterised by using a thermal infrared camera, along with the outputs provided by the USM machine. Their results allow us to successfully identify different stages during the heating of the polymer, but the relationship between the material temperature and the process parameters is not explained.

In the present chapter, the temperature and heating rate distributions obtained in solid cylindrical specimens of a commercial polymer submitted to ultrasonic heating are measured experimentally and analysed. Subsequently, a phenomenological viscoelastic model representative of this material is applied to a numerical modelling simulation based on a finite element analysis (FEA). The results obtained experimentally and numerically are compared.
The main objective of this study is to deepen the knowledge of the effect of the different variables of the USM process on the thermal behaviour of the polymer subjected to this forming technology.

4.2 Description of the experiment

In this research study, a simplified approach is adopted for studying the heating suffered by a polymeric material due to the application of high-power ultrasound energy. This approach consists in using a solid cylinder of regular dimensions instead of pellets as the target geometry. This cylinder is partially inserted into a mould cavity and a plunger is used to push it to a sonotrode (see Figure 4.1). In all the experiments, the force of the plunger and the amplitude of the movement of the sonotrode are controlled during the entire process, and the temperature over the time period is measured and analysed.

The main objective of this set of experiments is to evaluate the evolution of the temperature over time due to ultrasonic heating. Additional objectives include the study of the effect of the main factors (amplitude and pressure), as well as the analysis of the temperature distribution along the cylinder.

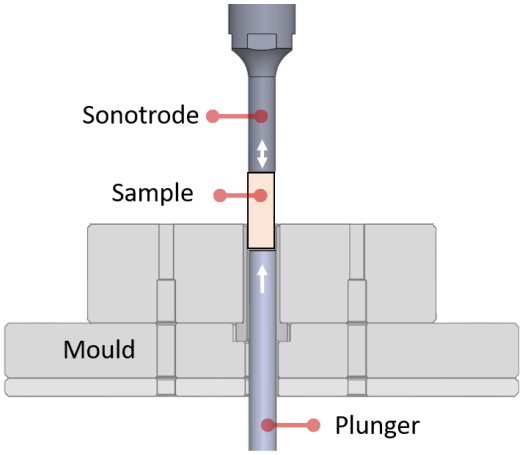

Figure 4.1: Sketch of the device configurations used for the ultrasonic heating experiments

4.3 Material characterisation

The material used in this work is a homo-polymer polypropylene Propil® produced by the firm *Plásticos Lutesor, S.A.*, with a density of 910 kg/m^3, a nominal Young's modulus of 1200 Mpa and a thermal conductivity of 0.22 $W/K \cdot m$, according to the manufacturer's datasheet [123]. All samples needed to perform the experimental tests and the material characterisation have been machined from the same extruded bar of this polymer.

In addition to the properties specified by the manufacturer, complementary tests were performed to characterise the material. The specific heat capacity was measured using the double needle method under ASTM 5334 regulation, obtaining a value of $c_p = 1598 \pm 40 J/(Kg \cdot K)$.

4.3.1 Elastic behaviour

The elastic behaviour of the material has been studied by applying cycles of loading and unloading in uniaxial compression tests. Incremental levels of loading have been applied on cylindrical specimens of polypropylene Propil® having 12 mm diameter and 20 mm height. The tests have been carried out using a 5 kN MTS Landmark ® servohydraulic machine, with several combinations of temperature and strain rate. A polytetrafluoroethylene (PTFE) film has been applied on both sides of the sample to allow its sliding with the press clamps (see Figure 4.2).

The results obtained from the test show that the static behaviour is highly non-linear for large strains, with a strong hysteresis. The progressive increase in the areas corresponding to this hysteresis, together with the plastic deformation of the stress-strain relationships in the figure, show that the material is not mechanically stabilised. The Mullins effect responsible for the

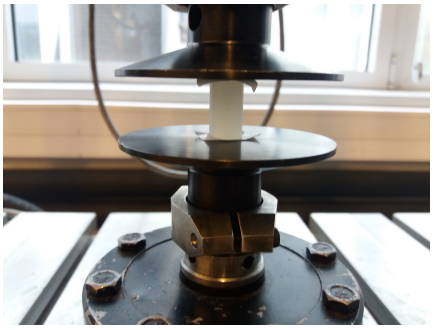

Figure 4.2: Detail of a compression test setup using the MTS793 servohydraulic press

cyclic softening of the polymer is also clear. Furthermore, as expected, this behaviour is dependent on temperature and strain rate.

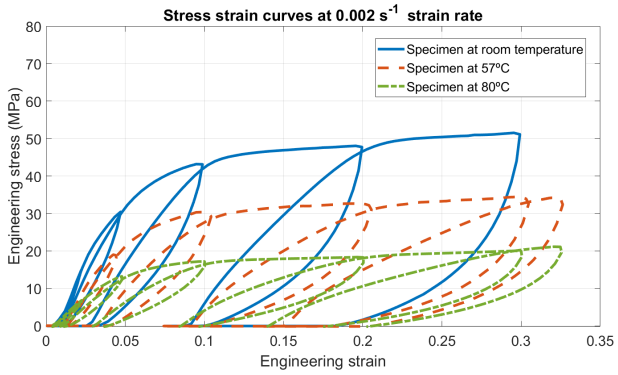

(a) Dependence of compression stress-strain relationship upon temperature

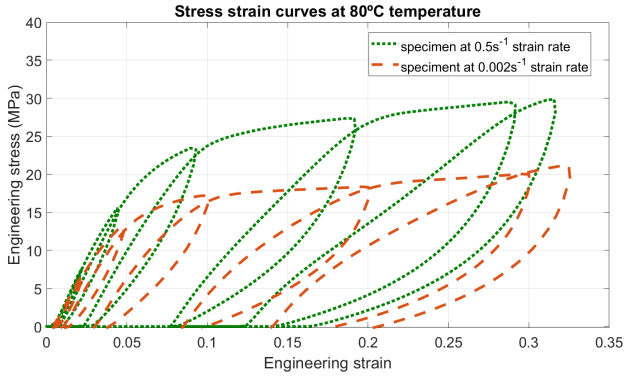

(b) Dependence of compression stress-strain relationship upon strain rate

Figure 4.3: Stress strain curves obtained from the cyclic compression tests of cylindrical specimens of polypropylene at different temperatures (upper figure) an different strain rates (lower figure)

The type of behaviour observed is usually represented by one of the well-known energy functions of the hyper-elastic models [124]. However, the complexity that hyper-elastic models bring to the numerical calculation, together with the low level of deformation to which the polymer is subjected during its ultrasonic heating, make it advisable to assume linear elastic behaviour. Thus, a linear viscoelastic model with a long-term elastic modulus has been used in the numerical analysis. This viscoelastic model is built based on dynamic experiments instead of static tests and it will be described in depth in section 4.5. As can be seen in Figure 4.4, the long term modulus used in the numerical model has a lower slope than the enveloping obtained in the experiments, as it is intended for long term static tests. Instead, the nominal Young's modulus obtained from the manufacturer datasheet presents a better adjustment with the initial slope found in experimental tests.
In this work, the long term moduli along with the viscoelastic model proposed in section 4.5 will be used in all the ultrasonic heating simulations performed.

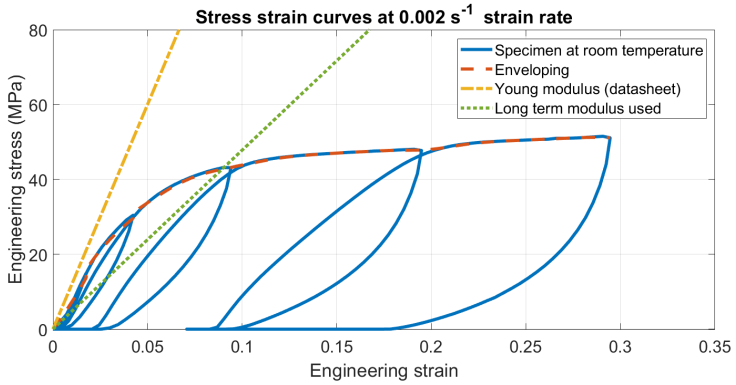

Figure 4.4: Comparison between the strain-stress relationship test, the Young modulus value of the material datasheet and the long term modulus obtained from the viscoelastic model

Dynamic mechanical analysis

The dependence of Young's modulus upon frequency and temperature was obtained from dynamic mechanical analysis (DMA) tests using a TA Instruments® DMA Q800 equipment with a liquid nitrogen bottle (see Figure 4.5).

A dual cantilever experiment was performed using samples of 20 mm free length (10 mm free length at each side) under the following experimental conditions:

- A frequency sweep from 0.1 to 100 Hz with 3 frequencies per decade in logarithmic scale
- A controlled strain of 0.02%
- A temperature sweep between -20 °C and 100 °C.

Before and after every frequency sweep, an isothermal stabilisation was performed to guarantee an uniform temperature throughout the sample. The sample was clamped to the equipment at environmental temperature with a force per unit of length of 0.8 N/m.

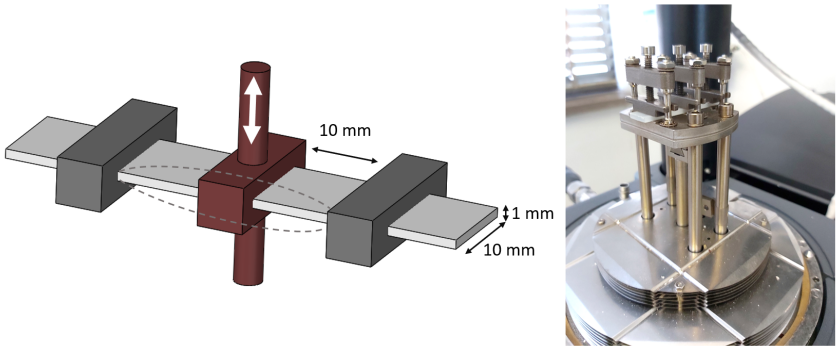

Figure 4.5: Sketch of the DMA test (left) and detail of sample clamping for double cantilever measurement with TA Instruments ® Q800 equipment (right)

The results showed that Young's modulus increases linearly with the logarithm of the testing frequency (see Figure 4.6), which is consistent with the results obtained in the literature [125] and with the previous results obtained from strain stress compression tests. The DMA results also provide the evolution of the Loss Modulus with temperature and frequency (see Appendix B). Based on these measurements, and using the Time Temperature Superposition (TTS) property [124], the master temperature and frequency curves can be obtained. These master curves describe the viscoelastic behaviour of the material and will be used in section 4.5 to build the viscoelastic model introduced in the numerical simulation.

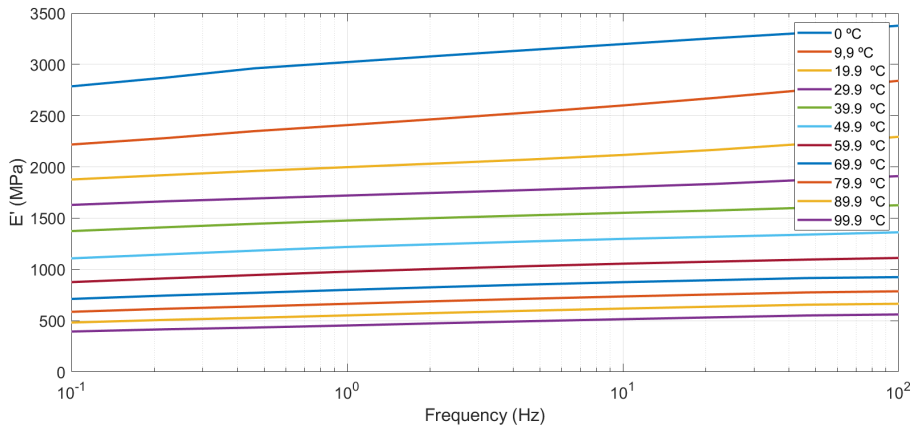

Figure 4.6: Propil ® storage Modulus values obtained from DMA measurement

4.4 Ultrasonic heating experiments

In this section, the experimental tests carried out in order to evaluate the polymer heating due to ultrasonic energy are reported and analysed. All the experiments described here were performed by the author at Eurecat facilities in Cerdanyola between 2017 and 2019.

4.4.1 Experimental setup

Cylindrical specimens with a diameter of 8 mm were submitted to ultrasonic heating with a commercial Sonorus® 1G machine. This USM device works with a Branson® DCX 30 kHz ultrasonic generator and a Langevin piezoelectric transducer to produce mechanical ultrasonic vibrations, as previously explained in section 2.5.2. A stepped sonotrode with a gain of 6.25 was used to amplify and apply these ultrasonic vibrations to the sample. Moreover, the lower part of a conventional USM mould was used to allocate the polymer sample and prevent it from slipping while a plunger was pushing it towards the sonotrode. Thus, in all the tests, samples were placed 5mm below the mould partition (see Figure 4.7 right).

A SC655 FLIR ® infrared camera was used to obtain the temperature during the ultrasonic heating process. In all the experiments, the camera was located at a distance of 50 cm from the sample (see Figure 4.7 left).

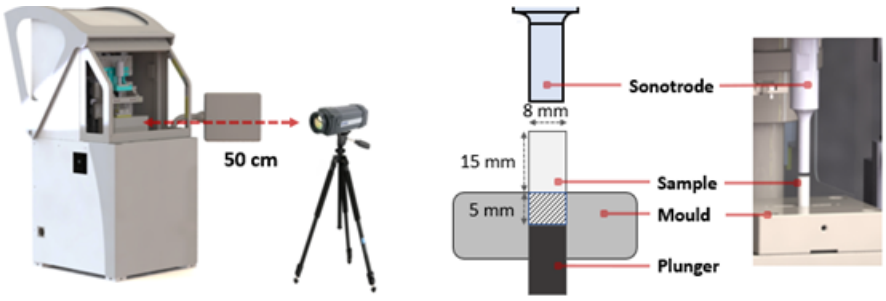

Figure 4.7: Experimental setup for ultrasonic heating evolution measurement. Sketch of the experimental setup (left) and detail of the sample allocation (right)

The infrared camera was calibrated using the results obtained with a J-type thermocouple inserted in a polypropylene cylinder. This cylinder was placed on a hot plate heated at different temperatures. When the system was in a thermal steady state, the cylinder temperatures measured from the thermocouple were compared with the temperatures recorded at the same position by the infrared camera. The best fit between both values was obtained for an emissivity of 0.92, giving an error of ± 0.3°between results.

An external trigger was applied to synchronise the ultrasonic cycle time with the infrared camera recording time. For each experiment, the temperature was obtained at a sampling rate of 200 Hz, and it was exported using the FLIR Thermacam Researcher® software. The data from infrared measurements were merged with the output from the ultrasonic machine and processed using the MATLAB R2019a® software.

4.4.2 Experimental procedure

Each processed sample was analysed according to four geometric regions as depicted in the image on the left of Figure 4.8: upper (AR01), middle (AR02), lower (AR03) and the whole sample (AR0), and the average temperature and heating rate from each region were computed. An additional region of the cylinder is hidden inside the mould, during most part of the measurement, as it is used to place the sample. Obviously, this region can not be measured experimentally, but has to be taken into account when comparing experimental and numerical results.

Temperature measurements can only be considered valid while the geometry of the defined regions is maintained. However, when a certain temperature is reached, the material gets softer and the cylinder starts to deform, as is seen in the image to the right of Figure 4.8. From this moment on, the recording area is different from the cylinder area and the temperature measurement is not correct any longer. This point is detected with a decrease in the average heating rate (as can be seen later in Figure 4.12), and is used as an ending time for the analysis of the results.

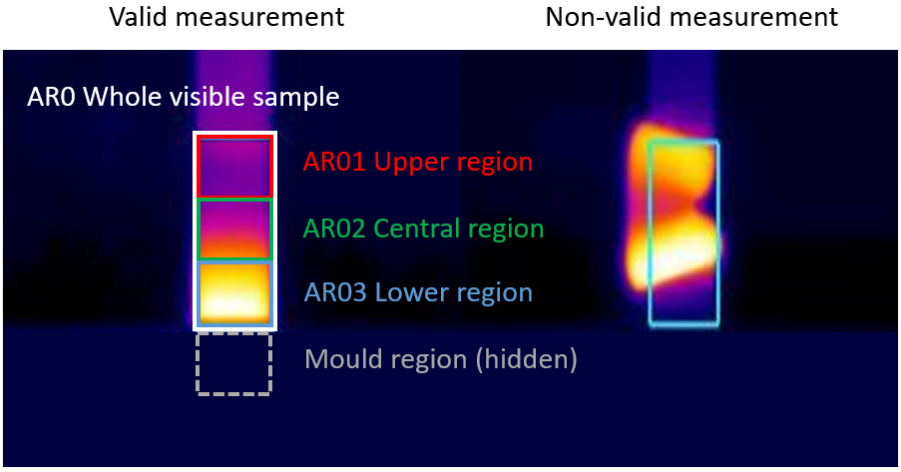

Figure 4.8: Sample measurement regions considered for the analysis (left). Defined regions are only maintained until the cylinder starts to deform (right)

Configuration	Cylinder length (mm)	Amplitude (μm)	Force (N)	Run numbers
1	20	28	1000	1-10
2	20	28	2000	11-20
3	20	44	1000	21-30
4	20	44	2000	31-40
5	16	37.5	1000	41-50
6	18	37.5	1000	51-60
7	20	37.5	1000	61-70
8	22	37.5	1000	71-80

Table 4.1: Experimental configurations for ultrasonic heating evolution measurement

In order to study the temperature evolution, a full factorial experiment was performed considering two factors (ultrasonic amplitude and applied force) and two levels. For each experimental set, ten runs were performed. The parameters used for each set are listed in Table 4.1, and the results are presented and explained in the following sections. Configurations 1 to 4 were used to analyse the evolution of the heating rate and its relationship with power consumption. Additional configurations 5 to 8 were tested to study the nature of a peak in the heating rate and will be discussed in section 4.6).

Across all configurations, the ultrasonic energy was imposed for 5 seconds. However, in those cases wherein the cylinder began to deform within 5 seconds, the post-processing of the measured data was adapted accordingly.

4.4.3 Results and discussion

Temperature and heating rate evolution during the ultrasonic heating process

The evolution of the maximum and average temperatures with time, in the three visible regions of the polymer cylinders tested, are represented in Figure 4.9. Based on these results, it can be determined that the temperature distribution in the cylindrical samples is not homogeneous. There is an important thermal gradient between the three regions (upper, middle and lower), defined along the height of the cylinder.

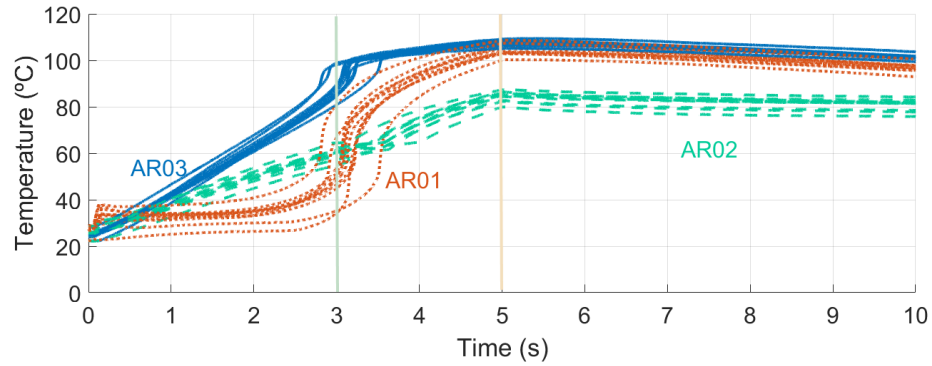

(a) Maximum temperature values

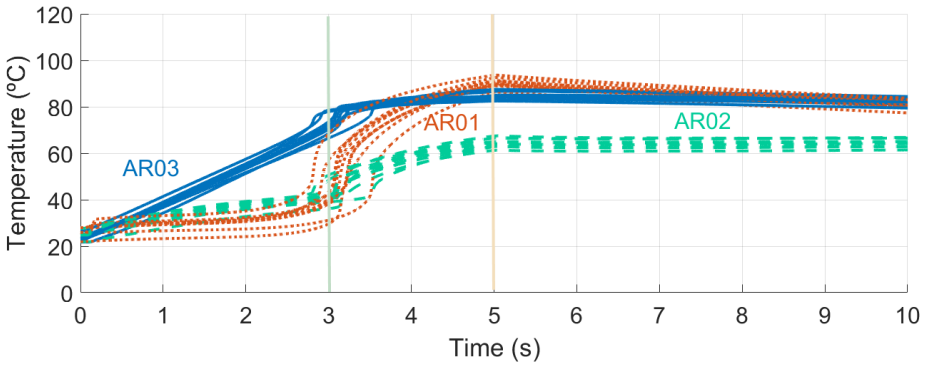

(b) Average temperature values

Figure 4.9: Temperature evolution for experimental runs of Configuration 1. Maximum recorded temperatures (a) and average recorded temperatures (b) are displayed for upper AR01 (dotted orange line), middle AR02 (dashed green) and lower AR03 (solid blue), regions of the cylinders. Solid green vertical lines indicate the average heating rate peak while dashed red vertical lines indicate the end of ultrasonic energy and the start of the cooling stage

The most constant temperature increase is obtained in the lower part, in the area that is near the mould partition. On the other hand, the upper region of the specimen, the one that receives the action of the sonotrode directly, has a slight initial heating and then maintains the temperature for a significant part of the test time (almost 2 out of 5 seconds of the test). In the third stage, the temperature evolution of the upper part follows a sigmoidal law type, with its inflexion point around the third second. This time coincides with a change in the slopes of the curves corresponding to the lower and middle regions. A very significant increase in temperature and heating rate is measured across the three regions considered, as it is also reflected in Figure 4.10, which shows the same results in terms of the derivative of the average temperature, that is, the evolution of the average heating rate during this process.

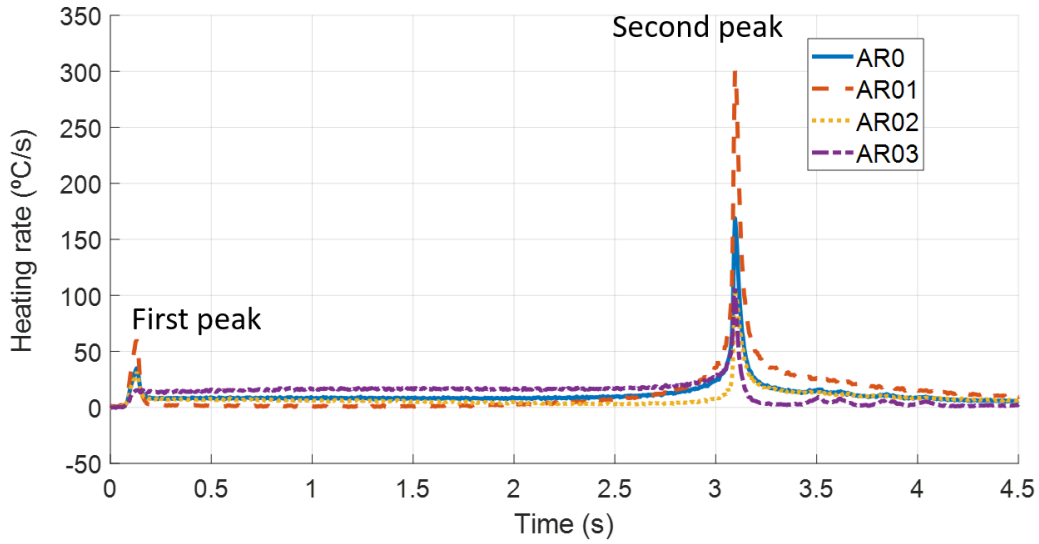

Figure 4.10: Heating rate results from an experiment performed using Configuration 1 parameters: different curves are obtained for the average heating rate for the whole sample (*AR0*), the upper region (*AR01*), the central region (*AR02*) and the lower region (*AR03*)

From this point onwards, the central zone undergoes an increase in the heating rate, probably due to the transfer of heat by conduction from the upper and lower regions, while, on the contrary, in the lower part of the cylinder, the heating rate is reduced. At the end of the ultrasonic time, the temperatures of the upper and lower parts of the specimen are equalised. The same does not happen with the central area of the cylinder, which maintains a considerable temperature difference from the ends. This behaviour can also be observed directly from the infrared camera images, shown in Figure 4.11.

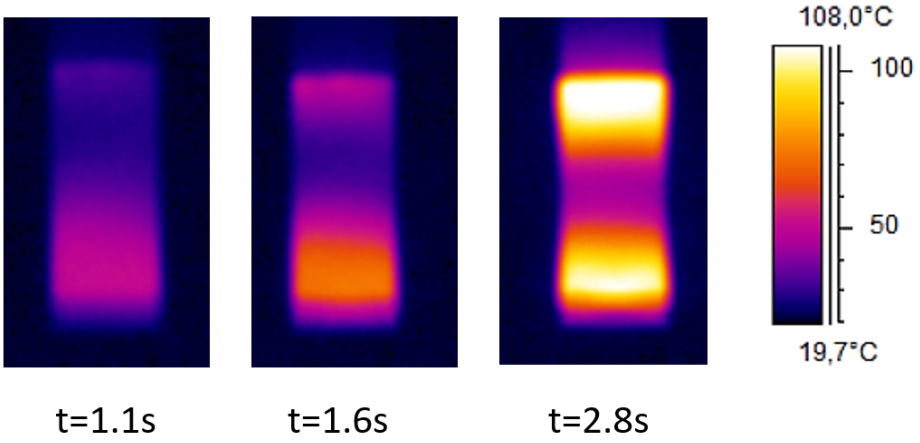

Figure 4.11: Infrared images captured at different time slots for a cycle in Configuration 1

When observing the heating rate, it can be seen that all the regions have a similar heating rate profile that changes over time. Two main peaks are identified in all the configurations with a flat region between them. This behaviour is similar across all the configurations tested. Thus, in order to analyse the mechanisms and phenomena responsible for the increment of temperature in this polymer due to ultrasonic vibrations, the three different steps represented in Figure 4.12 were defined (these steps should not be confused with the USM process steps described in Chapter 2).

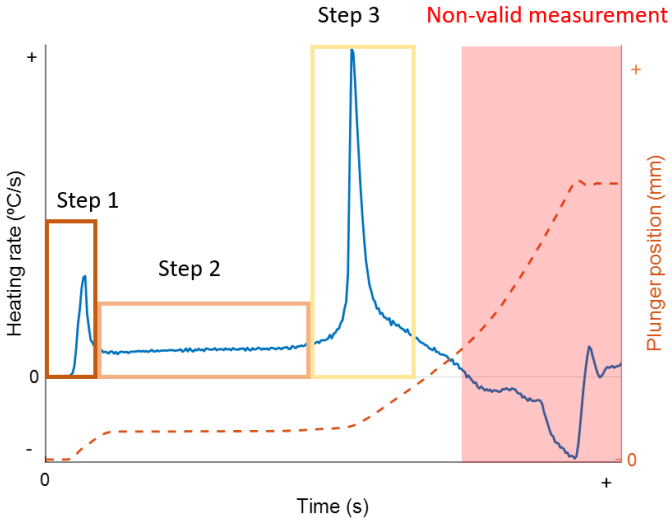

Figure 4.12: Generalised graph with proposed steps to study the heating rate evolution: the region excluded from the analysis is highlighted in red; plunger position evolution is displayed in dashed orange

In Step 1, the sonotrode impacts the polymer specimen and, as a result, the temperature rate increases abruptly for a short lapse of time. There is a significant movement of the plunger during this entire step that compresses the cylinder. As can be seen in Figure 4.13, the upper region of the cylinder (AR01) is the one with a higher heating rate and, although there is some dispersion in the results, the Pareto plot on the right side of Figure 4.13 demonstrates that the amplitude of the movement of the sonotrode is the most influential variable.

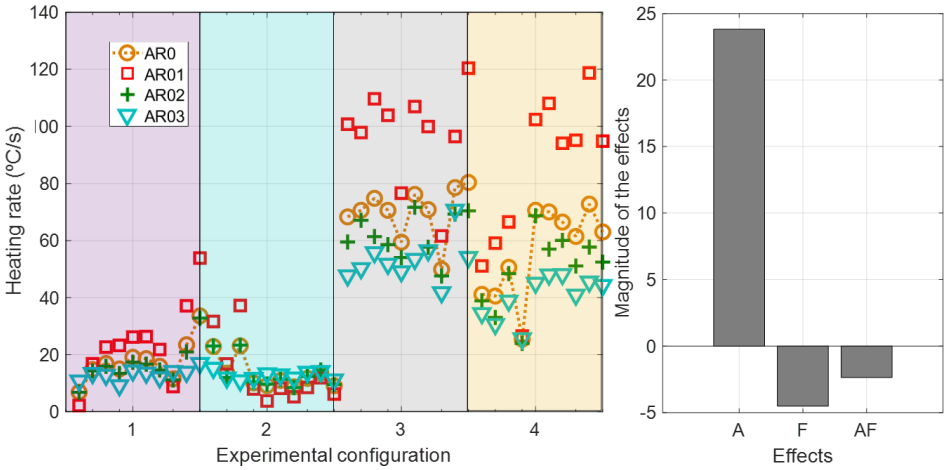

Figure 4.13: Average heating rate during Step 1 calculated for the different cylinder regions in each experimental run (left). Each colour box groups the experiments done with the same configuration. Pareto plot of the influence of the effects in the AR0 region (right) (A: ultrasonic amplitude, F: plunger force, AF: Interaction between variables)

In Step 2, the sonotrode is in complete contact with the cylinder and there is a constant (but lower) heating rate for all the cylinder regions. Again, amplitude is the most relevant parameter for the overall heating of the cylinder.

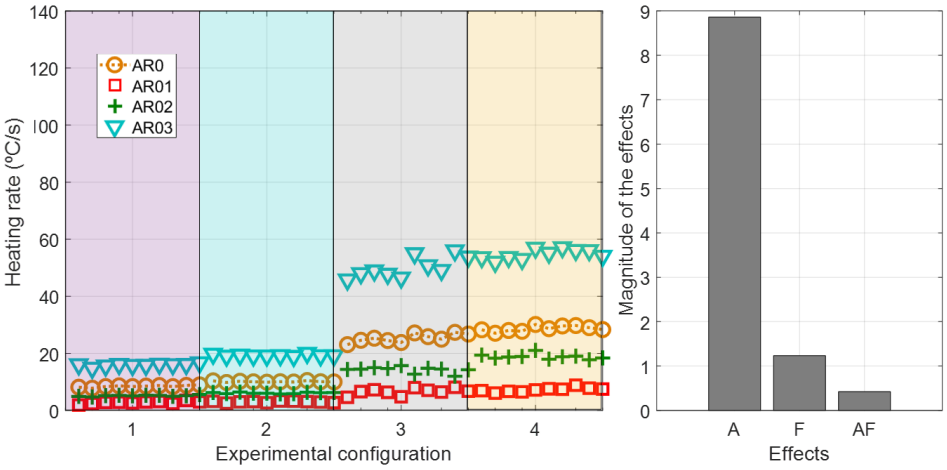

Figure 4.14: Average heating rate during Step 2 calculated for the different cylinder regions in each experimental run (left). Each colour box groups the experiments done with the same configuration. Pareto plot of the influence of the effects in the AR0 region (right) (A: ultrasonic amplitude, F: plunger force, AF: interaction between variables)

The average heating rate of the cylinder in this Step 2 is between 7 °C/s and 30 °C/s depending on the configuration. These values have the same order of magnitude as the ones obtained by Jiang et al. [126], and the heating phenomenon can be attributed to the viscoelastic effect. In this case, the lower region of the cylinder (AR03) is the one with the highest heating rate. As discussed later in section 4.6, this behaviour is probably caused by the contact between the polymer and the mould, and should be addressed in future experiments in order to avoid it.

When the material reaches a certain temperature, there is a sudden increment of temperature and this creates a high peak for the heating rate in all the cylinder regions (Step 3). In this step, the upper region of the cylinder reaches heating rate values of up to 133 °C/s. In this case, both the amplitude and force effects have a similar influence on the heating rate.

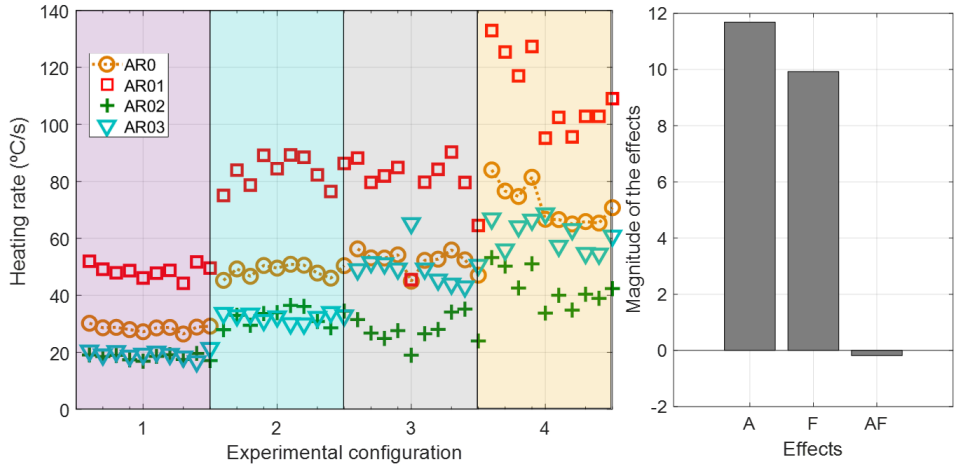

Figure 4.15: Average heating rate during Step 3 calculated for the different cylinder regions in each experimental run (left). Each colour box groups the experiments done with the same configuration. Pareto plot of the influence of the effects in the AR0 region (right) (A: ultrasonic amplitude, F: plunger force, AF: interaction between variables)

In some experimental configurations, a further Step 4 could be considered, wherein there is a flat region for the heating rate similar to the one in Step 2. However, in most of the configurations, this step is very short, because as soon as the polymer starts to deform, the results are invalid. Hence, this step has not been analysed in this study.

Relationship between the consumed energy and the polymer temperature

Ultrasonic power consumed by the ultrasonic generator presents the same evolution as the heating rate, as shown in the graph on top of Figure 4.16. The heating rate peaks in steps 1 and 3 are also replicated in the power

consumption graph, and similar peaks can also be observed during USM process of polypropylene pellets (see Figure 8 in Gülçür et al. [115]). Thus, there is a clear relationship between the output power of the acoustic unit and the average polymer heating rate. This relation is also fulfilled in its integral form between the increment of temperature and the consumed energy (see lower Figure 4.16). The knowledge of this relationship for each material and geometric shape could be very useful to estimate the temperature of the polymer melt during the process.

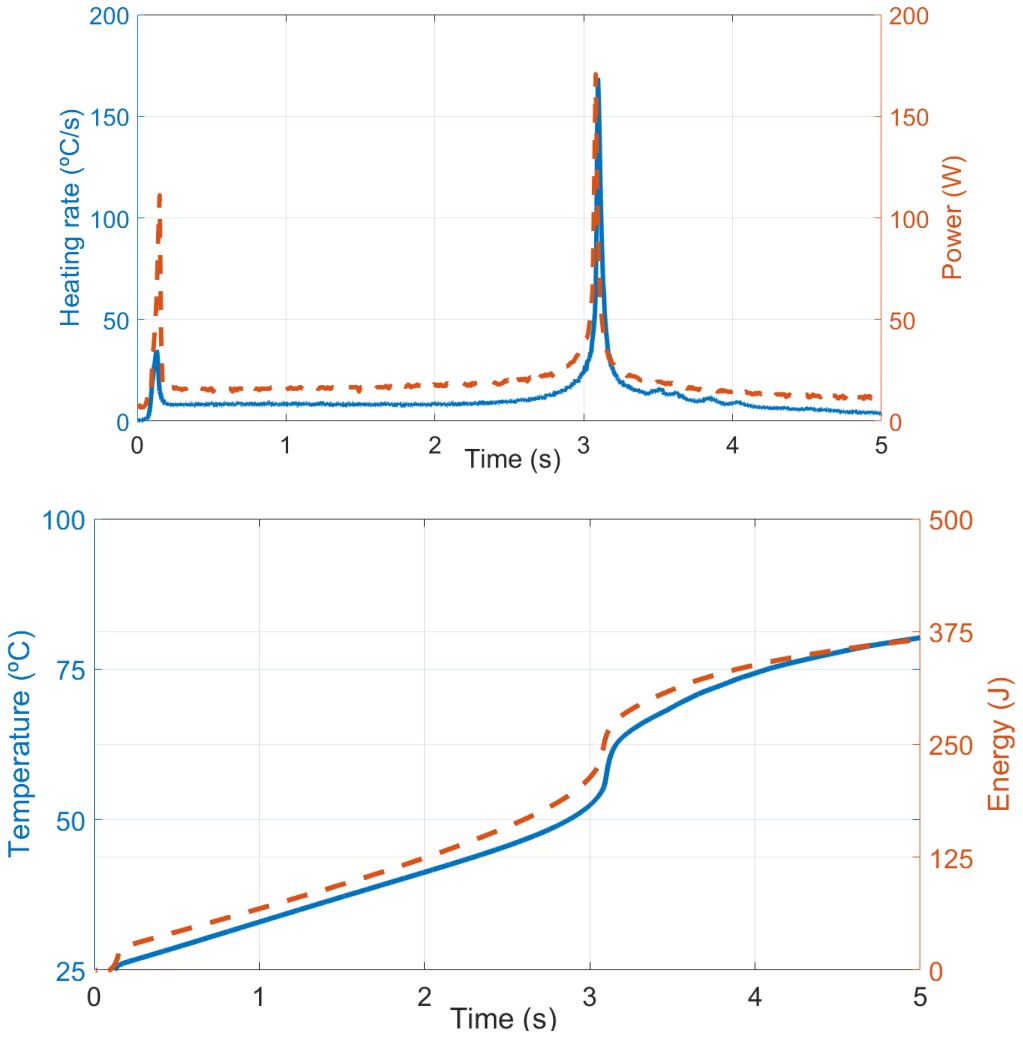

Figure 4.16: Relationship between heating rate evolution (solid blue) and power consumption (dashed orange) in the upper figure, and cumulative energy (solid blue) and temperature (dashed orange) in the lower figure for a cycle in Configuration 1)

In order to stablish this correlation, a linear fit between the energy of the transducer and the increment of temperature of the polymer is considered:

$$E = K_1(T - T_0) \tag{4.1}$$

Here E is the cumulative energy consumed by the ultrasonic generation since the start of the cycle, T is the temperature in Celsius, and T_0 is the initial temperature of the polymer. The coefficient K_1 is obtained using the least square method by minimizing the sum of the residuals R defined as:

$$R^2 = \sum [E_i - f(T_i, K_1)]^2 \tag{4.2}$$

The values of K_1 obtained for each experimental configuration are presented in Table 4.2.

The results obtained show that a range between 6 and 8 J of energy is needed to increase a single degree of temperature within the cylinder. Higher amplitudes have higher K_1 (spend more energy) while higher plunger forces have slightly lower values of K_1.

The same methodology can be used to explain the relationship between the heating rate and the power consumption of the ultrasonic generator. In this case, the correlation can be expressed as:

$$P = K_2 \frac{dT}{dt} \tag{4.3}$$

The least squares method is applied to obtain the values of K_2 that minimise the sum of the residuals:

$$R^2 = \sum \left[P_i - f\left(\frac{\Delta T_i}{\Delta t_i}, K_2 \right) \right] \tag{4.4}$$

In this case, the average value obtained for all the configurations is

$$K_2 = 6.5 \pm 0.6 W/°C \tag{4.5}$$

On the other hand, the heating needed to raise the temperature of the cylinder by 1 degree, is given by:

$$Q = c_p m \frac{dT}{dt} = K_3 \frac{dT}{dt} \tag{4.6}$$

Configuration	Amplitude (μm)	Force (N)	K_1 (J/°C)
1	22	1000	6.48 ± 0.22
2	22	2000	6.12 ± 0.36
3	44	1000	8.3 ± 0.5
4	44	2000	7.4 ± 0.5

Table 4.2: Linear fit of K_1 coefficient obtained for each experimental configuration

Here Q is the heat of the process, c_p is the specific heat capacity of the material and m is the mass processed. Substituting the material properties obtained in section 4.2, the theoretical energy needed to increase the temperature by 1 degree is:

$$K_3 = 1.46 W/°C \tag{4.7}$$

The process efficiency can be calculated as:

$$efficiency = \frac{K_3}{K_2} = 22\% \tag{4.8}$$

This value is in agreement with the results obtained by Grabalosa et al.[11] when estimating the efficiency of the USM process.

4.5 Viscoelastic model

Perfectly elastic solids and perfectly viscous fluids are idealisations that are valid only in very limiting conditions. In general, most materials (and particularly polymers) exhibit a combination of elastic and viscous responses when subjected to external loads and displacements. The simplest way to model this behaviour is trough linear viscoelasticity. The foundation of linear viscoelasticity relies on the Boltzmann superposition principle, which states that each loading step can be considered as an independent contribution, and the resultant strains add linearly [127]. In this dissertation, a linear viscoelastic phenomenological model is used for the modelling of the polypropylene cylinders.

4.5.1 Phenomenological constitutive models

Phenomenological models uses springs and dashpot elements to represent complicated material responses as a combination of simple responses. Usually, the elasticity is represented by a spring of stiffness E and the viscosity is given by a dashpot (a piston that moves in a cylinder filled with viscous fluid) of viscosity η. Thus, the simplest phenomenological models of a viscoelastic material is calculated as the combination of both elements either in parallel or in series.

Maxwell model

The Maxwell rheological model consists of a linear spring and a linear dashpot in series. In this case, the rate of change in strain of the system is given by

Here, ϵ_1 and ϵ_2 are the elastic and viscous strains, and σ is the applied stress.

$$\dot{\epsilon} = \frac{d}{dt}(\epsilon_1 + \epsilon_2) = \frac{\dot{\sigma}}{E} + \frac{\sigma}{\eta} \quad (4.9)$$

(a) Maxwell model equation

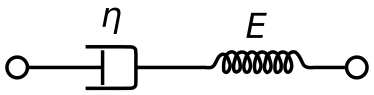

(b) Maxwell model representation

This model is suitable for describing stress relaxation. When a strain step $\epsilon(t) = \epsilon_0 H(t)$ is applied in a stress relaxation experiment (where *H(t)* is the Heaviside function), the differential equation can be solved in closed form, giving:

$$\sigma(t) = \sigma_0 \exp \frac{-t}{\eta / E} \quad (4.10)$$

This element can be represented by means of a single Prony series term.

Kelvin-Voigt model

The Kelvin-Voigt model is represented by a linear spring and a linear dashpot connected in parallel. In this case, the stress is given by:

$$\sigma = E\epsilon + \eta \frac{d\epsilon}{dt} \quad (4.11)$$

(a) Kelvin-Voigt model equation

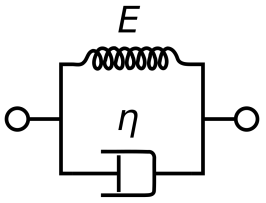

(b) Kelvin-Voigt model representation

This model is more suitable for describing strain retardation. If we suddenly apply some constant stress σ_0 to the Kelvin–Voigt material, then the strain obtained during the time period will be

$$\epsilon(t) = \frac{\sigma_0}{E}\left(1 - e^{-\lambda t}\right) \quad (4.12)$$

where the rate of relaxation is $\lambda = \frac{E}{\eta}$.

Based on these examples is easy to see that the Maxwell model is valid for the reproduction of a linear creep test while the Kelvin-Voigt model is capable of reproducing a linear relaxation test. However, in order to obtain a model for a material capable of accounting for multiple behaviours, more elements must be added.

Generalised Maxwell model

The Generalised Maxwell model (also known as Maxwell-Wiechert model) is the most general form of the linear model for viscoelasticity. In this model, several Maxwell elements are assembled in parallel. It takes into account that the relaxation does not occur at a single point of time, but over a set of times, due to the presence of molecular segments of different lengths, with shorter ones contributing lesser than longer ones. A generalised Maxwell model is composed of a multi-network Maxwell model in parallel with an elastic network (see Figure 4.19).This model could be represented by the relaxation moduli functions as follows [128]:

$$E(t) = E_\infty + \sum_{i=1}^{TN} E_i e^{-\frac{t}{\tau_i}} \tag{4.13}$$

where E_∞ is the long term modulus, and E_i and τ_i are the elastic components and relaxation time, respectively, associated with the i element. In addition, by substituting the equation for $t = 0$, we obtain the value for the instantaneous relaxation modulus, E_0.

$$E(t = 0) = E_\infty + \sum_{i=1}^{TN} E_i = E_0 \tag{4.14}$$

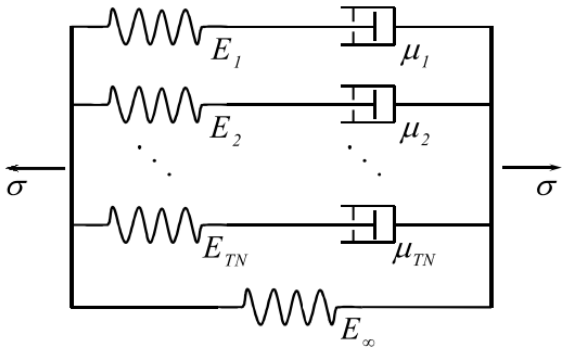

Figure 4.19: Generalized Maxwell model diagram reproduced from [128]

In this study, a Generalised Maxwell model has been considered for reproducing the viscoelastic behaviour of a polypropylene material.

4.5.2 Time-temperature superposition

When constructing a model for the viscoelastic behaviour of a material, the dependence of this behaviour upong the temperature must be taken into account. It has been shown experimentally that, in many cases, the temperature dependence can be modelled by a scaling of time. This empirical relation

is known as a *time-temperature equivalence* or *time-temperature superposition principle* (TTS) [129].

Observation suggests that if the relaxation modulus is known at one temperature, the relaxation modulus at any other temperature can be obtained from a known shift factor. When a material fulfils this property, it is called a *rheologically simple material*.

In polymers that obey the TTS, viscoelastic data measured at a temperature different from reference temperature can be shifted to form a single superposed curve called the *master curve* (see Figure 4.20).

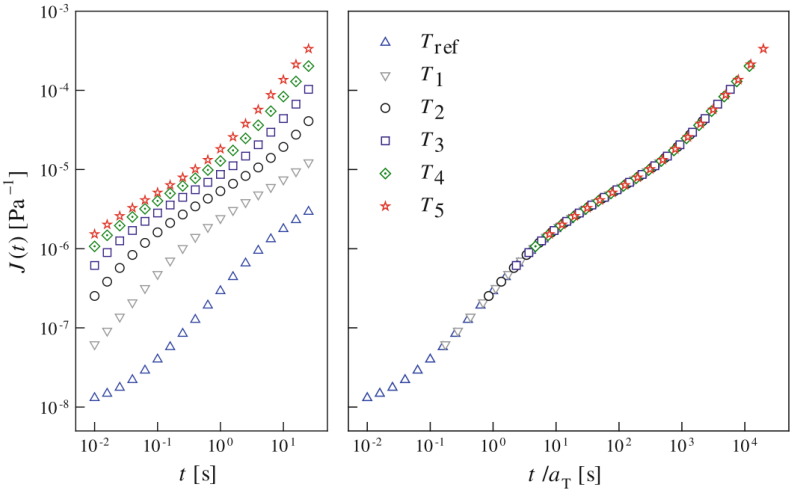

Figure 4.20: Schematic illustration of the master curve generation with time-temperature superposition. Creep compliance measurements obtained (left) are superposed in a unique curve (right). Reproduced from [124]

Since the distance of the shifting depends on the temperature, the horizontal and vertical shift factors are denoted by a_T and b_T respectively. For relaxation modules, the TTS means that the following relationship in time domain is fulfilled:

$$G(t,T) = \frac{\rho(T)T}{\rho(T_{ref})T_{ref}} G\left(\frac{t}{a_T}, T_{ref}\right) = b_T G\left(\frac{t}{a_T}, T_{ref}\right) \tag{4.15}$$

where G is the shear modulus (the same equation applies for the flexural modulus), ρ is the material density and T_{ref} is the reference temperature from which the shift factors are computed. In the frequency domain, this equation can be expressed for the storage and loss moduli as:

$$G'(w,T) = b_T G'(a_T w, T_{ref}) \tag{4.16}$$

$$G''(w,T) = b_T G''(a_T w, T_{ref}) \tag{4.17}$$

Since it is assumed that the relaxation times are all identically affected by the temperature in the same way, the vertical shift factor (b_T) can be neglected.

The horizontal shift factor, a_T, can be expressed as a relationship between the relaxation times as:

$$a_T = \frac{\tau(T)}{\tau_{ref}(T_{ref})} \tag{4.18}$$

The most common method for constructing the master curve is to choose the optimum shift factor, which gives the best superposition. This procedure can be carried out by visual inspection, but it can also be done using algorithms such as a non-linear regression method, or minimisation of arc length. In this study, the non-linear least square method has been used to obtain optimal shift factors from the modulus data measured at different frequencies and temperatures (see section 4.3 for details about experimental characterisation of the material, and Appendix B for the raw data obtained from measurements). As it can bee seen in Figure 4.21, there exists a lineal relation between the logarithm of the shift factors and the temperature.

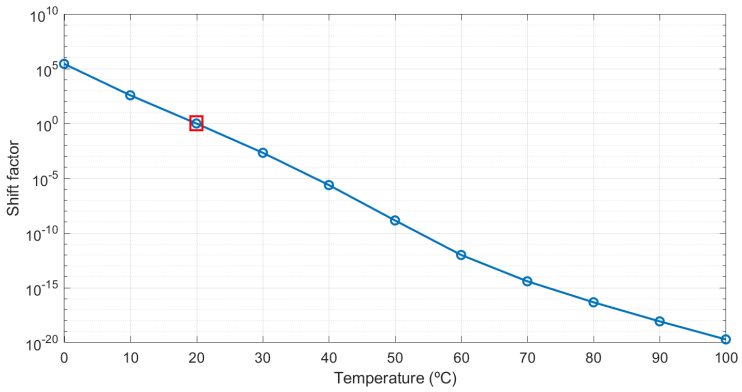

Figure 4.21: Shift factors obtained from DMA measured data: the reference temperature from which shift factors are computed (20 °C) is shown in red

Using the obtained shift factors, the master curve is determined. As it can be seen from Figure 4.22, the storage modulus master curve is smooth while loss modulus measures present some discontinuities in the superposed curve. Thus, in order to facilitate the introduction of these data in the simulation, a polynomial fit of each modulus has been performed and will be used in the following sections to obtain the Prony series.

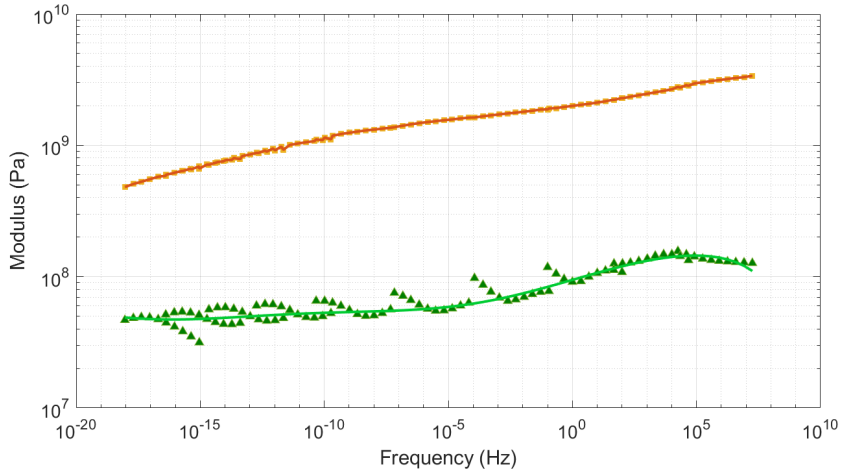

Figure 4.22: Master curve for storage modulus (orange dots) and loss modulus (green dots) at (20 °C). Lines indicate the polynomial fit for each modulus performed with MATLAB®

4.5.3 Equations to model the temperature dependence of the shift factor

The Williams-Landel-Ferry Equation

The Williams-Landel-Ferry (WLF) equation is an empirical equation that states the dependence of the shift factor on temperature as [130]:

$$\log a_T = \frac{-C_1(T - T_{ref})}{C_2 + T - T_{ref}} \tag{4.19}$$

where C_1 and C_2 are empirically obtained coefficients, and T_{ref} is usually chosen as the glass transition temperature (T_g).

The WLF equation has its basis in the viscosity model of Doolittle [131], which is a phenomenological model wherein the viscosity of glassy material is reciprocally proportional to the free volume fraction ($V_f = (V - V_c)/V$). The free volume fraction V_f is the normalised difference between the whole volume occupied by molecules (V), and the core volume of molecules (V_c). Viscosity is then given by

$$\eta = A \exp\left(\frac{B}{V_f}\right) \tag{4.20}$$

where A, and B are material constants. Doolittle assumed that the free volume fraction has a linear dependence on temperature as follows:

$$f = f_g + \alpha_f(T - T_g) \qquad for \qquad T > T_g \tag{4.21}$$

where f_g is the free volume fraction at glass transition temperature (T_g) and α_f is the expansion coefficient. Substituting:

$$\log a_T = \frac{B}{f_g + \alpha_f(T - T_g)} - \frac{B}{f_g + \alpha_f(T_{ref} - T_g)} \tag{4.22}$$

using the notation

$$c_1 = \frac{B}{f_g + \alpha_f(T_{ref} - T_g)} \tag{4.23}$$

$$c_2 = \frac{f_g}{\alpha_f} + T_{ref} - T_g \tag{4.24}$$

the WLF equation (4.19) is obtained.

Although the kinetic theory of polymers and TTS are valid only above the glass transition temperature, there is no consensus about the range of applicability of the WLF equation. In any case, it is expected to be valid between $T_g \pm 50°C$ for all polymers [129] and up to $T_g + 100°C$ in amorphous polymers [132].

The suggested universal values for WLF constants (considering the glass transition as a reference temperature) are: $C_1 \approx 17.44$ and $C_2 \approx 51.6K$. However, in practice, there are different constant values for multiple polymer and reference temperatures in existing literature (i.e, see table 13.10 in [133]).

The Arrhenius equation

The Arrhenius activation energy equation is obtained from the Eyring model for temperature dependence of viscosity [134]:

$$\eta(T) = A \exp\left(\frac{E_a}{RT}\right) \tag{4.25}$$

where A is the front factor, E_a is the activation energy, R is the gas constant and T is the absolute temperature. The Arrhenius equation then gives a one parameter model for the horizontal shift factor as:

$$\log a_T = \frac{E_a}{R}\left(\frac{1}{T} - \frac{1}{T_{ref}}\right) \tag{4.26}$$

In this equation, absolute temperature must be used.

Van Krevelen et al. [133] consider that an Arrhenius-type equation must be used for semi-crystalline polymers between T_g and T_m, where T_m is the melting temperature of the polymer.

Coefficient values obtained for Propil ® polypropylene

As mentioned previously, there is a clear relationship between the logarithm of the shift factor and the temperature for the data obtained in this work. In order to decide which empirical relation best represents the material used in this work, both WLF and Arrhenius equations have been applied and compared with experimental data. To obtain the best adjustment, all the coefficients have been found using linear square methods. As can be seen in Figure 4.23, both approaches give good results for optimised coefficients. However, WLF equation with *universal values* does not correctly simulate the experimental results [1].

The optimised coefficients obtained are $C_1 = 60.1$ and $C_2 = 165.5K$ for the WLF approach, and $E_a = 2.5 \cdot 10^2$ KJ/mol for the Arrhenius approach.

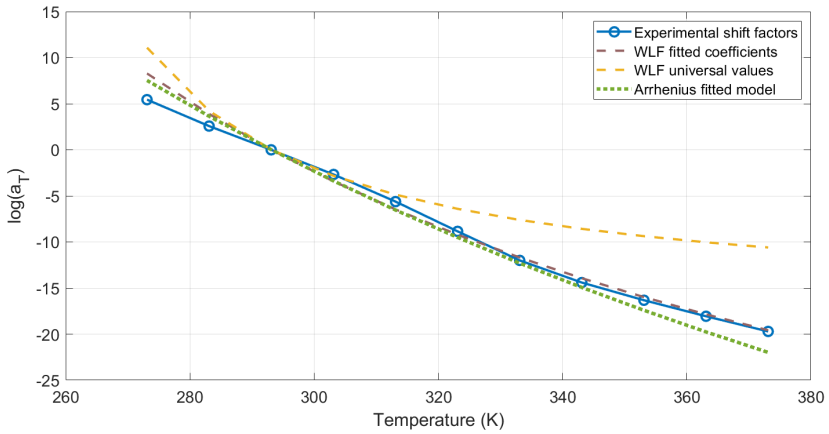

Figure 4.23: WLF and Arrehnius ajusted data to experimental shift factors

The temperature range analysed in this work is limited to the zone between the T_g and the T_m. Given that both methods provide an almost exact adjustment of experimental values, WLF equation will be used in the numerical model, as it can be used directly in the interactive modulus of ABAQUS®.

4.5.4 Validation of the model

In this section, the validity of the obtained moduli values and the TTS hypotesis are evaluated.

First of all, a Kramers-Kronig relation is applied to analyse the relation between the real part (storage) and the imaginary part (loss) of the moduli measured. This relation must be fulfilled for any response of a physical

[1] WLF *universal values* are expected to be used with T_g as the reference temperature. However, it is possible to convert WLF coefficients for different reference temperatures using the procedure described in [135]. In any case, this procedure did not provide good coefficient values for our experimental data.

system that involves causality. Although in this study, the Kramers-Kronig relation is used only to verify the obtained data, it can also be used to optimise the shift factors [136]. The application of a Kramers-Kronig relation can be easily implemented by using the following equations [137]:

$$E^{'}(w) = \frac{2w}{\pi}\left(\frac{d\left[E^{''}(u)/u\right]}{d\ln u}\right)_{u=w} \tag{4.27}$$

$$E^{''}(w) = \frac{2}{\pi}\left(\frac{dE^{'}(u)}{d\ln u}\right)_{u=w} \tag{4.28}$$

Using the last equation, loss modulus has been obtained and compared with the fitted experimental data, as can be seen in Figure 4.24.

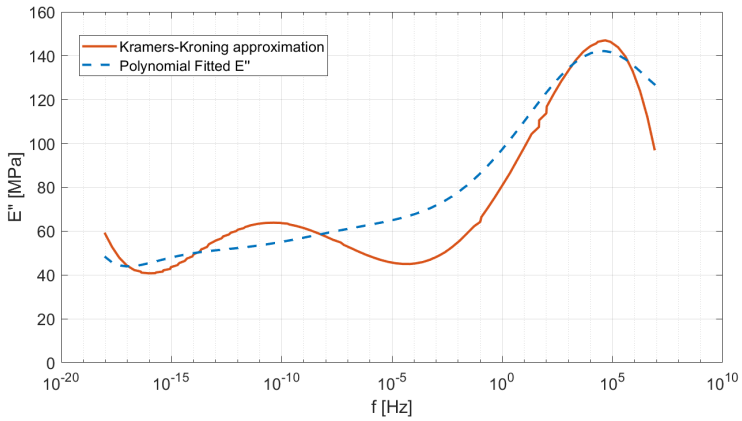

Figure 4.24: Loss modulus comparison with Kramers-Kronig relation obtained from storage modulus data

Another usual method for validating the results is the Cole-Cole plot [138]. This plot determines if the horizontal shift factor is enough to reproduce the behaviour of the material. If so, the relation between the loss modulus and the Young's modulus should be represented as a line in the logarithmic scale. In this case, as can be seen in Figure 4.25, the material of the present work does not have a linear Cole-Cole plot graph. This could indicate that the material is not fully rheologically simple, and that vertical shift factors may be needed. Although for the sake of simplicity, during simulation, the material will be treated as rheologically simple, this issue must be addressed in future works.

4.5.5 Prony series

Theoretical equations

The behaviour of a viscoelastic material can be modelled using the *Prony series*. This representation is fully equivalent to a generalised Maxwell

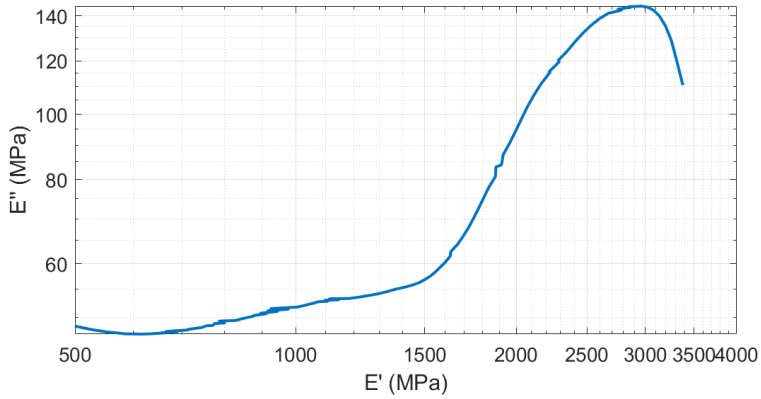

Figure 4.25: Cole-Cole plot obtained for polypropylene material

model (see section 4.5.1), and it is often applied in numerical analysis due to its remarkable computational efficiency resulting from its exponential basis function [139]. The representation of the relaxation modulus using Prony series is:

$$E(t) = E_\infty + \sum_{i=1}^{TN} E_i e^{-\frac{t}{\tau_i}} \tag{4.29}$$

which is the same equation as 4.13. This equation can be expressed in dimensionless terms, by defining the dimensionless relaxation modulus $e_r(t)$ as:

$$e_r(t) = \frac{E(t)}{E_0} \tag{4.30}$$

where E_0 is the instantaneous modulus, related to the long term modulus by:

$$E_\infty = E_0(1 - \sum_{i=1}^{N} E_i) \tag{4.31}$$

Replacing the dimensionless terms, equation 4.29 can be rewritten as:

$$E(t) = E_0 \left(1 - \sum_{i=1}^{N} 1 - E_i e^{-t/\tau_i}\right) \tag{4.32}$$

The same method can be applied for another modulus, such as shear modulus $G_r(t)$, thus obtaining analogue equations:

$$G_r(t) = G_0 \left(1 - \sum_{i=1}^{N} 1 - g_i e^{-t/\tau_i}\right) \tag{4.33}$$

$$\tag{4.34}$$

where

$$G_\infty = G_0(1 - \sum_{i=1}^{N} g_i) \tag{4.35}$$

In fact, most finite elements' codes such as ABAQUS ® consider the values of shear modulus in their Prony series implementation.

Prony series can also be written in the frequency domain. In this case, the equations are obtained through the application of the Fourier transforms. Using the dimensionless modulus, the Prony series for storage and loss modulus are written as:

$$G_s(w) = G_0 \left[1 - \sum_{i=1}^{N} g_i\right] + G_0 \sum_{i=1}^{N} \frac{g_i \tau_i^2 w^2}{1 + \tau_i^2 w^2} \tag{4.36}$$

$$G_l(w) = G_0 \sum_{i=1}^{N} \frac{g_i \tau_i w}{1 + \tau_i^2 w^2} \tag{4.37}$$

The above discussion thus explains the manner of introducing Prony series in ABAQUS®.

Obtaining Prony series

In order to obtain the values for Prony series from experimental data, curve fitting procedures for non-linear optimisation problems are needed. Some methods try to avoid the non-linear system of equations, by estimating the time constants (τ_i) from the total range of time domain (Schapery [139] suggested the use of a one-time constant for each time decade) and interfering values as E_0 from the scatter data at lower times.

The obtention of Prony series in the frequency domain is more difficult due to the ill-posed nature of the problem [140]. In this case, there are two different sets of equations to be adjusted using the same parameters. For fitting experimental data in the frequency domain, some researchers have proposed different methods that introduce regularisation techniques [141]. The ill-posed nature of these problems has been discussed in detail by Honerkamp [142].

In this study, the ReSpect MATLAB® toolbox developed by Takeh and Shanbhag[2] was used to obtain the Prony series of our material. The algorithm implemented in the software works in two steps [143]: first a continuous relaxation spectrum (CRS) is obtained from the experimental discrete data, and then a discrete relaxation spectrum is computed (DRS), which are the Prony series. The algorithm can be implemented both in time and frequency

[2]https://es.mathworks.com/matlabcentral/fileexchange/54322-respect-v2-0

domain and is provided with a GUI interface for MATLAB®, as seen in Figure 4.26.

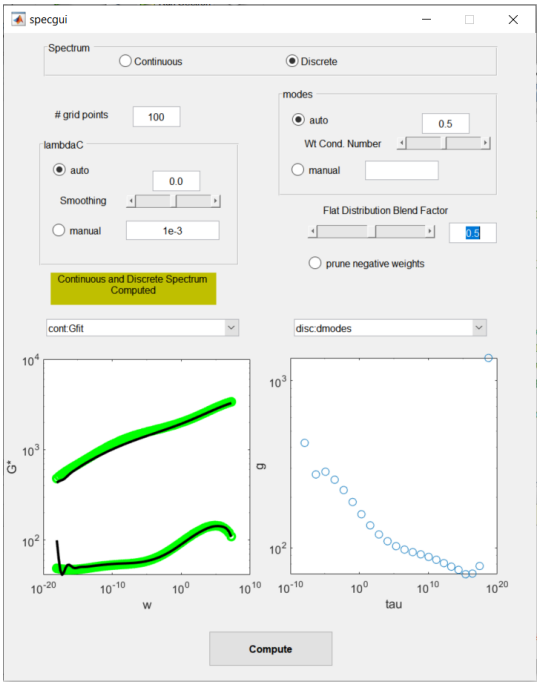

Figure 4.26: Screen capture of Respect v2.0 toolbox for MATLAB® [143]

In order to obtain the continuous spectrum in the frequency domain, the Tickhonov regularisation strategy was implemented [144], using a regularisation term λ_c that could be modified in the software. In addition, when computing the discrete relaxation modulus, the software allows the user to decide the number of modes, and the space between the τ_i values (*Flat Distribution Blend Factor* parameter in Figure 4.26). The algorithm also applies a condition number that can be used to control the relative importance of error and conditioning in determining the DRS values (see *ReSpect* manual for a detailed explanation). All of these parameters allowed a great control over the methodology to obtain the Prony values.

The master curve obtained in the previous section was used as an input in the *ReSpect* software to obtain the best Prony series fitting the data[3]. The values obtained for the discrete spectrum are displayed in Figure 4.27. For its implementation in the ABAQUS® numerical software, the last Prony term was considered as the long-term modulus ($E_\infty = 478$ MPa), and the rest of the terms were transformed to shear modulus. The values obtained are displayed in Appendix B.

[3]In this case, the fit is done for the complex Young modulus and then converted to shear modulus for its use in the numerical software.

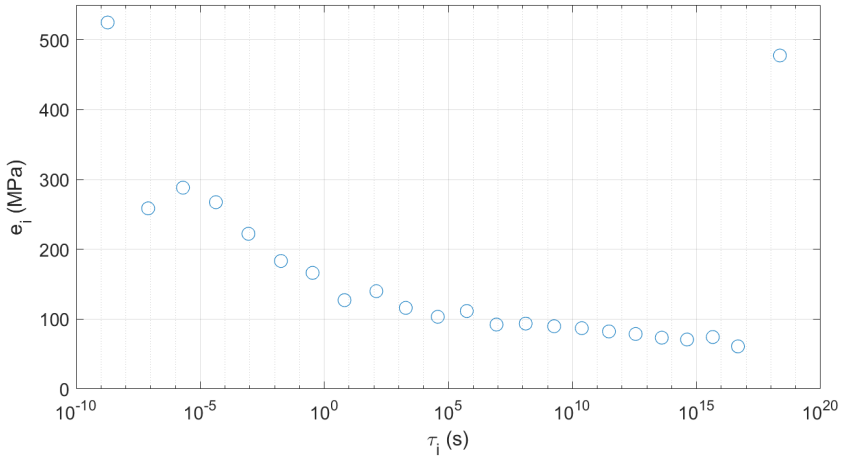

Figure 4.27: Prony series terms obtained from the experimental complex modulus master curve for Propil® material

Prony series validation

As the Prony modes are obtained as a numerical fit for experimental data, it is important to validate that the adjust is good enough. A way to perform this validation is to see if the resulting series are capable of reproducing the initial storage and loss modulus or if, on the contrary, the reproduced modulus are not good enough and more terms are needed.

First of all, it is important to understand the contribution of each Prony term in the storage and loss modulus. This is perfectly explained by Kraus and Niederwald [137] using a dummy 5-element series. One of the main conclusions of their analysis is that each Prony element has a influence of two decades in the storage modulus and up to four decades in the storage modulus (assuming that there is a τ_i per decade). This is graphically represented in Figure 4.28.

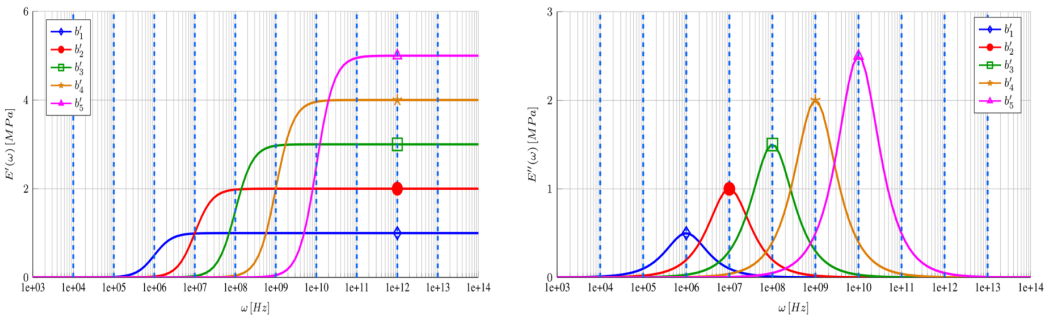

Figure 4.28: Influence of each Prony term in the storage (left) and loss (right) modulus. Reproduced from [137])

From Figure 4.29 and 4.30, it can be observed that the moduli reproduced from substituting the Prony series in equation 4.37 are very similar

to the initial experimental modulus. Instead, if a lower number of Prony terms is forced in *ReSpect* software, the resulting modulus obtained does not reproduce the experimental one. This is even more visible in the loss modulus, wherein lower terms can give very large fitting errors. Thus, it can be concluded that the Prony series obtained are capable of reproducing the experimental modulus in the frequency range considered.

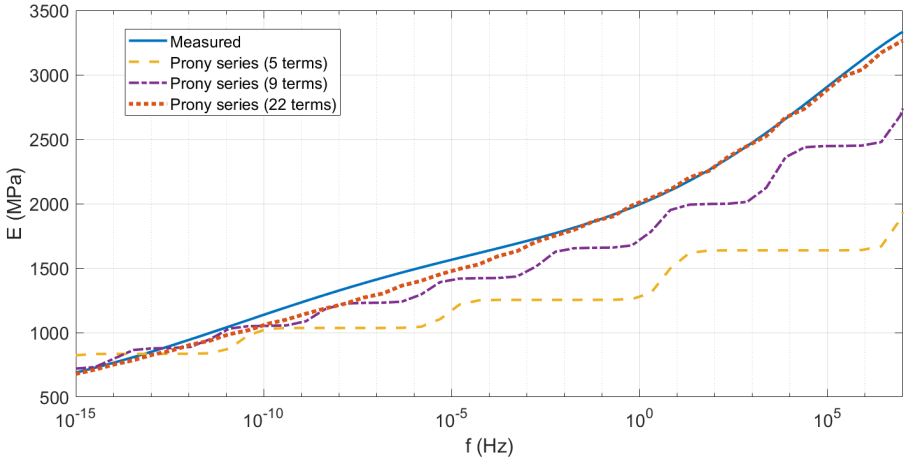

Figure 4.29: Comparison of the experimental storage modulus measured using the reproduced modulus from different Prony series

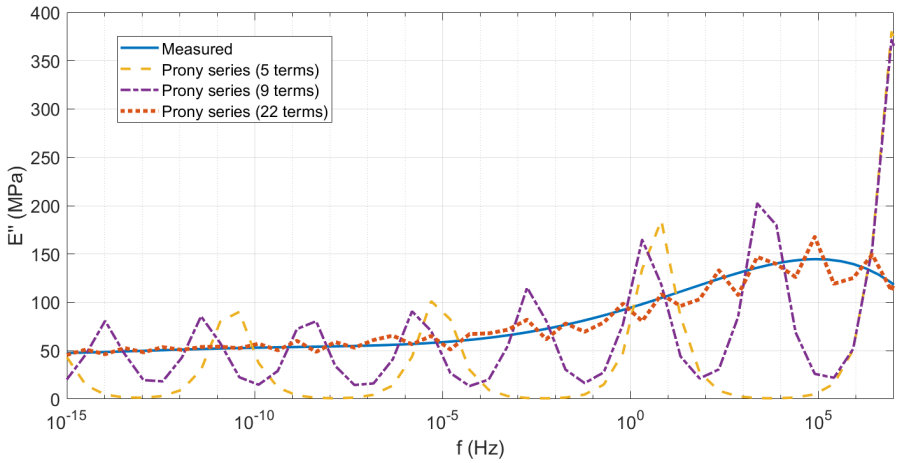

Figure 4.30: Comparison of the experimental loss modulus measured using the reproduced modulus from different Prony series

4.6 Numerical modelling approach

In this section a finite element analysis (FEA) of the heating process was performed to estimate the ultrasonic heating of a polymeric cylinder.
The thermal state of a polymer in USM process depends upon the thermomechanical state imposed by the action of the tools (the sonotrode, the plunger and the mould). This includes multiples effects such as viscoelastic deformation, friction and heat transfer due to conduction, convection and radiation. However, in the simulations presented in this section, it has been assumed that the polymeric cylinder is adiabatic due to the speed of the imposed process, the low thermal gradient developed and, also, the lack of knowledge of the thermal contact conductance.

The aim of the numerical simulation presented here is to reproduce the viscoelastic heating step of the polymer obtained in the experimental results displayed in section 4.4.3, and to obtain the influence of each component in the USM process, with the finality of finding its optimal values to process a given material.

In this work, ABAQUS® 2021 was used for the ultrasonic heating numerical simulations using a coupled thermomechanical model and an explicit solver. In addition COMSOL Multiphysics ® 5.3 was the commercial code employed for the eigenfrequency calculus in section 4.6.7.

4.6.1 FEA setup

The experimental model to be simulated is composed of an 8 mm diameter and 20 mm tall cylinder, which is subjected to the vibration of the sonotrode, the axial compression of the plunger and the influence of the mould in the lower zone. An axisymmetric numerical model was used for the simulation, considering a deformable element for polypropylene cylinder and rigid tools for the rest of the elements (see Figure 4.31). As the main goal is the prediction of the temperature in the cylinder, the use of rigid tools for the external elements is justified due to the rapidity of the process and the low thermal conductance between the elements (as a consequence of the low pressures used in the process, which does not allow a good contact between the surfaces). The boundary conditions imposed for each configuration are detailed in Table 4.4.

The default initial temperature used in the experiments is 293.15 Kelvin, although additional experiments starting at slightly different temperatures were performed to facilitate the comparison with experimental results. Even

though simulation results are given in Kelvin, temperatures were converted to Celsius degrees while being compared with experimental data.

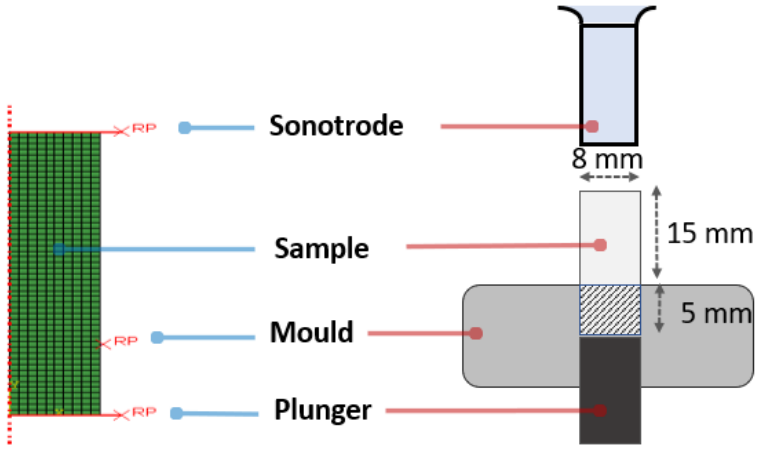

Figure 4.31: On the left, a finite element model with its mesh representing the simulated physical model shown on the right

The polypropylene cylinder was introduced in the model as a viscoelastic material whose temperature dependence is driven by the Prony series described in section 4.5. In addition, the temperature independent material properties were mainly obtained from the manufacturer's datasheet.
The material properties used in the simulation are summarised in Table 4.3, while the Prony values obtained for the cylinder can be found in Table B.1 in Appendix B.

Material	Physical property	Value	Reference
Propil® PP (Cylinder)	Density	910 Kg/m^3	[123]
	Young Modulus	478 MPa	Section 4.5
	Poisson's ration	0.3	[123]
	Specific heat	1598 $J/(Kg \cdot K)$	Section 4.3
	Heat conductance	0.22 $W/(K \cdot m)$	[123]

Table 4.3: Temperature independent material properties introduced in the numerical model

As previously stated, a coupled thermomechanical time dependent analysis was used in the simulation, involving two different physical fields simultaneously, that is, the mechanical and the thermal.
For the mechanical boundary conditions, prescribed displacements were

imposed in the model, as they generally give better convergence. Particularly, in order to introduce the movement of the sonotrode in the model, a sinusoidal displacement was prescribed for the direction along the axis of the cylinder, as:

$$u_z = a_{zero-peak} \sin(wt) \tag{4.38}$$

where $a_{zero-peak}$ is the *zero - peak* amplitude of the sonotrode for each configuration modelled. The standard way to represent ultrasonic amplitude values in the industry is using *peak - to - peak* measurements. Hence, half of the values of Table 4.1 must be considered in the amplitude value of the sonotrode boundary condition.

A prescribed displacement was also used as a boundary condition instead of a loading force when simulating the movement of the plunger. The displacement imposed consisted of averaged values from the experimental data measured. As can be seen in Figure 4.32, two-step piecewise functions were used to reproduce the experimental data, with a fast increment in the first 0.12 seconds (t_1, d_1) and a plateau during the remaining time (t_2, d_2). Experimental data from the plunger movement for each processed sample is displayed in Appendix B.

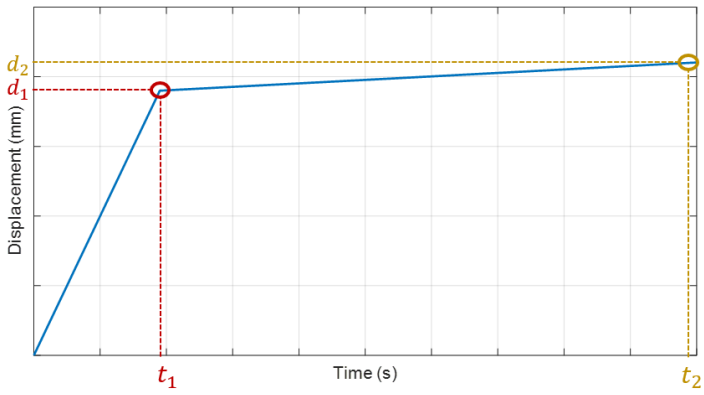

Figure 4.32: Piecewise representation of the movement of the plunger during time, used as a prescribed displacement for the FEA model

The mechanical boundary conditions used for each configuration are summarised in Table 4.4.

To model the contact pairing among the cylinder, the sonotrode and the plunger, the Coulomb law of friction was applied to the sliding behaviour, with a 0.1 coefficient. The mechanical transmission between surfaces is defined by a penalty exponential law that increases the material stiffness based on the distance between surfaces.

Element	Variable	Conf. 1	Conf. 2	Conf. 3	Conf. 4
Sonotrode	Frequency	30 kHz	30 kHz	30 kHz	30 kHz
	Zero-peak amplitude	14 μm	14 μm	22 μm	22 μm
Plunger Movement	Time (s)	Displacement (mm)			
	0	0	0	0	0
	0.12	0.55	0.84	0.55	0.84
	0.4	0.6	1.2	0.6	1.2
	1	0.6	1.2	0.6	1.2

Table 4.4: Values for mechanical boundary conditions

The thermal source in the cylinder is obtained from viscoelastic heating using an inelastic heat fraction of 0.9.

4.6.2 FEA solver selection

The selection of the FEA solver was one of the first decisions to be made. The ultrasonic heating of a polymer is a high speed event in a highly dynamic, mechanical situation. In this case, a correct representation of the ultrasonic waves within the cylinder was needed. Thus, it seemed that an explicit solver could be a better fit for this type of analysis.

In order to demonstrate this hypothesis, a simplified model was created considering the plunger and the sonotrode as rigid tools, and imposing the boundary conditions of Configuration 3 in Table 4.4. The thermo-mechanical state of the cylinder was obtained using implicit and explicit solvers. In both cases, two vibration cycles were analysed using a transient coupled thermomechanical model with a step time of 1e-6 seconds. A comparison of the displacement evolution in the axial direction between the implicit and explicit solvers is presented in Figure 4.33. A significant difference can be observed between both solvers. The implicit calculus does not model the ultrasonic wave transmission correctly along the cylinder, as all the nodes suffer simultaneous displacement. On the other hand, the dynamic explicit calculus clearly shows the movement of the ultrasonic wave along the different nodes of the cylinder.

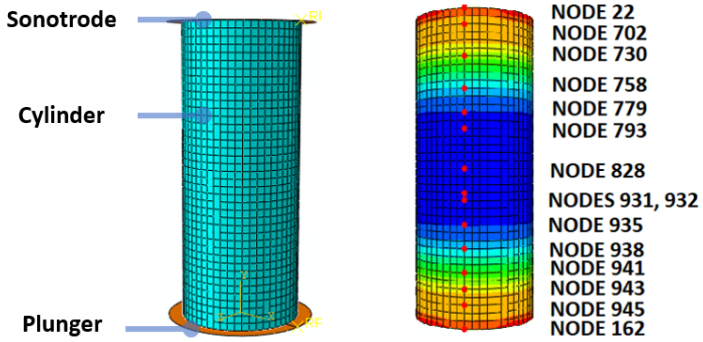

(a) Geometric model with hexaedric coupled temperature-displacement elements

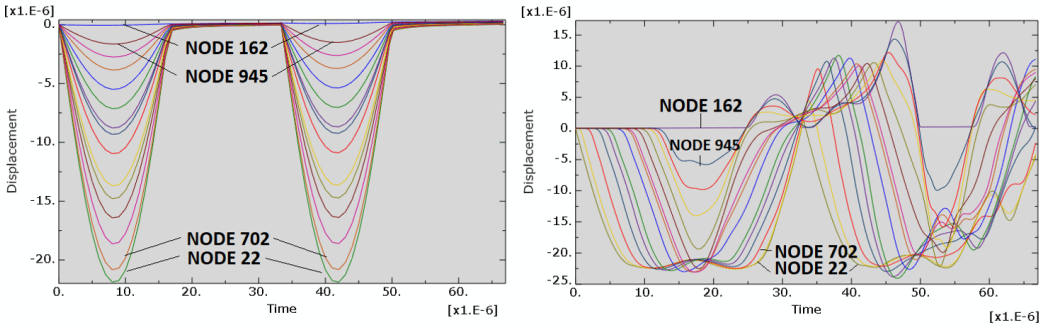

(b) Distribution of the displacement in the axial direction (in meters) for implicit model (left) and explicit model (right)

Figure 4.33: Comparison between the displacement distribution in the control nodes for the implicit and explicit solvers

A remarkable difference is also found in the viscoelastic energy obtained from the whole cylinder (ALLCD magnitude in ABAQUS ®), as can be observed in Figure 4.34. It can be seen that the viscoelastic energy for the explicit model is more than one order of magnitude greater than the energy obtained in the implicit model.

In order to obtain a simple estimation of the viscoelastic heating expected for this material, a simple analytical thermal model was used, following the approach used by Villegas et al. [145]. In this case, the loss modulus at 30 kHz was obtained from the frequency master curve (see Figure 4.22) and used to compute the heating ratio per volume in equation 4.39.

$$W = \pi f \epsilon_0^2 E'' \tag{4.39}$$

Ans ϵ_0 is computed as the engineering strain

$$\epsilon_0 = a_{zero-peak} / L_0 \tag{4.40}$$

where $a_{zero-peak}$ is the applied ultrasonic amplitude, and L_0 is the initial

length of the cylinder. Although the analytical equation is a very simple approximation that considers a constant unidirectional strain for the entire cylinder, the estimated viscoelastic energy obtained is more similar to the one obtained using the explicit method.

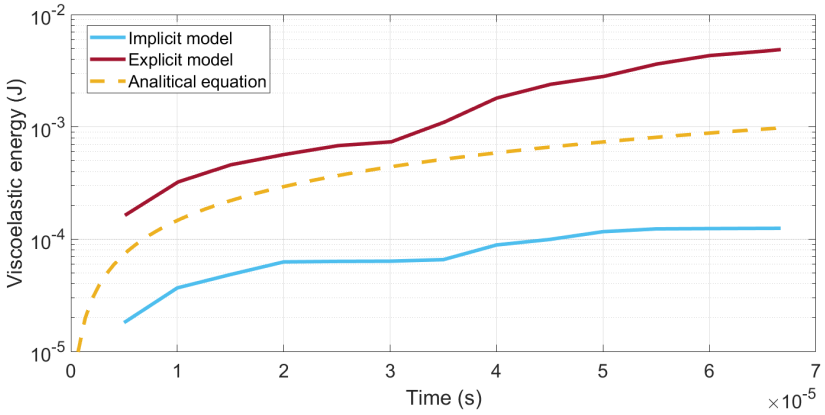

Figure 4.34: Viscoelastic energy evolution in the whole cylinder for two complete cycles obtained from the implicit model (blue), explicit model (red) and analytical formulation (dashed orange) using Configuration 3 parameters. A logarithmic scale is used along the Y axis to facilitate the comparison among the values

However, when the calculus was performed at lower frequencies (i.e. 4 Hz), the behaviours of both solvers were much more similar, as can be seen in Figure 4.35. The only remarkable difference between both methods at low frequency excitation is the bouncing of the polymer during the *discharge* for the explicit model. This effect is not observed in the implicit model.

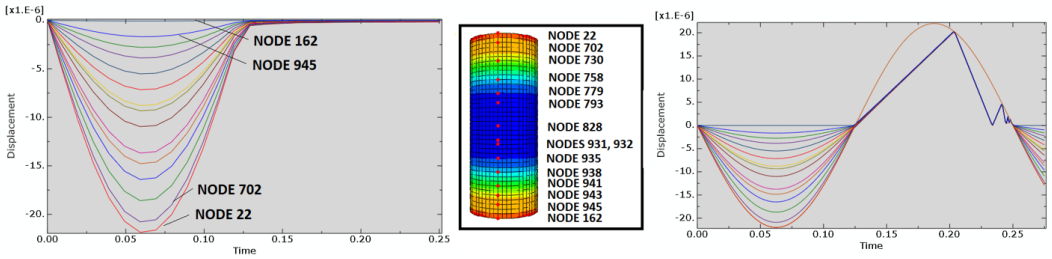

Figure 4.35: Comparison of axial displacement during a charge-discharge cycle at 4 Hz for the implicit model (left) and the explicit model (right)

4.6.3 Viscoelastic heating simulation and temperature distribution

Once the simulation strategy was defined (axisymmetric geometry and a transient coupled thermomechanical analysis using an explicit solver), the viscoelastic heating due to the effect of an ultrasonic mechanical wave was

analysed.

Upon comparing the results obtained from the numerical analysis with the experimental measurements, the first conclusion reached is that the temperature distribution along the axis of the cylinder shows remarkable differences (see Figure 4.36).

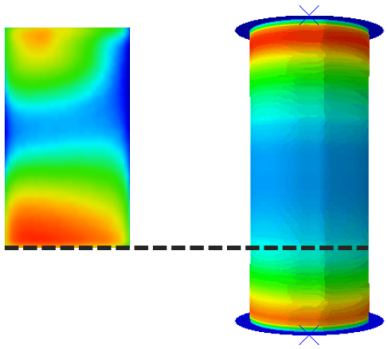

Figure 4.36: Qualitative comparison of the temperature distribution along the cylinder from experimental measurements (left) with the one obtained from the numerical model calculated with ABAQUS® including the sonotrode and the plunger movement (right). The dashed black line represents de mould partition. Only the region above the line is visible in the experiments

The temperature distribution in the experimental sample is stratified but not uniform, indicating that the contact among the cylinder, the sonotrode and plunger is not regular, or that the sample does not maintain an exactly vertical position while being deformed (may be due to the bouncing to which it is subjected by the vibration and compression of the plunger).

In contrast, the results of the numerical simulation are more regular, as would be expected from a numerical model. Here, the area directly affected by the sonotrode is the one with the highest temperature, followed by the area at the bottom of the cylinder, which bears the plunger compression, and finally the intermediate zone, which is much colder.

However, the most notable aspect of the experimental result is perhaps the intense concentration of heat in the region in contact with the upper end of the mould, which can only be explained by a sticking between the circular ring of the mould and the outer skin of the cylinder, as it will be discussed at the end of this section. Obviously, this phenomenon does not appear in the simulation because a contact algorithm has been implemented according to Coulomb's law with a relatively low coefficient of friction.

While in the experimental tests the lower region is the one that achieves more temperature, the numerical predictions give a remarkably different distribution. In the simulations, the upper region is the one with a higher heating rate and the lower region above the mould partition almost does not increase its temperature (see Figure 4.36). The numerical simulation predicts a higher temperature in the upper part of the cylinder, which is the nearest zone to the sonotrode, than in the lower part. These results match with the ones found in the literature (see [63]) but do not match with the experimental results.
This divergence in the results shows that there is an unexpected influence from the mould.

A possible hypothesis of this difference is related with the effect of the mould. Although the cylinders were machined to have a gap of around 0.1 mm with the mould cavity, they deform during the heating experiments and get in touch with the mould. This creates a region above the mould partition, wherein the cylinder expands beyond the mould cavity dimension. This effect is observed in processed cylinders, where the region that has remained inside the mould cavity has a lower diameter than the region outside the mould cavity (see Figure 4.37).

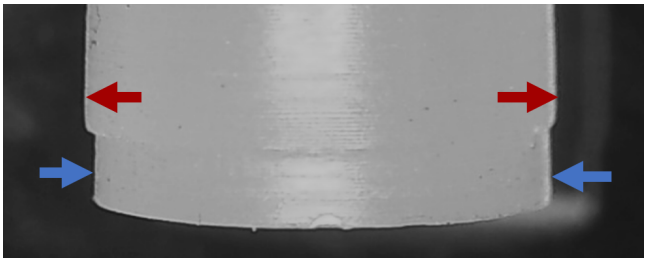

Figure 4.37: Image of the lower part of a cylinder after being processed with Configuration 1 parameters. A step change of the diameter is observed in the mould partition. Below the mould partition, the cylinder is compressed by the mould (blue arrows), while above this point, it expands its diameter (red arrows)

To simulate this effect of the mould, a modified geometry was considered for the cylinder with a step increase in the diameter around the mould partition. This change of diameter resulted the presence of sharp edges due to the contact between the mould and the cylinder (see Figure 4.38).

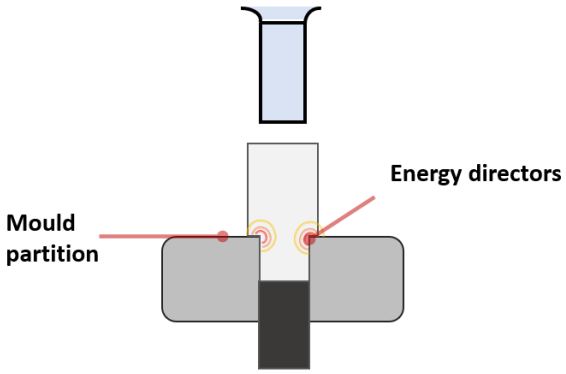

Figure 4.38: Sketch with a new geometry in the presence of energy directors in the mould partition

The effect of this contact could be considered analogous with the presence of energy directors. Energy directors are widely used in ultrasonic welding [145], and they are of critical importance in far-field ultrasonic welding, wherein the ultrasonic energy is transmitted through the polymer sample until it reaches an interface [92]. In this case, energy directors are used to magnify the heating in the desired interface and not around the sonotrode. Somehow, the experimental results obtained in the ultrasonic heating of the polymer resemble the behaviour of a far-field ultrasonic welding.

To study the effect of this geometry in the numerical model, the change of diameter in the cylinder was magnified x 10, with a resulting difference of 1 mm between the upper and the lower parts. This provided enough elements of an acceptable size to perform the simulation.

The results obtained using this new configuration show a change of tendency in the temperature distribution along the cylinder. This is because, in this case, the lower part of the visible cylinder (the one near the partition mould) has a higher temperature evolution than the rest of the workpiece (see Figure 4.40).

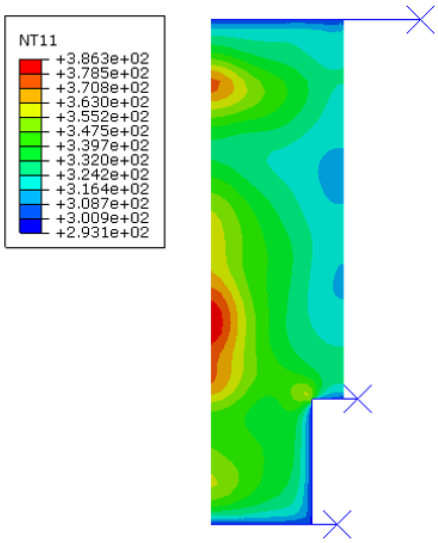

Figure 4.39: Temperature distribution in the modified geometry created to take into account the effect of a strong interference between the cylinder and the mould

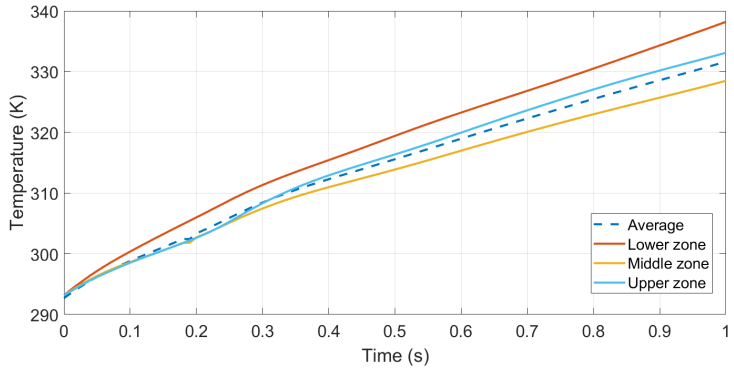

Figure 4.40: Temperature evolution considering the modified geometry

As can be deduced from the analysis of Figures 4.9, 4.11 and 4.36, across all the experimental tests, a sticking seems to develop between the specimen and the mould responsible for the particular distribution of the measured temperature. The numerical simulation only reproduces this phenomenon if the geometric defect in the cylinder that has been exposed above is incorporated. Under these conditions, the analysis of the effect of USM parameters on viscoelastic heating is carried out in the following sections using an ideal finite element model.

4.6.4 Effect of the ultrasonic amplitude

In the experimental measurements, the amplitude delivered by the sonotrode is the parameter with the greatest influence upon the ultrasonic heating of the polymer. Thus, in order to study the effect of this parameter in the simulation, a numerical model with no mould and without plunger displacement was constructed.

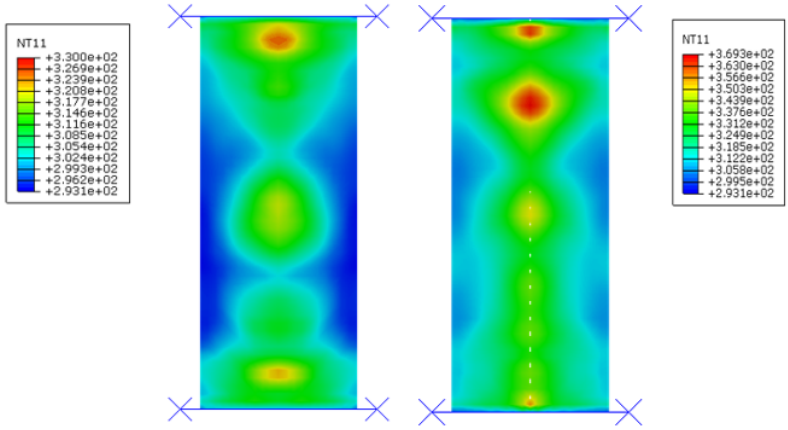

Figure 4.41: Mirror axisymmetric model with temperature distribution (in K) at 1 second under 14μm ultrasonic amplitude (left) and 22 μm ultrasonic amplitude (right)

The results of the simulation show a significant influence of the sonotrode amplitude in the viscoelastic heating of the material (see Figure 4.41). These results also show an irregular temperature distribution along the cylinder height, with the hottest zones being always around the axis of the cylinder.

Upon comparing the temperature distribution with the one obtained from the experimental results in Figure 4.36, it can be observed that the numerical simulation has no stratification but only an irregular distribution along the height of the cylinder. On the other hand, a comparison of the average heating rate of the visible part of the cylinder, shows that the numerical values are in agreement with the experimental results (see Figure 4.42).

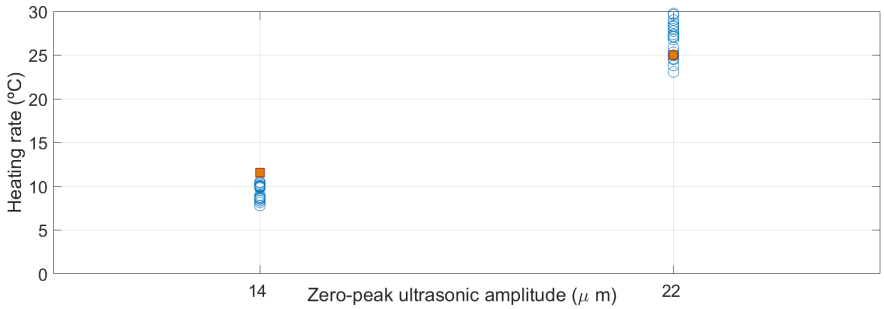

Figure 4.42: Comparison of the heating rate in the visible part of the cylinder between the experimental results (blue circles) and the numerical simulation (orange squares). Experimental configurations with different plunger values are used

A good prediction of the numerical simulation is also observed when the average temperature evolution is plotted against the numerical prediction obtained (see Figure 4.43).

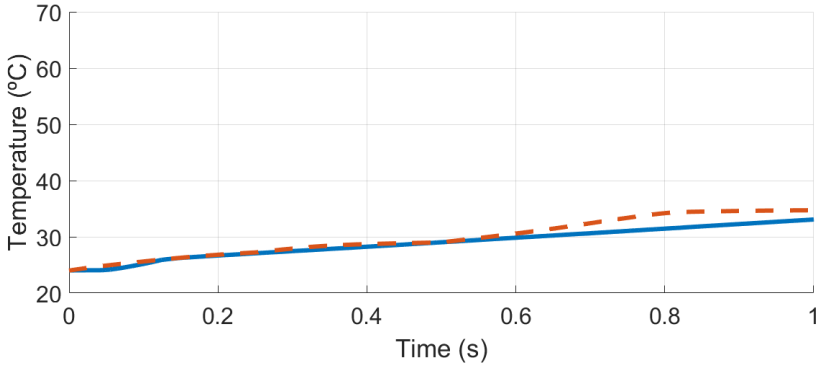

(a) Temperature evolution with zero-peak ultrasonic amplitude of 14 μm

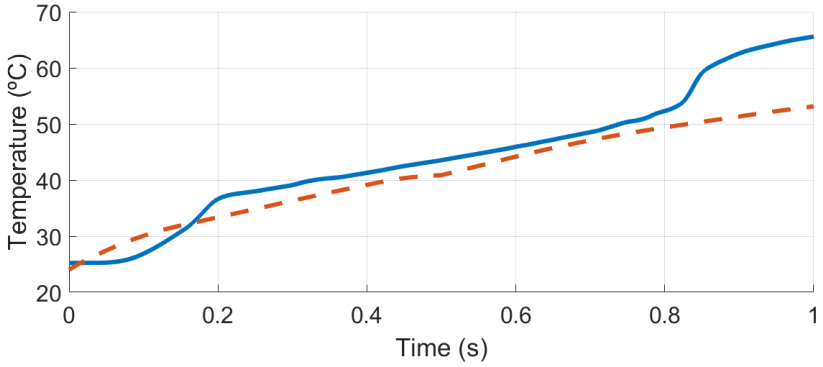

(b) Temperature evolution with zero-peak ultrasonic amplitude of 22 μm

Figure 4.43: Comparison of the average temperature evolution in the visible cylinder obtained in experimental tests (blue line) and numerical model (dashed red line): for the experimental results, cycle number 5 from configuration 1 (top) and cycle number 1 from configuration 3 (down) are used

The previous images show a precise correlation between the effect of the

ultrasonic amplitude on the average temperature of the cylinder predicted by the numerical model, and the experimental results obtained. In addition, it can be observed that the slope of the curve increases with an increment in the ultrasonic amplitude.
However, as explained in the previous section, the comparison between the numerical model and the experimental measurement for temperature evolution in each region of the cylinder shows remarkable differences (see Figure 4.44).

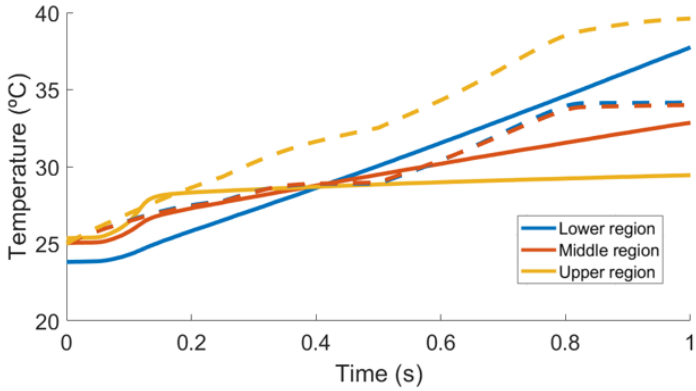

Figure 4.44: Comparison of the heating rate in the different regions of the visible part of the cylinder between the experimental results (solid line) and the numerical simulation (dashed line) without mould or plunger, for Configuration 1 parameters

In order to compare the numerical results with measurements obtained in ideal conditions, an additional set of experiments have been performed with very low plunger force (500N) and 14μm of amplitude *zero-to-peak*. These experiments are not discussed in section 4.4.3, as they are not repetitive enough, and the steps identified in Figure 4.12 are not clear in some of the experimental runs. However, the temperature evolution of one sample processed under these conditions shows a good agreement with the results estimated by the numerical model (see Figure 4.45).

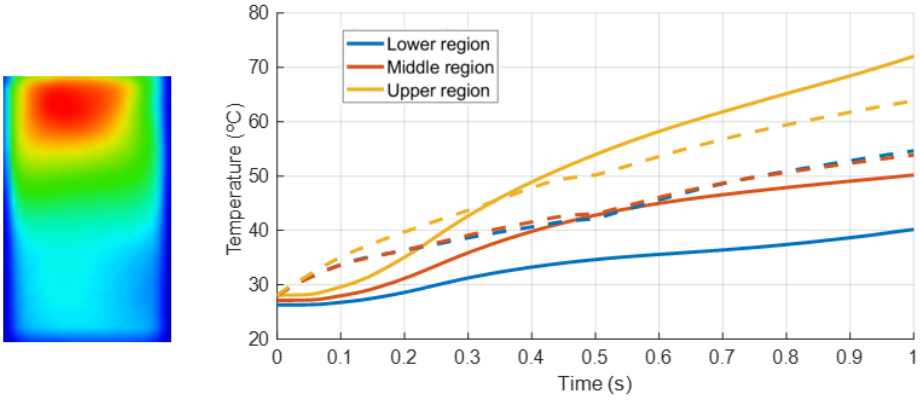

Figure 4.45: Experimental temperature distribution in a sample processed using a configuration with low force of the plunger (left); and comparison between the experimental values (solid line) and the numerical model created without plunger or mould (dashed line) using an amplitude of 14 μm (right)

The similarity with the previous results shows that the attachment between the cylinder and the mould does not take place for lower values of plunger force. In this case, the temperature distribution is much more similar to the one obtained in the numerical model.

4.6.5 Effect of the plunger movement

This section deals with the movement of the plunger, which is introduced into a model with sonotrode vibration and without mould. As previously described in section 4.6.1, the movement of the plunger is introduced as a prescribed displacement boundary condition with regard to the average values obtained in the experimental measurements.
As can be observed in Figure 4.46, the influence of the plunger in the temperature of the cylinder (difference between Configuration 1 and Configuration 2) is much lower than the influence of the ultrasonic amplitude (difference between Configuration 1 and Configuration 3). These results are in accordance with the ones obtained experimentally (see Figure 4.14).

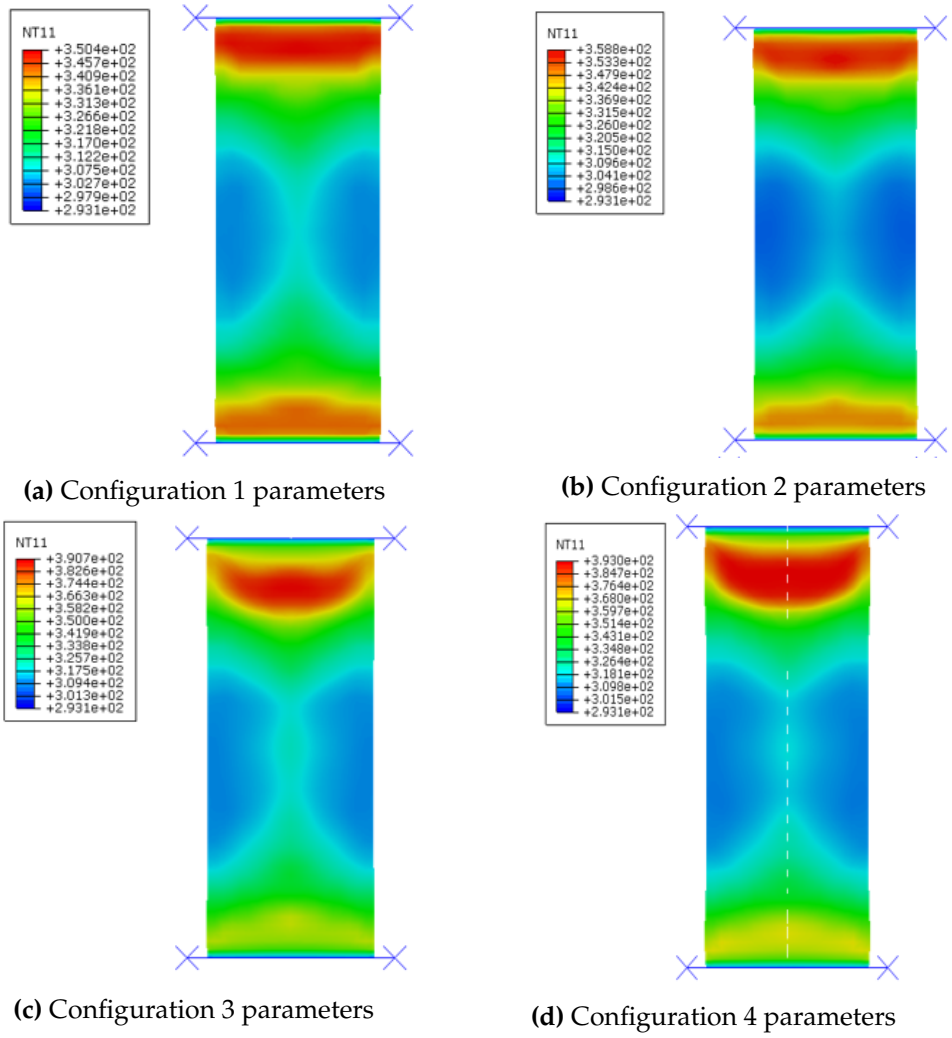

(a) Configuration 1 parameters

(b) Configuration 2 parameters

(c) Configuration 3 parameters

(d) Configuration 4 parameters

Figure 4.46: Temperature distribution (in Kelvin) at 1 second with different values of ultrasonic amplitude and plunger force

The displacement experimented upon the plunger occurs at a very high speed only at the beginning of the process, and then it almost stops during the rest of the cycle (see Figure 4.32). This behaviour is replicated with regard to the increment of temperature also. When the plunger movement is introduced into the numerical model, a significant increment of temperature is observed at the beginning of the process, followed by a thermal saturation (or stabilisation). This behaviour of the temperature is seen across all the zones of the cylinder for all the tested configurations wherein the plunger movement is introduced (see Figure 4.47).

In addition, the introduction of the plunger movement into the numerical model also affects the distribution of temperature along the horizontal axis of the cylinder. The temperature distribution becomes more stratified due to the action of the plunger, as can be seen in Figure 4.48.

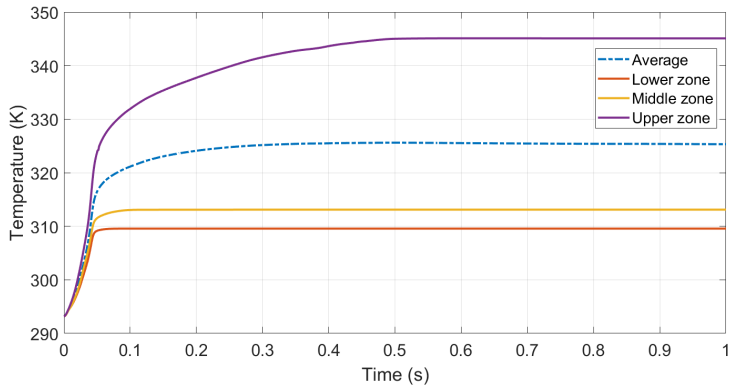

(a) Temperature evolution of the cylinder with plunger movement for configuration 2 parameters

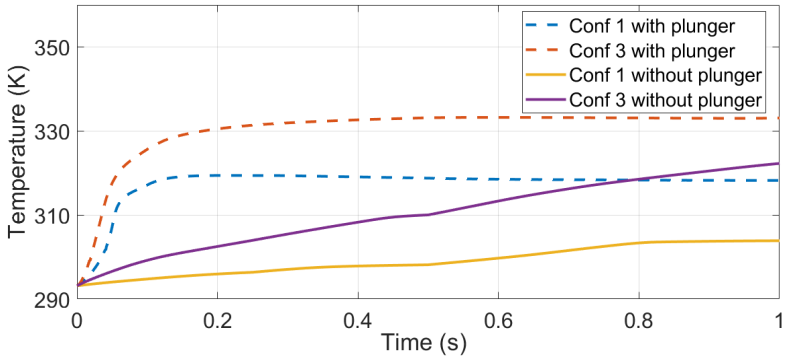

(b) Comparison between average temperature evolution of the cylinder with and without the movement of the plunger

Figure 4.47: Average temperature evolution of the cylinder obtained in the numerical model with plunger movement; Upper figure: Evolution of the temperature for each zone of the cylinder; Lower figure: comparison between the evolution with and without plunger

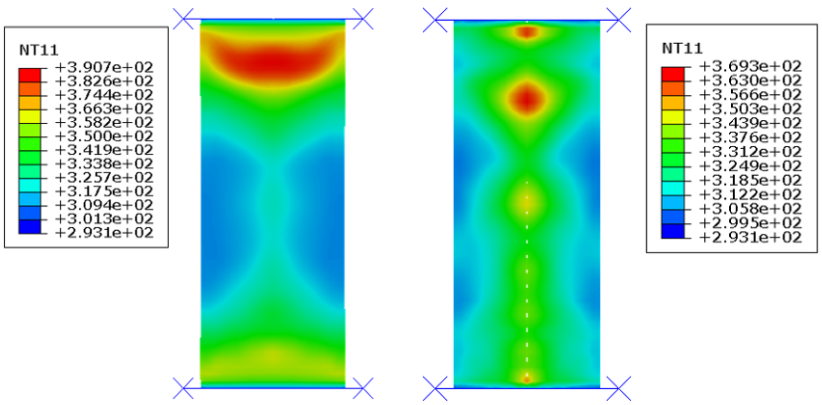

Figure 4.48: Temperature distribution (in K) for Configuration 3 parameters after 1 second with plunger movement (left) and without plunger movement (right)

In any case, the great thermal difference resulting from the presence or absence of plunger action originates precisely from the different levels of deformation developed in the material. In Figure 4.49, the logarithmic strain along the direction of the length of the cylinder, *LE22*, with and without the influence of the plunger is plotted. It should be noted that the addition of the plunger completely modifies the strain of the sample. The same figure also shows how this strain is caused by plunger displacement over time.

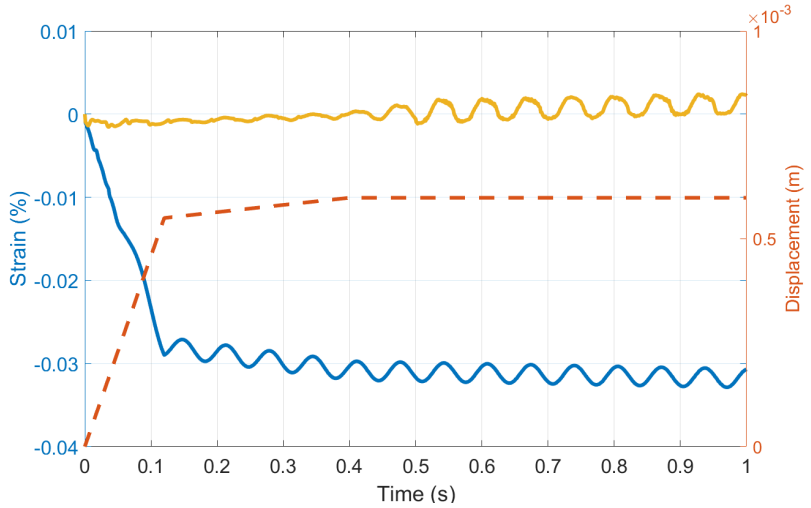

Figure 4.49: Logarithmic strain obtained for Configuration 3 parameters including the plunger influence (blue) and including only the sonotrode vibration (yellow). The displacement of the plunger is also displayed along the right axis (orange)

4.6.6 Effect of the mould

As previously discussed, the interaction between the cylinder and the mould is affecting the experimental results. As the cylinder gets stuck in the mould during the process, the edge of the mould partition acts as an energy director and the zone nearer to the mould is heated faster than the rest of the cylinder. Although this behaviour has been reproduced qualitatively in section 4.6.3 by magnifying the cylinder deformation, in this section a different approach is used. In this case, the mould is introduced as a rigid tool with friction interference with the cylinder.

This interaction between the mould and the cylinder creates a ring of stress, as a result of the strain generated around the mould partition (see Figure 4.50).

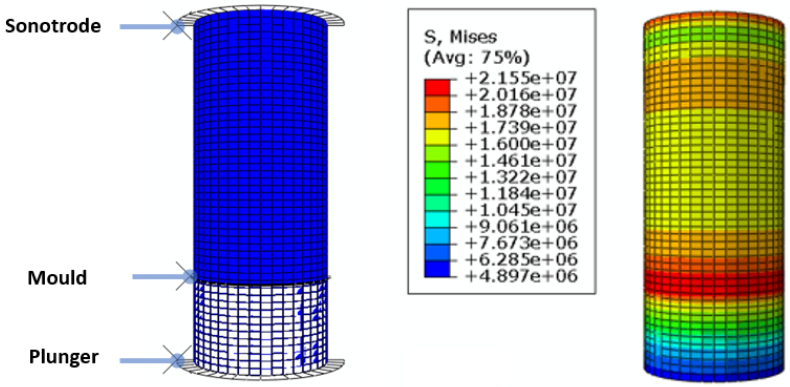

Figure 4.50: Revolved view of the cylinder with the rigid tools defined (sonotrode, plunger and mould) (left) and the resulting von Mises principal stress (in Pa) at 1 second for Configuration 1 parameters (right)

If we look into the details of the mechanical behaviour of the cylinder in this region, it can be seen that the radial component of the stress (S11) component below the mould partition is a compressive component, while the same variable is tensional above the mould (see Figure 4.51). This state of stress is responsible for the experimental results and its observed expansion during the process. The predicted radial displacement just above the mould partition is around 0.01mm. Instead, the average expansion measured in the processed cylinders is 0.04 ± 0.02 mm. The experimental value is expected to be greater because it is measured at the end of the polymer processing (the 4 steps identified in section 4.4), while the numerical model is valid only until the end of *Step 2*.

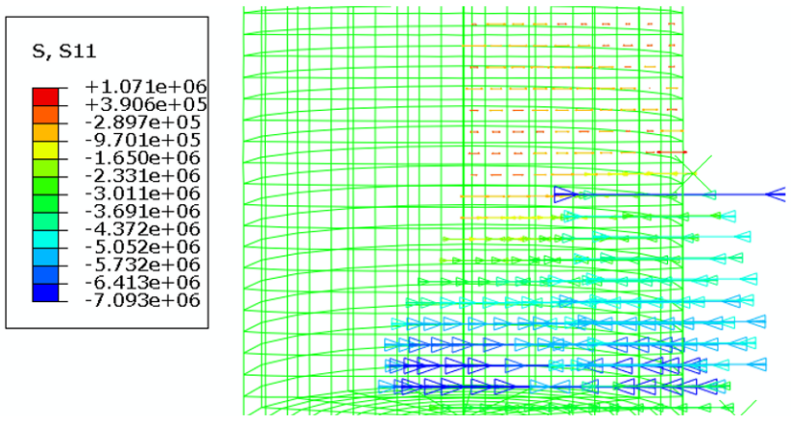

(a) Detail of the stress in radial direction (in Pa)

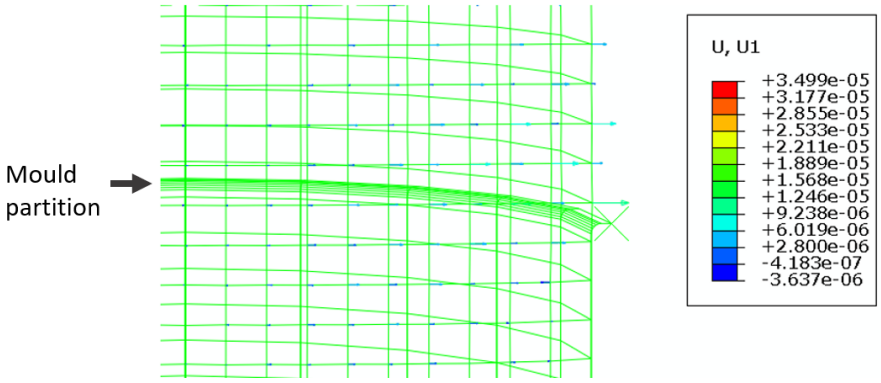

(b) Detail of the displacement of the cylinder in radial direction (in meters)

Figure 4.51: Detail of radial stress and displacement in the zone of the cylinder around the mould partition processed under Configuration 1 parameters

The presence of the mould modifies the temperature distribution in the cylinder and creates a localised hotspot around the mould partition, as can be seen in Figure 4.52. However, the effect of the plunger still creates a highly inhomogeneous temperature evolution, with a very swift rate of temperature increment at the beginning and an almost flat behaviour during the rest of the process. In addition, the effect of the mould does not change the average temperature distribution within the cylinder.

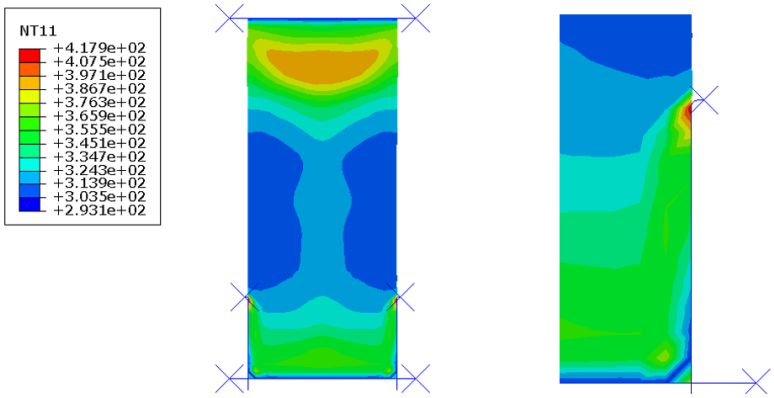

(a) Temperature distribution along the cylinder (left), and detail around the mould partition (right)

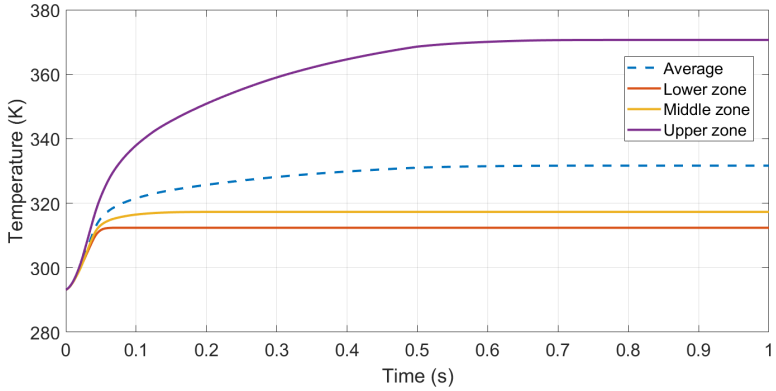

(b) Average temperature evolution of the visible part of the cylinder

Figure 4.52: Temperature evolution of a cylinder processed under Configuration 3 parameters taking into account the effect of the plunger and the mould

The results show that the introduction of the mould as a rigid tool with displacement constraints changes the stress distribution and creates a localised increment of temperature around the mould partition. However, its effect is not observed in the average temperature distribution, and the numerical prediction is not able to reproduce the behaviour observed in the experiments.

To summarise the results obtained in the previous sections, the effect of each of the tools on the average temperature distribution of the cylinder is summarised in Figure 4.53, for an ultrasonic amplitude of 22 μm.

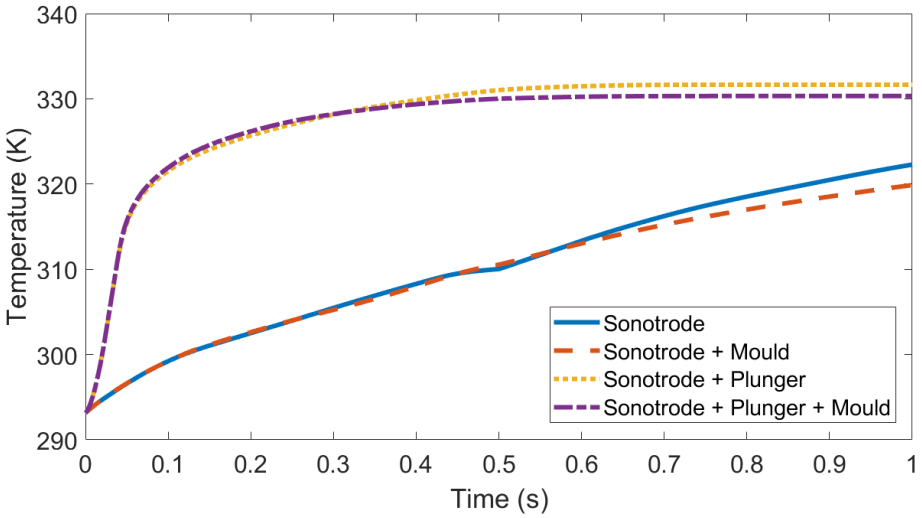

Figure 4.53: Average temperature evolution of the visible zone of the cylinder (in K) for different models that introduce the effect of the tools using Configuration 3 parameters

4.6.7 Study of the heating rate peak

The numerical results presented in the previous sections are related to *Step 1* stage and, mostly, to *Step 2* stage, as described in Figure 4.12 . However, during the experimentation process, a sharp peak in the heating rate is observed across all the cycles in *Step 3*. This peak substantially increases the temperature of the cylinder within a very short period of time. In addition, the results presented in Figure 4.16 show that there is a strong relation between the ultrasonic power consumed by the ultrasonic generator, and the heating rate of the cylinder. A similar increment in temperature was observed by Jiang et al. [126] and it was attributed to the glass transition temperature of the material (T_g). However, this cannot be the cause in this case, as typical values for T_g in polypropylenes are below 0 degrees Celsius.

In this research study, the origin of the peak in the heating rate is considered to have been caused by a resonance effect. In order to validate this hypothesis, varied cylinder lengths have been tested (see configurations 5 to 8 from Table 4.1). The results obtained from the temperature measurement show that the peaking of the heating rate takes place earlier in time and at lower temperatures when the longitude of the cylinder increases (see Figure 4.54). This indicates that this peak is somewhat related to the geometry of the cylinder.

On the other hand, the data obtained from the ultrasonic equipment show an abrupt change in the phase of the signal along with a change in the frequency of the equipment, which is a typical resonance behaviour (see Figure 4.55).

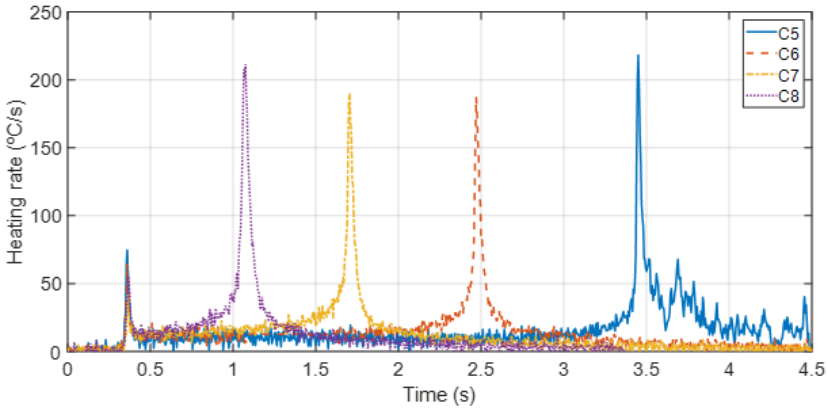

Figure 4.54: Heating rate evolution for configurations 5-8

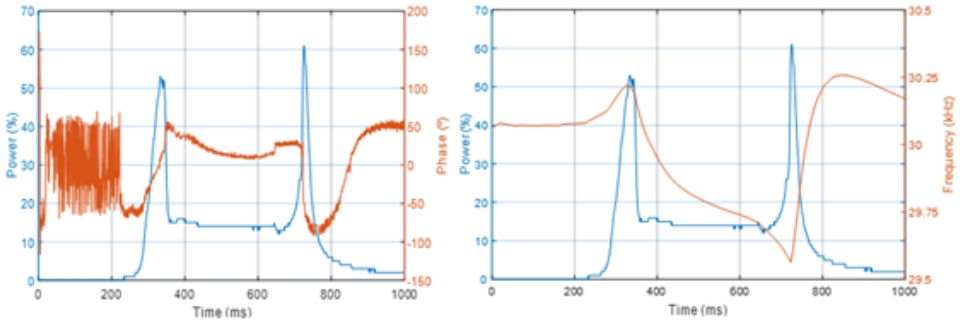

Figure 4.55: Graphs obtained from ultrasonic generator during an experimental test for 22 mm cylinder. First peak of power takes place when the sonotrode is coupled with the cylinder. It can be observed that the phase and frequency changes in the second peak

According to these results, it seems that the second peak occurs when the cylinder is in resonance mode with the acoustic unit. For this resonance to take place, the length of the cylinder must be equal to $\lambda_{res}/2$, where λ_{res} is the resonance wavelength. In order to study this behaviour, the master curve of Young modulus with temperature calculated at 30 kHz was introduced into COMSOL Multiphysics® software, and an eigenfrequency analysis was performed. For each cylinder configuration, the temperature at which the longitudinal vibration mode equals the resonance frequency of the equipment (30 kHz) was obtained. In Figure 4.56, the comparison between the temperature obtained by FEA and the average temperature obtained experimentally across all the cylinders is displayed.

Although the temperature values obtained using the numerical analysis are quite different from the average experimental temperatures recorded at the peak point, the results reveal the same tendency and seem to validate the hypothesis that the peak is caused by a resonance process. Differences

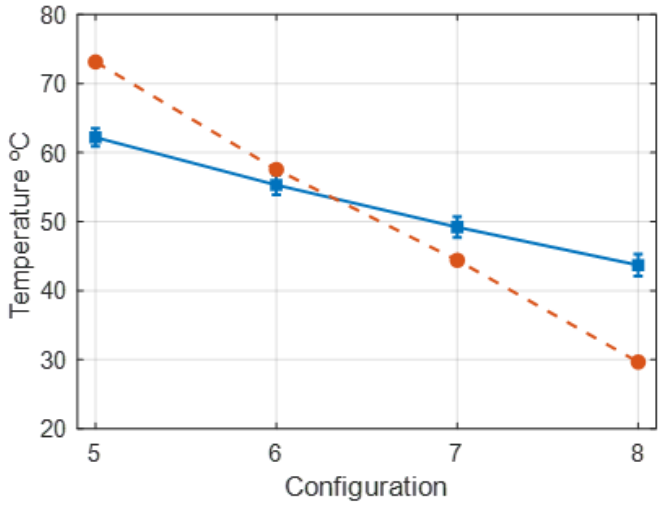

Figure 4.56: Comparison between simulated and measured temperatures at heating rate peak for each configuration. In dashed orange, temperatures at which the longitudinal eigenfrequency mode calculated using COMSOL Multiphysics® of each cylinder stands at 30 kHz. In blue, the average temperature at heating rate peak and its error bar for each tested configuration

between simulation and experimental results could be related to the fact that a homogeneous temperature has been considered for the entire cylinder in the numerical model.

4.7 Conclusions

The results obtained in this study show that the temperature evolution in polypropylene cylinders under ultrasonic excitation shows a non-linear behaviour over time. Moreover, different regions of the specimen increase their temperatures at different rates, showing an important thermal gradient along the height of the cylinder. In order to analyse this behaviour during the experiments, three regions have been defined within the cylinder (upper, middle and lower). In addition, three main steps have been established, based on the evolution of the heating rate over time, which shows an initial peak (Step 1), followed by a flat region (Step 2) and a high peak (Step 3), and then the material starts to deform. The lower region shows the most constant increment of temperature during the whole process, while the upper region almost maintains its temperature until Step 3, when it rises abruptly following a sigmoidal law. Although the values are significantly different, the shape of the heating rate curve is similar for all the geometric regions of the cylinder. After the first step wherein the sonotrode comes into contact with the cylinder, a constant heating rate region is found (Step 2). This region has a heating rate between 7 °C/s and 30 °C/s that seems to be linked with

the viscoelastic heating of the material. After that, a high heating rate peak is found, and the temperature of the cylinder rises abruptly (Step 3). In addition, both heating rate and consumed power of the ultrasonic generator have the same evolution profile. The correlation between these magnitudes could be used in the future to estimate the temperature of the polymer melt, without the need to use in-mould sensors. Besides, based on the correlation coefficients it may be estimated that the efficiency of ultrasonic heating is around 22%.

In order to model the behaviour of the material, a time-temperature master curve has been obtained based on DMA measurements, and a set of Prony terms has been obtained, which successfully reproduce the measured storage and loss modulus. The viscoelastic model has been used in the numerical simulations to reproduce the observed ultrasonic heating.

An explicit model has been generated using the ABAQUS ® FEM software. The numerical model is able to predict the average heating rate of the sample, but presents significant divergences in the estimation of the temperature distribution along the cylinder.
Differences between the numerical model and the experimental results are assumed to be related to the influence of the mould during the experimentation.

The mould, in its role of containing the specimen, alters the state of stresses and strains of the cylinder and, therefore, can condition the temperature distribution of its lower part. This hypothesis has been validated by applying the model to a magnified deformed cylinder. This model has been found to be able to qualitatively reproduce the experimentally obtained temperature distributions.

The numerical model also correctly identifies the ultrasonic amplitude as the parameter with the greatest effect upon the viscoelastic heating process, while the influence of the plunger and the mould is less significant. In any case, the introduction of plunger displacement into the numerical model abruptly changes the temperature evolution in the cylinder, resulting in a rapid heating followed by a thermal saturation. Although the effect of the interaction between the plunger and the vibration has been presented in this chapter, it should be analysed in-depth in future research.

In this chapter, the study of the nature of the heating rate peak has also been addressed. Additional configuration tests are carried out to discover that the time and temperature of the peak varies with the cylinder length. In addition, there is a phase change and an asymptotic behaviour of the ultrasonic generator frequency in the vicinity of the power peak. These results indicate that the peak could be associated with a resonance behaviour. The results obtained from a numerical eigenvalue analysis show that polypropylene cylinders indeed have a longitudinal resonance mode near the ultrasonic generator frequency (30 kHz). This mode is found at different temperatures depending on the cylinder length.

5 Conclusions

The results obtained in this research study have allowed us to improve the repeatability and robustness of USM technology, by developing a new configuration resulting in a new patent. In addition, advances have been made towards understanding the ultrasonic heating of polymers and its relationship with the main parameters of the USM process. The major conclusions related to the specific objectives of this research study are presented here.

USM technology conclusions

- The application of USM to thermoplastic polymers has been reviewed, thereby proving that this technology is capable of moulding a large quantity of thermoplastic polymers. However, the influence of the processing factors on the measurable responses (filling, mechanical properties, degradation) has still not been completely understood.
- Most of the published articles are based on the study of USM ability to process materials, but very little information has been found about the repeatability of the technology.

New configuration for ultrasonic moulding process

- The use of the nodal point concept in USM technology shows an improvement in the quality of the manufactured parts (as well as in the repeatability of this quality), while processing a polyoxymethylene and a cyclic olefin polymer.
- Melt temperature and pressure obtained for the best processing conditions of NPUSM match the material providers recommendations.
- Best process parameters have allowed the manufacture, under stable conditions, of a large number of tensile specimens, whose physical and mechanical properties (geometry, presence / absence of defects, stress-strain ratio in uniaxial tensile tests, molecular weight and stress patterns) meet the requirements for this type of components.
- The results obtained for NPUSM processing are comparable with those obtained in equal specimens manufactured using the well-established conventional injection moulding technology. The ability to process these materials has improved greatly with the use of NPUSM configuration, in comparison to standard USM.
- The results of this research show that NPUSM is a robust technique, which improves the processability of polyoxymethylene and cyclic olefin polymer, and that it stands as a convincing industrial technique for manufacturing of polymeric parts.

Ultrasonic heating evolution

- The temperature evolution in polypropylene cylinders under ultrasonic excitation has a non-linear behaviour over time, and different regions of the specimen increase its temperature at different rates, showing an important thermal gradient along the height of the cylinder.
- The lower region shows the most constant increment in temperature during the entire process, while the upper region almost maintains its temperature until a certain time, when it rises abruptly following a sigmoidal law.
- Although the values are significantly different, the shape of the heating rate curve is similar for all the geometric regions of the cylinder.
- The average viscoelastic heating rate measured in the sample is between 7°C/s and 30°C/s, depending on the conditions.

- Both heating rate and consumed power of the ultrasonic generator have the same evolution profile. Based on the correlation coefficients, it may be estimated that the efficiency of ultrasonic heating is around 22%.
- A time-temperature master curve has been obtained from DMA measurements. From it, a set of Prony terms has been achieved that successfully reproduce the measured storage and loss modulus.
- An explicit thermomechanical model using ABAQUS ® software has been developed. The model is able to correctly predict the average heating rate of the sample, but shows differences in the estimation of the temperature distribution along the cylinder.
- The differences between the numerical model and the experimental results are related to the influence of the mould during the experimentation, and can be minimised if a deformed cylinder is used in the model. However, further work is needed to fully reproduce the experimental behaviour.
- The numerical model agrees with the experimental results in highlighting the sonotrode amplitude as the main parameter having the biggest influence upon viscoelastic heating. However, there is a strong interaction between the ultrasonic amplitude and the plunger, as the introduction of the plunger into the numerical model significantly changes the temperature evolution.
- The peak in the heating rate could be associated with a resonance behaviour. This hypothesis agrees with the modes obtained from different cylinder lengths using a numerical eigenvalue analysis

Future work

This research study has taken some important steps towards improving the robustness of the USM and its applicability to industrial environments. However, there remains much research work to be carried out in the future, in order to further advance the understanding and development of this technology. Further areas for further research are outlined below.

- *Nodal point* methodology has improved the standard USM method in almost every aspect (repeatability, sample contamination, sample quality), but has considerably increased the sprue needed to manufacture a sample. In order to facilitate the adoption of this technology for industries processing costly materials, this sprue needs to be reduced. The solution to this issue would probably involve a major redesign of the sonotrode and/or other machine components.

- In this study, the validation of the repeatability of an experimental configuration is done by using data from in-mould sensors. Although this is a very reliable method, the sensor specifications limit the maximum mould temperatures and melt pressures used in the process. Some technical materials exceed these limits; hence, in such cases, no repeatability validation could be performed. In order to overcome this limitation, the study of indirect measurements of in-mould data should be examined and considered.

- Ultrasonic heating is a very fast process and hence very difficult to isolate during a simple experimentation. The experiments carried out in this study involved an undesirable interaction between the samples and mould, which changed the temperature distributions along the cylinder. Simpler experiments using high-speed thermal cameras should be performed, in order to obtain a more precise measurement of the viscoelastic heating of the polymer.

- The correlation between the heating rate measured and the power consumed by the ultrasonic generator could be used to estimate the temperature of the polymer melt, without the need to use in-mould sensors. The study of this relationship in more complex scenarios (pellets, cavity filling) should be considered.

- The numerical model presented here provides a lot of information about the influence of the parameters in USM. However, more work is needed to obtain a model able to completely reproduce the experimental behaviour. Future numerical implementations should contemplate the use of hyper-elastic models and, even visco-plastic models to simulate the ultrasonic heating of polymer pellets.

Bibliography

[1] W. Michaeli, R Maesing, T Kampes, S Hessner, A. Spennemann, and R. Gärtner. New plastification concepts for micro injection moulding. *Microsystem technologies*, 8(1):55–57, 2002.

[2] B. Zhao, Y. Qiang, W. Wu, and B. Jiang. Tuning power ultrasound for enhanced performance of thermoplastic micro-injection molding: Principles, methods, and performances. *Polymers*, 13(17):2877, 2021.

[3] A. Benatar. *Ultrasonic welding of advanced thermoplastic composites*. PhD thesis, Massachusetts Institute of Technology, 1987.

[4] M. Lucas, J. N. Petzing, A. Cardoni, and L. J. Smith. Design and characterisation of ultrasonic cutting tools. *CIRP Annals - Manufacturing Technology*, 50(1):149–152, 2001.

[5] J. Sackmann, K. Burlage, C. Gerhardy, B. Memering, S. Liao, W.K. K Schomburg, C. Gerhardy, J. Sackmann, S. Liao, K. Burlage, B. Memering, C. Gerhardy, B. Memering, S. Liao, and W.K. K Schomburg. Review on ultrasonic fabrication of polymer micro devices. *Ultrasonics*, 56:189–200, 2015.

[6] A. Sato, H. Sakaguchi, H. Ito, and K. Koyama. Evaluation of replication properties on moulded surface by ultrasonic injection moulding system. *Plastics, Rubber and Composites*, 39(7):315–320, 2010.

[7] BCC Research. Micro Injection Molding: Global Markets, 2020.

[8] M. Janer, X. Plantà, and D. Riera. Ultrasonic moulding: Current state of the technology. *Ultrasonics*, 102, 2020.

[9] M. Janer, T. López, X.r Plantà, and D. Riera. Ultrasonic nodal point, a new configuration for ultrasonic moulding technology. *Ultrasonics*, 114(June 2020):1–10, 2021.

[10] M. Sacristán, X. Plantá, M. Morell, and J. Puiggalí. Effects of ultrasonic vibration on the micro-molding processing of polylactide. *Ultrasonics Sonochemistry*, 21(1):376–386, 2014.

[11] J. Grabalosa, I. Ferrer, A. Elías-Zúñiga, and J. Ciurana. Influence of processing conditions on manufacturing polyamide parts by ultrasonic molding. *Materials and Design*, 98:20–30, 2016.

[12] M. Planellas, M. Sacristán, L. Rey, C. Olmo, J. Aymamí, M. T. Casas, L. J. Del Valle, L. Franco, and J. Puiggalí. Micro-molding with ultrasonic vibration energy: New method to disperse nanoclays in polymer matrices. *Ultrasonics Sonochemistry*, 21(4):1557–1569, 2014.

[13] P. Negre, J. Grabalosa, I. Ferrer, J. Ciurana, A Elías-Zúñiga, and F. Rivillas. Study of the ultrasonic molding process parameters for manufacturing polypropylene parts. *Procedia Engineering*, 132:7–14, 2015.

[14] U. Heredia, E. Vázquez, I. Ferrer, Ciro A. Rodríguez, and J. Ciurana. Feasibility of manufacturing low aspect ratio parts of PLA by ultrasonic moulding technology. *Procedia Manufacturing*, 13:251–258, 2017.

[15] T. Dorf, K. Perkowska, M. Janiszewska, I. Ferrer, and J. Ciurana. Effect of the main process parameters on the mechanical strength of polyphenylsulfone (PPSU) in ultrasonic micro-moulding process. *Ultrasonics Sonochemistry*, 46:46–58, 2018.

[16] M. Sortino, G. Totis, and E. Kuljanic. Comparison of injection molding technologies for the production of micro-optical devices. *Procedia Engineering*, 69:1296–1305, 2014.

[17] D. Ensminger and L. J. Bond. *Ultrasonics: fundamentals, technologies, and applications*. CRC press, 2011.

[18] Y. Yao, Y. Pan, and S. Liu. Power ultrasound and its applications: A state-of-the-art review. *Ultrasonics Sonochemistry*, 62:104722, 2020.

[19] D. Ensminger and F. B. Stulen. *Ultrasonics: data, equations and their practical uses*. CRC press, 2008.

[20] A. I. Isayev, R. Kumar, and T. M. Lewis. Ultrasound assisted twin screw extrusion of polymer-nanocomposites containing carbon nanotubes. *Polymer(Guildf)*, 50(1):250–260, 2009.

[21] M. Moles, A. Roy, and V. Silberschmidt. Ultrasonically-assisted Polymer Molding: An Evaluation. In *Physics Procedia*, volume 87, pages 61–71, 2016.

[22] Y. J. Yang, C. C. Huang, S. K. Lin, and J. Tao. Characteristics analysis and mold design for ultrasonic-assisted injection molding. *Journal of Polymer Engineering*, 34(7):673–681, 2014.

[23] H. Zheng, S. Gao, X. Yang, Z. Qiu, and F. Fang. Investigation of micro-injection molding based on longitudinal ultrasonic vibration core. *Applied Optics*, 54(28):8399, 2015.

[24] C. Espinoza-González, G. Martínez-Colunga, A. Maffezzoli, F. Lionetto, D. Bueno-Baqués, and C. Ávila-Orta. An Overview of Progress and Current Challenges in Ultrasonic Treatment of Polymer Melts. *Advances in Polymer Technology*, 32(S1):E582–E602, 2012.

[25] A. Levy, S. Le Corre, and I. F. Villegas. Modeling of the heating phenomena in ultrasonic welding of thermoplastic composites with flat energy directors. *Journal of Materials Processing Technology*, 214(7):1361–1371, 2014.

[26] M. N. Tolunay, P. R. Dawson, and K. K. Wang. Heating and bonding mechanisms in ultrasonic welding of thermoplastics. *Polymer Engineering & Science*, 23(13):726–733, 1983.

[27] H. Mekaru, H. Goto, and M. Takahashi. Development of ultrasonic micro hot embossing technology. *Microelectronic Engineering*, 84(5):1282–1287, 2007.

[28] A. Levy, S. Le Corre, and A. Poitou. Ultrasonic welding of thermoplastic composites: A numerical analysis at the mesoscopic scale relating processing parameters, flow of polymer and quality of adhesion. *International Journal of Material Forming*, 7(1):39–51, 2014.

[29] W. Kardyś, A. Milewski, P. Kogut, and P. Kluk. Universal ultrasonic generator for welding. *Acta Physica Polonica A*, 124(3):456–458, 2013.

[30] A. Ramos-Fernandez, J. A. Gallego-Juarez, and F. Montoya-Vitini. Automatic system for dynamic control of resonance in high power and high Q ultrasonic transducers. *Ultrasonics*, 23(4):151–156, 1985.

[31] S. Ghenna, F. Giraud, C. Giraud-Audine, M. Amberg, and B. Lemaire-Semail. Vector control applied to a Langevin transducer. In *2015 17th European Conference on Power Electronics and Applications (EPE'15 ECCE-Europe)*, pages 1–9. IEEE, 2015.

[32] S. H. Kristensen. Design, construction and characterization of high power ultrasound sources. Master's thesis, Univ. of Southern Denmark, 2009.

[33] E. Moreno, P. Acevedo, M. Fuentes, A. Sotomayor, L. Borroto, M. E. Villafuerte, and L. Leija. Design and construction of a bolt-clamped Langevin transducer. In *2005 2nd International Conference on Electrical and Electronics Engineering*, number Cie, pages 393–395. IEEE, 2005.

[34] Emerson ultrasonics. Branson horn catalog. https://www.emerson.com/documents/automation/catalog-ultrasonic-horn-branson-en-us-160126.pdf. Accessed:2022-07-24.

[35] M.J. Troughton. *Handbook ofPlastics Joining: A Practical Guide*. The Welding Institute:Cambridge, 2008.

[36] Weber ultrasonics. https://www.weber-ultrasonics.com/en/cutting/. Accessed:2010-09-03.

[37] J. Grabalosa, I. Ferrer, O. Martínez-Romero, A. Elías-Zúñiga, X. Plantá, and F. Rivillas. Assessing a stepped sonotrode in ultrasonic molding technology. *Journal of Materials Processing Technology*, 229:687–696, 2016.

[38] A. S. Nanu, N. I. Marinescu, and D. Ghiculescu. Study on ultrasonic stepped horn geometry design and FEM simulation. *Nonconventional Technologies Review*, 15(4):25–30, 2011.

[39] J. J. Yang, Z. D. Fang, B. Y. Wei, and X. Z. Deng. Theoretical explanation of the 'local resonance' in stepped acoustic horn based on Four-End Network method. *Journal of Materials Processing Technology*, 209(6):3106–3110, 2009.

[40] M. Tadvi, A. Pandey, J. Prajapati, and J. Shah. Design and Development of Sonotrode for Ultrasonic Drilling. In *ASME International Mechanical Engineering Congress and Exposition*, 2015.

[41] H. Al-Budairi. *Design and analysis of ultrasonic horns operating in longitudinal and torsional vibration*. PhD thesis, University of Glasgow, 2012.

[42] Atcp ultrasonics. https://www.atcp-ndt.com/en/. Accesed: 2021-12-03.

[43] R. Zheng, R. I. Tanner, and X. J. Fan. *Injection molding: integration of theory and modeling methods*. Springer Berlin Heidelberg, Berlin, Heidelberg, 2011.

[44] G. Tosello. *Micro Injection Molding*. Carl Hanser Verlag GmbH & Co. KG, 2018.

[45] P. R. Hornsby, P. D. Coates, P. S. Allan, G. Greenway, M. T. Martyn, B. R. Whiteside, M. T. Martyn, P. D. Coates, P. S. Allan, P. R. Hornsby, and G. Greenway. Micromoulding: process characteristics and product properties. *Plastics, Rubber and Composites*, 32(6):231–239, 2003.

[46] B. Sha, S. Dimov, C. Griffiths, and M. S. Packianather. Investigation of micro-injection moulding: Factors affecting the replication quality. *Journal of Materials Processing Technology*, 183(2-3):284–296, 2007.

[47] I. Fassi and D. Shipley. Micro-Manufacturing Technologies and Their Applications. *Springer Tracts in Mechanical Engineering*, 10:978–3, 2017.

[48] G. Fantoni, G. Tosello, D. Gabelloni, and H. N. Hansen. Modelling injection moulding machines for micro manufacture applications through functional analysis. *Procedia Cirp*, 2:107–112, 2012.

[49] F. Kennedy. Frictional heating and contact temperatures. *Modern Tribology Handbook*, 1:235–272, 2001.

[50] R. Surace, G. Trotta, V. Bellantone, and I. Fassi. *The micro injection moulding process for polymeric components manufacturing*. New Technologies - Trends, Innovations and Research, Prof. Constantin Volosencu (Ed.), 2012.

[51] J. Giboz, T. Copponnex, and P. Mélé. Microinjection molding of thermoplastic polymers: A review. *Journal of Micromechanics and Microengineering*, 17(6):R96, 2007.

[52] Q. Wang, X. Zhao, J. Zhang, P. Zhang, X. Wang, C. Yang, J. Wang, and Z. Wu. Research on quality characterization method of micro-injection products based on cavity pressure. *Polymers*, 13(16):1–13, 2021.

[53] J Z Liang and J.N. Ness. The calculation of cooling time in injection moulding. *Journal of materials processing technology*, 57:62–64, 1996.

[54] G. Lucchetta, M. Sorgato, S. Carmignato, and E. Savio. Investigating the technological limits of micro-injection molding in replicating high aspect ratio micro-structured surfaces. *CIRP Annals - Manufacturing Technology*, 63(1):521–524, 2014.

[55] J.R. Lerma Valero. *Manual avanzado de transformación de termoplásticos por inyección: scientific injection molding : recomendaciones y buenas prácticas para un proceso de inyección avanzado*. Ed. 9Disseny, 2014.

[56] Davide Masato, Jitendra Rathore, Marco Sorgato, Simone Carmignato, and Giovanni Lucchetta. Analysis of the shrinkage of injection-molded fiber-reinforced thin-wall parts. *Materials and Design*, 132(2016):496–504, 2017.

[57] W. Michaeli, T. Kamps, and C. Hopmann. Manufacturing of polymer micro parts by ultrasonic plasticization and direct injection. *Microsystem Technologies*, 17(2):243–249, mar 2011.

[58] J. Chen, Y. Chen, H. Li, S.Y. Y. Lai, and J. Jow. Physical and chemical effects of ultrasound vibration on polymer melt in extrusion. *Ultrasonics Sonochemistry*, 17(1):66–71, jan 2010.

[59] G. Chen, S. Guo, and H. Li. Ultrasonic improvement of rheological behavior of polystyrene. *Journal of Applied Polymer Science*, 84(13):2451–2460, 2002.

[60] D. Masato, M. Babenko, B. Shriky, T. Gough, G. Lucchetta, and B. Whiteside. Comparison of crystallization characteristics and mechanical properties of polypropylene processed by ultrasound and conventional micro-injection molding. *International Journal of Advanced Manufacturing Technology*, 99(1-4):113–125, 2018.

[61] W. Michaeli and D. Opfermann. Ultrasonic plasticising for micro injection moulding. In *4M 2006 - Second International Conference on Multi-Material Micro Manufacture*, pages 345–348. Woodhead Publishing Limited, 2006.

[62] W. Wu, H. Peng, Y. Jia, and B. Jiang. Characteristics and mechanisms of polymer interfacial friction heating in ultrasonic plasticization for micro injection molding. *Microsystem Technologies*, 23(5):1385–1392, 2017.

[63] B. Jiang, H. Peng, W. Wu, Y. Jia, and Y. Zhang. Numerical simulation and experimental investigation of the viscoelastic heating mechanism in ultrasonic plasticizing of amorphous polymers for micro injection molding. *Polymers*, 8(5):199, 2016.

[64] X. Sánchez-Sánchez, M. Hernández-Avila, L. E. Elizalde, O. Martínez, I. Ferrer, and A. Elías-Zuñiga. Micro injection molding processing of UHMWPE using ultrasonic vibration energy. *Materials and Design*, 132:1–12, 2017.

[65] X. Sánchez-Sánchez, A. Elias-Zuñiga, and M. Hernández-Avila. Processing of ultra-high molecular weight polyethylene/graphite composites by ultrasonic injection moulding: Taguchi optimization. *Ultrasonics Sonochemistry*, 44:350–358, 2018.

[66] U. Heredia-Rivera, I. Ferrer, and E. Vázquez. Ultrasonic molding technology: Recent advances and potential applications in the medical industry. *Polymers*, 11(4):667, 2019.

[67] R. Gaxiola-Cockburn, O. Martínez-Romero, A. Elías-Zúñiga, D. Olvera-Trejo, J. E. Reséndiz-Hernández, and C. G. Soria-Hernández. Investigation of the Mechanical Properties of Parts Fabricated with Ultrasonic Micro Injection Molding Process Using Polypropylene Recycled Material. *Polymers*, 12(9):2020, 2020.

[68] Y. Yang and C. Huang. Effects of ultrasonic injection molding conditions on the plate processing characteristics of PMMA. *Journal of Polymer Engineering*, 2018.

[69] H. V. Fairbanks. Applying ultrasonics to the moulding of plastic powders. *Ultrasonics*, 12(1):22–24, 1974.

[70] M. Kellomäki and P. Törmälä. Ultrasonic moulding of bioabsorbable polymers and polymer/drug composites. *Journal of Materials Science Letters*, 16(21):1786–1789, 1997.

[71] K. Zeng, X. Y. Wu, X. Liang, B. Xu, Y. T. Wang, X. Q. Chen, R. Cheng, and F. Luo. Process and properties of micro-ultrasonic powder molding with polypropylene. *International Journal of Advanced Manufacturing Technology*, 70(1-4):515–522, 2014.

[72] F. Puliga, M. Sacristán, A. Fauria, and F. J. Plantà. Pellet dosing apparatus, 2015. US Patent 9,174,364.

[73] J. A. Marfil, M. Janer, and F. J. Plantà-Torralba. Device and method for feeding molten plastic material into a molding cavity, 2021. US Patent 10,953,570.

[74] C. Olmo. *Micromoldeo por ultrasonidos de ácido poliláctico: Preparación de nanocompuestos y carga con fármacos*. PhD thesis, Master Thesis, Universitat Politècnica de Catalunya, http://hdl.handle.net/2117/86995, 2015.

[75] D. Montes. *Estudi dels parámetres del procés de micromoldeig per ultrasons mitjançant disseny experimental*. PhD thesis, Master Thesis, Universitat Politécnica de Catalunya, http://hdl.handle.net/2117/165706, Barcelona, Spain, 2016.

[76] M. S. Huang. Cavity pressure based grey prediction of the filling-to-packing switchover point for injection molding. *Journal of materials processing technology*, 183(2-3):419–424, 2007.

[77] M. Janer, D. Montes, C. M. Rubio, X. Plantá, and M.D. Riera. Applying ultrasonic moulding to process polyoxymethylene. In *Ultrasonics 2018 Proceedings Book*, pages 173–174. Bioscope-Protomass, 2018.

[78] F. J. P. Torralba, E E Martínez, A. S. Descalzo, P. L. M. López, J. F. B. F., M. E. R. Sierra, and F. Puliga. Ultrasonic device for moulding micro plastic parts, 2012. US Patent 8,328,548.

[79] Fundacio privada ASCAMM, Promolding B.V., Plastiasite S.A., Mateu y Solé S.A., Cedrat Technologies S.A., and Fraunhofer Gesellshaft Haidlmar GmbH. New process and machinery for microparts moulding based on ultrasound excitation. *FP7-SME: ID 222378*, 2010.

[80] J. Grabalosa, E. Vázquez, I. Ferrer, A. Elias-Zúñiga, E. Sirera, and F. Rivillas. Processing of polyamide by ultrasonic molding for medical applications. Preliminar study. In *Proceedings of the 2nd International Conference on Design and Processes for Medical Devices*, pages 52–56. Ed. Rodríguez et al., 2014.

[81] L. Rodríguez. Microprocesado de matrices termoplásticas mediante ultrasonidos: Evaluación de las propiedades químicas y físicas de los materiales procesados. Technical report, Master Thesis, Universitat Politècnica de Catalunya ,http://hdl.handle.net/2099.1/18471, 2012.

[82] B. Jiang, Y. Zou, T. Liu, and W. Wu. Characterization of the Fluidity of the Ultrasonic Plasticized Polymer Melt by Spiral Flow Testing under Micro-Scale. *Polymers*, 11(2):357, 2019.

[83] B. Jiang, J. Hu, J. Li, and X. Liu. Ultrasonic plastification speed of polymer and its influencing factors. *Journal of Central South University*, 19:380–383, 2012.

[84] F. Puliga, M. Sacristán, F. J. Plantà, and A. Navarro. Apparatus for moulding plastics micro-pieces by ultrasounds, 2014. US Patent 8,758,000.

[85] Ultrasion S.L. http://ultrasion.com/. Accessed:2022-07-24.

[86] A. Díaz, L. Franco, M. T. Casas, L. J. Del Valle, J. Aymamí, C. Olmo, and J. Puiggalí. Preparation of micro-molded exfoliated clay nanocomposites by means of ultrasonic technology. *Journal of Polymer Research*, 21(11), 2014.

[87] C. Olmo, H. Amestoy, M. T. Casas, J. C. Martínez, L. Franco, J. R. Sarasua, and J. Puiggalí. Preparation of nanocomposites of poly("-caprolactone) and multi-walled carbon nanotubes by ultrasound micromolding. influence of nanotubes on melting and crystallization. *Polymers*, 9(8):1–18, 2017.

[88] A. Díaz, M. Casas, and J. Puiggalí. Dispersion of Functionalized Silica Micro- and Nanoparticles into Poly(nonamethylene Azelate) by Ultrasonic Micro-Molding. *Applied Sciences*, 5(4):1252–1271, 2015.

[89] T. Dorf, I. Ferrer, and J. Ciurana. Characterizing Ultrasonic Micro-Molding Process of Polyetheretherketone (PEEK). *International Polymer Processing*, 33(4):442–452, 2018.

[90] I. Ferrer, M. Vives-Mestres, A. Manresa, and M. L. Garcia-Romeu. Replicability of Ultrasonic Molding for Processing Thin-Wall Polystyrene Plates with a Microchannel. *Materials*, 11(8):1320, 2018.

[91] X. Sánchez Sánchez. *Application of ultrasonic micro injection molding for manufacturing of UHMWPE microparts*. PhD thesis, Thesis. School of Engineering and Sciences,Técnologico de Monterrey, 2017.

[92] A. Benatar, R. V. Eswaran, S. K. Nayar, and Z. Chengi. Ultrasonic welding of thermoplastics in the near-field. *Polymer Engineering & Science*, 29(23):1689–1698, 1989.

[93] D. Ha Minh. *Couplages thermo-mécaniques lors de la soudure par ultrasons. application aux thermoplastiques*. PhD thesis, PhD thesis, Ecole Nationale des Ponts et Chaussées. ParisTech, https://tel.archivesouvertes. fr, 2009.

[94] K.S. S. Suresh, M. Roopa Rani, K. Prakasan, and R. Rudramoorthy. Modeling of temperature distribution in ultrasonic welding of thermoplastics for various joint designs. *Journal of Materials Processing Technology*, 186(1):138–146, may 2007.

[95] D. M. Marhöfer, G. Tosello, H. N. Hansen, and A. Islam. Advancements on the simulation of the micro injection moulding process. In *Proceedings of the 10th International Conference on Multi-Material Micro Manufacture*, pages 77–81. 4M Association, 2013.

[96] S. L. Peshkovskii, M. L. Friedman, A. I. Tukachinskii, G. V. Vinogradov, and N. S. Enikolopian. Acoustic cavitation and its effect on flow in polymers and filled systems. *Polymer composites*, 4(2):126–134, 1983.

[97] A. Levy, S. Le Corre, N. Chevaugeon, and A. Poitou. A level set based approach for the finite element simulation of a forming process involving multiphysics coupling: Ultrasonic welding of thermoplastic composites. *European Journal of Mechanics, A/Solids*, 30(4):501–509, 2011.

[98] S.C. Chou, K.D. Robertson, and J.H. Rainey. The effect of strain rate and heat developed during deformation on the stress strain curve of plastics. *Experimental Mechanics*, 13(10):422–432, 1973.

[99] J.J. Mason, A.J. Rosakis, and G. Ravichandran. On the strain and strain rate dependence of the fraction of plastic work converted to heat:an experimental study using high speed infrared detectros and the Kolsky bar. *Mechanics of Materials*, 17(2-3):135–145, 1994.

[100] D. Rittel. Investigation of the heat generated during cyclic loading of two glassy polymers. Part I: Experimental. *Mechanics of Materials*, 32:149–159, 2000.

[101] M. A. Meyers and K. K. Chawla. *Mechanical behavior of materials*. Cambridge university press, 2008.

[102] J. De Cazenove, D. Rade, A. M. G. De De Lima, and E. Pagnacco. A study of self-heating effects in viscoelastic damping devices. *11th Pan-American Congress of Applied Mechanics*, (1998), 2009.

[103] B. Jiang, Y. Zou, G. Wei, and W. Wu. Evolution of interfacial friction angle and contact area of polymer pellets during the initial stage of ultrasonic plasticization. *Polymers*, 11(12), 2019.

[104] E. A. Neppiras. Acoustic cavitation. *Physics reports*, pages 159–251, 1980.

[105] M. Hauptmann, H. Struyf, P. Mertens, M. Heyns, S. De Gendt, C. Glorieux, and S. Brems. Towards an understanding and control of cavitation activity in 1 MHz ultrasound fields. *Ultrasonics Sonochemistry*, 20(1):77–88, 2013.

[106] B. Jiang, J. L. Hu, W. Q. Wu, and S. Pan. Research on the polymer ultrasonic plastification. *Advanced Materials Research*, 87-88:542–549, 2009.

[107] H. Mavridis, A. N. Hrymak, and J. Vlachopoulos. Mathematical modeling of injection mold filling: A review. *Advances in Polymer Technology*, 6(4):457–466, 1986.

[108] CoreTech System Hsinchu. Moldex 3D "User Manual and Material Database", 2015.

[109] Z. Longzhi, C. Binghui, Y. Min, and Z. Shangbing. Application of Moldflow software in design of injection mold. In *2010 International Conference on Mechanic Automation and Control Engineering*, pages 243–245, 2010.

[110] P. J. Carreau, D. De Kee, and M. Daroux. An analysis of the viscous behaviour of polymeric solutions. *The Canadian Journal of Chemical Engineering*, 57(2):135–140, 1979.

[111] C. A. Griffiths, S. S. Dimov, E. B. Brousseau, and R. T. Hoyle. The effects of tool surface quality in micro-injection moulding. *Journal of Materials Processing Technology*, 189(1-3):418–427, 2007.

[112] N. Zobeiry. *Viscoelastic constitutive models for evaluation of residual stresses in thermoset composites during cure*. PhD thesis, Thesis. The University of British Columbia, 2006.

[113] Jiang Li, Shaoyun Guo, and Xiaonan Li. Degradation kinetics of polystyrene and EPDM melts under ultrasonic irradiation. *Polymer Degradation and Stability*, 89(1):6–14, jul 2005.

[114] M. Janer, D. Montes, J. A. Marfil, and F. J. Plantà. Ultrasonic Device For A Polymer Injector Apparatus, 2021. US Patent App. 17/264,028.

[115] M. Gülçür, E. Brown, T. Gough, J. M. Romano, P. Penchev, S. Dimov, and B. Whiteside. Ultrasonic micromoulding: Process characterisation using extensive in-line monitoring for micro-scaled products. *Journal of Manufacturing Processes*, 58(April):289–301, 2020.

[116] M. Patrikios, R. S. Soloff, and S. Vargas. "System and method for mounting ultrasonic tools." U.S. Patent, 2015. US Patent 8,950,458.

[117] G. Perez. *Application of ultrasound in twin-screw extrusion and microinjection molding : improvements of properties of processed materials and nanocomposites*. PhD thesis, Universitat Politècnica de Catalunya, 02 2022.

[118] A. Sato, H. Ito, and K. Koyama. Study of application of ultrasonic wave to injection molding. *Polymer Engineering & Science*, 49(4):768–773, 2009.

[119] J. Lu, Y. Qiang, W. Wu, and B. Jiang. Effects of the processing parameters on the shear viscosity of cyclic olefin copolymer plasticized by ultrasonic vibration energy. *Polymers*, 12(3), 2020.

[120] Dupont POM Delrin datasheet. https://dupont.materialdatacenter.com/. Accessed:2022-07-24.

[121] Zeonex processing guidelines. https://www.zeonex.com/processing-guidelines.aspx.html. Accessed:2022-07-24.

[122] Zeonex E48R datasheet. https://www.zeon.co.jp/en/business/enterprise/resin/pdf/200323391.pdf. Accessed:2022-07-24.

[123] Propil® polypropylene technical datasheet. https://www.lutesor.com/p_propil.htm. Accesed: 2022-07-24.

[124] K. S. Cho. *Viscoelasticity of Polymers: Theory and numerical algorithms, Springer Series in Material Science*. Springer, 2018.

[125] N. Lagakos, J. Jarzynski, J. H. Cole, and J. A. Bucaro. Frequency and temperature dependence of elastic moduli of polymers. *Journal of Applied Physics*, 59(12):4017–4031, 1986.

[126] J. Jiang, S. Wang, B. Sun, S. Ma, J. Zhang, Q. Li, and G. Hu. Effect of mold temperature on the structures and mechanical properties of micro-injection molded polypropylene. *Materials and Design*, 88:245–251, 2015.

[127] M. T. Shaw and W. J. MacKnight. *Introduction to Polymer Viscoelasticity: Third Edition*. John Wiley & Sons, 2005.

[128] J. E. L. L. Pacheco, C. A. Bavastri, and J. T. Pereira. Viscoelastic relaxation modulus characterization using Prony series. *Latin American Journal of Solids and Structures*, 12(2):420–445, 2015.

[129] H. H. Winter and J. Jackson. Linear Viscoelasticity. In *Rheological Fundamentals of Polymer Processing*, pages 61–92. Springer, 1995.

[130] M. L. Williams, R. F. Landel, and J. D. Ferry. The Temperature Dependence of Relaxation Mechanisms in Amorphous Polymers and Other Glass-forming Liquids. *Journal of the American Chemical Society*, 77(14):3701–3707, 1955.

[131] A. K. Doolittle. Studies in Newtonian Flow. II. The Dependence of the Viscosity of Liquids on Free-Space. *Journal of Applied Physics*, 22(12):1471, apr 2004.

[132] Y. Shangguan, F. Chen, E. Jia, Y. Lin, J. Hu, and Q. Zheng. New insight into Time-Temperature correlation for polymer relaxations ranging from secondary relaxation to terminal flow: Application of a Universal and developed WLF equation. *Polymers*, 9(11), 2017.

[133] D.W. Van Krevelen and K. Te Nijenhuis. *Properties of polymers: their correlation with chemical structure; their numerical estimation and prediction from additive group contributions*. Elsevier, 2009.

[134] H. Eyring. The Activated Complex in Chemical Reactions. *The Journal of Chemical Physics*, 3(2):107, nov 2004.

[135] E. Chailleux, G. Ramond, C. Such, and C. De La Roche. A mathematical-based master-curve construction method applied to complex modulus of bituminous materials A mathematical-based master-curve construction method applied to complex modulus of bituminous materials. *Road Materials and Pavement Design*, pages 75–92, 2006.

[136] L. Rouleau, J. F. Deü, A. Legay, and F. Le Lay. Application of Kramers-Kronig relations to time-temperature superposition for viscoelastic materials. *Mechanics of Materials*, 65:66–75, 2013.

[137] M. A. Kraus and M. Niederwald. Generalized collocation method using stiffness matrices in the context of the theory of linear viscoelasticity (GUSTL). *Technische Mechanik*, 37(1):82–106, 2017.

[138] P. Butaud, V. Placet, J. Klesa, M. Ouisse, E. Foltête, and X. Gabrion. Investigations on the frequency and temperature effects on mechanical properties of a shape memory polymer (Veriflex). *Mechanics of Materials*, 87:50–60, 2015.

[139] R. A. A. Schapery. Nonlinear viscoelastic solids. *International Journal of Solids and Structures*, 37(1-2):359–366, 2000.

[140] S. W. Park and Y. R. Kim. Fitting prony-series viscoelastic models with power-law presmoothing. *Journal of Materials in Civil Engineering*, 13(1):26–32, 2001.

[141] C. Elster, J. Honerkamp, and J. Weese. Using regularization methods for the determination of relaxation and retardation spectra of polymeric liquids. *Rheologica Acta*, 31(2):161–174, 1992.

[142] J. Honerkamp. Ill-posed problems in rheology. *Rheologica Acta*, 28(5):363–371, 1989.

[143] A. Takeh and S. Shanbhag. A computer program to extract the continuous and discrete relaxation spectra from dynamic viscoelastic measurements. *Applied Rheology*, 23(2):1–10, 2013.

[144] G. H. Golub, P. C. Hansen, and D. P. O'Leary. Tikhonov Regularization and Total Least Squares. *https://doi.org/10.1137/S0895479897326432*, 21(1):185–194, jul 2006.

[145] I. F. Villegas. Strength development versus process data in ultrasonic welding of thermoplastic composites with flat energy directors and its application to the definition of optimum processing parameters. *Composites Part A: Applied Science and Manufacturing*, 65:27–37, 2014.

Appendices

A

Appendix A: Experimental results

In this appendix, the data obtained from in-mould sensors for the materials processed in Chapter 3 is represented. In addition, results obtained from mechanical tensile test are also displayed.

POM processed with standard USM. In-mould temperatures and pressures

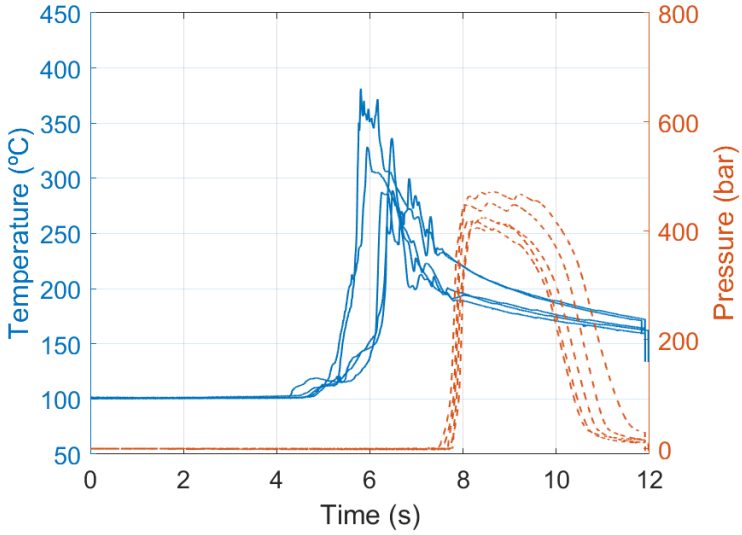

Figure A.1: In-mould temperatures and pressures for 5 samples of POM Delrin ® processed with standard USM at 50% ultrasonic amplitude and 3 mm/s plunger velocity

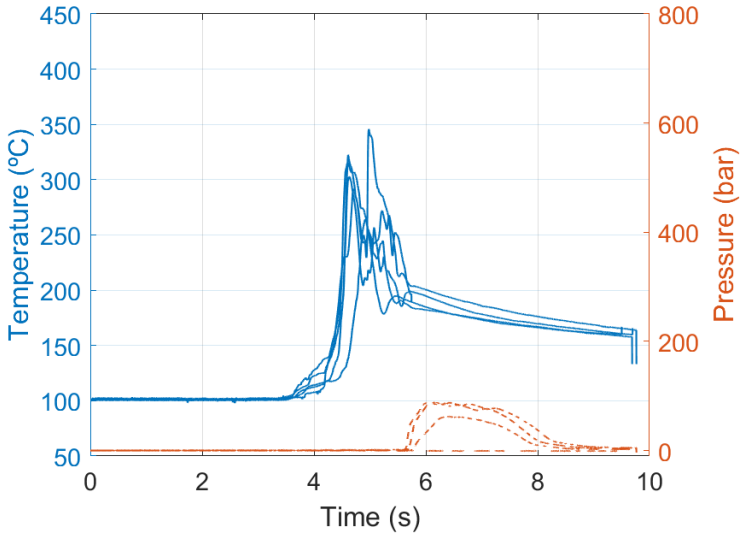

Figure A.2: In-mould temperatures and pressures for 5 samples of POM Delrin ® processed with standard USM at 50% ultrasonic amplitude and 4 mm/s plunger velocity

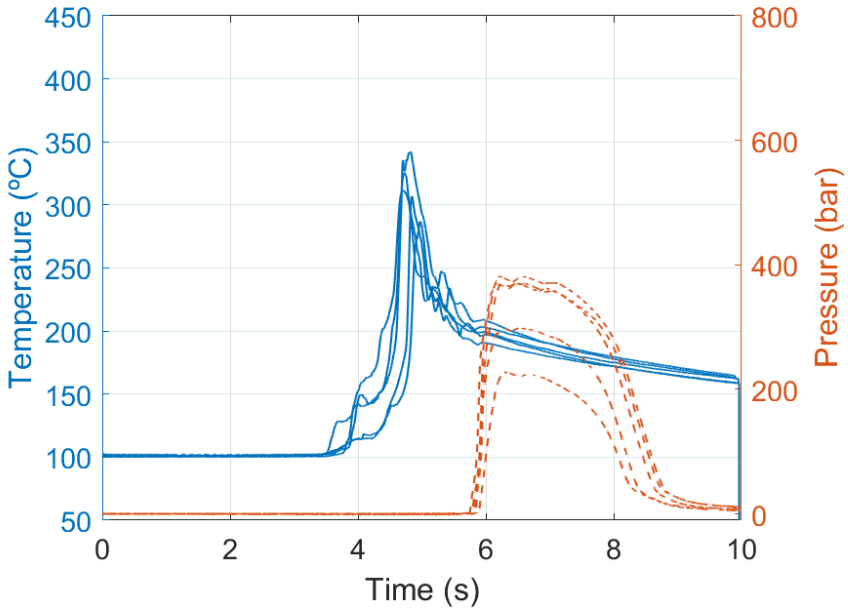

Figure A.3: In-mould temperatures and pressures for 5 samples of POM Delrin ® processed with standard USM at 55% ultrasonic amplitude and 4 mm/s plunger velocity

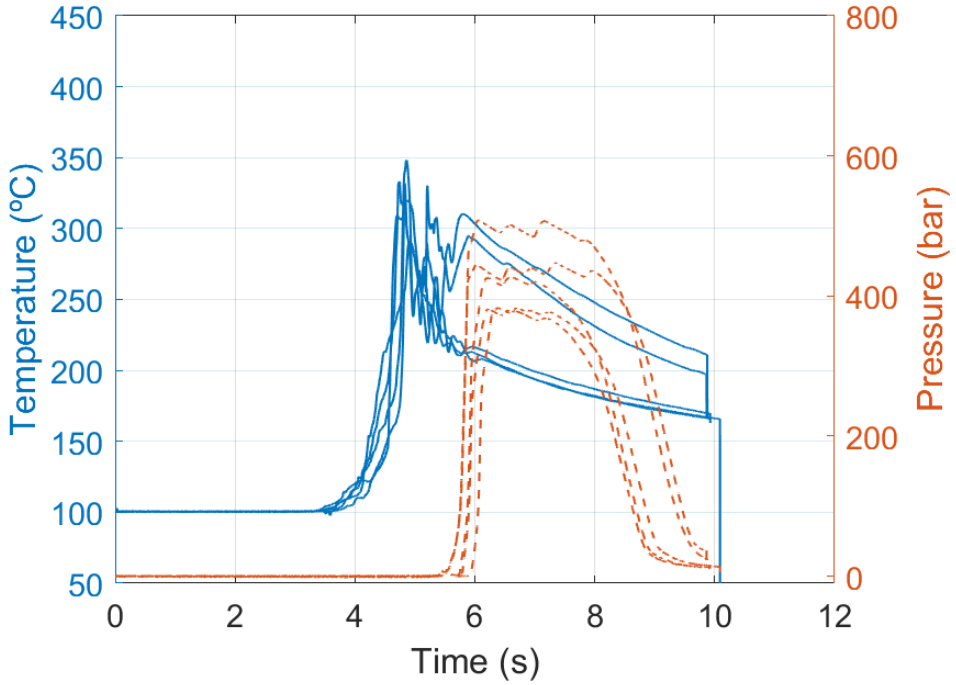

Figure A.4: In-mould temperatures and pressures for 5 samples of POM Delrin ® processed with standard USM at 60% ultrasonic amplitude and 4 mm/s plunger velocity

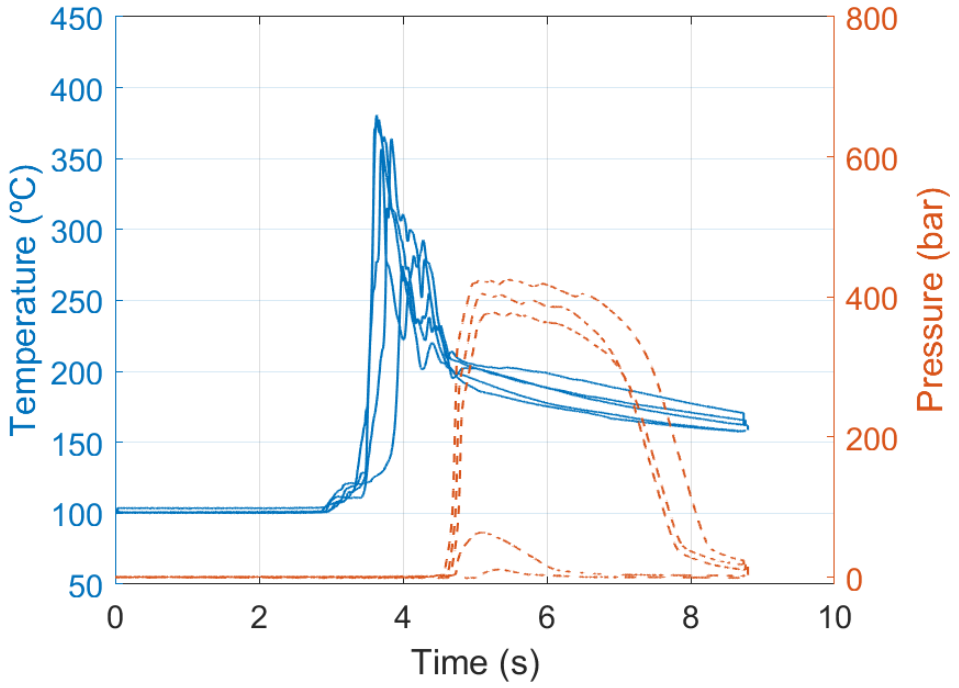

Figure A.5: In-mould temperatures and pressures for 5 samples of POM Delrin ® processed with standard USM at 60% ultrasonic amplitude and 5 mm/s plunger velocity

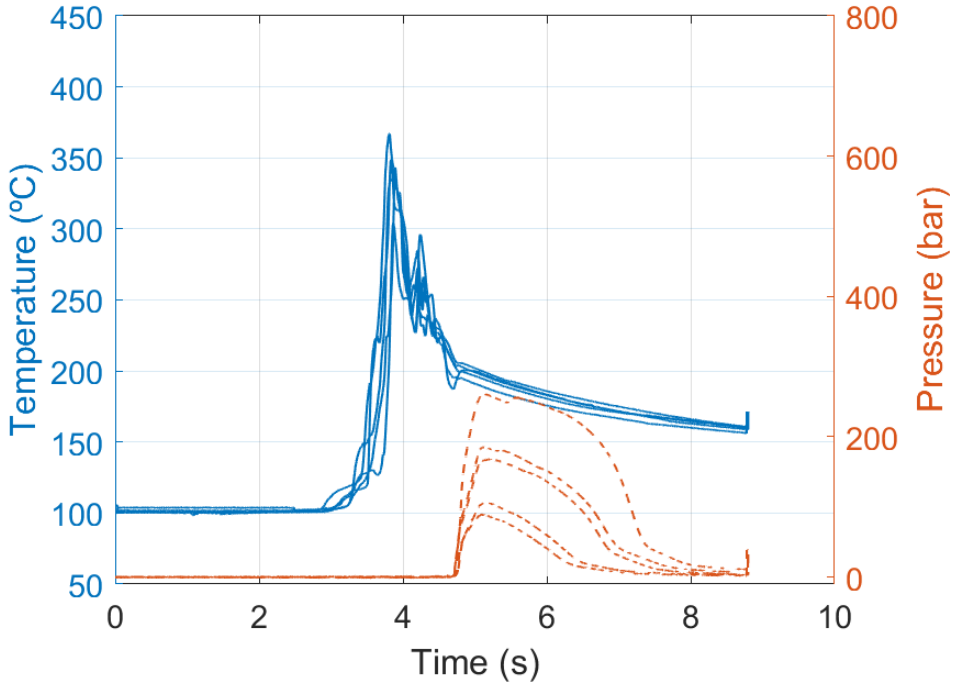

Figure A.6: In-mould temperatures and pressures for 5 samples of POM Delrin ® processed with standard USM at 55% ultrasonic amplitude and 5 mm/s plunger velocity

POM processed with NPUSM. In-mould temperatures and pressures

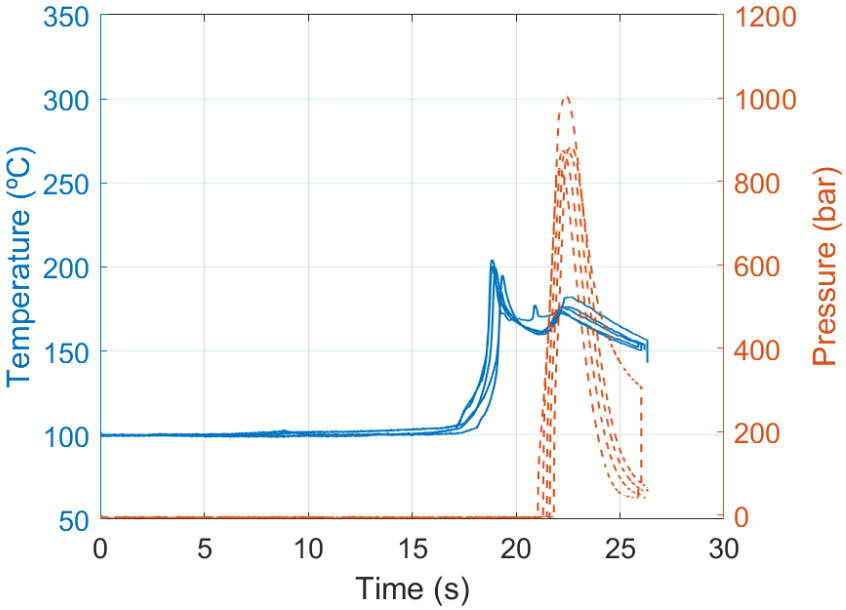

Figure A.7: In-mould temperatures and pressures for 5 samples of POM Delrin ® processed with NPUSM at 55% ultrasonic amplitude and 2 mm/s plunger velocity

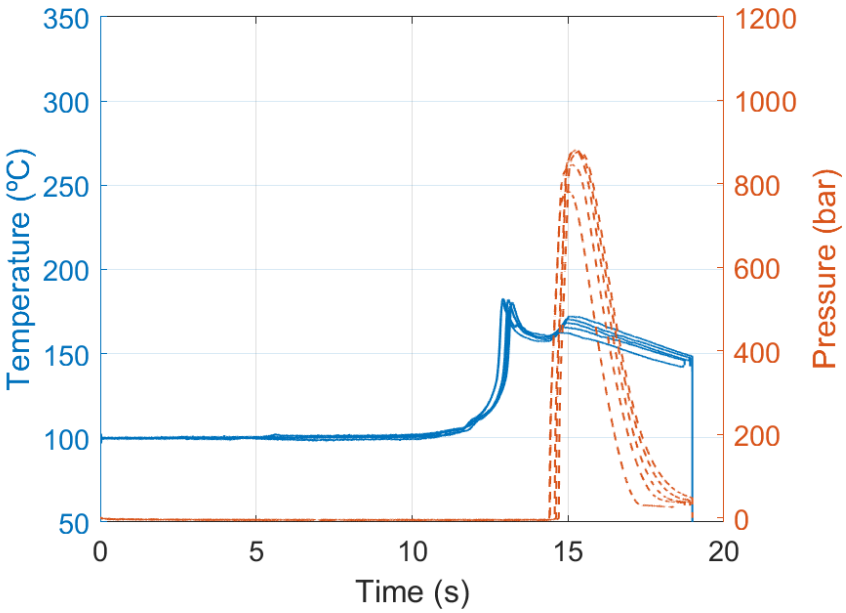

Figure A.8: In-mould temperatures and pressures for 5 samples of POM Delrin ® processed with NPUSM at 50% ultrasonic amplitude and 3 mm/s plunger velocity

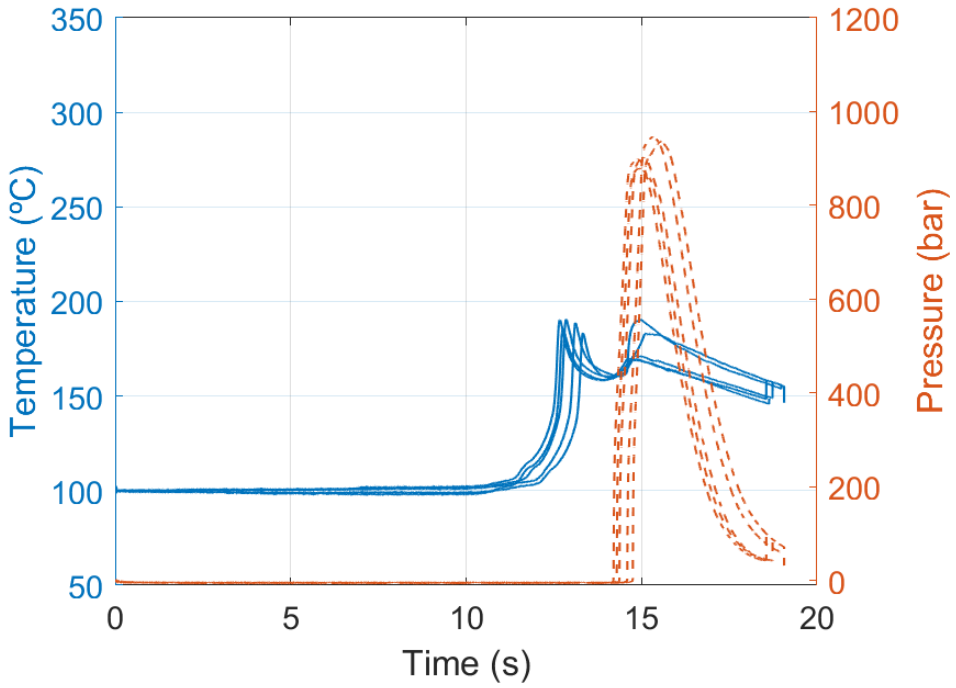

Figure A.9: In-mould temperatures and pressures for 5 samples of POM Delrin ® processed with NPUSM at 55% ultrasonic amplitude and 3 mm/s plunger velocity

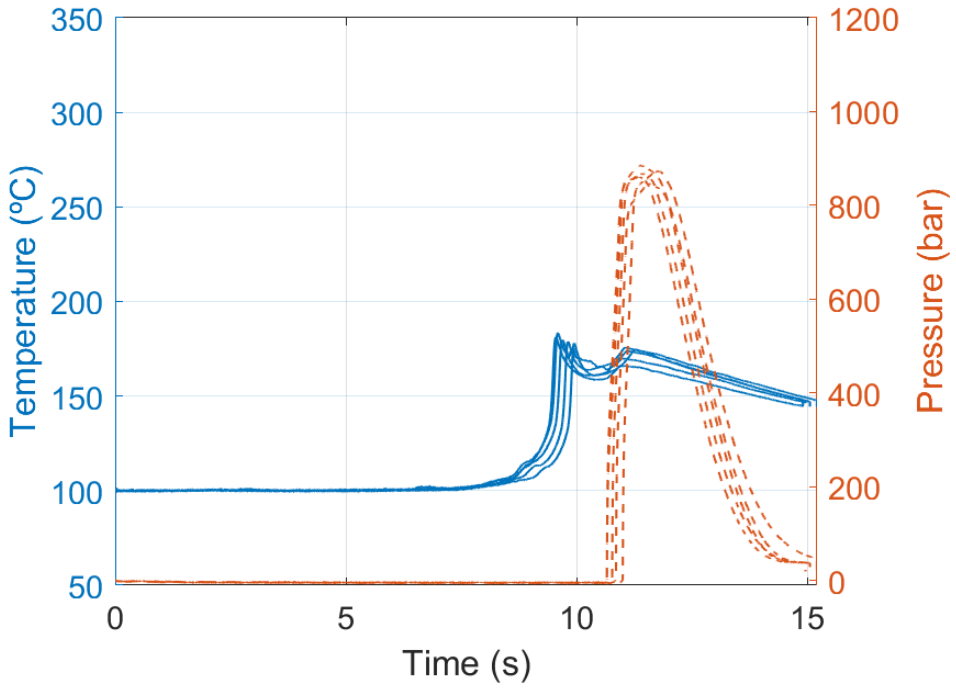

Figure A.10: In-mould temperatures and pressures for 5 samples of POM Delrin ® processed with NPUSM at 55% ultrasonic amplitude and 4 mm/s plunger velocity

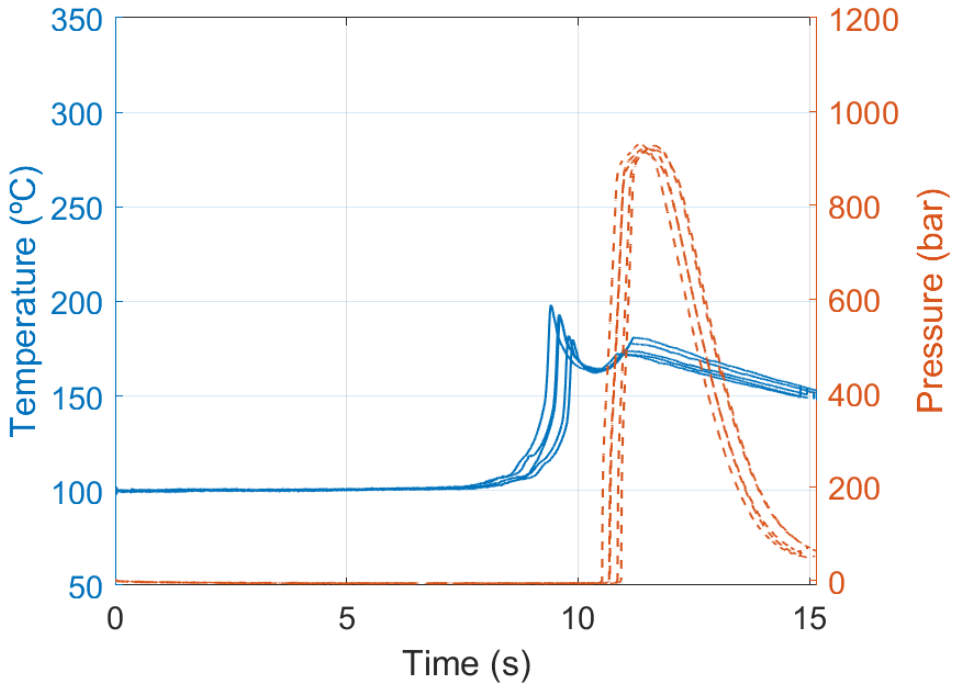

Figure A.11: In-mould temperatures and pressures for 5 samples of POM Delrin ® processed with NPUSM at 60% ultrasonic amplitude and 4 mm/s plunger velocity

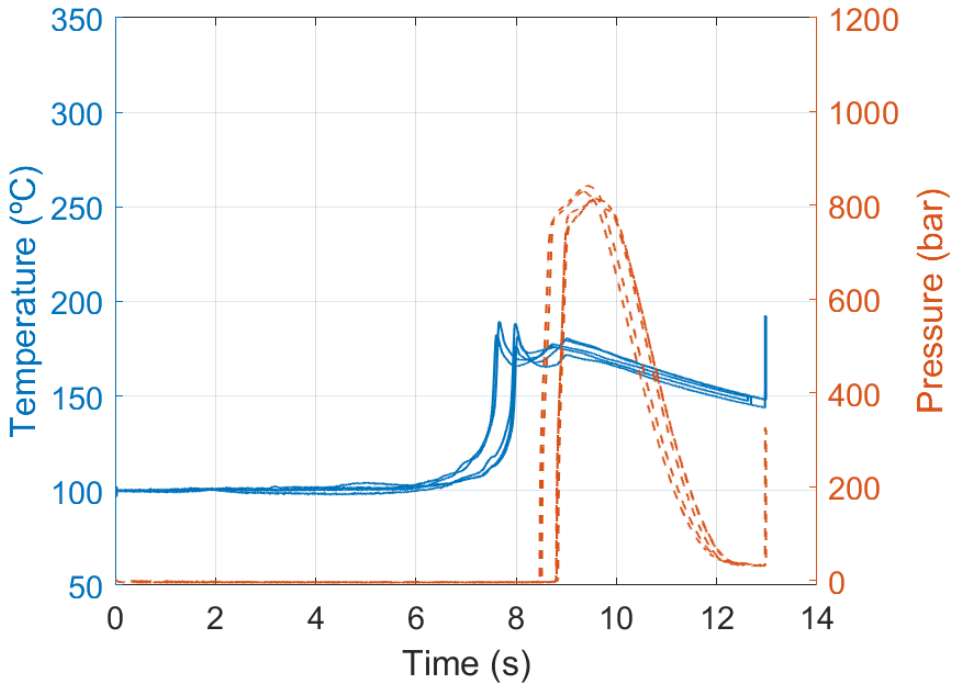

Figure A.12: In-mould temperatures and pressures for 5 samples of POM Delrin ® processed with NPUSM at 60% ultrasonic amplitude and 5 mm/s plunger velocity

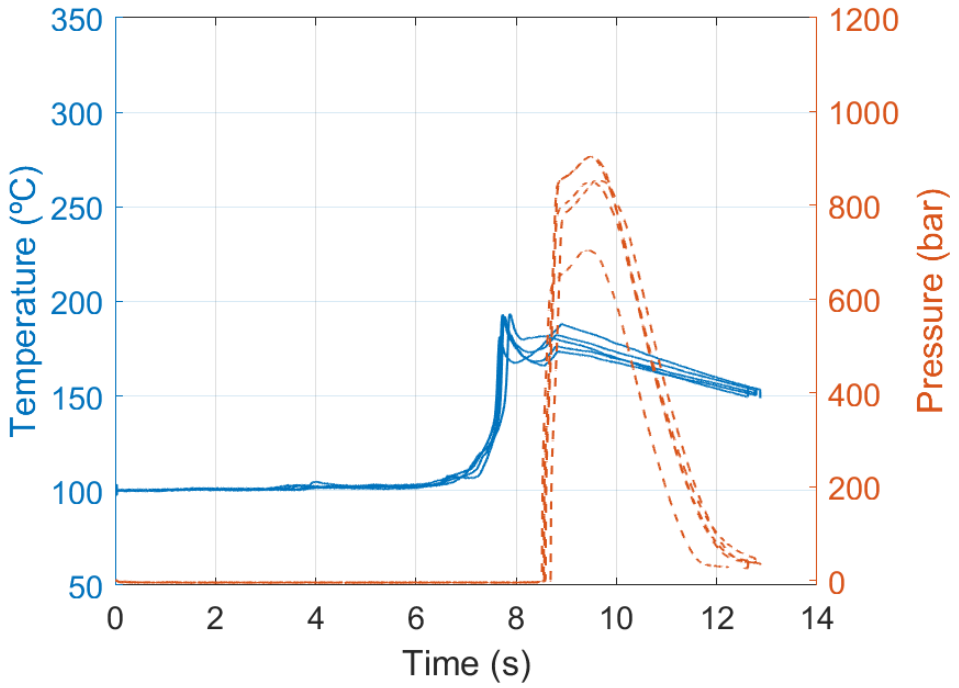

Figure A.13: In-mould temperatures and pressures for 5 samples of POM Delrin ® processed with NPUSM at 65% ultrasonic amplitude and 5 mm/s plunger velocity

POM processed with conventional injection moulding. In-mould temperatures and pressures

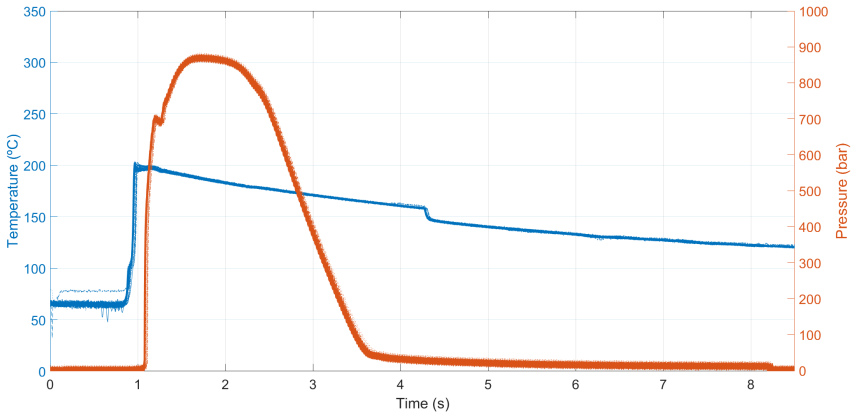

Figure A.14: In-mould temperatures and pressures for 50 samples of POM Delrin ® processed with conventional injection moulding using a Babyplast ® machine

COP processed with standard USM. In-mould temperatures and pressures

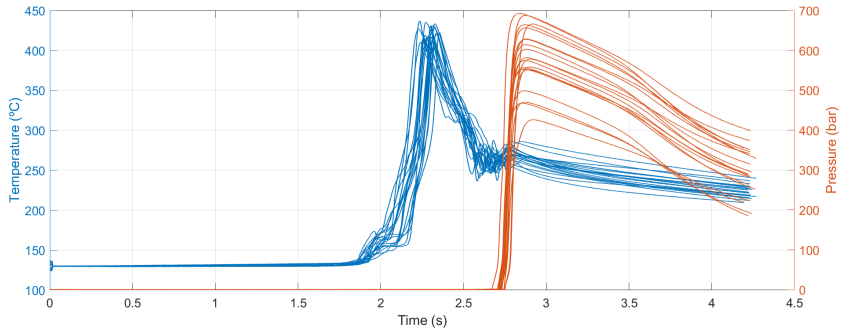

Figure A.15: In-mould temperatures and pressures for 20 samples of COP Zeonex ® processed with standard USM at 100% ultrasonic amplitude and 5 mm/s plunger velocity

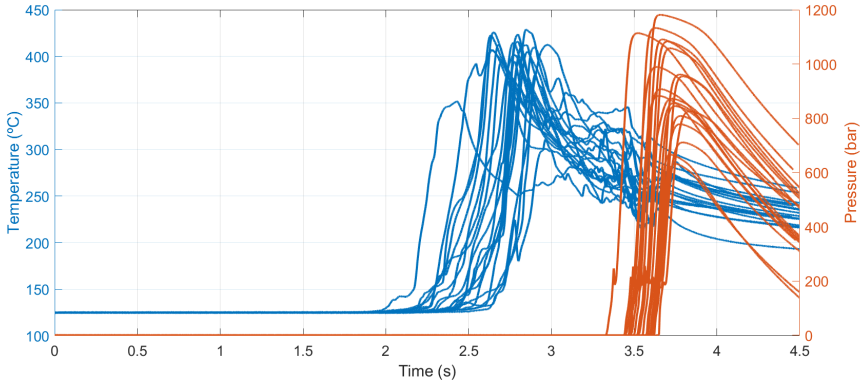

Figure A.16: In-mould temperatures and pressures for 20 samples of COP Zeonex® processed with standard USM at 80% ultrasonic amplitude and 5 mm/s plunger velocity

COP processed with NPUSM. In-mould temperatures and pressures

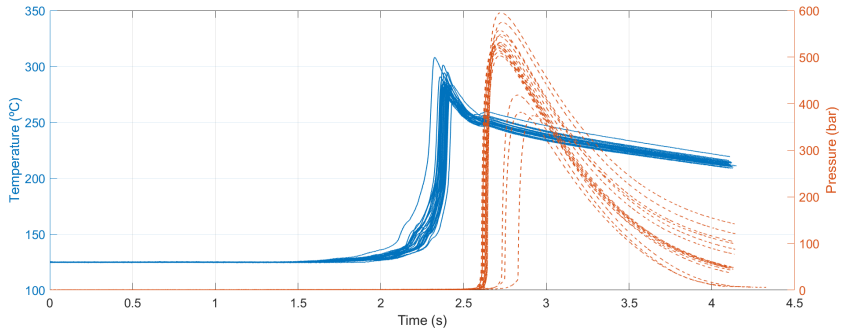

Figure A.17: In-mould temperatures and pressures for 30 samples of COP Zeonex ® processed with NPUSM at 80% ultrasonic amplitude and 10 mm/s plunger velocity

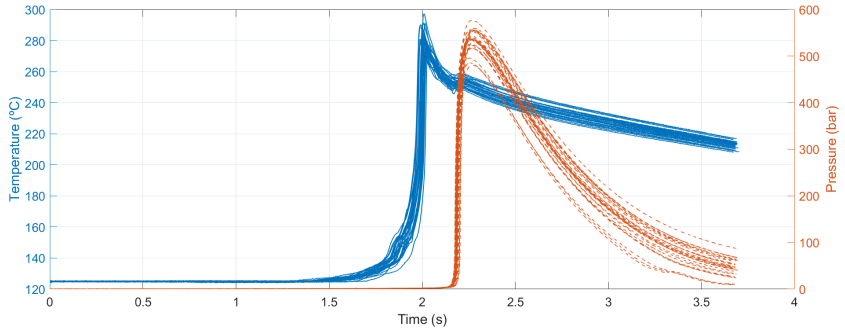

Figure A.18: In-mould temperatures and pressures for 30 samples of COP Zeonex ® processed with NPUSM at 80% ultrasonic amplitude and 12 mm/s plunger velocity

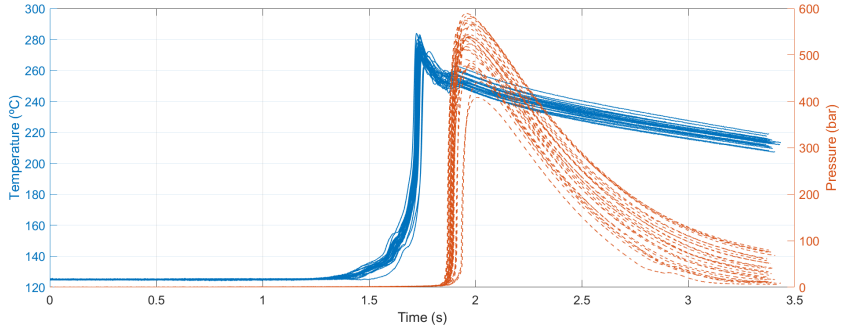

Figure A.19: In-mould temperatures and pressures for 30 samples of COP Zeonex ® processed with NPUSM at 80% ultrasonic amplitude and 14 mm/s plunger velocity

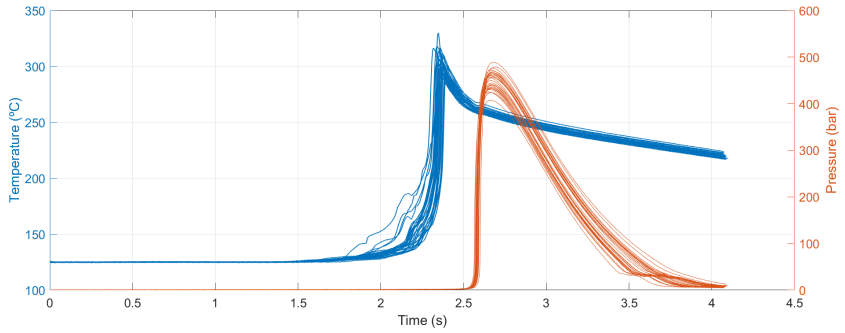

Figure A.20: In-mould temperatures and pressures for 30 samples of COP Zeonex ® processed with NPUSM at 90% ultrasonic amplitude and 10 mm/s plunger velocity

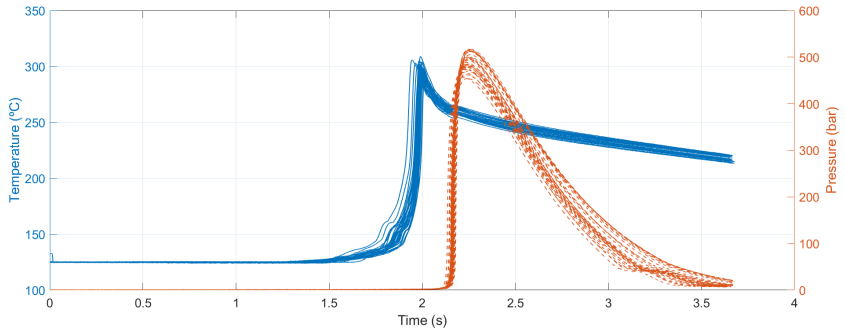

Figure A.21: In-mould temperatures and pressures for 30 samples of COP Zeonex ® processed with NPUSM at 90% ultrasonic amplitude and 12 mm/s plunger velocity

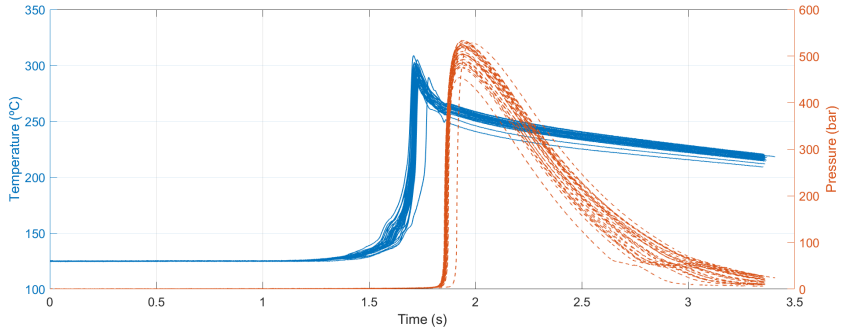

Figure A.22: In-mould temperatures and pressures for 30 samples of COP Zeonex ® processed with NPUSM at 90% ultrasonic amplitude and 14 mm/s plunger velocity

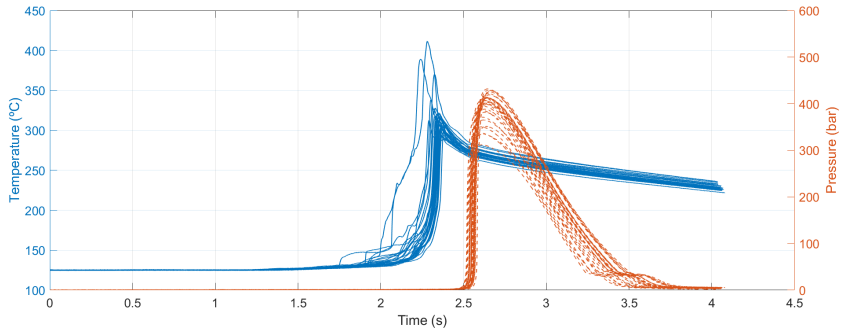

Figure A.23: In-mould temperatures and pressures for 30 samples of COP Zeonex ® processed with NPUSM at 100% ultrasonic amplitude and 10 mm/s plunger velocity

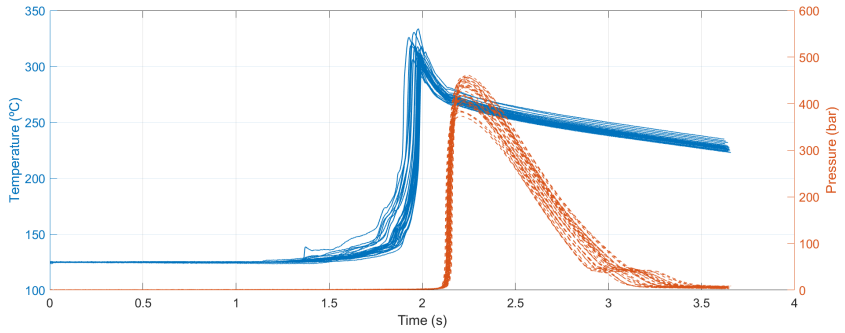

Figure A.24: In-mould temperatures and pressures for 30 samples of COP Zeonex ® processed with NPUSM at 100% ultrasonic amplitude and 12 mm/s plunger velocity

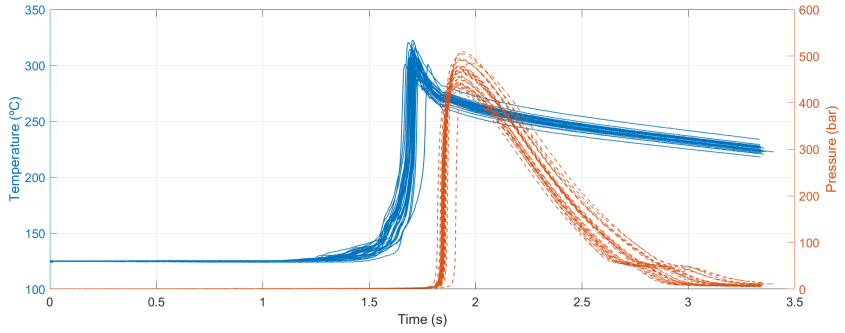

Figure A.25: In-mould temperatures and pressures for 30 samples of COP Zeonex ® processed with NPUSM at 100% ultrasonic amplitude and 14 mm/s plunger velocity

COP processed with conventional injection moulding. In-mould temperatures and pressures

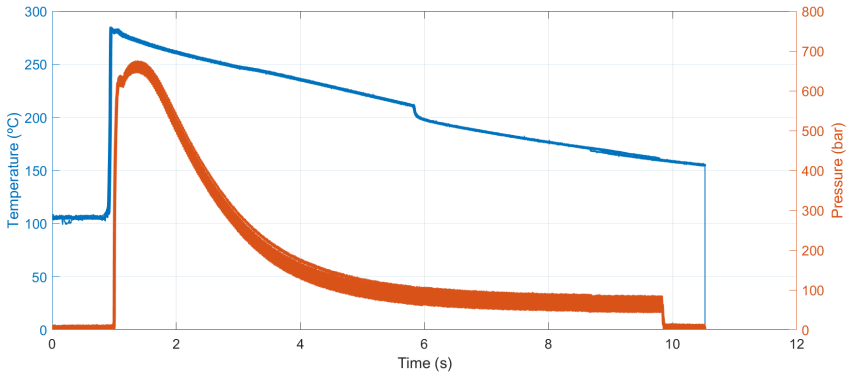

Figure A.26: In-mould temperatures and pressures for 50 samples of COP Zeonex ® processed with conventional injection moulding using a Babyplast ® machine

COP processed with NPUSM. Mechanical properties

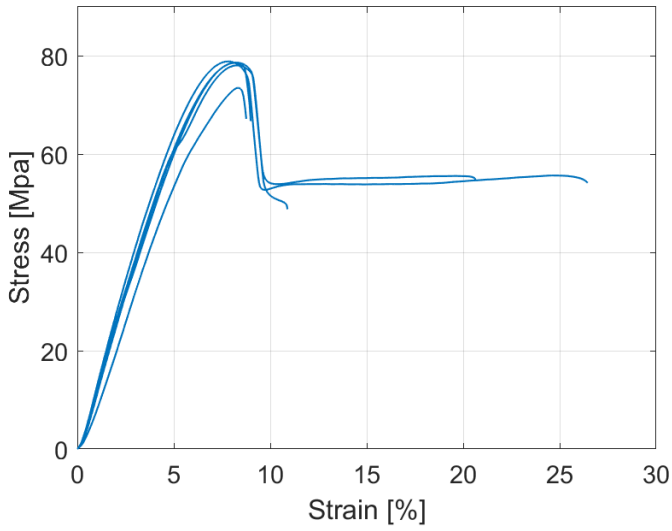

Figure A.27: Stress – strain behaviour in uniaxial tensile tests of 5 specimens manufactured with the NPUSM process at 80 % ultrasonic amplitude and 10 mm/s plunger velocity

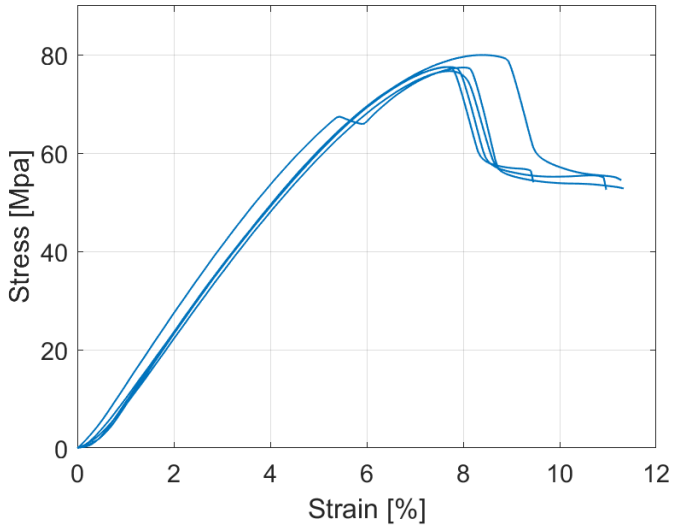

Figure A.28: Stress – strain behaviour in uniaxial tensile tests of 5 specimens manufactured with the NPUSM process at 80 % ultrasonic amplitude and 12 mm/s plunger velocity

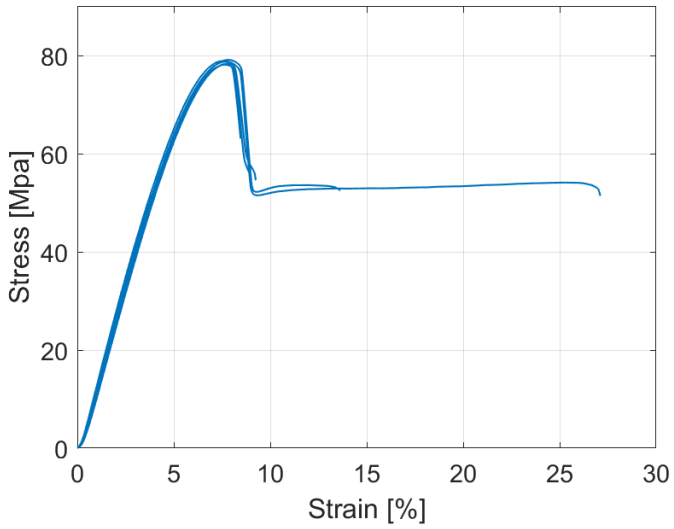

Figure A.29: Stress – strain behaviour in uniaxial tensile tests of 5 specimens manufactured with the NPUSM process at 80 % ultrasonic amplitude and 14 mm/s plunger velocity

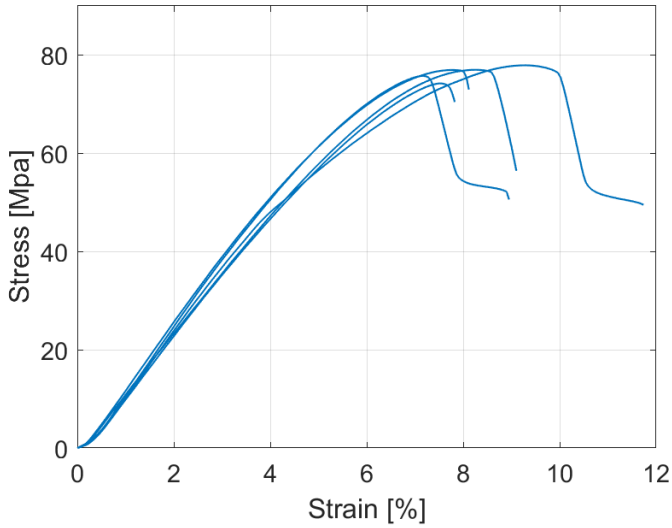

Figure A.30: Stress – strain behaviour in uniaxial tensile tests of 5 specimens manufactured with the NPUSM process at 90 % ultrasonic amplitude and 10 mm/s plunger velocity

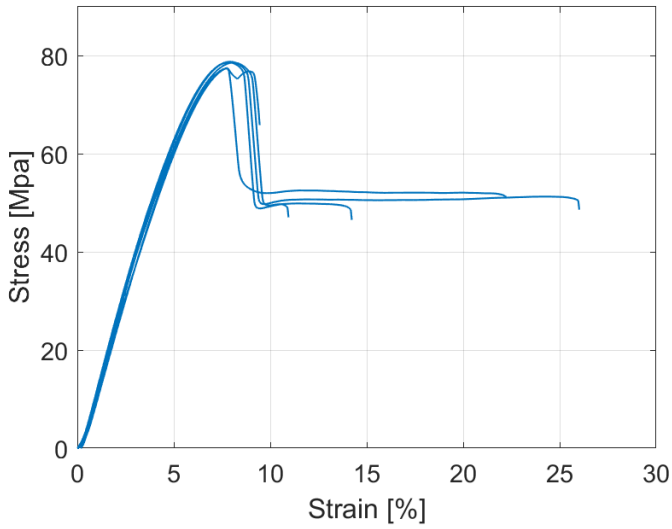

Figure A.31: Stress – strain behaviour in uniaxial tensile tests of 5 specimens manufactured with the NPUSM process at 90 % ultrasonic amplitude and 12 mm/s plunger velocity

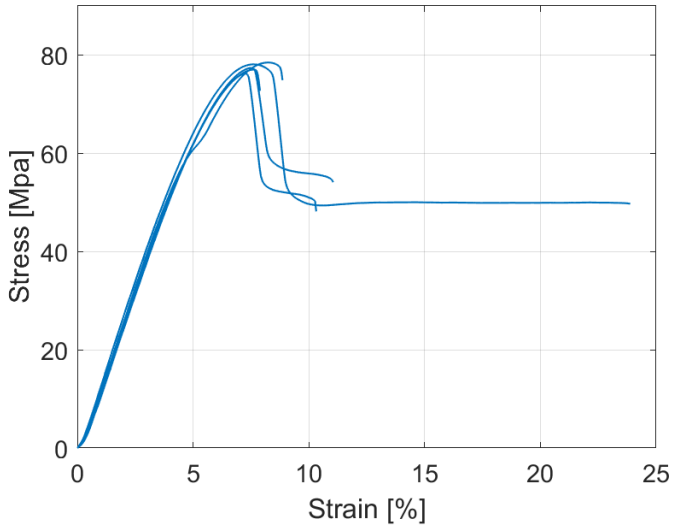

Figure A.32: Stress – strain behaviour in uniaxial tensile tests of 5 specimens manufactured with the NPUSM process at 90 % ultrasonic amplitude and 14 mm/s plunger velocity

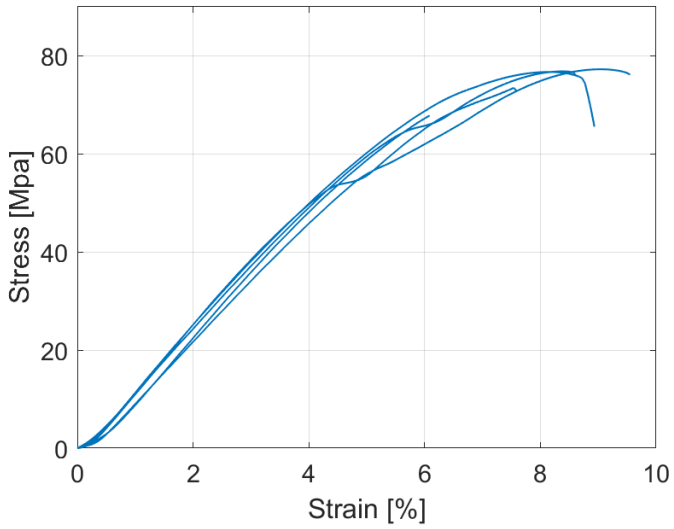

Figure A.33: Stress – strain behaviour in uniaxial tensile tests of 5 specimens manufactured with the NPUSM process at 100 % ultrasonic amplitude and 10 mm/s plunger velocity

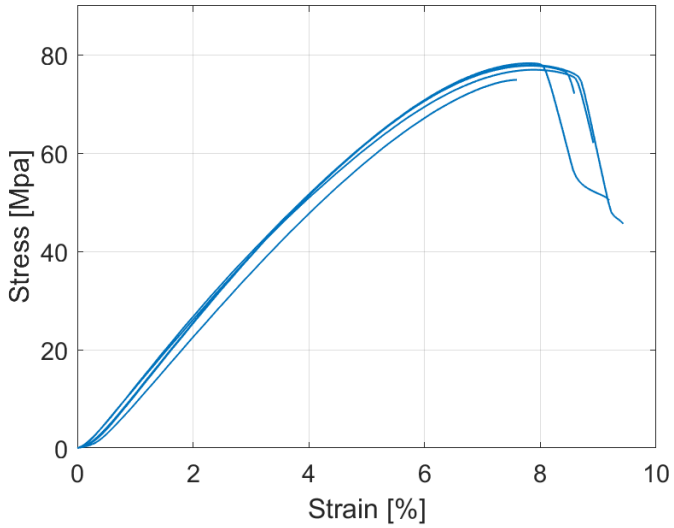

Figure A.34: Stress – strain behaviour in uniaxial tensile tests of 5 specimens manufactured with the NPUSM process at 100 % ultrasonic amplitude and 12 mm/s plunger velocity

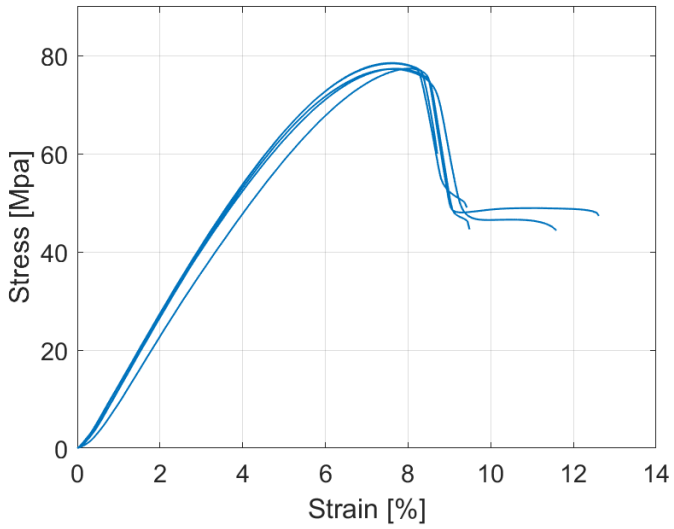

Figure A.35: Stress – strain behaviour in uniaxial tensile tests of 5 specimens manufactured with the NPUSM process at 100 % ultrasonic amplitude and 14 mm/s plunger velocity

COP processed with standard USM. Mechanical properties

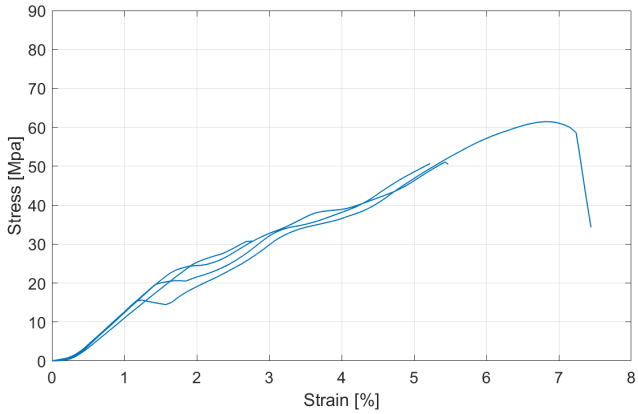

Figure A.36: Stress – strain behaviour in uniaxial tensile tests of 5 specimens manufactured with standard USM process at 100 % ultrasonic amplitude and 5 mm/s plunger velocity

B

Appendix B: Simulation data

In this appendix, additional data used in Chapter 4 is presented.

Polypropilene Viscoelastic model

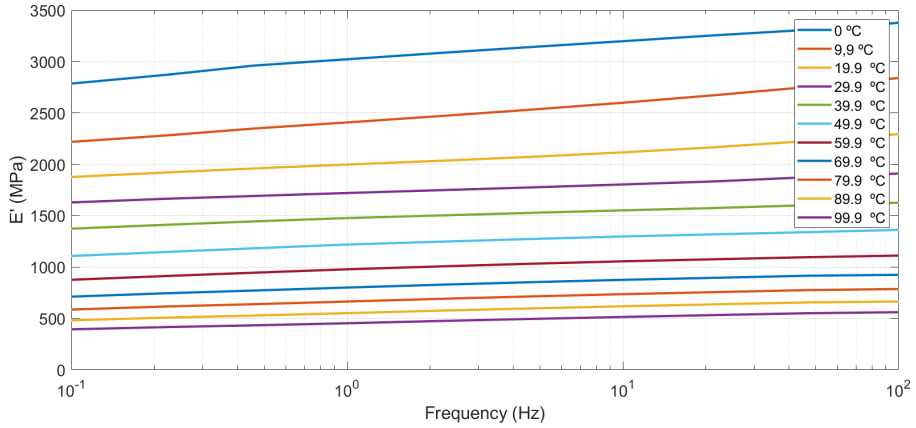

Figure B.1: Propil ® storage Modulus values obtained from a DMA measurement at different frequencies and temperatures

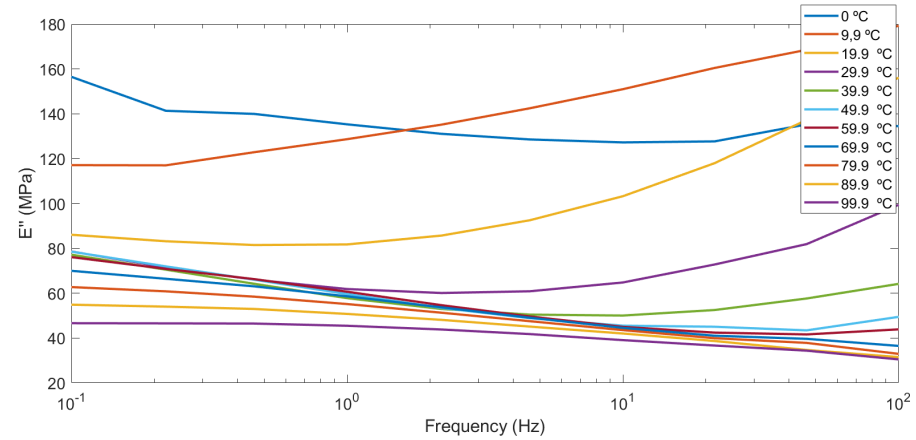

Figure B.2: Propil ® loss Modulus values obtained from a DMA measurement at different frequencies and temperatures

Mode number	τ_i (s)	G_i (Pa)	g_i (%)
1	1.86E-09	1.96E+08	1.38E-01
2	7.97E-08	9.65E+07	6.82E-02
3	2.02E-06	1.08E+08	7.61E-02
4	4.29E-05	9.98E+07	7.06E-02
5	8.78E-04	8.29E+07	5.86E-02
6	1.79E-02	6.84E+07	4.84E-02
7	3.38E-01	6.20E+07	4.39E-02
8	6.54E+00	4.75E+07	3.36E-02
9	1.25E+02	5.22E+07	3.69E-02
10	1.92E+03	4.33E+07	3.06E-02
11	3.73E+04	3.86E+07	2.73E-02
12	5.53E+05	4.17E+07	2.95E-02
13	8.71E+06	3.44E+07	2.43E-02
14	1.31E+08	3.49E+07	2.47E-02
15	1.83E+09	3.35E+07	2.37E-02
16	2.38E+10	3.25E+07	2.30E-02
17	2.96E+11	3.07E+07	2.17E-02
18	3.52E+12	2.94E+07	2.08E-02
19	4.00E+13	2.74E+07	1.94E-02
20	4.17E+14	2.64E+07	1.87E-02
21	4.53E+15	2.78E+07	1.96E-02
22	4.68E+16	2.28E+07	1.61E-02

Table B.1: Prony series obtained from Propil ® polypropylene, in Pa (2^{nd} column) and its dimensionless form in % as used in Abaqus ®(3^{rd} column). In the latter case, a value of $G_0 = 1.41E09$ is obtained

Plunger movement measured

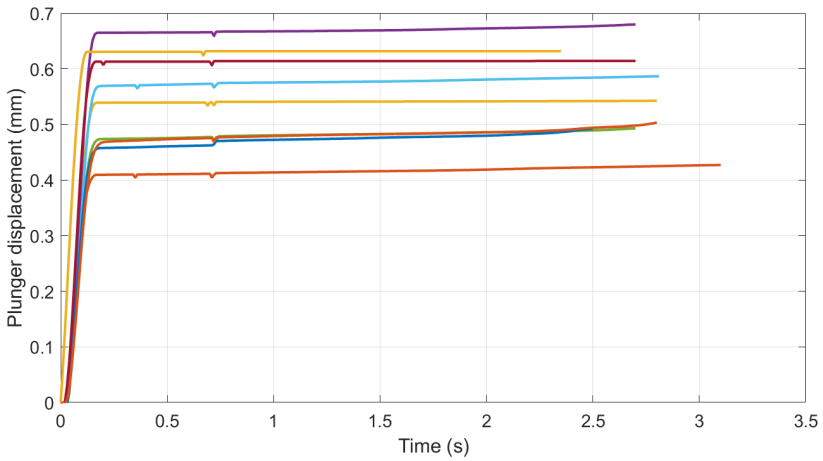

Figure B.3: Plunger movement measured for samples processed with Configuration 1 parameters

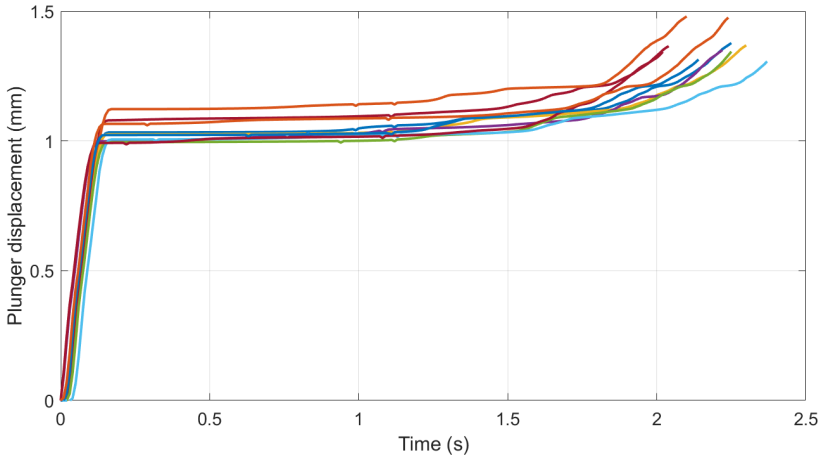

Figure B.4: Plunger movement measured for samples processed with Configuration 2 parameters

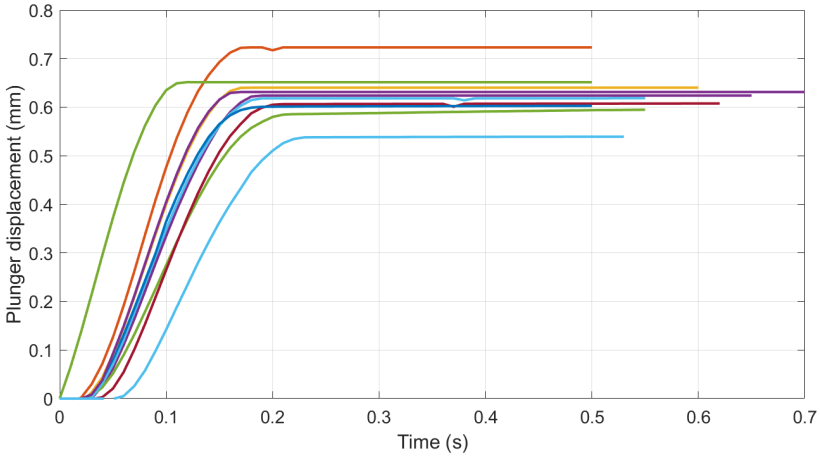

Figure B.5: Plunger movement measured for samples processed with Configuration 3 parameters

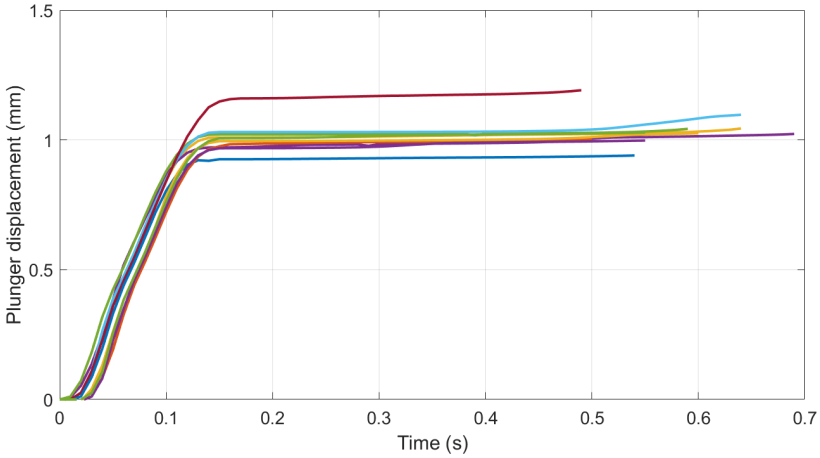

Figure B.6: Plunger movement measured for samples processed with Configuration 4 parameters